T.C.
YEDİTEPE UNIVERSITY
INSTITUTE OF HEALTH SCIENCES
DEPARTMENT OF HISTOLOGY AND EMBRYOLOGY

DETERMINATION OF THE ANTI-CANCER EFFECT OF VERTEPORFIN IN TCam-2 HUMAN SEMINOMA CELLS

THE DOCTOR OF HISTOLOGY AND EMBRYOLOGY THESIS

TUĞÇE ÖNEL

İSTANBUL-2023

T.C.
YEDİTEPE UNIVERSITY
INSTITUTE OF HEALTH SCIENCES
DEPARTMENT OF HISTOLOGY AND EMBRYOLOGY

DETERMINATION OF THE ANTI-CANCER EFFECT OF VERTEPORFIN IN TCam-2 HUMAN SEMINOMA CELLS

THE DOCTOR OF HISTOLOGY AND EMBRYOLOGY THESIS

TUĞÇE ÖNEL

SUPERVISOR
ASSOC. PROF. AYLİN YABA UÇAR

İSTANBUL-2023

APPROVAL

Institute : Yeditepe University Institute of Health Sciences
Programme : Doctoral Program in Histology and Embryology
Title of the Thesis : Determination of The Anti-cancer Effect of Verteporfin in TCam-2 Human Seminoma Cells
Owner of the Thesis : Tuğçe Önel
Examination Date : 25/01/2023
The Jury judges that the candidate named above has satisfactorily completed his thesis.

Supervisor:	Assoc. Prof. Aylin Yaba Uçar (Yeditepe University, Faculty of Medicine, Department of Histology and Embryology)
Member/Examiner:	Prof. Ahmet Çevik Tufan (Yıldırım Beyazıt University, Faculty of Medicine, Department of Histology and Embryology)
Member/Examiner:	Prof. Gülderen Yanıkkaya Demirel (Yeditepe University, Faculty of Medicine, Department of Immunology)
Member/Examiner:	Assoc. Prof. Yasemin Seval Çelik (İzmir Ekonomi University, Faculty of Medicine, Department of Histology and Embryology)
Member/Examiner:	Assist. Dr. Alev Cumbul (Yeditepe University, Faculty of Medicine, Department of Histology and Embryology)

APPROVAL
This thesis has been deemed by the jury in accordance with the relevant articles of Yeditepe University Graduate Education and Examinations Regulation and has been approved by Administrative Board of Institute with decision dated ..... and numbered .....

Prof. Dr. Bayram Yılmaz
Director of Institute of Health Sciences

DECLARATION

I hereby declare that this thesis is my own work and that, to the best of my knowledge and belief, it contains no material previously published or written by another person nor material which has been accepted for the award of any other degree except where due acknowledgment has been made in the text.

../../20..

Tuğçe Önel

DEDICATION

To my family…

ACKNOWLEDGEMENTS

I exceptionally would like to thank my supervisor and counsel Assoc. Prof. Aylin Yaba UÇAR who encouraged me and has been very helpful to me in my laboratory experiments. I am also appreciative for the checks and corrections she has made about my thesis. I am grateful to Assoc. Prof. Aylin Yaba UÇAR for her psychological support and friendliness also. Working with Assoc. Prof. Aylin Yaba UÇAR has been a privilege for me; I think she has contributed greatly to my academic point of view.

I have taken pleasure in working with Ecem Yıldırım and Cihan Süleyman Erdoğan while doing my experiments; I give them endless thanks for their understanding and encouragement. I am also appreciative for their interest and help in conducting the thesis experiments.

I was deeply affected with the help of my close friends Dr. Mehmet Şerif Aydın and Olgu Enis Tok really thank them for the close interest and supportive approache they showed me throughout my studies.

I would also like to thank Prof. Bayram Yılmaz, Prof. Gülderen Yanıkkaya Demirel and PhD Başak Aru for their support and help during the experiments for my thesis.

And the last thanks are for my mom Şermin Önel, my father Fevzi Önel and my sister Buse Önel; the work they spent on me and the patience they showed can never be paid. I am also grateful to them for their unconditional, real love and endless interest.

TABLE OF CONTENTS

LIST OF TABLES

LIST OF FIGURES

LIST OF SYMBOLS AND ABBREVIATIONS

ABP: Androgen binding proteins

AFP: α-fetoprotein

AMD: Age-related macular degeneration

AMH: Anti-Müllerian hormone

ASA: Anti sperm antibody

BBB: Blood Brain Barrier

BCA: Bicinchoninic acid

BMP4: Bone Morphonegenetic Protein 4

BRB: Blood Retina Barrier

BTB: Blood Testis Barrier

CTGF: Connective Tissue Growth Factor

DPBS: Dulbecco's phosphate buffered saline solution

EC: Embryonal Carcinoma

ESC: Embryonic stem cell

FBS: Fetal Bovine Serum

FSH: Follicle stimulating hormone

GCNIS: Germ Cell Neoplasia in situ

GCT: Germ cell tumor

H&E: Hematoxylen&Eosin

Immunoflourecence: IF

KRT18: Keratin 18

LATS1/2: Large tumor suppressor homologues 1 and 2

LH: Luteinizian Hormone

MST1/2: Mammalian sterile 20-protein kinase 1 and 2

PBS: Phosphate Buffer Saline

PDT: Photodynamic therapy

PGC: Primodial Germ Cell

PGC: Primordial Germ Cell

PI: Propidium iodide

PIC: Protein inhibitor cocktail

PMSF: Phenylmethylsulphonyl fluoride

PS: Phosphatidylserine

PS: Photosensitizing properties

q-RT-PCR: Quantitative Real Time Polymerase Chain Reaction (qRT-PCR)

SC: Spermatogonial Cell

SOX2: SRY-Box-Transcription Factor 2

TAOK1/2/3: TAO kinases

TAZ: Two homologs of *Drosophila* Yki

TDGR1: Testicular development-related gene 1

TEAD: TEA domain family member

TGFβ: Transforming Growth Factor β

TGTC: Testicular germ cell tumor

VP: Verteporfin

YAP1: Yes-associated protein 1

ZO-1: Zonula Ocludens-1

β–hCG: β-human chorionic gonadotropin

ABSTRACT

Önel, T. (2023). Determinatıon of The Anti-cancer Effect of Verteporfin in TCam-2 Human Seminoma Cells, Yeditepe University, Institute of Health Sciences, Department of Histology and Embryology, PhD Thesis, İstanbul.

Testicular cancer is the most common solid organ malignancy in young men. The Hippo pathway is a highly conserved signaling pathway with crucial roles in organ size, tissue homeostasis, and cancer development. Verteporfin is an inhibitor of Hippo pathway with promising roles in anticancer therapy. In the thesis study, we hypothesized that verteporfin may have anti-cancer effect on TCam-2 human seminoma cells. Therefore, the aim of the study was to investigate the effect of verteporfin treatment at different doses and concentrations on the proliferation, migration and apoptosis process in TCam-2 cells. Hippo signaling pathway protein expression in testis, embryonal carcinoma and seminoma tissues was determined by immunohistochemistry staining. TCam-2 cells were treated with different concentrations of verteporfin (1, 5, 10, 20 and 40 μM) for 24, 48 and 72 h. Protein and mRNA levels of Hippo pathway proteins, as well as their localization were investigated. Effect of verteporfin on cell migration, proliferation and apoptosis were also evaluated. In human testis, embryonal carcinoma and seminoma tissues, Hippo pathway proteins were detected as specifically and differentially localized. *In vitro*, as the duration and dose of verteporfin treatment increased, the level of the Hippo pathway proteins decreased, and mRNA levels remained unchanged. We also showed that Hippo signaling pathway proteins localized in the cell nucleus were translocated to cytoplasm depending on the increasing dose of verteporfin in TCam-2 cells. Verteporfin decreased the cell proliferation, migration and cell viability, as well as increased the apoptosis in TCam-2 human seminoma cells depending on the dose. In conclusion, we suggest that the Hippo pathway and verteporfin relationship may be a therapeutic target for seminoma by affecting cell proliferation, viability, migration and apoptosis processes. Further *in vivo* and *in vitro* studies are needed to better understand the underlying mechanism of seminoma and the role of Hippo pathway to earn new insights on the seminoma therapies.

Key words: Human testis tissue, Seminoma, TCam-2, Hippo, Verteporfin.

ÖZET

Önel, T. (2023). Verteporfinin TCam-2 İnsan Seminoma Hücrelerinde Kanser Önleyici Etkisinin Belirlenmesi, Yeditepe Üniversitesi, Sağlık Bilimleri Enstitüsü, Histoloji ve Embryoloji Anabilim Dalı, Doktora Tezi, İstanbul.

Testis kanseri, genç erkeklerde en sık görülen katı organ malignitesidir. Hippo sinyal yolağı, organ boyutu, doku homeostazı ve kanser gelişiminde çok önemli rollere sahip, oldukça korunmuş bir sinyal yolağıdır. Verteporfin, antikanser tedavisinde önemli rollere sahip bir Hippo sinyal yolağı inhibitörüdür. Bu çalışmada, verteporfinin TCam-2 insan seminoma hücreleri üzerinde anti-kanser etkisi olabileceğini varsaydık. Bu nedenle çalışmanın amacı, farklı doz ve konsantrasyonlarda verteporfin uygulamasının TCam-2 hücrelerinde proliferasyon, migrasyon ve apoptoz sürecine etkisinin araştırılmasıdır. Testis, embriyonal karsinom ve seminom dokularında Hippo sinyal yolağı protein ekspresyonu, immünohistokimya ile belirlendi. TCam-2 hücrelerine, 24, 48 ve 72 saat boyunca farklı konsantrasyonlarda verteporfin (1, 5, 10, 20 ve 40 μM) uygulandı. Hippo sinyal yolağı protein ve mRNA seviyeleri ile bu proteinlerin lokalizasyonu araştırıldı. Verteporfinin hücre migrasyonu, proliferasyonu ve apoptoz üzerindeki etkisi de değerlendirildi. Testis, embriyonal karsinom ve seminom dokularında, Hippo sinyal yolağı proteinlerinin diferansiyel olarak lokalize olduğu tespit edildi. *İn vitro*, verteporfin tedavisinin süresi ve dozu arttıkça, Hippo sinyal yolağı protein seviyeleri azaldı ve mRNA seviyeleri değişmeden kaldı. TCam-2 hücrelerinde, çekirdekte lokalize olan Hippo sinyal yolağı proteinleri, verteporfin dozuna bağlı olarak sitoplazmaya yer değiştirmiştir. Verteporfin, doza bağlı olarak *in vitro* hücre proliferasyonu, migrasyonu ve hücre canlılığını azaltmış, apoptozu ise arttırmıştır. Sonuç olarak, Hippo sinyal yolağı ve verteporfin ilişkisinin, hücre proliferasyonu, canlılığı, göçü ve apoptoz süreçlerini etkileyerek seminoma için terapötik bir hedef olabileceğini öneriyoruz. Seminomun altında yatan mekanizmayı ve Hippo sinyal yolunun tedavideki rolünü daha iyi anlamak ve seminoma terapileri hakkında yeni bilgiler edinmek için daha fazla *in vivo* ve *in vitro* seminoma çalışmalarına ihtiyaç vardır.

Anahtar kelimeler: İnsan testis dokusu, Seminoma, TCam-2, Hippo, Verteporfin.

1. INTRODUCTION AND PURPOSE

The testicles are arranged in two separate sections: the seminiferous tubules, where germ cells differentiate into mature spermatozoa, and the interstitial space composed of testosterone-secreting Leydig cells, blood vessels, nerve fibers, and connective tissue (1). Spermatogenesis is a cellular process in which spermatogonia transform into mature spermatids within the seminiferous tubules under the regulation of endocrine factors and structural and nutritional support of Sertoli cells (2). In the testis, Sertoli cells act as “mother cells” to support and nurture the development of different germ cell types during spermatogenesis (3) and form the blood-testis barrier, which is a special junctional complex with neighboring germ cells (4). Testicular cancer is the most common type of cancer in men aged 15–35 years and accounts for approximately 45% of all primary testicular tumors (5). Testicular tumors are largely composed of germ cell tumors, sex cord - stromal tumors, germ cell / sex cord - stromal tumors and various types of tumors (6). Testicular cancer is one of the most important causes of infertility in male reproductive life and has increased significantly in the last forty years. Although the exact cause of testicular cancer has not been determined yet, cryptorchidism, infertility, the presence of contralateral tumors and some genetic factors are known as associated risk factors (7).

Hippo signaling pathway is involved in cell-cell contact inhibition, control of organ size and regulation of cancer development in mammals (8, 9) and it is an evolutionarily conserved pathway (10). It also plays an important role in the formation and progression of many different types of cancer in humans (11). The Hippo signaling pathway consists of Mammalian sterile 20-protein kinase 1 and 2 (MST1/2), large tumor suppressor homologues 1 and 2 (LATS1/2), Yes-associated protein (YAP1), and its transcriptional cofactor Two homologs of *Drosophila* Yki (TAZ) (12). YAP1 is a central transcription coactivator that acts as an oncogene in numerous experimental systems (13). It is involved in cell differentiation, transformation and control of organ size. When the Hippo signaling pathway is active, YAP/TAZ is transcriptionally active and phosphorylates YAP/TAZ activity in the cytoplasm. In contrast, when the Hippo pathway is inactive, YAP/TAZ is transcriptionally active and localizes to the nucleus to regulate gene expression (14).

Among the germ cell lines that mimic germ cells, TCam-2 is the germ cell line available that shows the most similarity to human germ cells. TCam-2 cells are known as suitable for both *in vitro* and *in vivo* studies of seminoma pathophysiology (15). This cell line is derived from human seminoma, a type of testicular germ cell tumor (TGCT), and represents male germ cells in the early phase of prenatal development (16).

Verteporfin is known as the one of Hippo signaling pathway inhibitors. Verteporfin (VP) has been used clinically for many years for the treatment of age-related macular degeneration (AMD) with photodynamic therapy (PDT). However, recent studies have demonstreated that VP also exerts anti-tumor activities. YAP is a key effector of the Hippo pathway that is aberrantly expressed in various cancer types and regulates tumorigenesis and organ size and is also a pro-tumorigenic factor as mentioned.

In the thesis study, we hypothesized that verteporfin may have anti-cancer effect on TCam-2 human seminoma cells. Therefore, the aim of the study was to investigate the effect of verteporfin treatment at different doses and concentrations on the proliferation, migration and apoptosis process in TCam-2 cells. We suggest that the findings obtained in our study may contribute to the development of new treatment approaches in seminoma treatment as well as in the process of restoration of testicular functions and preservation of fertility.

2. LITERATURE REVIEW

2.1. Male Genital System

Male reproductive system in mammals is divided into two groups as internal and external genitalia. The testes, vas deferens, epididymis and accessory glands (seminal vesicle and prostate) form the internal genital organs. Epididymis where the spermatozoa are transmitted and stored (Figure 1) is consists of head (caput), body, tail (cauda). The spermatozoa formed in the testis enter the head part of the epididymis and pass to the tail part and are stored there. The part of the canal that transmits spermatozoa after the epididymis is the vas deferens, starting from the tail of the epididymis and extending upwards at the posterior edge of the testis (17, 18). During ejaculation, sperm is transferred from epididymis to the vas deferens, then from vas deferens to the urethra (19-23). Scrotum and penis are known as the external genitalial organs (Figure 1). Scrotum is the place where the testis is located, and the penis carries the ejaculate to the vagina. Penis also excretes the urine from the body. There are sensitive nerve endings that provide sexual arousal on its surface (20). The main task of these internal and external organs, which work together but have different functions, is to produce spermatozoa and transport them to the female reproductive organ (24, 25).

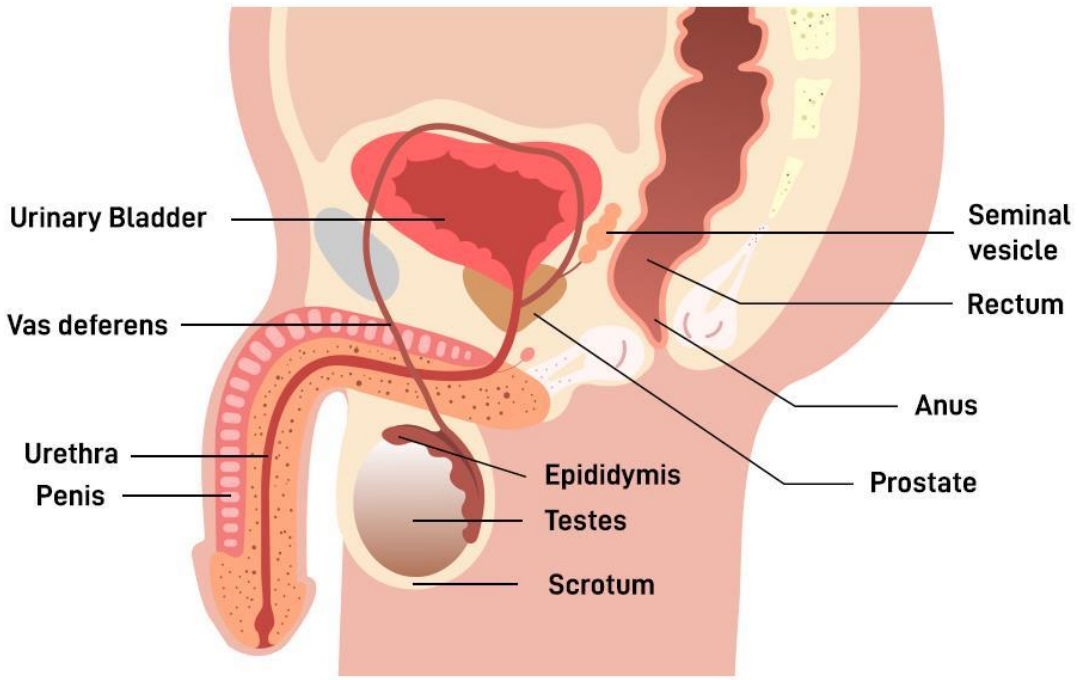

Figure 1. Components of the male genital system (26).

2.1.1. Testis

The testis is the pair of organs of the male reproductive system where spermatogenesis and steroidogenesis take place. The testis is surrounded by thick dense connective tissue called thick tunica albuginea. Fibrous extensions emerging from this capsule divide the testicular mass into approximately 250 lobules (27). Testes surrounded by tunica albuginea are located in the scrotum which consists of skin and fibromuscular tissue. The structure and location of the scrotum is very crucial for the function of testis. The skin of the scrotum is thin and densely packed with nerve endings. Because of these nerve endings, it is quite sensitive to heat. The reason why the structure is outside the body is that sperms need an environment whose temperature is lower than the body temperature (35 °C) in order to stay alive. The scrotum maintains a balance of temperature through various physiological mechanisms, such as a cremasteric reflex, a change in blood flow to the spermatid cord, a fold of the skin and the role of the sweat glands of the scrotal skin (28, 29).

The testes, accepted as the center of the male reproductive system consist of two parts, the interstitial tissue and the seminiferous tubules (20). The two ends of each of the convoluted seminiferous tubule loops open into a network of channels at the head of the epididymis. The interstitial space contains blood and lymph vessels, fibroblastic support cells, macrophages, mast cells and Leydig cells. There are Sertoli cells in the seminiferous tubules of the testes and spermatogenic cells between Sertoli cells (Figure 2).

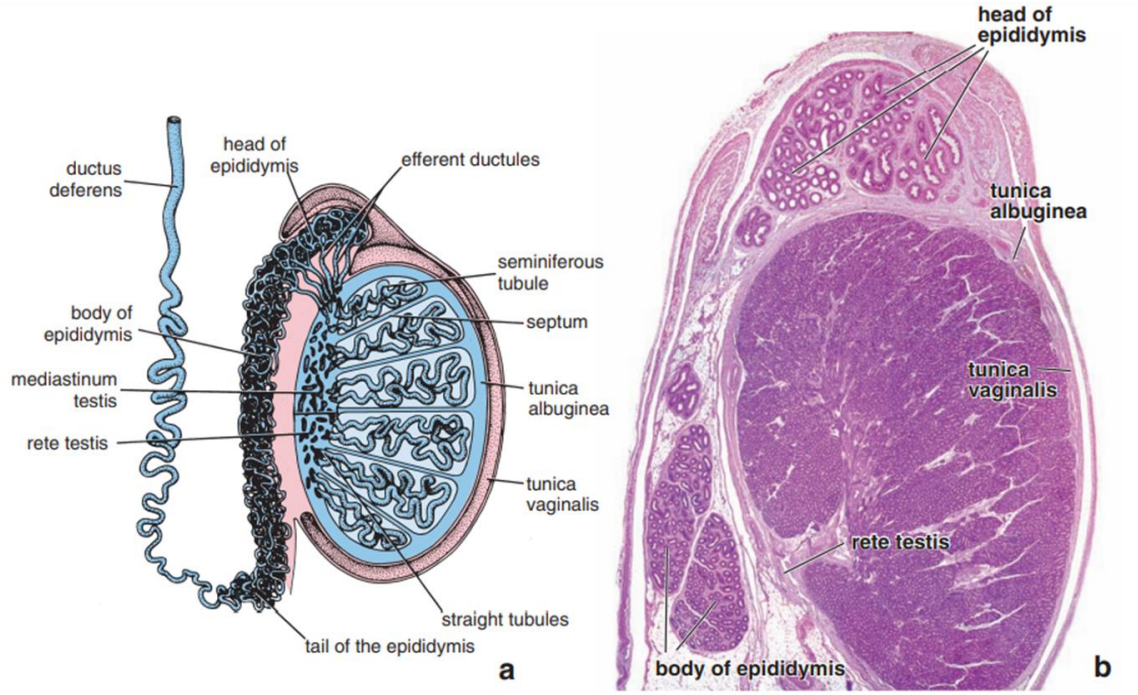

Figure 2. Section of human testis. **a.** This schematic diagram shows of the human testis. **b.** Hematoxylin & Eosin (H&E) stained section of the head and body of the epididymis and testis (13).

Sertoli cells are somatic cells that spread from the basal lamina to the lumen. Sertoli cells play a critical role in the development of sperm cells, both functionally and structurally (30, 31). We summarized the functions of Sertoli cells below:

- Sertoli cells express the enzyme CYP19 (aromatase). CYP19 enzyme converts testosterone secreted from Leydig cells into estradiol.
- Sertoli cells also produce androgen binding proteins (ABP). ABP binds testosterone and provide high concentration of testosterone level in the testes, which is very important for spermatogenesis.
- Sertoli cells provide the movement of spermatozoa to the epididymis via secretions.
- Sertoli cells eliminate the apoptotic spermatogenic cells and residual bodies through phagocytosis.
- Sertoli cells, which have an important endocrine role, secrete Anti-Müllerian hormone (AMH) and inhibin hormone.

Sertoli cells are tightly interconnected and create the blood- testis barrier. The purpose of this tight connection is to prevent passage of the fluid in the lumen of seminiferous tubule, which is quite different from the plasma in content into the circulation and prevent formation of immune response in case of passage (20, 30-32). Sertoli cells express androgen and Follicle Stimulating Hormone (FSH) receptors. Therefore, all these functions of Sertoli cells mentioned above are organized by the hormonal (FSH, testosterone) and the paracrine control.

Another specialized cell found in testis are Leydig cells. These cells are located in the peritubular compartment and through Sertoli cells, Leydig cells supply nutrients to the seminiferous tubules. Also, they cells form a network with the capillaries and play a role in the transportation of testosterone to the peripheral circulation (20). Leydig cells are the source of androgens or testosterone in males. Luteinizing hormone (LH) creates the receptor stimulation in Leydig cells and testosterone production takes place. LH

secretion supports the growth and proliferation of Leydig cells in the long term (21, 30, 31).

2.1.1.1. Spermatogenesis

Spermatogenesis is the process of the formation of spermatozoa in testes. During the spermatogenesis the spermatogonia pass through the stages of primary spermatocyte, secondary spermatocyte and spermatid. It is a very complex and well-organized process and includes three stages of germ cell development, mitosis (proliferation of spermatogonia), meiosis (spermatocyte formation and DNA recombination) and spermiogenesis (spermatid differentiation). Spermatogenesis generates highly specialized sperms from undifferentiated spermatogonia.

In human, spermatogonial stem cells contain two cell populations as type A dark and type A pale undifferentiated spermatogonia (Figure 3). Type B1 spermatogonia is formed through mitotic divisions of type A pale spermatogonia. All mammals are capable of spermatogenesis, type B/B1 spermatogonia go through mitotic divisions to form preleptotene spermatocytes, which marks the beginning of meiosis. After the formation of preleptotene spermatocytes, they enter the prophase of meiosis and differentiate into pachytene, zygotene, leptotene, and diplotene spermatocytes. During prophase, which is the longest stage of meiosis, various changes occur like migration, genetic recombination and chromosome condensation of primary spermatocytes (44+XY) spread the basal seminiferous tubule to the adluminal compartment. Following the prophase stage, meiosis is completed rapidly and secondary spermatocytes containing 23 chromosomes (22+X or 22+Y) are formed. As a result of the second meiosis, spermatids are formed (33). During this differentiation process, the cells are embedded in the cytoplasmic wall of Sertoli cells. Sertoli cells play different roles in nourishing, protecting and supporting the developing germ cells along the seminiferous tubules (34). On the other hand, type A dark spermatogonia form the stem cell population in testes by self-renewal (Figure 3).

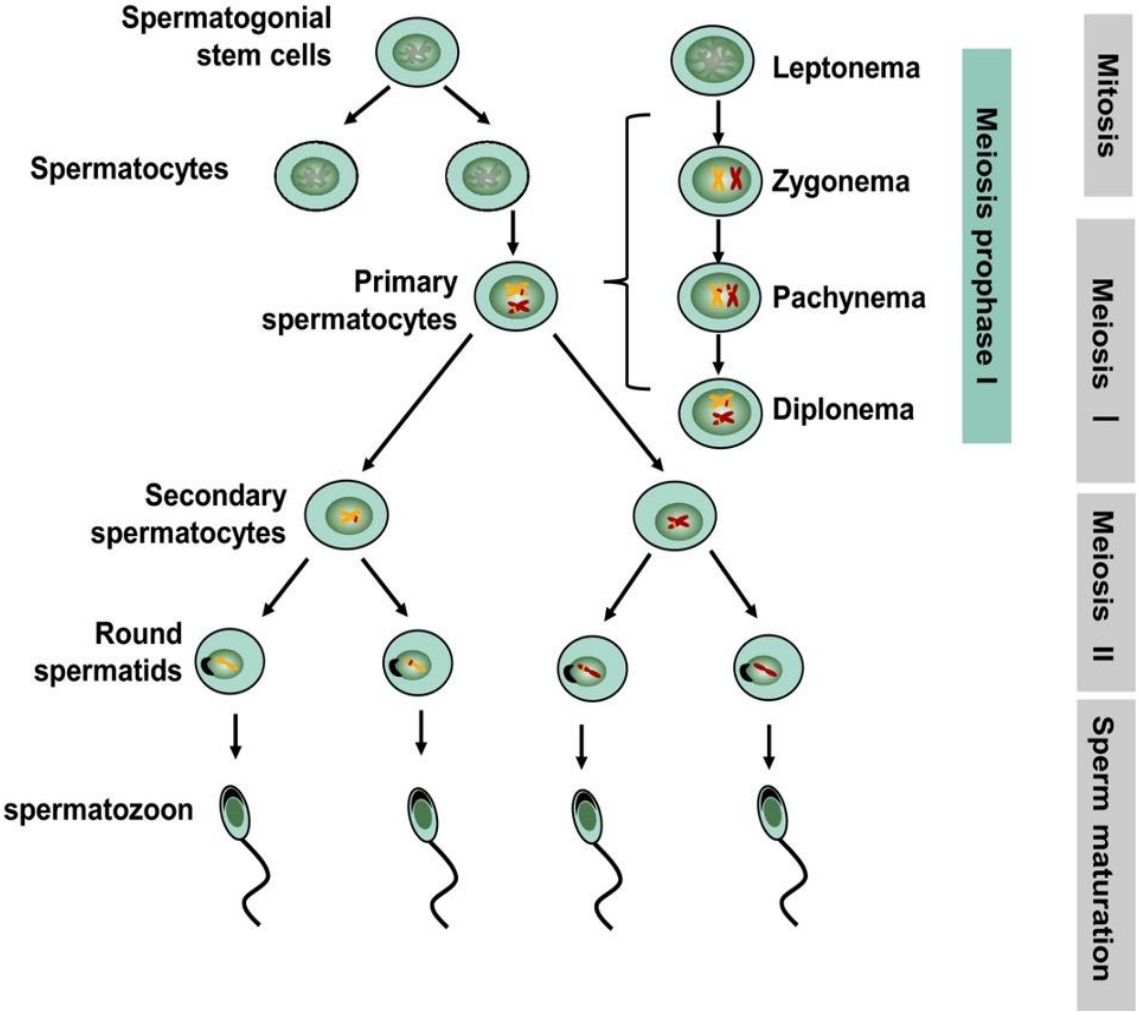

Figure 3. Schematic diagram of spermatogenic cells. This diagram shows the spermatogenic cell lines, respectively. Cytoplasmic division is seen only in primitive type A dark spermatogonia, which act as stem cells. All other spermatogenic cells undergo mitotic and meiotic divisions and undergo the process of differentiation of spermatids. The cells transform into spermatozoa as they pass through the lumen. Sertoli cells phagocytize residual bodies in the environment (17).

2.1.1.2. Spermiogenesis

Spermatids undergo a highly differentiated cell process called spermiogenesis. The final stage of spermatogenesis is spermiogenesis. This process takes place in three stages;

a. Golgi Phase: The spermatid cytoplasm found at this stage contains the nucleus, Golgi complex, mitochondria, ribosome, and flat-faced endoplasmic reticulum. Hydrolytic enzymes are transferred from the Golgi apparatus to the acrosomal vesicle.

The flagellum, which will provide sperm movement in the future, begins to form at this stage.

b. Acrosomal Phase: The acrosomal granule is spread to cover the nucleus and the acrosome is formed. The distal centriole forms the flagellum, which consists of pair of microtubules. Mitochondria, which are necessary for sperm movement, create the middle part of the sperm.

c. Maturation Phase: After all organelles have taken a certain arrangement, sertoli cells phagocytized residual bodies. Mature sperm disperse from the lumen of the seminiferous tubule.

Sperm cells are transferred from the seminiferous tubule lumen by passive transport, where they are both stored and directed to the epididymis where they will function functionally. From here, they reach the urethra via the vas deferens. The time required for the spermatogonia to develop into mature sperm is approximately 64 days. As shown in Figure 4 the mature sperm consists of two parts as the head and the tail. The head contains the nucleus surrounded by an acrosome. The nucleus has a flattened dense structure. The acrosome covers the anterior half of the nucleus. Acrosomal enzymes are released at the time of fertilization to facilitate sperm entry. The tail is divided into three parts as the main part, the middle part and the last part. The middle part contains mitochondria that provide the energy needed for movement.

One of the main changes that occur in the nucleus during spermiogenesis is the formation of nuclear condensation when somatic histones are replaced by arginine and lysine-rich protoamines. As a result of these events, transcription ends in the nucleus and the sperm genomic DNA structure is stabilized and protected (35).

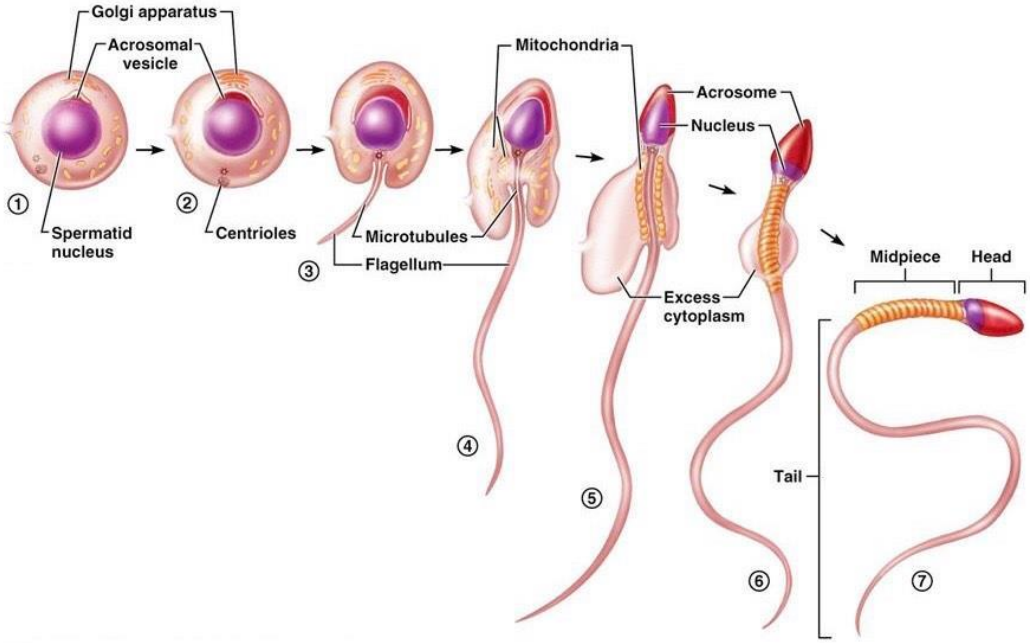

Figure 4. Schematic diagram of spermiogenesis stages (17).

2.1.1.3. Blood-Testis Barrier

The concept of the blood-tissue barrier was introduced in the early 20th century, when it was observed that the brain and testis were not completely stained with vital dyes (36). At the same time, researchers have seen that the content of fluid obtained from testicular lymph and blood plasma and the content of fluid obtained from the lumen of the rete testis and seminiferous tubules differ from each other (37, 38). While other barrier structures in the body, like the Blood-Brain Barrier (BBB) and the Blood-Retina Barrier (BRB), are composed of tight junctions between capillary endothelial cells and supporting pericyte and perivascular macrophages, the Blood-Testis Barrier (BTB) composed of specialized connections between Sertoli cells that sit on the basement membrane only in the seminiferous tubules (Figure 5). BTB is considered to be the one of the tightest barrier structures in the body (39, 40).

BTB divides the seminiferous tubule epithelium into two basal and adluminal compartments (Fig. 5). The most important task of BTB is to prevent certain substances such as water, ions, electrolytes, paracrine factors, hormones and biological molecules from reaching the apex between Sertoli cells. Its secondary mission is providing defense system. It enables spermatocytes that have passed into the adluminal compartment from the preleptotene stage to complete spermatogenesis in an isolated microenvironment (41).

In addition to these functions, an environment that may cause male infertility is eliminated by preventing the entry of anti-sperm antibodies (ASAs) that may occur during spermiogenesis into this isolated environment (42). Studies have shown that the main reason for the formation of ASA is permeability in the BTB structure (43). However, it has been shown to cause ASA formation in mechanical obstructions that may occur as a result of congenital anomalies, vasectomy or traumas (44, 45). As a result of increased BTB permeability, ASAs enter the lumen of the seminiferous tubule and are transmitted to the epididymis and vas deferens via channels. These antibodies bind to sperm and cause agglutination (46). Besides sperm agglutination (47), ASAs cause inhibition of sperm migration (48). In addition, since the sperm heads are coated with antibodies, they cannot bind and penetrate the zona pellucida (49, 50).

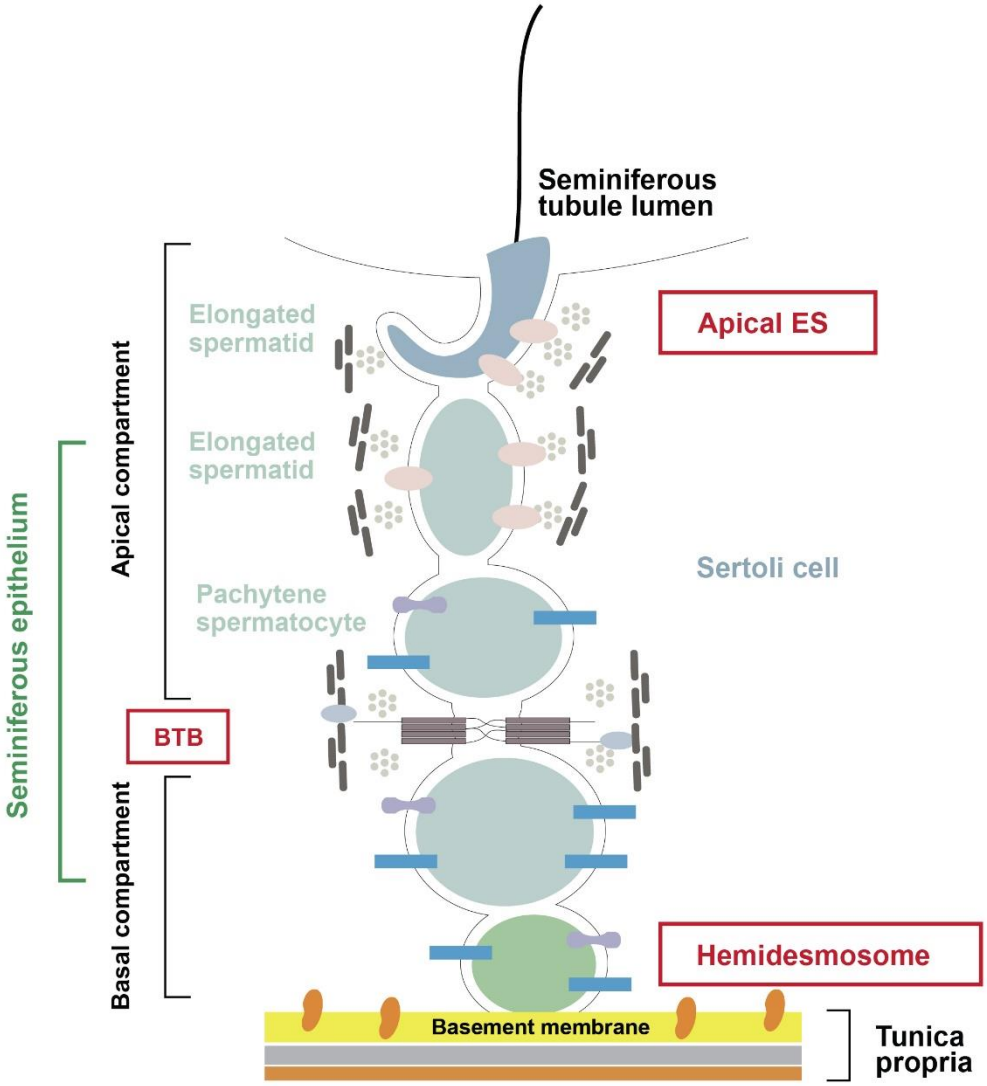

Figure 5. Concept of the blood-testicular barrier (BTB). BTB consists of tight junctions, desmosome and gap junctions, basal ectoplasmic specialization, and bundles of actin filaments sandwiched between the endoplasmic reticulum cisterna and the plasma membranes of two opposing Sertoli cells (51).

BTB consist of 4 types of junctions: ectoplasmic specializations, tight junctions, gap junctions and desmosomes (41). Desmosomes are the type of junction that connects cell-cell-intermediate filaments. It contains the integral membrane proteins desmoglein-2 and desmocollin-2. Gap junctions are an actin-based type of junction and are responsible for the communication of cells with each other. They are formed by the combination of connexins. It is found in the testis, especially in the areas where basal and apical ectoplasmic specializations are located. Ectoplasmic specializations are testis-specific connections made up of hexagonal actin microfilaments between the endoplasmic reticulum and the plasma membrane. The tight junctions in the BTB structure are in the class of integral membrane proteins and are grouped under the three headings: occludins, claudins and cell adhesion molecules (52). Occludins are involved in controlling the localization of proteins required for establishing cell polarization and controlling cell orientation. Claudins (claudin 3, 5, 11) expressed in the BTB structure, together with occludins, contribute to maintaining the integrity of the BTB. Zonula occludens-1 (ZO-1) is a found peripheral membrane protein associated with tight junction proteins. It binds occludin and claudins to the actin skeleton. It colocalizes with Connexin-43 and regulates the communication between the gap junctions (53).

2.2. Testicular Cancer

Testicular cancer is the most general types of malignancies in men aged between 15 and 35 years (54, 55). Testicular cancer accounts for approximately 1% of tumors seen in men (56, 57). Currently, more than 80% of testicular cancer patients can be cured. In patients in the early stage, the cure rate reaches up to 100% (58).

2.2.1. Testicular Cancer Development

Despite extensive research, the etiology of Testicular Germ Cell Tumor (TGCT) remains unclear. Studies suggest that environmental factors may effect on tumor development in testicular cancer (59). Moreover, many genetic mutations have been identified that positively affect TGCT rates in familial and sporadic TGCT cases (60).

Risk factors identified for TGCT are cryptorchidism, family history of TGCT, Klinefelter Syndrome, spermatic and testicular dysgenesis, testicular atrophy, inguinal hernia, and hydrocele (61, 62). Moreover, studies at the genome level have shown a connection between TGCT and a number of single nucleotide polymorphisms (63, 64). Environmental factors such as disruptions in androgen hormone secretion, perinatal characteristics, and lifestyle factors do not have a clear relationship with TGCT (65, 66). The combined effect of (micro)environmental and (epi)genetic factors is likely to lead to TGCT (67).

A previous study suggests two different theories which can be linked to the formation of the testicular cancer. Spermatogonial Cell (SCs) in connection with GCNIS (Germ Cell Neoplasia *in situ*) are prepubertal cells whose differentiation processes are arrested through environmental agents such as antitestosterones, xenoestrogens and/or genetic anomalies (68). Primordial Germ Cell (PGC) PGC/gonocytes requires a favorable microenvironment in order to live in the postnatal testes however immature SCs that are unable to induce germ cells cannot fulfill these requirements. GCNIS can be formed when PGC/gonocytes fail the differentiation process into prespermatogonia (69, 70). There are two main theories around this process. First theory debates whether these SCs are contribute to GCNIS development (Figure 6) or adult cells that differentiate under the factor of GCNIS and/or the underlying process. There is an ongoing debate and the fact that adult SCs are talented of differentiation support the second theory. For example, Keratin18 (KRT18) has been shown to be reexpressed in monkey testis following heat application (71). According to these two theories, in a co-culture model using SC (FS1) cells and seminoma cell line TCam-2 alternative to GCNIS, GCNIS-associated SCs were shown to be secondary differentiated adult cells but not than immature cells that contribute to GCNIS development. TCam-2 cells co-cultured with FS1 cells reported an upregulation of genes associated with reprogramming and pluripotency and SRY-Box Transcription Factor 2 (SOX2) expression, suggesting a possible transition from seminoma to embryonal carcinoma (EC) (Figure 6)(72).

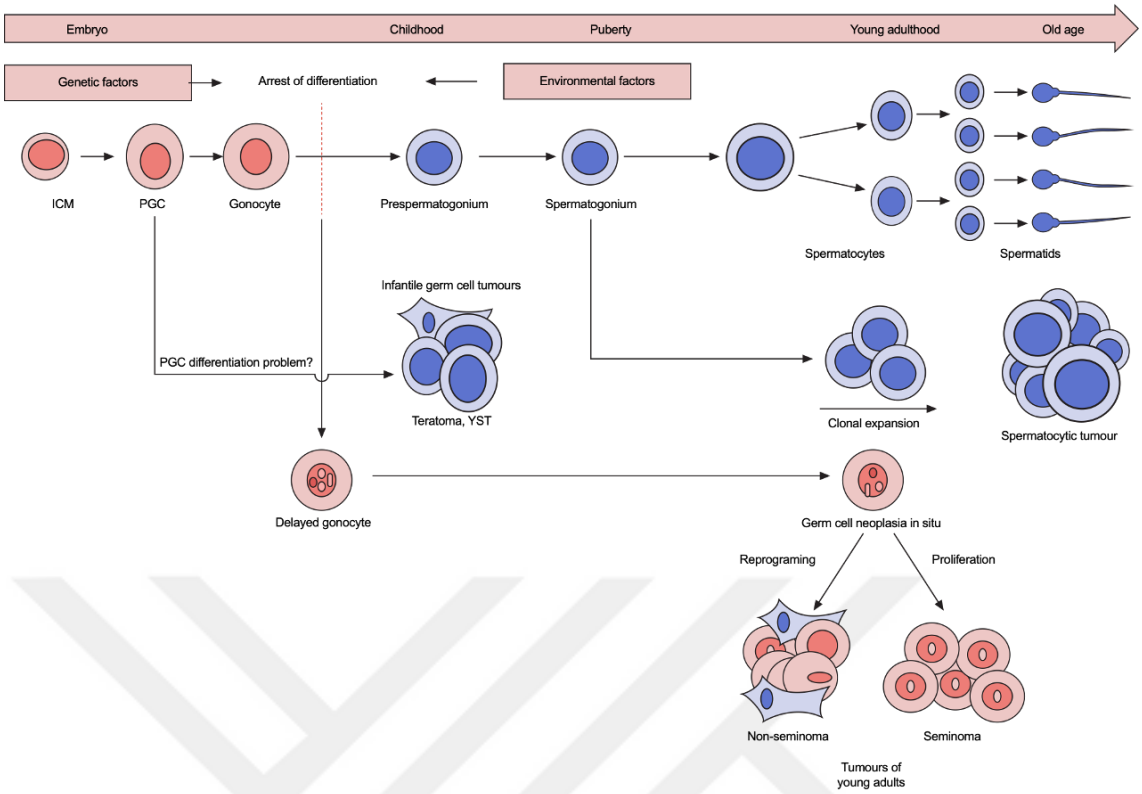

Figure 6. Development of Different Types of Testicular Cancer. The arrest of differentiation in PGC or gonocytes in the prenatal stage leads to the formation of GCNIS in the seminiferous tubules. After puberty, GCNIS cells may begin to differentiate into nonseminoma, seminoma, or both. GCNIS originates from corrupted SC. The current hypothesis proposes that there are prepubertal cells that have been arrested during differentiation of impaired SCs. These cells are not capable of supporting normal spermatogonial development, resulting in delays and disruptions in germ cell differentiation. Furthermore, these SCs are thought to be adult cells differentiating under the influence of GCNIS and/or the underlying pathological process (72).

2.2.2. Testicular Cancer Types

Germ cell tumors (GCT) account for 95% of testicular cancer (56, 73) and testicular cancers can be divided into three groups (Figure 7) (74): Type I testicular germ cell tumors (TGCTs) occur mainly in neonatal and young children, including benign teratomas and malignant yolk sac tumors (75). Type II TGCTs most commonly act men aged 20-40 years, but this tumor type has its origin earlier in fetal development (76). Type III TGCT affects men over 50 years of age and is originate from the dissemination of growing type B spermatogonia (77).

Type II TGCT is divided into two main subgroups as seminoma and nonseminoma (Figure 7). Seminoma constitutes 50% of germ cell tumors and is frequently observed in the 40s. Nonseminomatous histology (choriocarcinoma, teratoma, yolk sac tumor and embryonic carcinoma) constitute the remainder of the germ cell tumors and are frequently encountered in the 30s (78). There are three histological types of seminoma: classical (85%), anaplastic (5-10%), and spermatocytic (4-6%) (79). Classical seminoma constitutes 85% of all seminomas and is mostly seen at the age of 40. Anaplastic seminoma constitutes 10% of seminomas and has a high mitotic rate and its survival rate is lower than the rate seen in seminoma (55). Spermatocytic seminoma is a rare seminoma and usually occurs in older men (80). Although these tumors can usually be treated with orchiectomy alone, many patients also receive radiation therapy as a preventive measure (81). Its metastatic potential is minimal (82). Nonseminoma tumors consist of yolk sac tumor, choriocarcinoma teratoma and embryonal carcinoma (Figure 7) (78, 82). Embryonal carcinoma accounts for 20% of testicular tumors (83). Although these tumors can be treated with chemotherapy, they are very aggressive and more lethal than seminomas (84). Choriocarcinoma is rare (84) however it is the most aggressive of germ cell tumors due to early spread by blood and lymphatic routes (83). Yolk sac tumor mimics embryonic yolk sac histology. It is the most common tumor in newborns and infants up to 3 years of age and has a good prognosis (85). Terotamas are tumors that contain at least 2 or 3 germinal layers. They are the tumors with the least metastatic potential compared to the other germ cell tumors (54).

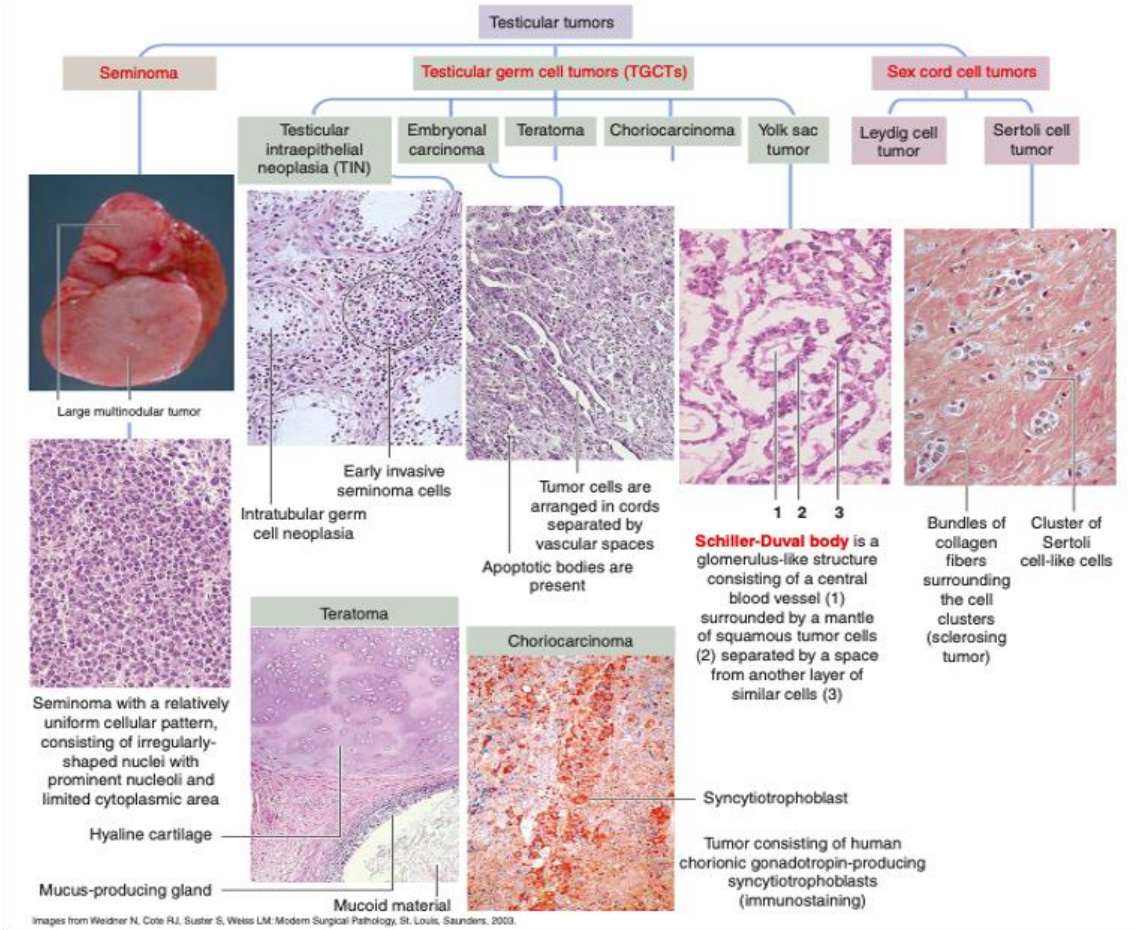

Figure 7. Types of testicular tumors. Testicular cancer types are examined in 3 groups as seminoma, testicular germ cell tumors and sex cord cell tumors. Testicular germ cell tumors include testicular intraepithelial neoplasia, embryonal carcinoma, teratoma, choriocarcinoma, and yolk sac tumor subgroups. Sex cord cell tumors are divided into two subgroups as leydig and sertoli cell tumors. The figure contains histological images of all testicular cancer types and subgroups (79).

2.2.3. Testicular Cancer Treatment

For the testicular cancer treatment, tumor markers are very crucial. Because tumor markers provide information for the identification of small or undetectable malignant cells and tumor type. There are three tumor markers used in testicular cancer. These are α-fetoprotein (AFP), a glycoprotein found in large quantities in fetal serum, β-human chorionic gonadotropin (β-hCG), a hormone produced by the placenta of pregnant women and not normally found in men, and lactate dehydrogenase, a cellular enzyme normally found in muscle, liver, kidney, and brain (86). AFP is a marker for nonseminoma, especially for yolk sac tumor. β-hCG is produced in both seminoma and nonseminoma.

However, it is at low levels in seminoma (87). Serological measurement of β-hCG and AFP is used in the monitoring and diagnosis of testicular cancer treatment. AFP is not produced in pure seminoma or choriocarcinoma. In addition, the enzyme lactate dehydrogenase is a marker for tumor size (88, 89).

The treatment for testicular cancer it depends on the type and stage of the tumor. There are three basic treatment methods: surgery, radiotherapy, and chemotherapy. Testes contains cancerous tissue are removed from the body by surgical method. With radiotherapy, cancer cells are damaged, and their growth is stopped. Seminomas are very sensitive to radiation and are also susceptible to cis-platinum-based chemotherapy drugs (76). After the surgical treatment of seminoma patients, radiotherapy is applied to the abdominal lymph nodes. However, since nonseminomas are not sensitive to radiation, chemotherapy is used to treat this type of cancer. Anti-cancer drugs are generally preferred when the disease metastasized to other parts of the body. These drugs can sometimes be used to shrink the tumor before surgery (90).

2.2.4. TCam-2 Cell Line

Type II germ cell tumors (GCT) are mostly observed in men aged 18-35 years (91). All type II GCTs derivate from a common precursor lesion called GCNIS (92, 93), suggesting that a defective PGC development might cause these cells. TGCTs are examined in two groups as non-seminomas and seminomas. Seminomas display a like epigenetic profiles and gene expressions as primordial germ cells, while the nonseminomatous EC stem cell population is similar to the malignant embryonic stem cells. As a result, ECs can differentiate into extra-embryonic tissue-like cells (yolk-sac tumor, choriocarcinoma) as well as cells that are cabable of making up the three germ layers (teratomas). Embryonal carcinomas (ECs; stem cell part of non-seminomas) and seminomas shows significant differences in their histology, epigenetics and gene expression profiles. While seminomas are like to GCNIS and PGCs, ECs are similar to the malignant embryonic stem cells (92).

Among the germ cell lines that mimic germ cells, TCam-2 is the germ cell line available that shows the most similarity to human germ cells. TCam-2 cells are known as suitable for the studies on seminoma pathophysiology both *in vitro* and *in vivo* (15).

TCam-2 was derived from human seminoma, a type of TGCT, and indicates male germ cells in the early phase of prenatal development (16). This cell line exhibits a broad state of aneuploidy, including gain in chromosomes 7p, 8q, 12p, 20 and loss in 9q, 13, 17p, 22 and Y (94, 95).

TCam-2 cells specifically express GCNIS and PGC determinant genes and determine a typical seminoma/GCNIS morphology (a large nucleus and large round cells with clear cytoplasm) (94, 96, 97). Like seminomas, TCam-2 cells express some markers in connection with different stages of PGC development. Seminomas can also transform into non-seminomas likely yolk-sac tumors, ECs, choriocarcinomas or teratomas (92). TCam-2 cells have been shown to be reprogrammed to an EC-like cell fate upon development in a somatic microenvironment such as brain or the murine flank (97, 98). In one study, molecular analyzes showed that seminoma TCam-2 cells are reprogrammed to an EC-like cell fate upon an inhibition of the Bone morphogenetic factor (BMP) signaling pathway triggered by the *in vivo* (mouse brain or wing) microenvironment. SOX2, which is activated upon inhibition of BMP that mediates the reprogramming process, has been identified as the key factor regulating epigenetic factors and pluripotency reprogramming. In fact, a seminoma cell fate was maintained for approximately six weeks *in viv*o when SOX2 was deleted by the CRISPR/Cas9 method in TCam-2 cells, and only small subpopulations were observed to initiate differentiation six weeks later in vivo.

Studies from the 1970s have shown that when aggressive cancer cells were placed in an embryonic microenvironment, they are capable of being reprogramed towards a less aggressive phenotype (99-102). Another study investigated whether a culture medium supplemented with 10% Egg White (EW) using the TCam-2 cell line could organize seminoma cell phenotype and behavior by providing an appropriate morphogenetic signaling. This substance added to the culture medium has been shown to alter the cell proliferation rate and cell-substrate complex formation without changing the viability and proliferation rates of TCam-2 cells. Organization of substrate-cell adhesion is an important step for the early stages of metastatic process, where small or individual groups of cancer cells can gain differentiation from the primary tumor (103).

TCam-2 cells share many features with fetal germ cells such as BMP4, activin and retinoic acid responsiveness, including Transforming growth factorβ (TGFβ) superfamily

signaling components (104). Their ability to differentiate in response to BMP4 has been documented by xenotransplantation studies in mice (105, 106). In literature, there are different studies which are cunducted with TCam-2 cell line. For instance, TCam-2 cell line was used for the evaluation of the expression of genes associated with human gonocyte differentiation (15). In another study on the proliferation and survival of seminoma cells, TCam-2 cell line was also used (107).

Besides, there are also many studies using the TCam-2 cell line to mimic seminoma cells. One of these research topics is mechanotransduction. There are many experimental studies supporting the importance of cell behavior and mechanotransduction. In a study, cytoskeletal modifications induced by the acute effect of microgravity and its autophagic activation in the TCam-2 cell line were investigated for the first time. Ultimately, TCam-2 cells have been shown to respond rapidly to acute exposure to microgravity and induce adaptive biological processes like autophagy (108). In another study, testicular development-related gene 1 (TDRG1), which is highly expressed in seminoma tissues, was shown to increase the chemoresistance of TCam-2 cells to CDDP by inducing autophagy through the p110β/Rab5/Vps34 (PI3-Kinase Class III) signaling pathway (109).

TCam-2 cell line also pioneered the elucidation of the function of certain factors. For instance, high expression of CSE1L in various tumor types has been showed in many studies but there was no reporting on the the clinical importance of CSE1L for testicular cancer. It was shown that CSE1L is significantly overexpressed in seminoma compared to non-tumor normal testicular tissues. Deletion of the CSE1L gene in the seminoma cell line TCam-2 has been demonstrate to impair cell cycle and cell proliferation. The results of the studies showed that CSE1L could play a critical role in seminoma tumorigenesis (110). In another study, leptin (Ob) and leptin receptor (ObR) expression was determined for the first time in human testicular seminoma and testicular tumors showed a significant increase in expression levels compared to non-neoplastic testicular tissues. *In vitro* results reported that leptin release and Ob expression in TCam-2 cells that are comparable to seminomas. Moreover, it was stated that the administration of the ObR antagonist peptide LDFI significantly decreased motility and leptin-induced growth in TCam-2 cells (111).

2.3. Hippo Signaling Pathway

The Hippo pathway is evolutionarily conserved in humans and mice and was first demonstrated in Drosophila as a tumor suppressor (112). The core of the Hippo signaling pathway consists of transcription coactivators, kinase cascade and DNA binding complexes. Previously, the Hippo signaling pathway was expanded as a complex 30-component signaling interaction (113). This signaling pathway is organised by a wide variety of signals, consists of internal cell mechanisms such as cell polarity and cell-cell contact, cellular energy metabolism, mechanical responses and hormonal signals acting through the G-protein (114). Moreover, Hippo signaling pathway play a crucial role in limiting cell proliferation, cell migration, differentiation and tissue growth processes in developing organs. In addition, dysregulation in the Hippo signaling pathway cause neoplasia and abnormal cell develop which leads, tumor formation (Figure 8) (115).

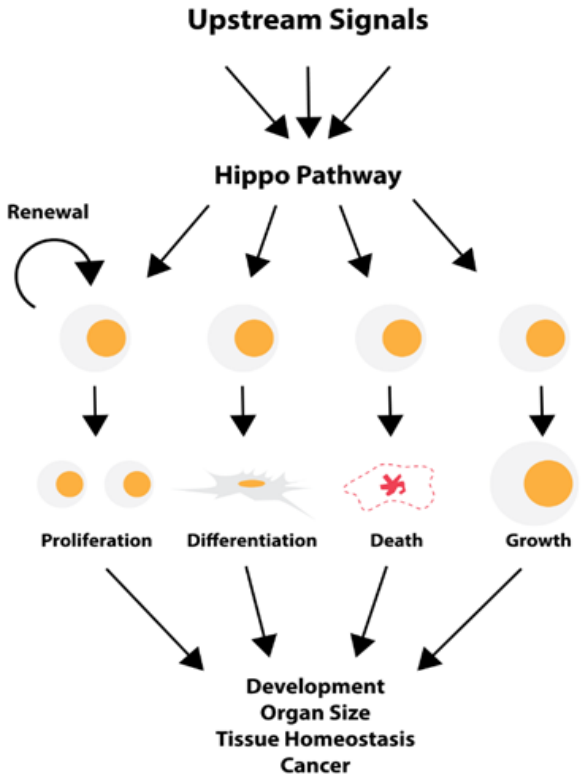

Figure 8. Roles of Hippo signaling pathway. Hippo signaling pathway regulates cell proliferation, differentiation, growth and death (116).

2.3.1. Hippo Signaling Pathway in Mammals

In mammals, the major element of the Hippo signaling pathway is a kinase cascade. This kinase cascade includes LATS1/2 (Homolog of *Drosophila* Wts) that is

phosphorylated and activated by MST1/2 (homolog of *Drosophila* Hpo). Two transcriptional coactivators YAP and transcriptional coactivator with PDZ-binding motif TAZ (two homologs of *Drosophila* Yki) are restricted. When activated, YAP and TAZ interact with each other and create a complex with TEAD (TEA domain family member) transcription factor and stimulates the expression of many genes involved in cell proliferation, migration and survival (115). TAO kinases (TAOK1/2/3) can can also activate the Hippo pathway by phosphorylating the the activation loop of MST1/2 (117, 118). Moreover, MST1/2 can be activated by the autophosphorylation of activation loop by dimerization (119, 120. Because of this, MST1/2 can be activated by dimerization without needing any upstream kinases. When MST1/2 is activated, two scaffold proteins, SAV1, a homolog of Drosophila Sav and MOB1A/B, homolog of Drosophila Mats, are phosphorylated {Callus, 2006 #45). In the phosphorylation and recruitment of LATS1/2, these proteins assist MST1/2. T1079 is hydrophobic motif for T1041 and LATS1 is hydrophobic motif for LATS2 (Figure 9) (121, 122). NF2/Merlin is another crucial element in this process. By interacting with LATS1/2, LATS1/2 phosphorylation of by the MST1/2-SAV1 complex is facilitated (122). LATS1/2 is also activated by autophosphorylation. Then, phoysphorylation of YAP and TAZ leads to inactivation of them (Figure 10) (123).

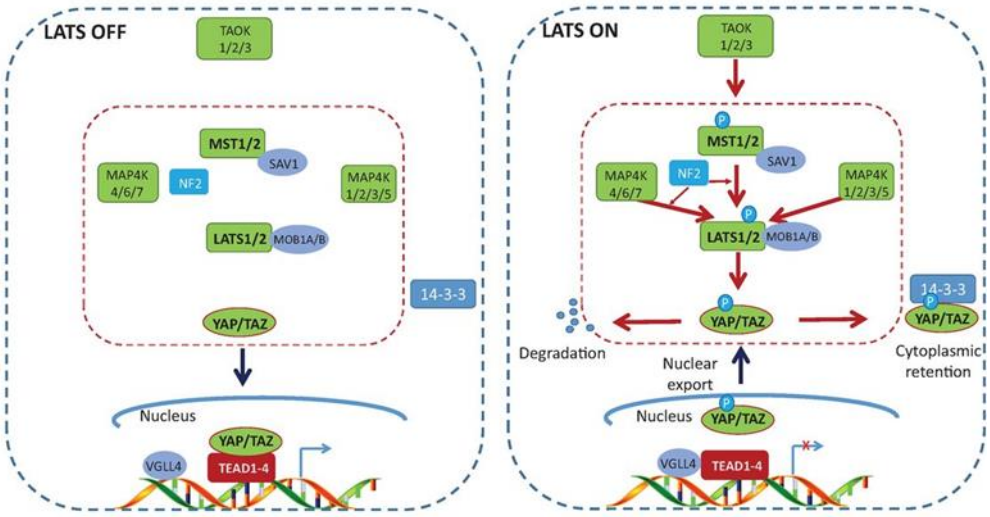

Figure 9. Hippo signaling pathway components (115).

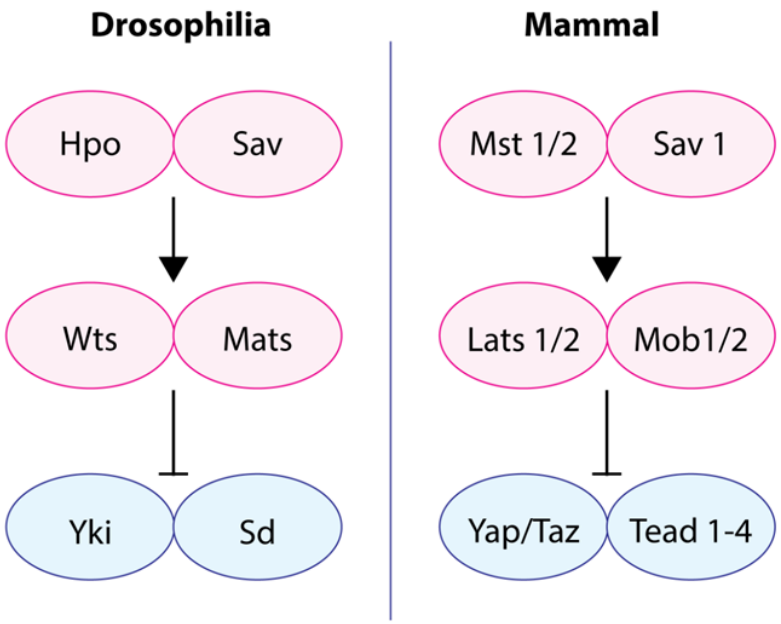

Figure 10. Components of Hippo Signaling Pathway. Comparison of Hippo signaling pathway core components between *Drosophila* and mammals (124).

The Hippo signaling pathway is organised by cell or tissue properties such as apico-basal polarity, mechanotransduction, cell-cell contact, and contact inhibition. Also, the Hippo signaling pathway and its components regulate very important processes such as cell viability, cell proliferation, cell competition, preservation of stem cell characteristics, regeneration and metastasis (Figure 11) (112). This pathway is conserved in mammals and has an important role in limiting cancer development. Regulation of the Hippo signaling pathway therefore presents a potential therapeutic case for treating cancer, but the targeted pathway needs to be explored in more detail (125).

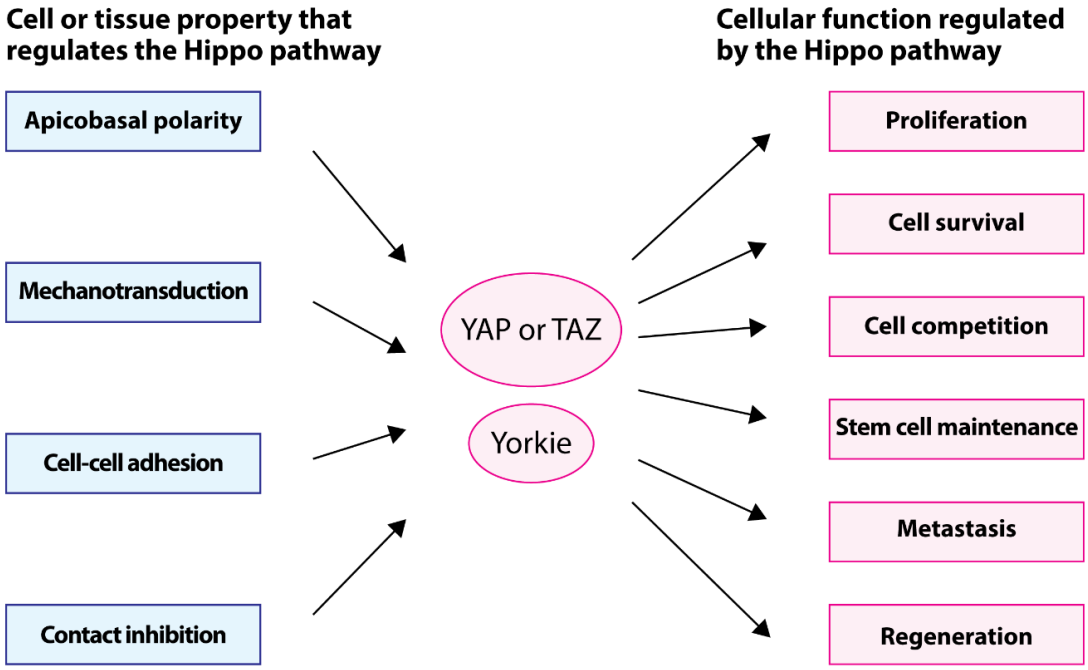

Figure 11. Hippo signaling pathway activity responds to and regulates many cellular features associated with tumorigenesis. In *Drosophila melanogaster*, the orthologs of Yorkie Yes-associated protein (YAP) and transcriptional co-activator with PDZ-binding motif (TAZ) are channels for Hippo pathway regulation and output (126).

2.3.2. Hippo Signaling Pathway in Reproductive System

Few studies have reported different functions of the Hippo signaling pathway in the male reproductive system. It was found that deletion of YAP and LATS2 were lethal at embryonic 9.5 and 12.5 days in mice (127, 128), and mice with Taz deletion were unable to complete their postnatal development (129). In another study, it was suggested that in male mice with LATS1 deletion, fertility rates were reduced that was accompanied with reduced luteinizing hormone (LH) secretion (130). Moreover, YAP and TAZ activity in testicular tissue in mice organise the expression of markers involved in sex differentiation (131). Also, Hippo signaling pathway proteins were reported to be expressed in Sertoli cells of Atlantic salmon (132). In another study, YAP was determined to be a regulator of cyclic AMP signaling in pubertal and adult rat Sertoli cells (133). In a study, the knockout of Kindlin-2, an important integrin-binding protein, in Sertoli cells caused YAP to be phosphorylated by passing into the cytoplasm, resulting in decreased Sertoli cell proliferation and increased apoptosis. Kindlin-2 inhibits YAP phosphorylation by LATS1 by isolating the interaction between LATS1 and YAP (134).

Previous studies have not evaluated the function of the Hippo signaling pathway in mammalian testicular germ cells, but two relevant studies have offered a critical role for the Hippo signaling pathway in germ cell development. First study offered that miRNA-372 and miRNA-373 might play a role in testicular tumorigenesis by inhibiting LATS2 (133). Second one reported high levels of YAP expression in spermatogonia (131), indicating the role of the Hippo signaling pathway and YAP in the early stages of spermatogenesis (135). The role of the Hippo signaling pathway in mammalian testicular germ cells has not been evaluated yet. Although there are some studies on the interaction between Hippo signaling pathway and male reproductive system in some animals such as mice, rat or salmon, the role of Hippo signaling pathway on male reproductive system in humans have not been studied yet except human prostate cancer (136). There is no study in the literature regarding the evaluation of the proteins of the Hippo signaling pathway in the human testis.

2.3.3. Hippo Signaling in Human Cancer

The Hippo signaling pathway regulates several cellular features associated with tumorigenesis and is regulated by different signaling pathways. In different cancer types it has been shown that the Hippo signaling pathway activity is frequently deregulated (137). Because Hippo signaling pathway is an evolutionarily conserved pathway in regulation of tissue develop, it is not surprising that Hippo signaling pathway might be interacted with the cancer. Uncontrolled cell proliferation is known as a key feature of neoplasia. It has been shown that mutations in Hippo pathway in flies and mice cause tumor formation (138). Mutations in Hippo signaling pathway proteins that cause hyperactivation of YKI in flies or YAP-TAZ in mammalians reason ectopic cell proliferation (139). YAP hyperactivation or overexpression causes overproliferation in many tissues, including the skin, liver, heart and gastrointestinal tract (140-142). The immobility, irreversible cell cycle exit (senescence) is a tumor suppressor program, and oncogene-induced senescence in cancer cells (143).

Although apoptosis by the Hippo pathway has not yet been demonstrated in mammals, suppression of the Hippo signaling pathway has been reported to lead to tissue overgrowth in D. melanogaster (139). This situation is known as central to carcinogenesis, so it can be said that dysregulation of the Hippo pathway could provide a strong competitive advantage to the cancer cell and live in tumor tissues. (139). In

addition, it was stated that YAP overexpression preserves cell viability both in vivo and in vitro. YAP overexpression inhibits CD95 (also known as FAS) and necrosis-induced apoptosis in mouse tumors (144).

There are studies showing the relationship between hippo signaling pathway and stem cell. For example, expression profiling studies have demonstrated high expression of both YAP and TEAD transcription factors in various stem cell types (145) and YAP are usually localized in the stem cell compartment of different tissues (146). Both YAP and TAZ stimulate the pluripotency character of embryonic stem (ES) cells (147, 148) and TAZ organizes mesenchymal stem cell differentiation (149). In addition, overexpression of YAP in the gastrointestinal tract in rodents stimulates the expansion of progenitor cells (140). It has been reported that YAP and TAZ activity are increased in basal breast cancers with more stem cell-like characteristics (150). Thus, TAZ and YAP hyperactivity may increase the tumorigenic potential by enhancing stem cell-like properties. Since tumor cells are known to share common features with progenitor or stem cells, the role play by the Hippo signaling pathway in maintaining the stem cell phenotype actually reveals the relationship of this pathway with cancer (151).

Hippo signaling pathway is also known as the regulator of the cellular architecture. There are some studies shows that the derangement of tissue architecture is associated with the solid human tumors and some cancer types. That’s why it is thought that Hippo signaling pathway might be the underlying factor in this situation (116).

Contact inhibition is another key property which is found in transformed cancer cells. It is known that the loos of the upstream Hippo signaling pathway protein NF2, or overexpression of YAP might lead cells to overcome contact inhibition and provoke tumor formation (152).

Besides, mechanical properties of tumors are known to be linked with their growth and progression and by this way with cancer formation. Therefore, it is thought that signaling pathways which are sensitive to the mechanical properties, might modulate the microenvironment of tumor cells and modulate cancer formation. Hippo signaling pathway is very important for responding mechanical factors. It has been suggested that Hippo signaling pathway is the underlying factor of hyperactivation of YAP and TAZ

that has been determined in human tumors as a consequence of response to the mechanical cues (153).

The role of Hippo signaling pathway dysregulation in human cancer metastasis has been also reported in both prostate and breast cancer. It has been shown that YAP and TAZ activity was increased in high-grade metastatic breast cancer and the expression of YAP and TAZ inhibitors LATS1 and LATS2 was lower in metastatic prostate cancer (154).

It is known that regeneration might stimulate carcinogenesis especially in regenerative organs. Therefore, the relationship between Hippo signaling pathway and regeneration was also be studied. These studies reported that YAP and TAZ hyperactivation would trigger cancer formation in chronically regenerated tissues. It sould be noted that Hippo signaling pathway has important role in regenerative growth of mammalian epithelial tissues (155). Tissue damage leads to the suppression of the Hippo signaling pathway. Therefore, YAP and TAZ induce the self-renewal of the progenitor cells and stimulate tissue repair. In case of a damage in cultured cells, YAP is activated. Nuclear YAP supports wound healing by directing cell migration and proliferation *in vitro* (156). This regenerative feature of Hippo signaling pathway is thought to lead formation of cancer.

Studies also reported that few germline or somatic mutations were found in Hippo signaling pathway genes which are widespread in human cancers, compared with those in other oncogenic signaling pathways (157).

There are many studies reporting the dysregulation of the Hippo signaling pathway in different human carcinomas such as colorectal, lung, liver, ovarian and prostate cancers, but no studies on testicular cancer types.

The role of Hippo signaling pathway in cancer and its formation is very crucial as indicated above. The studies on the underlying mechanism of Hippo signaling pathway were very necessary and important to suggest new therapies for the treatment of cancer. For instance, YAP1, an important component of the Hippo signaling pathway, is activated in various human cancers and acts as an oncogene (158, 159). YAP1 regulates not only the proliferation of cancer cells, also plays a critical role in cancer treatments like targeted therapies, radiotherapy, chemotherapy, immunotherapies (160, 161). In a related study,

the administration of metformin, an anticancer agent, in TCam-2, a seminoma cell line, and NTERA-2, an embryonal carcinoma cell line, reduced cell proliferation and induced apoptosis, depending on dose and time, by regulating YAP1 phosphorylation (162). Therefore, it is thought that some inhibiting factors for Hippo signaling pathway components might be useful for cancer treatment.

2.3.4. The Role of Verteporfin as Hippo Signaling Pathway Inhibitor

Verteporfin (VP), a benzoporphyrin derivative monoacid ring A, is a photosensitising drug for photodynamic therapy (PDT) activated by low-intensity, nonheat-generating light of 689nm wavelength. Activation generates cytotoxic oxygen free radicals. The specificity and uptake of verteporfin for target cells with a high expression of low density lipoprotein (LDL) receptors, such as tumour and neovascular endothelial cells, is enhanced by the use of a liposomal formulation and its rapid uptake by plasma LDL. Verteporfin therapy (at light doses < 150 J/cm2) selectively damages neovascular endothelial cells leading to thrombus formation and specific occlusion of choroidal neovascular vessels in subfoveal lesions in patients with age-related macular degeneration (AMD). Verteporfin (VP) has been used clinically for many years for the treatment of age-related macular degeneration (AMD) with photodynamic therapy (PDT). Verteporfin used for photoactivator therapy is diffused intravenously as a laser over the entire neovascular lesion. Penetrating into the neovascular lesion, the drug is activated. Photoactivation selectively eliminates the lesion by generating reactive oxygen species such as hydroxide radicals and superoxide without damaging the viable retinal tissue overlying neovascularization. Repeated applications of verteporfin therapy 6 mg/m2 improved or maintained visual acuity in the majority of patients with some classic subfoveal choroidal neovascularisation (CNV) secondary to AMD at 1 year's follow-up in 2 large multicentre, placebocontrolled, double-blind trials. Furthermore, in a subgroup of these patients with predominantly classic CNV secondary to AMD, there was a significantly more marked visual acuity (VA) benefit with 67.3% of verteporfin-treated eyes experiencing less than a 15-letter loss of VA versus 39.3% with placebo treatment. Multiple applications of verteporfin therapy were well tolerated in patients with subfoveal CNV secondary to AMD. The most common adverse events were visual disturbances, injection site reactions, photosensitivity reactions and infusion-related back pain. Also, verteporfin is known as the one of Hippo signaling pathway inhibitors (163). However,

recent studies have reported that VP has also a significant anti-tumor effect. YAP is a central effector of the Hippo signaling pathway, which is aberrantly expressed in various types of cancer and regulates tumorigenesis and organ size, and is also a pro-tumorigenic factor as mentioned. Although VP is well-known as photosensitizer and its photosensitizing properties (PS) effectively function in anti-tumor PDT (Figure 12) (164), it has been reported that VP also inhibits YAP expression in independent of photoactivation and suppress autophagy.

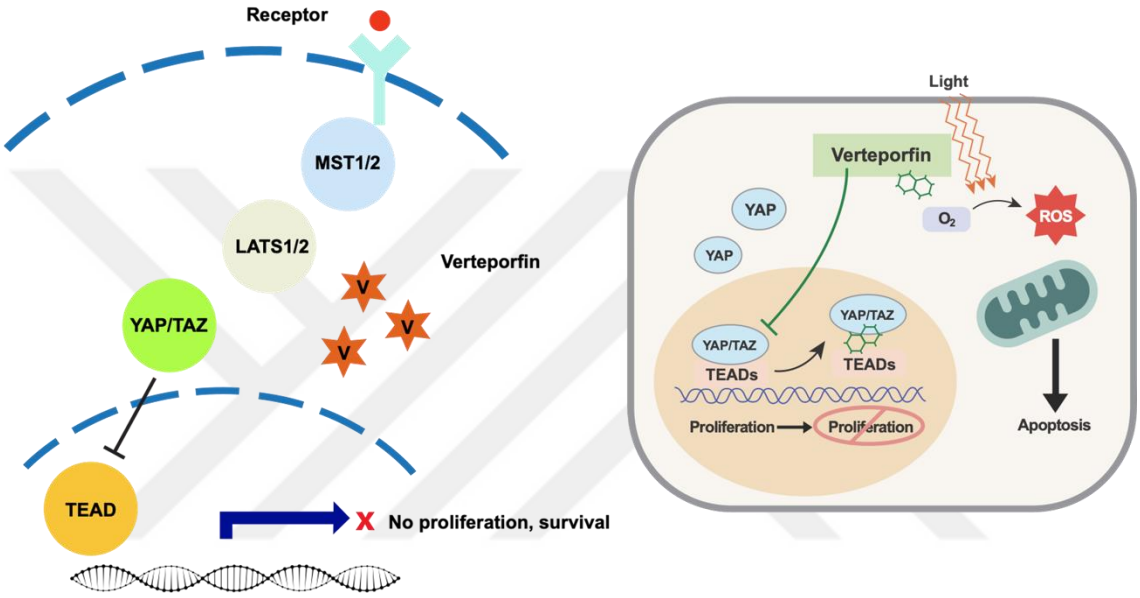

Figure 12. Hippo Signaling Pathway Inhibitor Verteporfin. Dual mechanism by which decrease of cell proliferation and survival (left) through inhibition of YAP/TAZ-TEAD complex and induction of cellular apoptosis (right) by light activation causing oxidative stress (165).

YAP is overactivated in different types of malignancies, and tumor metastasis and progression represent a poor prognosis. Thus, recent studies suggested YAP as a target in anti-tumor treatment (166). Besides, The YAP-TEAD complex is a central effector and thus this complex is also a potential target for cancer therapy. Similarly, VP inhibits cell proliferation in pancreatic ductal carcinoma (167), non-small cell lung cancer (168), myxoid liposarcoma (169), and melanoma cells (167, 170) and xenografts in mice. *Helicobacter pylori* infection of gastric epithelial cells stimulates nuclear translocation of YAP, promoting nuclear translocation of YAP. VP was reported to inhibit *H. pyroli*-induced invasion, proliferation, and metastasis of gastric cancer cells by inhibiting the YAP1/TEAD4-Connective Tissue Growth Factor (CTGF) axis of the pathway (171, 172).

Pharmacological inhibition of YAP/TAZ in endothelial cells by verteporfin reduced the growth of melanomas (173). Similarly, it was demonstrated that verteporfin administration in dose- and time-dependent forms suppressed tumor formation by inhibiting human pancreatic ductal adenocarcinoma cell proliferation in G1 phase and inducing apoptosis (167). In another study, dose-dependent administration of verteporfin inhibited bladder cancer cell growth (174).

Besides direct inhibiting effect of VP on YAP and YAP1/TEAD4 complex, it has been suggested that VP might regulate Hippo-YAP Cross-Signaling. It has been shown that VP inhibits YAP and TAZ in endometrial cancer cells and downregulates GAB2-dependent PI3K/AKT and p-mTOR and target genes p-4EBP1 and p-S6 in liver and endometrial cancer cells and reduces growth. xenografts. In another study, it was reported that VP increased the effect of metformin on YAP in lung cancer cells (175). VP suppresses NRAS, KRAS and HRAS transcription by inhibiting YAP-TEAD, which reduces cell proliferation and significantly delays xenograft growth in mouse thyroid cancer cells (176). VP also inhibits proliferation of osteosarcoma (U-2OS) and mesothelioma (211H, H2052) cell lines by affecting YAP and its target genes (177, 178). Inhibits non-photoactivated VP, YAP, FGF1 and FGF2 and reduces proliferation of LATS knockout ovarian cancer cells, induces apoptosis (179).

In the thesis study, we hypothesize that Hippo signaling pathway proteins may be among important markers for testicular cancer. Based on this, we aim to show the expression of Hippo signaling pathway proteins in human testis, seminoma and non-seminoma testicular tissues and to determine the relationship between this basic mechanism and testicular cancer and Hippo signaling pathway proteins. Also, we hypothesized that verteporfin therapy in vitro as well as in vivo experiments may be beneficial in the treatment of testicular cancer. In this thesis, our aim was to investigate the expression pattern of Hippo signaling pathway proteins in the TCam-2 cell line after verteporfin treatment. We aim to contribute to the development of potential treatment approaches for seminoma patients in the process of restoring testicular functions and preserving fertility.

3. MATERIAL and METHODS

3.1. Human Sample Groups and Design

Germ cell tumors according to the current 2016 WHO classification; it is classified as seminoma and non-seminoma tumors, including embryonal carcinoma, yolk sac tumor, or post-pubertal teratoma, trophoblastic tumor (180).

Seminomas consist of germ cells that are transformed into distinct cells during their development into mature gonocytes or their differentiation into a particular cell lineage. Non-seminoma tumors have the potential to differentiate into a variety of somatic, extraembryonic and embryonic tissues (Figure 1), their differentiation potential can often be limited and sometimes they arrest at certain stages (181).

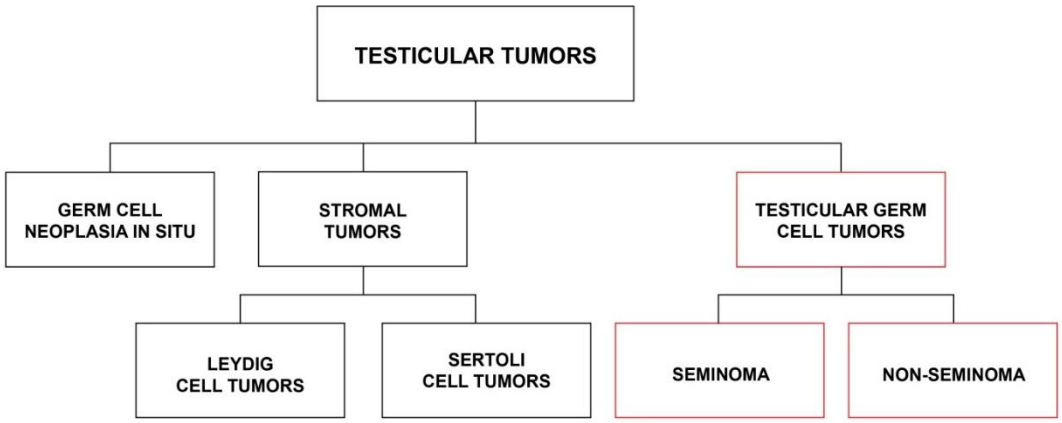

Figure 13. Testicular tumor classification. Testicular cancer types are summarized in the figure. We can divide them into two groups: stromal tumors (Sertoli cell and Leydig cell tumors) and germ cell tumors with their common source, germ cell neoplasia in situ (GCNIS).

In our study, 11 normal, 24 seminoma and 11 non-seminoma testicular blocks taken in the last 4 years. Inclusion criteria of the patients in our study;

- For normal patients: Absence of tumor and in situ germ cell neoplasia, continuation of spermatogenesis.

- For seminoma patients: Histological subtyping, diagnosis of pure seminoma, and availability of paraffin blocks.

- For non-seminoma patients: Histological subtyping, diagnosis of pure embryonal carcinoma or mixed germ cell tumor containing at least 40% embryonal carcinoma component, and availability of paraffin blocks.

The criteria for not including the patients in our study are; Tru-cut or incisional biopsy, History of neoadjuvant and/or palliative chemotherapy, Infarction and Orchitis.

3.1.1. Morphological Evaluation

In our study, control (n=11), seminoma (n=24) and non-seminoma (n=11) testicular blocks taken in the last four years were used. For the histological analyses of all experimental groups, paraffin sections of 5 μm thickness were taken from the paraffin-embedded tissues to the grounded straight microscope slide using a microtome, and Hematoxylin & Eosin (H&E) staining was applied to these sections.

3.1.1.1. Hematoxylin and Eosin Staining

Sections were stained with hematoxylin and eosin for morphological analysis. All the sections were incubated for 40 min at 60ºC to remove paraffin and for two times for 20 min left in xylene for complete removal of paraffin. Then sections were rehydrated by decreasing alcohol series for 10 min for each (100%, 96%, 90%, 80% and 70%). After rehydration, sections were washed with distilled water and stained with hematoxylin (Gill's hematoxylin No.3, Bio-Optica, 05-06015/L) for 2 min. Then, the sections were washed in running tap water. Eosin (Eosin Y Alcoholic Solution, Bio-Optica, 05-10003/L) staining was performed for 1 min. Sections were washed with distilled water for 2 min. Sections were dehydrated with increasing alcohol series and cleared with xylene for 40 min. Finally, the sections were covered with coverslip using xylene-based mounting medium (Bio Mount HM, Bio-Optica, 05-BMHM500) examination was performed by using light microscope (Leica CTR 6000).

3.1.2. Immunohistochemistry Staining

Immunohistochemistry staining of paraffin sections of 5 μm thickness taken on a poly-lysine-coated slide (Poly-Lysine, Thermo Fisher Scientific, 165014) to determine the localization of MST1/2, LATS1/2, YAP1, TEAD4, p-MST1/2, p-LATS1/2, p-YAP1 and ZO-1 proteins.

All slides were deparaffinized in the incubator (60ºC) for 1 hour. To be able to remove paraffin from the sections, they were cleared with xylene for 2 times for 20

minutes. Sections were rehydrated by decreasing alcohol series (100%, 90%, 80% and 70%) in order to remove xylene. Sections were washed by distilled water for 5 min then by PBS (Phosphate Buffer Saline, pH:7.2-7.4) for 5 min. For antigen retrieval, sections were heated in microwave (around 600 Watts) in Citrate buffer (10mM, pH 6.0) prepared by dissolving sodium citrate tribasic dihydrate (Sodium Citrate Tribasic Dihydrate, Sigma Aldrich, 6132-04-3) in distilled water, followed by about 5 min low watt (300 Watt). After the sections were heated in microwave, they were left in room temperature to cool down and this process was repeated two times more. Then sections were cool down at the room temperature for 20 min. Then a circle was drawn around the tissues on the slides with a hydrophobic barrier pen and slides were washed with PBS for 3 times 5 min. For blocking endogenous peroxidase enzymes, sections were incubated with 3% hydrogen peroxide (prepared in methanol) for 10 min. Sections were washed with distilled water for 2 times for 5 min, then with PBS for 2 times for 5 min. 2.5% Normal Horse Serum (Vector Laboratories, 30022) was used for blocking and the sections were incubated with Normal Horse Serum for 1h at room temperature. After removal of blocking solution, sections were not washed, and they were incubated with the primary antibodies MST1/2 Polyclonal Antibody in 1:100 (MST1/2 Polyclonal Antibody, İnvitrogen, PA5-36100), LATS1/2 Polyclonal Antibody in 1:100 (LATS1/2 Polyclonal Antibody, Bioss, bs4081R), YAP1 Polyclonal Antibody in 1:100 (YAP1 Polyclonal Antibody, Cell Signaling, 14074), TEAD4 Polyclonal Antibody in 1:100 (TEAD4 Polyclonal Antibody, İnvitrogen, PA5-21977), p-MST1/2 Polyclonal Antibody in 1:100 (p-MST1/2 Polyclonal Antibody, Bioss, bs3294R), p-LATS1/2 Polyclonal Antibody in 1:100 (p-LATS1/2 Polyclonal Antibody, İnvitrogen, PA5-37834), p-YAP1 Polyclonal Antibody in 1:100 (p-YAP1 Polyclonal Antibody, Abcam, ab62751), ZO-1Polyclonal antibody (ZO-1 Polyclonal antibody, Invitrogen, 61-7300) which were prepared in PBS solution at 4ºC for overnight. After the incubation with primary antibodies, sections were washed with PBS for 3 times for 5 min and then incubated with biotinylated pan-specific secondary antibody (Vector Laboratories, 30144) for 1.5h at room temperature. Sections were washed with PBS for 3 times for 5 min and then incubated with streptavidin/peroxidase complex (Vector Laboratories, 30143) for 1,5h at room incubated at room temperature. After slides were washed with PPS for 3 times for 5 min, slides were incubated with the mix of DAB and DAB substrate 1:20 (UltraVision Detection System Large Volume DAB Substrate System (RTU), Thermo Fisher Scientific HD16378). Sections were washed

with PBS for 3 times for 5 minutes. Counterstaining was performed with hematoxylin (Gill's hematoxylin No.3, Bio-Optica, 05-06015/L) and counterstaining slides were washed with tap water. Sections were dehydrated by increasing alcohol series (70%, 80%, 90% and 100%). Then they were cleared with xylene for 2 times for 20 min. The sections were covered with coverslip using xylene-based mounting medium (Bio Mount HM, Bio-Optica, 05-BMHM500) and examination was performed by using light microscope (Leica CTR 6000). Three different patient tissues were used in the analyzes done according to the staining densities. In these tissues, 100 cell type-specific cell counts were made in different areas. Cell count according to staining intensities was performed by two individuals independently of each other. Analyzes were used in GraphPad Prism Version 8.0 (GraphPad Software, USA).

3.2. TCam-2 Cell Culture Studies

3.2.1. Experimental Overview

The human TCam-2 cell line was produced primarily from a testicular tumor sample of pure classical seminoma. The TCam-2 cell line was retrieved from Prof. Dr. Hubert Schorle (Department of Developmental Pathology and Institute of Molecular Diagnostic Pathology, Faculty of Medicine, Germany, Bonn). TCam-2 cells were cultured in RPMI medium; supplemented with 10% fetal bovine serum (FBS) with 100 IU penicillin and 0.1 mg streptomycin. Trypsin-EDTA solution (with /phenol red, 0.25%) was used for detaching cells. TCam-2 cells used in this study were between 8th and 10th passages. Cells were incubated at 37°C and 5% CO_2. Verteporfin, an inhibitor of the YAP-TEAD complexes, was administered to cultured TCam-2 cells. The adhesion rate and morphology of the cells were checked every 24 hours. Also, medium of cells was changed every two days until density of cells reached 70%. Then verteporfin treatment were applied when the rate of cell density and healthy cells reached 70%. For flow cytometric, wound-healing strength, cell counting, qRT-PCR analysis and western blotting, cells were seeded as 500.000 cells per well into 6-well test plates as triplicates. For confocal microscopy, cells were seeded on Millicell® EZ Slides (Merck Millipore, USA) as 50.000 cell per well. Verteporfin treatment was applied in five different doses which were 1 μM, 5 μM, 10 μM, 20 μM and 40 μM and cells were cultured for 24, 48 and 72 hours (182). There were no verteporfin treatment for control group and they were cultured same time period with treatment groups. After an additional 24, 48 and 72 hours,

cells were detached with tyrpsin-EDTA. For flow cytometric analyses, cells were washed twice with Dulbecco's phosphate buffered saline solution (DPBS). Dose-dependent viability, early-late apoptosis and necrosis ratios 24, 48 and 72 hours were analyzed by Annexin V/propidium iodide (PI) staining. For western blotting, protein extraction was performed. Dose-dependent protein expression levels of MST1/2, LATS1/2, YAP1, TEAD4, p-MST1/2, p-LATS1/2, p-YAP1 for 24, 48 and 72 h were analyzed by western blot assay. For qRT-PCR, RNA isolation was performed and dose-dependent mRNA expression levels of *MST1*, *MST2*, *LATS1*, *LATS2*, *YAP1*, *TEAD4* for 24, 48 and 72 hours were analyzed. MST1/2, LATS1/2, YAP1, TEAD4, p-MST1/2, p-LATS1/2, p-YAP1 protein localization was performed in TCam-2 cells under confocal microscopy with immunofluorescence staining (IF). Dose-dependent migration ratios 24, 48 and 72 h were analyzed by wound-healing assay. Dose-dependent cell counting ratios 24, 48 and 72 h were evaluated by an automated cell counter. General outline of TCam-2 cell culture and post procedures were shown below in Figure 14.

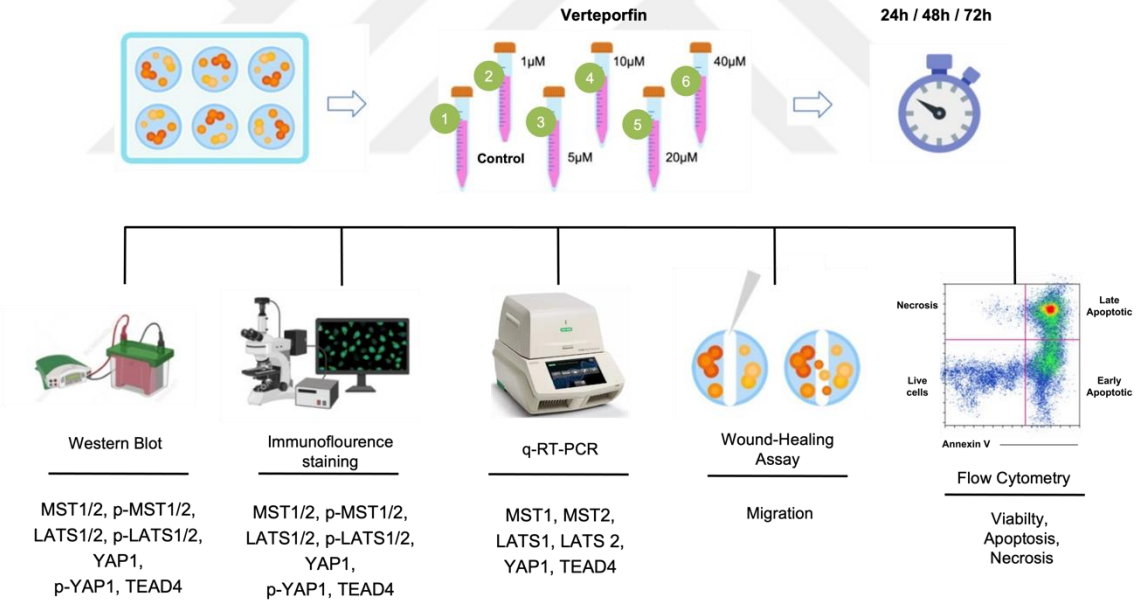

Figure 14. General outline of TCam-2 human seminoma cell culture and post procedures.

3.2.2. Cell Counting Assay

15 µL of sample mixture and 15uL of trypan blue solution (Trypan blue stain 0.4%, Invitrogen by Thermo Fischer Scientific, 1948601) were mixed. Then, 15 µL from this mixture was transferred onto cell counting chamber slide (Countess™ Cell Counting Chamber Slides, Invitrogen by Thermo Fischer Scientific, C10228) and live cells were counted by an

automated cell counter (CountessTM II FL Automated Cell Counter, Invitrogen by Thermo Fischer Scientific, AMQAF1000). Then, live, dead and total cell number was calculated by applying necessary calculations.

3.2.3. Western Blotting

All growth medium in wells was removed and 1ml of 1X trypsin was added into each well. Cells were incubated in trypsin for 3 minutes and 1ml of RPMI was added into each well. Each well was stripped by cell scraper and samples were transferred into different falcon tubes. Then, 500 µL of 0.25% trypsin was added into each well and controlled under the light microscope. After 5 minutes, 500 µL of RPMI was added into each well and each well was stripped again by cell scraper. Samples were transferred into same falcon tubes and centrifugation was applied for 10 minutes at 4000 rpm. Then, supernatant was removed and 1 ml of RPMI was added into each falcon tube. Samples were transferred into eppendorf tubes. Centrifugation was applied for 6 minutes at 10,000 rpm. Supernatant was removed and 200 µL of complete RIPA (194 µL RIPA lysis buffer, 2 µL sodium ortho-vanadate, 2 µL protein inhibitor cocktail (PIC), and 2 µL phenylmethylsulphonyl fluoride (PMSF) (RIPA Lysis Buffer System, SantaCruz Biotechnology, sc-24948A) was added into each eppendorf tube. Then samples were stored at -20ºC.

Samples were resuspended and incubated on the ice for 5 minutes. Then, centrifugation was applied at 14,800 rpm for 15 minutes. Supernatants were collected into new sterile eppendorf tubes and stored at -80ºC. Protein concentrations were determined by Pierce bicinchoninic acid (BCA) assay Kit (BCA Protein Assay Kit, Thermo Fisher Scientific, 23225).

After the total protein concentrations was determined, samples were equalized with distilled water, 5 µL LDS sample buffer (NuPAGE LDS Sample Buffer (4X), Invitrogen, NP0007) and 2 µL reducing agent (NuPAGE Sample Reducing Agent (10X), Invitrogen (10X), NP0009). Then, each sample mixture was heated at 95ºC for 5 minutes by using Thermal Cycler.

Tape which was on the gel was removed. Then, casette including gel was washed by distilled water. Gel was put into the tank which was filled with running buffer including 950 mL distilled water and 50 mL running buffer (NuPAGE MES SDS Running Buffer (20X), Novex, NP0002). Firstly, all wells were washed by running

buffer. Then, 8 µL ladder and all samples were loaded into the wells respectively. Then, gel was run at 100-120V and 80W for 2 h.

After gel electrophoresis was completed, cassette including gel removed from the tank. Then, cassette was washed with distilled water. Filter papers were placed into transfer buffer including 3 g Tris (Tris(hydroxymethyl)aminomethane, Thermo Fisher Scientific, 17926), 14.3 gr glycine (Glycine für die Molekularbiologie, BioFroxx, 56-40-6), 200 mL methanol and 800 mL distilled water. Also, membrane was activated by methanol for 20 minutes. Then, sandwich model was prepared from bottom to top as two filter papers, membrane, gel and two filter papers respectively. This model was transferred into the tank including transfer buffer. Wet transfer was conducted at 15V and +4ºC for overnight. After transfer, membrane was removed from the tank and washed with TBS-T before proceeding. Blocking solution was prepared with 10ml TBS-T and 0.5 g milk powder. Membrane was blocked in 5% milk powder solution at room temperature for 1 h.

3.2.3.1. Antibodies and Probing

After blocking solution was removed, membrane was incubated with primary antibodies at +4ºC overnight. Primary antibodies were diluted in 5% blocking solution. Primary antibodies were MST1/2 Polyclonal Antibody in 1:1000 (MST1/2 Rabbit Polyclonal Antibody, İnvitrogen, PA5-103144), LATS1/2 Polyclonal Antibody in 1:1000 (LATS1/2 Rabbit Polyclonal Antibody, Bioss, bs4081R), YAP1 Polyclonal Antibody in 1:1000 (YAP1 Rabbit Polyclonal Antibody, Cell Signaling, #14074), TEAD4 Polyclonal Antibody in 1:1000 (TEAD4 Rabbit Polyclonal Antibody, İnvitrogen, PA5-21977), p-MST1/2 Polyclonal Antibody in 1:1000 (p-MST1/2 Rabbit Polyclonal Antibody, Bioss, bs3294R), p-LATS1/2 Polyclonal Antibody in 1:1000 (p-LATS1/2 Rabbit Polyclonal Antibody, Cell Signaling, #9157), p-YAP1 Polyclonal Antibody in 1:1000 (p-YAP1 Rabbit Polyclonal Antibody, Abcam, ab62751). Also, β-actin (β-actin (H10D10), Mouse Monoclonal Antibody, Cell Signaling, #3700) was prepared in 1:1000 as an internal control. After primary antibody incubation was completed, membrane was washed by TBS-T for 5 minutes for 3 times.

Table 1. List of primary antibodies for western blot analysis.

Antibody	Isotype	Catalog Number	Dilution
MST1/2	Rabbit Polyclonal	Invitrogen, PA5-103144	1:1000
p-MST1/2	Rabbit Polyclonal	Bioss, bs3294R	1:1000
LATS1/2	Rabbit Polyclonal	Bioss, bs4081R	1:1000
p-LATS1/2	Rabbit Polyclonal	Cell Signaling, #9157	1:1000
YAP1	Rabbit Polyclonal	Cell Signaling, #14074	1:1000
p-YAP1	Rabbit Polyclonal	Abcam, ab62751	1:1000
TEAD4	Rabbit Polyclonal	Invitrogen, PA5-21977	1:1000
β-actin	Mouse Monoclonal	Cell Signaling, #3700	1:1000

The membranes were incubated with the appropriate secondary antibodies for 2 hours at room temperature. Anti-rabbit secondary antibody (Anti-rabbit IgG, HRP-linked Antibody, Cell Signaling, #7074S) was prepared in 1:5000 dilution rate. Anti-mouse secondary antibody (ECL Mouse IgG, HRP-linked Antibody, Amersham, #NA931V) in 1:5000 was prepared in 5% milk powder and used for β-actin. After secondary antibody incubation was completed, membrane was washed by TBS-T for 6 times for 5 minutes.

3.2.3.2. Chemiluminescent detection and analysis

Mixture of ECL substrate and ECL (Pierce ECL Western Blotting Substrate, Thermo Fisher Scientific, 32106) in 1:1 was used for one membrane. ECL mixture was added on top of the membrane drop by drop and ChemiDoc^{TM} MP Imaging System (170-8280) was use for gel imaging. ImageLab software was used for further analyses.

3.2.4. Immunofluorescence Staining

Localization of Hippo signaling pathway proteins in TCam-2 cells was visualized by confocal microscopy. Cells seeded on 8-well microscopy slides were treated with respective verteporfin doses of the compounds and incubated 24, 48 and 72 hours. Cells

were fixed by incubating cells witin 4% PFA solution prepared in PBS for 30 minutes, washed with PBS in three times for 5 minutes. Then, the cells were permeabilized with 0.1% Triton-X-100 in PBS for 30 minutes at +4ºC and blocked with 5% bovine serum albumin with 0.05% Triton-X-100 prepared in PBS for 1 hour. Cells were then incubated with the MST1/2 (1:100; MST1/2 Polyclonal Antibody, İnvitrogen, PA5-103144), LATS1/2 Polyclonal Antibody (1:100; LATS1/2 Polyclonal Antibody, Bioss, bs4081R), YAP1 (1:100; YAP1 Polyclonal Antibody, Cell Signaling, 14074), TEAD4 (1:100; TEAD4 Polyclonal Antibody, İnvitrogen, PA5-21977), p-MST1/2 (1:100; p-MST1/2 Polyclonal Antibody, Bioss, bs3294R), p-LATS1/2 (1:100; p-LATS1/2 Polyclonal Antibody, İnvitrogen, PA5-37834), p-YAP1 (1:100; p-YAP1 Polyclonal Antibody, Abcam, ab62751) which were prepared in 1% bovine serum albumin with 0.05% Triton-X-100 in PBS at +4ºC for overnight. Then the cells were washed with PBS for 5 minutes for 3 times and incubated with second secondary antibody (Alexa flour-488 goat anti-rabbit IgG) for 1.5 hours at room temperature. Coverslips were washed with PBS for 5 minutes for 3 times. Then, slides were mounted with DAPI (Fluoroshield with DAPI, Sigma-Aldrich, F6057) for nucleus staining, the observation was performed by using confocal microscopy (Zeiss, LSM780).

3.2.5. Quantitative Real Time Polymerase Chain Reaction (qRT-PCR)

3.2.5.1. RNA Isolation

qRT-PCR method was applied to show the mRNA levels of Hippo signaling pathway proteins. For the qRT-PCR method, 300 µL of lysis buffer was added to the TCam-2 cells to be collected.

Columns were washed with 100 µL of activation buffer for 30 second and centrifuged at 10,000xG. Add 300 µL of isopropanol to the eppendorf containing the sample supernatant and vortex. After the activation buffer settled to the bottom of the colon of eppendorf is emptied (eppendorf under the colon), the samples to which iso-propanol is added was transferred to the colon of eppendorf and 30 second. It was centrifuged at 10,000 g. Eppendorf remaining under the colon was emptied, sample RNAs were remain in the colon at this stage. Colons containing RNA was washed with 700 µL of primary buffer washing solution, 30 second. It was centrifuged at 10,000xG. The eppendorf located under the colon was emptied. 700 µl of secondary buffer washing solution was added on the colon and wait for 30 seconds. It was centrifuged at 10,000 g.

The tube under the colon was emptied. The colon portion was transferred to a new autoclaved tube. On the colon, 40 µl of elution buffer was transferred to the center of the colon and placed on the colon for 3 minutes. was incubated at room temperature for 2 minutes. It was centrifuged at 10,000 g. RNAs were collected in the lower ependorf and the upper colon was be discarded. Sample RNAs was stored at -20°C.

3.2.5.2. cDNA Synthesis

RNA measurement was made optionally from the separated RNAs, a determined/calculated amount of RNA-template, 0.5 µLOligo-DT and water mixture were prepared. 5-10 min at 70°C. were subjected to the heating process (denaturation process). First stage used in preparation and DNA amplification volumes are indicated in Table 2.

Table 2. cDNA synthesis reaction contents.

Content	**Volume (µL)**
SCRIPT RT Buffer	4
dNTP Mix	1
DTT Stock Solution	1
RNase inhibitor	1
SCRIPT Reverse Transcriptase	0.5
RNase-free Water	2.5
Total	**10 µl mix**

10 µL of the mix solution obtained as a result of this process was mixed with 10 µL of sample RNA. It was inserted into the PCR device by entering the appropriate program information (45 minutes at 50°C, 10 minutes at 42°C). After the cDNA synthesis process is completed, the samples were stored at -20°C.

The qRT-PCR reaction was prepared according to the manufacturer's instruction. The reaction volumes are given in Table 3. The reaction cycles are given in Table 4. The primer sequences used in the reactions are given in Table 5.

Table 3. qRT-PCR reaction contents.

Maxima SYBR Green qPCR Master Mix (2x)	**10 µl**
PCR Grade Water	7.8 µl
Forward Primer	0.6 µl
Reverse Primer	0.6 µl
Template DNA	1 µl

Table 4. qRT-PCR reaction protocol.

Step	**Temperature (Duration (sec))**	**Number of Cycles**
Initial Denaturation	95ºC (30)	1
Denaturation	95ºC (15)	**45**
Annealing	53ºC (20)	
Extension	60ºC (20)	

Table 5. Primer sequences used in qRT-PCR.

Transcript	**Primer**	**Sequence (5´-3´)**
MST1	***Forward***	CCTCCCACATTCCGAAAACCA
	Reverse	GCACTCCTGACAAATGGGTG (Xu et al., 2013)(183)
MST2	***Forward***	GCACTCCTGACAAATGGGTG

	Reverse	CCTCCCACATTCCGAAAACCA (Xu et al., 2013)(183)
LATS1	***Forward***	GTTAAGGGGAGAGCCAGGTCCTT
	Reverse	TCAAGGAAGTCCCCAGGACTGT (Najafi et al., 2016)(184)
LATS2	***Forward***	ACTTTTCCTGCCACGACTTATTC
	Reverse	GATGGCTGTTTTAACCCCTCA (Najafi et al., 2016)(184)
YAP1	***Forward***	CGCTCTTCAACGCCGTCA
	Reverse	AGTACTGGCCTGTCGGGAGT (Liu et al., 2013)(185)
TEAD4	***Forward***	GGACACTACTCTTACCGCATCC
	Reverse	TCAAAGACATAGGCAATGCACA (Zhang et al., 2019)(186)
β-ACTIN	***Forward***	ATAGCACAGCCTGGATAGCAACGTAC
	Reverse	CACCTTCTACAATGAGCTGCGTGTG (Liu et al., 2013)(185)

3.2.6. Wound-Healing Scratch Assay

A total of 50.000 cells per well were seeded on six-well plates and let attached overnight. After overnight attachment, a straight line was created by scratching with a 100 μL pipette tip. Then the medium was removed, fresh medium with respective drug concentrations were added and images were obtained for t=0 h. The migration/healing was determined for 48 and 72 hours by obtaining microscopy images of the same area (Axiovert 135; Carl Zeiss Microscopy). Migration/wound healing was determined as previously described by using Image J/Fiji® (NIH, USA) and the percent healing against the control group was determined (187).

3.2.7. Flow Cytometry

Early-late apoptosis, necrosis and viability were evaluated with Annexin V/propidium iodide staining, which is considered as the gold standard for apoptosis detection (188). Annexin V binds to phosphatidylserine (PS) residues which mainly located in the inner leaflet of the cellular membrane. PS residues translocate to the outer leaflet of the cellular membrane upon induction of apoptosis, enabling Annexin V to bind and label early apoptotic cells. Annexin V can also enter cells with compromised membranes and binds PS located at the inner leaflet, labelling cells during the last apoptotic stages. Propidium iodide (PI) which is a cell impermeable DNA intercalating agent that is used for discriminating apoptotic cells from living and necrotic cells (189). In this study, cells were seeded into six-well plates as 50.000 cell per well and incubated for overnight for attachment. Cells were then treated with verteporfin at respective doses for 24, 48 and 72 hours. For Annexin V/PI staining, cells were detached by trypsinization, washed twice with DPBS (Thermo Fisher Scientific, #14190144) and then suspended in Annexin V Binding Buffer (BioVision Inc.) followed by staining with Annexin V-FITC reagent (1μl/1×10^5 cells) (Biovision Inc.) and 1 μL Propidium Iodide (PI) solution (0.25 μg/1×10^5 cells) (Thermo Fisher Scientific, #P3566, at 250 μg/mL in DPBS) by incubating for 10 minutes under dark conditions at room temperature. A total of 2.5 × 10^4 cells per test were read with DxFLEX (Beckman Coulter Inc.) and analyzed by CytExpert software 20. All experiments were performed as triplicates.

3.2.8. Statistical Analysis

GraphPad Prism Version 8.0 (GraphPad Software, USA) was used for statistical analysis. Two-way analysis of variance (ANOVA) followed by Tukey's multiple

comparison test, western blot, qRT-PCR, proliferation, and flow cytometry experiments were compared using two-way ANOVA for the effects of treatment within cell lines compared to respective controls. P values less than 0.05 were considered statistically significant.

4. RESULTS

4.1. Morphological Evaluation of Experimental Groups by Hematoxylin-Eosin (H&E) Staining

Human testis (190), embryonal carcinoma (191) and seminoma (192) tissues were selected morphologically in accordance with the literature. Morphological evaluation with Hematoxylin-Eosin staining was performed to seminoma, embryonal carcinoma, and control group testicular tissues.

In sections taken from human testicular tissue, seminiferous tubules, Leydig cells and seminiferous tubule basement membrane were observed in normal structure. Interstitial connective tissue was observed in regular morphology (Figure 15A, A', A'', asterix). It was observed that the seminiferous tubules were lined with stratified cuboidal epithelium, and the tubule wall was composed of spermatogenic cell lines and Sertoli cells. Sertoli cells were distinguished by their characteristic nuclei shape (pyramid) that stained pale. Many spermatogenic series cells (Figure 15A, A', A'', round dot) with normal morphology were observed, located between the lateral folds of Sertoli cells resting on the basal lamina. Spermatogonia with oval-shaped nuclei were observed close to the basal lamina. Primary spermatocytes were distinguished by their larger voluminous nuclei due to having 4n DNA just above the spermatogonia. Depending on the developmental stages, secondary spermatocytes and spermatids were seen in higher ranks. Early spermatids were distinguished by their cap-shaped acrosome structure sitting on the nucleus, and late spermatids that would turn into spermatozoa with their tails extending into the lumen and dark long heads. Sperm were found in many seminiferous tubule lumens (Figure 15A, A', A'').

Seminiferous tubule degeneration, reduction in tubule diameters and tubular atrophy were observed in sections taken from embryonal carcinoma (non-seminoma) tissues. Carcinoma cells in the tubules have prominent nuclei, large vesicular nuclei and extensive cytoplasm (Figure 15B, B', B''). The cell borders were indistinct and showed agglomerations. Numerous carcinoma cells were found in the intertubular space (Figure 14B, B', B'', asterix). At the same time, glandular and tubular structures are observed in carcinoma areas (Figure 15B, B', B'').

In sections taken from seminoma testicular tissues, seminiferous tubule degeneration and tubular atrophy, which is remarkable with the decrease in tubule

diameters, were clearly observed. Large, neoplastic seminoma cells were seen (Figure 15C, C', C''). An increase in the number of blood vessels in the interstitial area was observed. Although the distance between the seminiferous tubules was not very wide, infiltration of lenfocyte cells towards the interstitial area was observed (Figure 15C, C', C'').

Different from normal testicular tissues, more atypical cells were found in seminoma testis tissues. The distances of the cells are regular, and they are arranged in clusters. Seminoma cells were observed to have prominent nucleoli, light colored, large cytoplasm, and large nuclei. Nuclei richer in chromatin are seen and there is more than one nucleoli (Figure 15C, C', C''). Many lymphocyte cells are seen among the seminoma cells, which are distributed in clusters. Nodule structures formed by lymphocyte cells are seen (Figure 15C, C', C'').

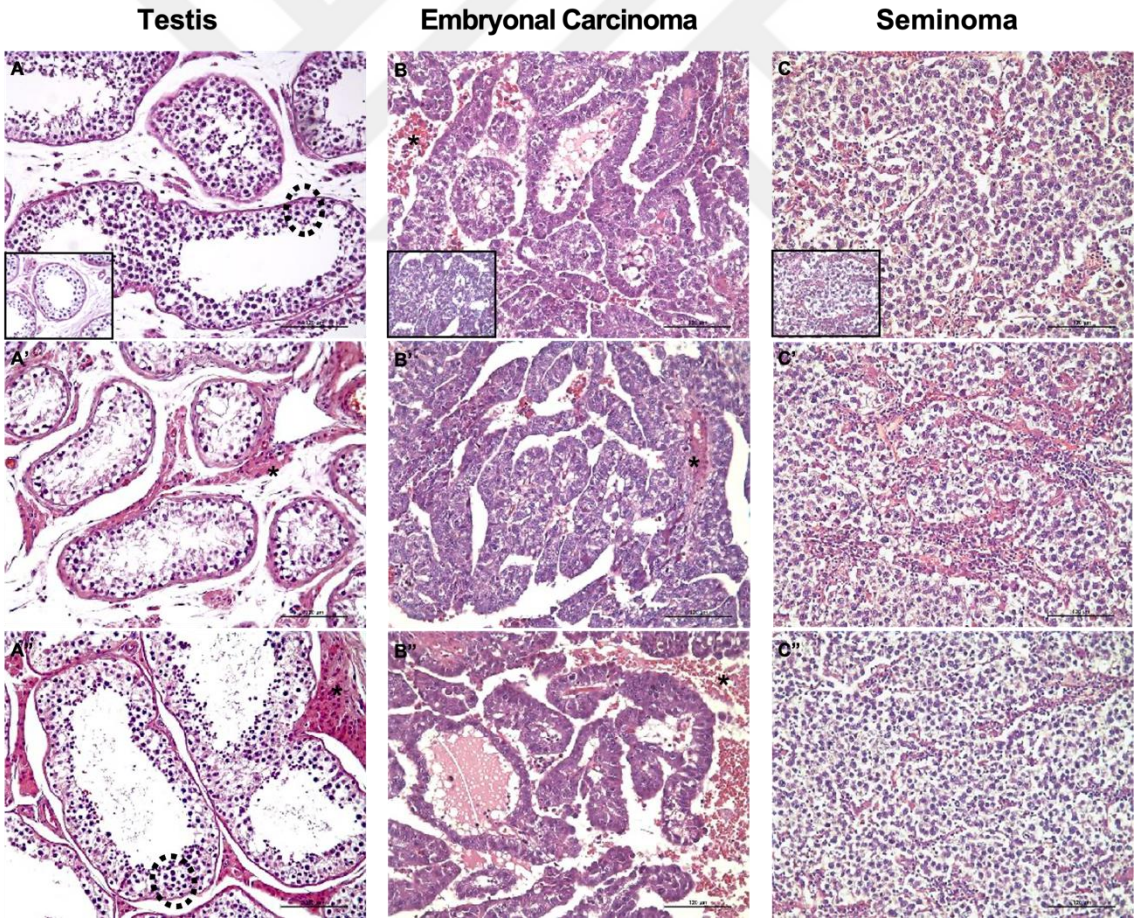

Figure 15. Morphological evaluation of experimental groups by Hematoxylin-Eosin (H&E) staining. A, A', A''. In control human testicular tissue; seminiferous tubules, Leydig cells (asterix) and seminiferous tubule basement membrane were observed in

normal structure. Sperm were found in many seminiferous tubule lumens (round dot). B, B', B''. carcinoma cells, the cell borders were indistinct and showed agglomerations. Cells have prominent nuclei, large vesicular nuclei and extensive cytoplasm. Blood cells are seen among the carcinoma cells (asterix). C, C', C''. The distances of the cells are regular and they are arranged in clusters. Seminoma cells were observed to have prominent nucleoli, light colored, large cytoplasm and large nuclei. Nuclei richer in chromatin are seen and there is more than one nucleus. A large number of lymphocyte cells are seen among the seminoma cells, which are distributed in clusters. An increase in the number of blood vessels in the interstitial area was observed.

4.2. Localization of Hippo Signaling Pathway Proteins by Immunohistochemistry

We performed immunohistochemistry staining to evaluate Hippo signaling pathway proteins in human control, embryonal carcinoma and seminoma tissues. Localization of Hippo signaling pathway proteins (MST1/2, p-MST1/2, LATS1/2, p-LATS1/2, YAP1, p-YAP1, TEAD4, ZO-1) in human control, embryonal carcinoma and seminoma testicular tissues was determined, counterstaining was performed with hematoxylin and images were evaluated with light microscope.

MST1 and MST2, components of the Hippo signaling pathway, control cell proliferation, differentiation and apoptosis during development (11). To elucidate in detail the cell type and developmental stage-specific localization of the MST1/2 protein in the human testis, we examined the expression of the MST1/2 protein in germ cells at various stages of seminiferous tubule classification. Leydig cells and blood vessels in the interstitial space between the seminiferous tubules showed strong positive immunoreactivity for MST1/2 (Figure 16, star and Figure 48, Table 6). Strong cytoplasmic MST1/2 expression was observed in myoid cells (Figure 16, thin arrow and Figure 48, Table 6). The cytoplasm of spermatogonium cells located at the base of the seminiferous tubule showed a positive staining pattern for the MST1/2 protein (Figure 16, arrowhead and 48, Table 6). We also determined cytoplasmic MST1/2 expression in spermatocytes (Figure 16, thick arrow and Figure 48, Table 6). Strong cytoplasmic MST1/2 expression was observed in round spermatids in the adluminal compartment of the seminiferous tubule (Figure 16, ellipse and Figure 48, Table 6), while MST1/2 expression was not detected in elongated spermatids (Figure 16, square and Figure 48, Table 6).

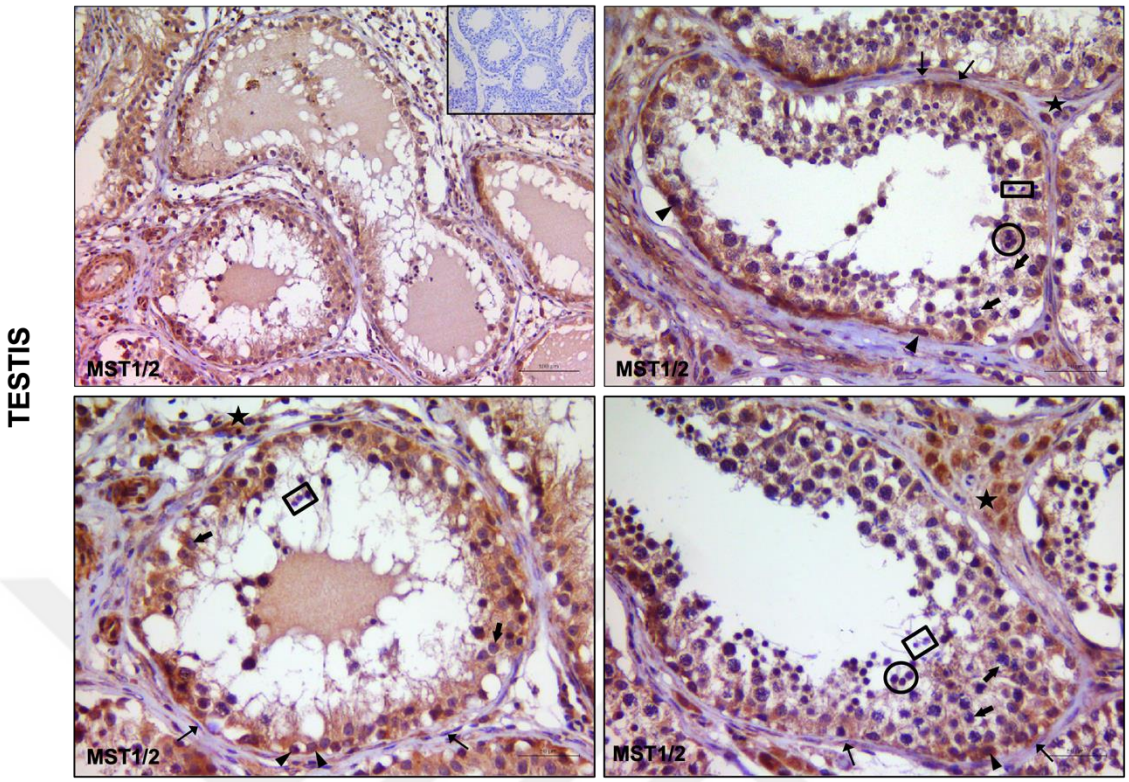

Figure 16. MST1/2 protein localization in human testis tissue is demonstrated by immunohistochemistry staining. The star refers to Leydig and blood cells in the interstitial space between the seminiferous tubules. Thin arrow, myoid cells; arrowhead, spermatogonium; thick arrow, spermatocytes; ellipse represents round spermatids and square represents elongated spermatids. There is no staining pattern in the negative control which is indicated in the insert image.

Embryonal carcinoma human testicular tissue showed a large number of carcinoma cells with large cytoplasm and vesicular nuclei and prominent nucleoli. It is observed that carcinoma cells are found in groups and form a glandular structure. Cells with atypical (Figure 16, arrowhead) and neutrophils (Figure 17, ellipse and Figure 49, Table 7) are seen in tissue (Figure 17 and 49). The MST1/2 showed strong cytoplasmic staining pattern in carcinoma cells (Figure 17 and 49). Positive MST1/2 immunoreactivity is observed in atypical (Figure 17, arrowhead and Figure 49, Table 7) and neutrophil (Figure 17, ellipse and Figure 49, Table 7) cells. We detected strong MST1/2 expression in the vascular endothelium (Figure 17, chevrons and Figure 49, Table 7).

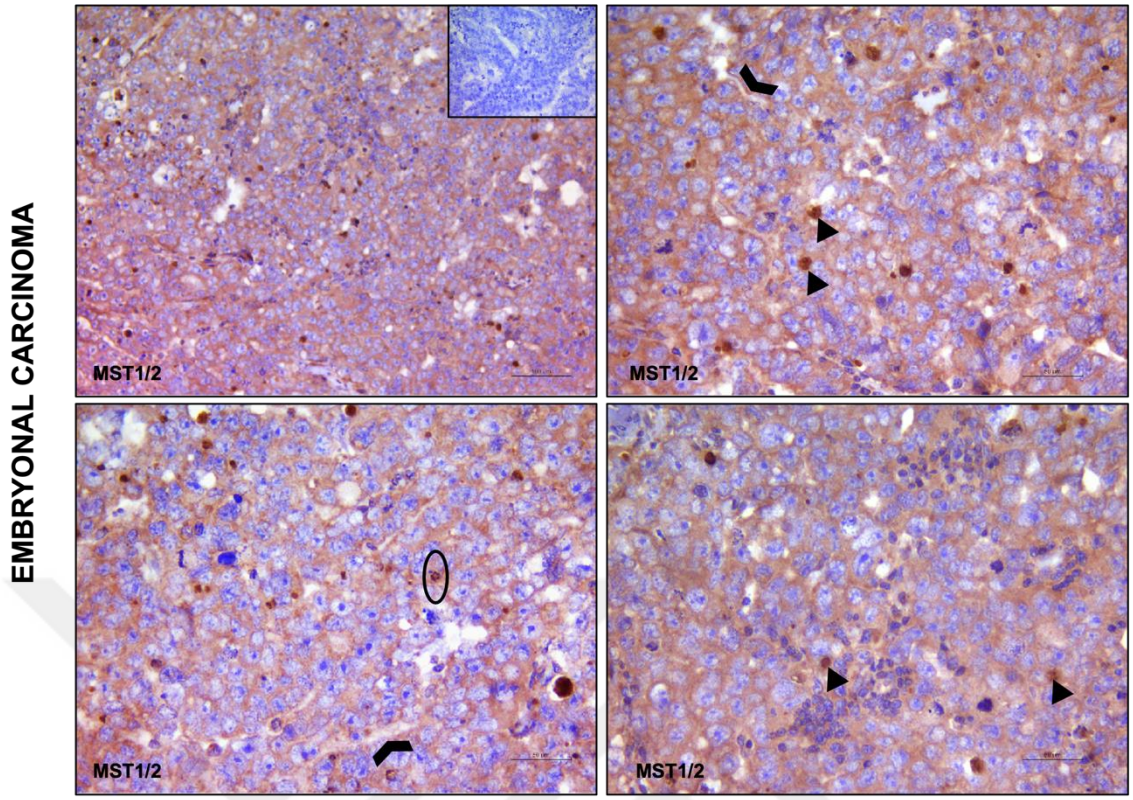

Figure 17. MST1/2 protein localization in human embryonal carcinoma tissue is demonstrated by immunohistochemistry staining. The ellipse includes neutrophils among the carcinoma cells; arrowhead represents atypical cells. The chevrons indicate the vascular endothelium. There is no staining pattern in the negative control which is indicated in the insert image.

In seminoma human testis tissue, we found seminoma cells to be large uniform round to polygonal cells with distinct cell borders, clear cytoplasm, and round nuclei (Figure 18 and 50). Lymphocyte cell infiltration is observed in the fibrous septa between the seminoma cells (Figure 18, dashed line and Figure 50, Table 8). We detected strong MST1/2 expression in the cytoplasm of seminoma cells. We showed strong cytoplasmic MST1/2 expression in the lymphocyte cells (Figure 18, dashed line and Figure 50, Table 8), which are abundant on the septa separating the seminoma cells.

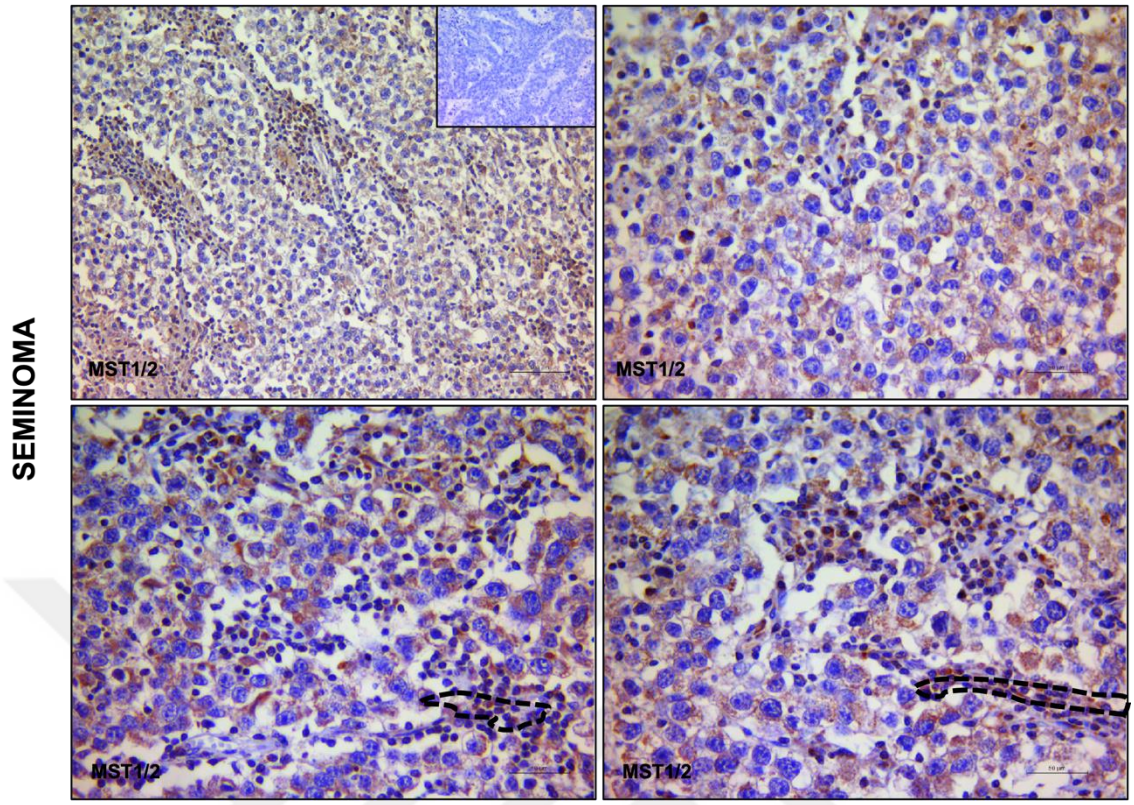

Figure 18. MST1/2 protein localization in human seminoma tissue is demonstrated by immunohistochemistry staining. Dashed line indicates lymphocytes arrayed on fibrous septa between seminoma cells. There is no staining pattern in the negative control which is indicated in the insert image.

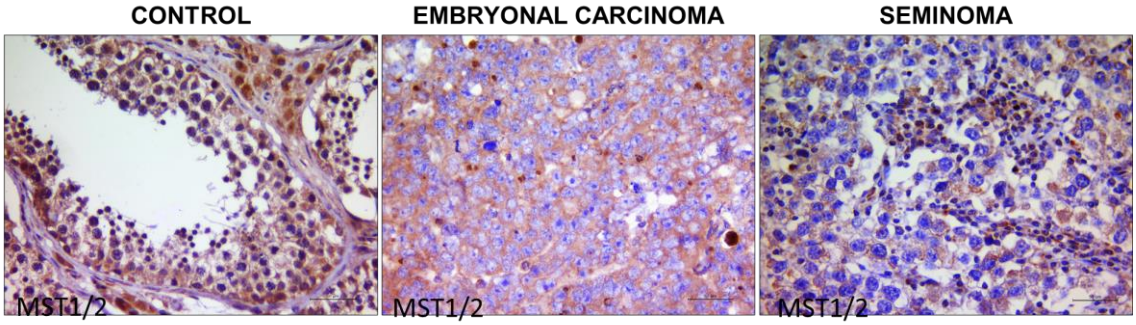

Figure 19. MST1/2 protein localization in human control, embryonal carcinoma and seminoma tissue is demonstrated by immunohistochemistry staining.

To elucidate in detail the cell type and developmental stage-specific localization of the p-MST1/2 protein in the human testis, we examined the expression of the p-MST1/2 protein in germ cells at various stages of seminiferous tubule classification. Leydig cells and blood vessels in the interstitial space between the seminiferous tubules

showed strong cytoplasmic immunoreactivity for p-MST1/2 (Figure 20, star and Figure 48, Table 6). p-MST1/2 expression was not observed in myoid cells (Figure 20, thin arrow and Figure 48, Table 6). The cytoplasm of spermatogonium cells located at the base of the seminiferous tubule showed strong cytoplasmic staining pattern for the p-MST1/2 protein (Figure 20, arrowhead and Figure 48, Table 6). We also determined very weak p-MST1/2 expression in spermatocytes (Figure 20, thick arrow and Figure 48, Table 6). Strong cytoplasmic p-MST1/2 expression was observed in round spermatids in the adluminal compartment of the seminiferous tubule (Figure 20, ellipse and Figure 48, Table 6), while p-MST1/2 expression was not detected in elongated spermatids (Figure 20, square and Figure 48, Table 6).

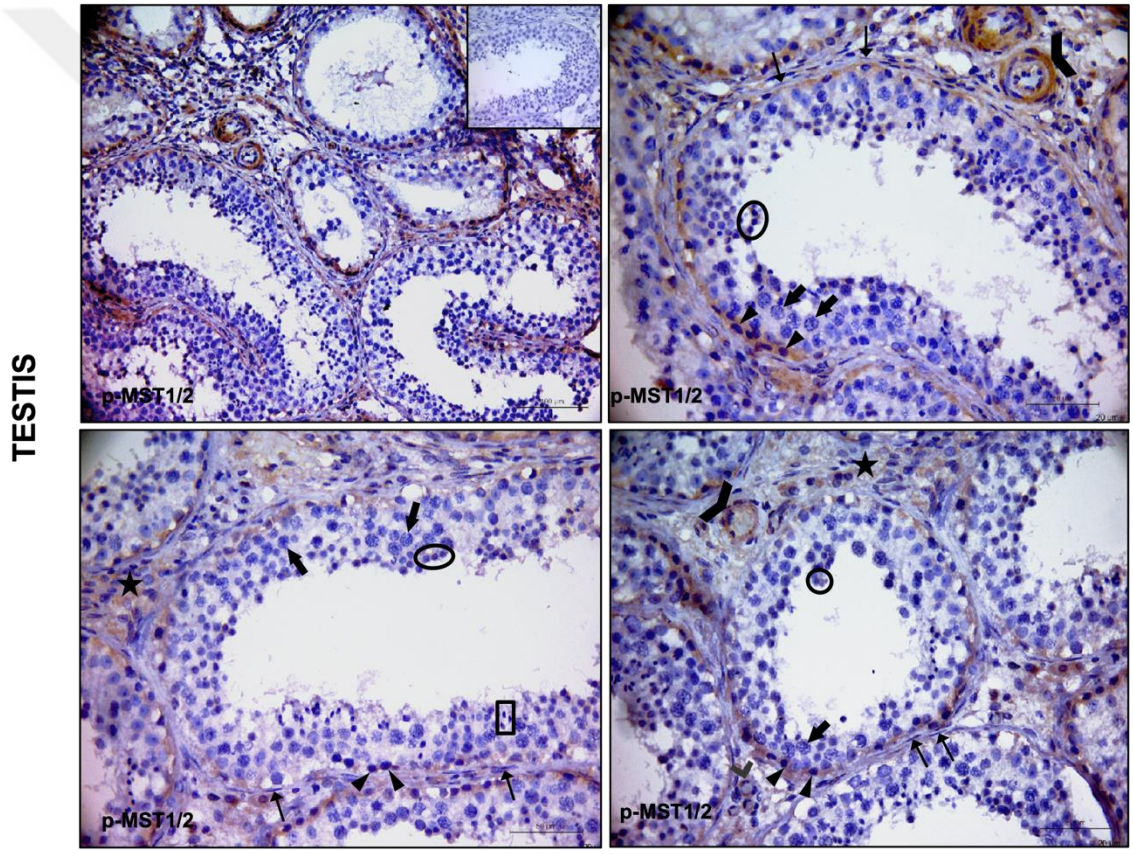

Figure 20. p-MST1/2 protein localization in human testis tissue is demonstrated by immunohistochemistry staining. The star refers to Leydig and blood cells in the interstitial space between the seminiferous tubules. Thin arrow, myoid cells; arrowhead, spermatogonium; thick arrow, spermatocytes; ellipse represents round spermatids and square represents elongated spermatids. There is no staining pattern in the negative control which is indicated in the insert image.

Embryonal carcinoma human testicular tissue showed a large number of carcinoma cells with large cytoplasm and vesicular nuclei and prominent nucleoli. It is observed that carcinoma cells are found in groups and form a glandular structure. The p-MST1/2 showed cytoplasmic staining pattern in carcinoma cells (Figure 21 and 49). We detected strong p-MST1/2 expression in the vascular endothelium (Figure 21 and 49, Table 7).

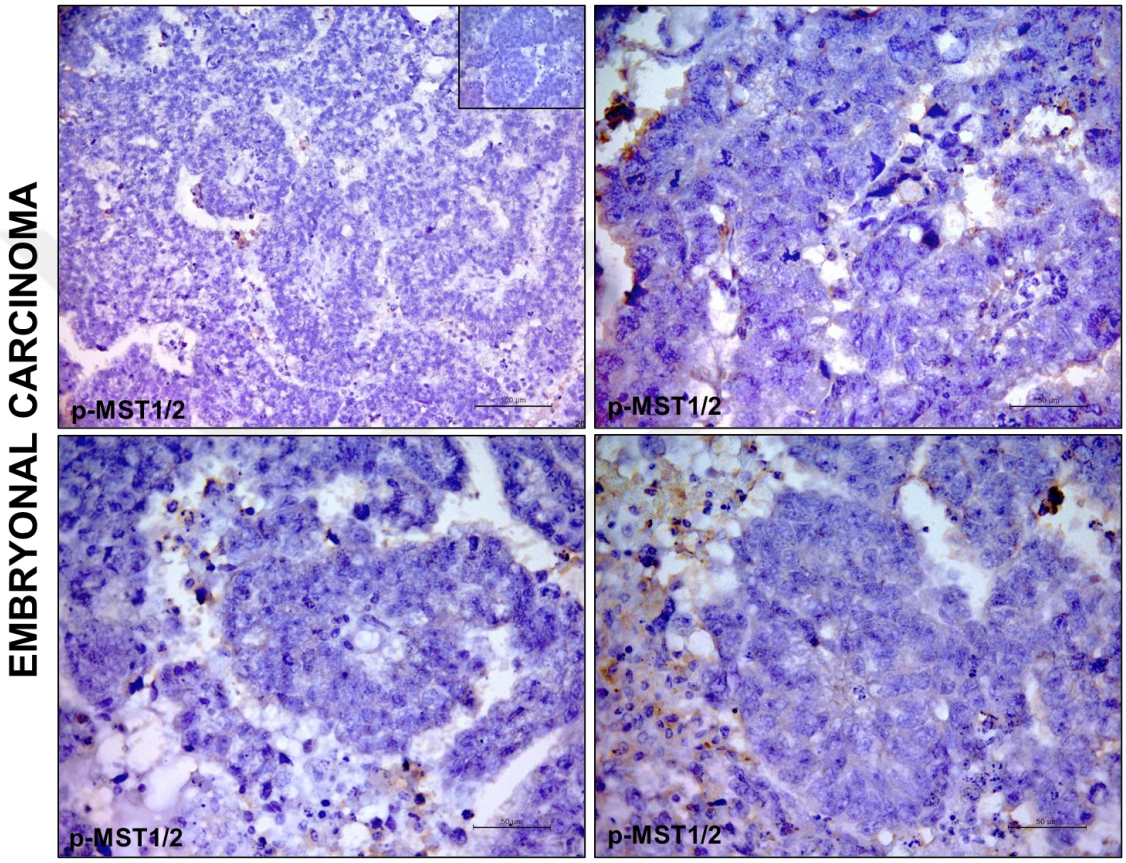

Figure 21. p-MST1/2 protein localization in human embryonal carcinoma tissue is demonstrated by immunohistochemistry staining. The chevrons indicate the vascular endothelium. There is no staining pattern in the negative control which is indicated in the insert image.

In seminoma human testis tissue, we found seminoma cells to be large uniform round to polygonal cells with distinct cell borders, clear cytoplasm, and round nuclei (Figure 22 and 50). Lymphocyte cell infiltration is observed in the fibrous septa between the seminoma cells (Figure 22, dashed line and Figure 50, Table 8). We detected a weak p-MST1/2 expression in the cytoplasm of seminoma cells. We showed a very weak

cytoplasmic p-MST1/2 expression in the lymphocyte cells (Figure 22, dashed line and Figure 50, Table 8), which are abundant on the septa separating the seminoma cells.

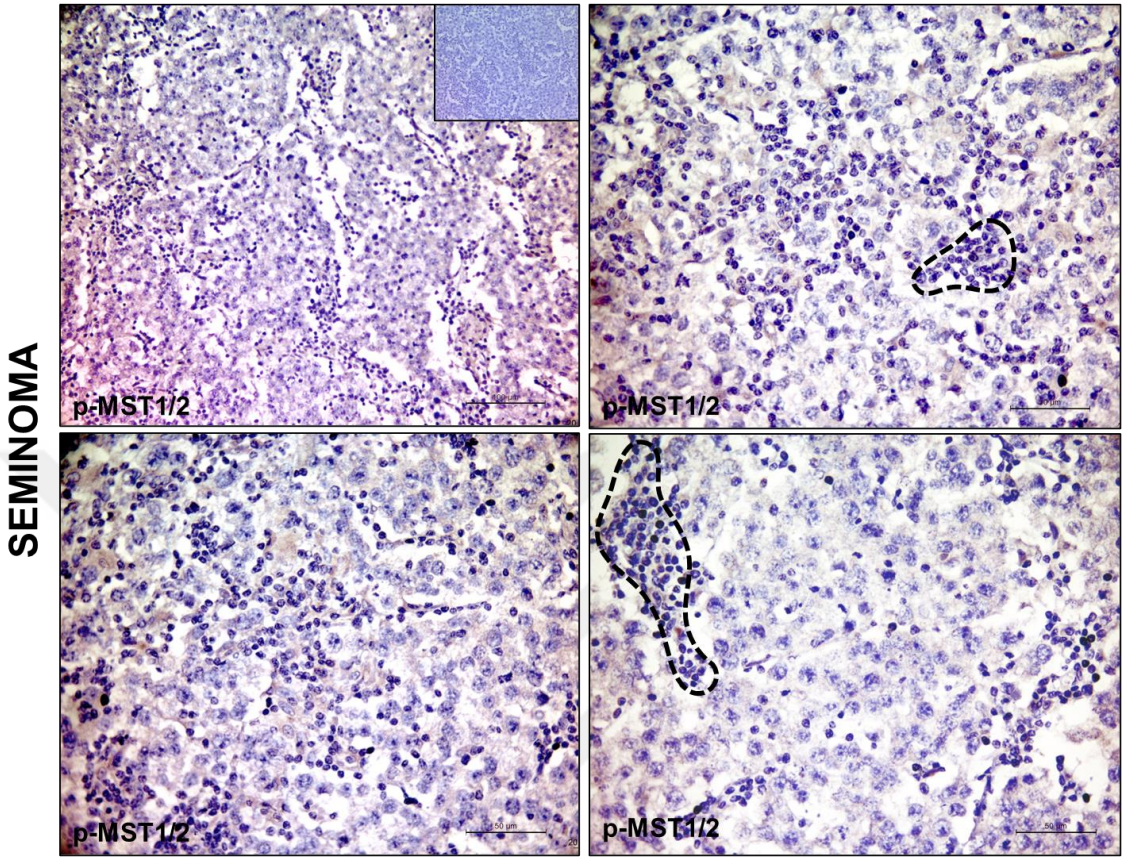

Figure 22. p-MST1/2 protein localization in human seminoma tissue is demonstrated by immunohistochemistry staining. Dashed line indicates lymphocytes arrayed on fibrous septa between seminoma cells. There is no staining pattern in the negative control which is indicated in the insert image.

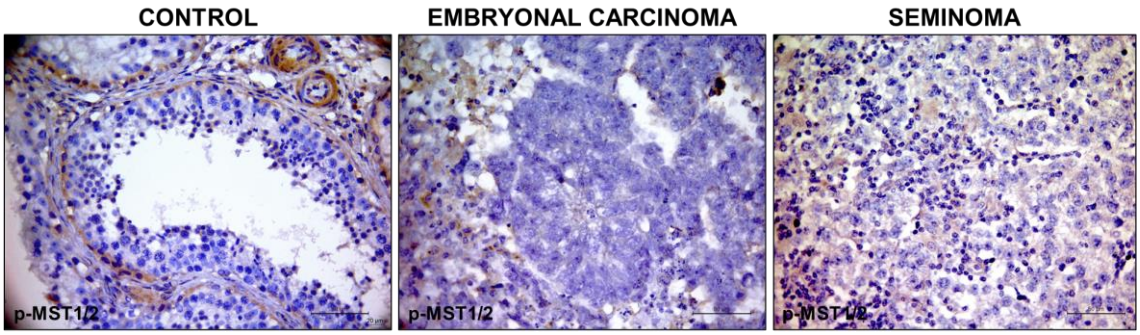

Figure 23. p-MST1/2 protein localization in human control, embryonal carcinoma and seminoma tissue is demonstrated by immunohistochemistry staining.

LATS1/2, the core Hippo kinases are critical for organismal fitness, genome integrity and cancer prevention (193). To elucidate in detail the cell type and developmental stage-specific localization of the LATS1/2 protein in the human testis, we examined the expression of the LATS1/2 protein in germ cells at various stages of seminiferous tubule classification. Leydig cells and vascular endothelia in the interstitial space between the seminiferous tubules showed cytoplasmic immunoreactivity for LATS1/2 (Figure 24, star and Figure 48, Table 6). LATS1/2 expression was not observed in myoid cells (Figure 24, thin arrow and Figure 48, Table 6). The nuclei of spermatogonium cells located at the base of the seminiferous tubule showed for the first time a strong nuclear staining pattern for the LATS1/2 protein (Figure 24, arrowhead and Figure 48, Table 6). We also determined a weak LATS1/2 expression in spermatocytes (Figure 24, thick arrow and Figure 48, Table 6). Cytoplasmic LATS1/2 expression was observed in round spermatids in the adluminal compartment of the seminiferous tubule (Figure 24, ellipse and Figure 48, Table 6), while LATS1/2 expression was not detected in elongated spermatids (Figure 24, square and Figure 48, Table 6).

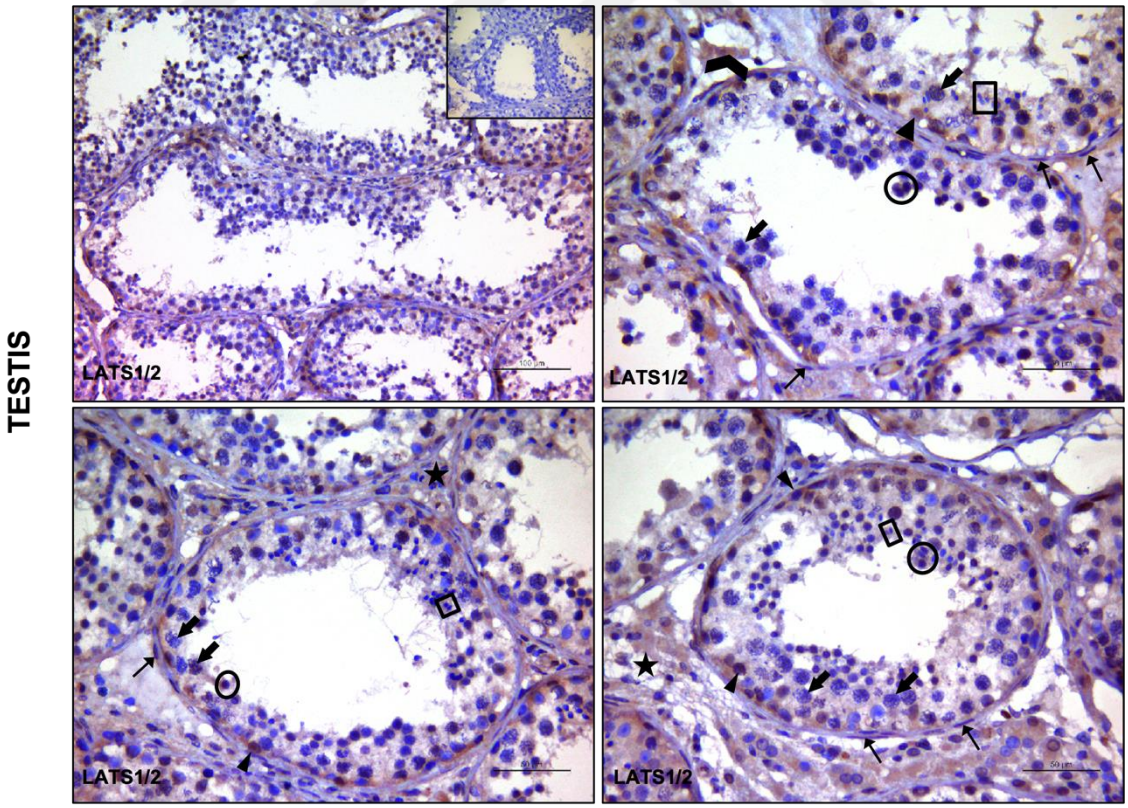

Figure 24. LATS1/2 protein localization in human testis tissue is demonstrated by immunohistochemistry staining. The star refersa to Leydig and blood cells in the

interstitial space between the seminiferous tubules. Thin arrow, myoid cells; arrowhead, spermatogonium; thick arrow, spermatocytes; ellipse represents round spermatids and square represents elongated spermatids. There is no staining pattern in the negative control which is indicated in the insert image.

Embryonal carcinoma human testicular tissue showed many carcinoma cells with large cytoplasm and vesicular nuclei and prominent nucleoli. It is observed that carcinoma cells are found in groups and form a glandular structure. The LATS1/2 showed cytoplasmic staining pattern in carcinoma cells (Figure 25 and 49). We detected strong LATS1/2 expression in the vascular endothelium (Figure 25, chevrons and Figure 49, Table 7).

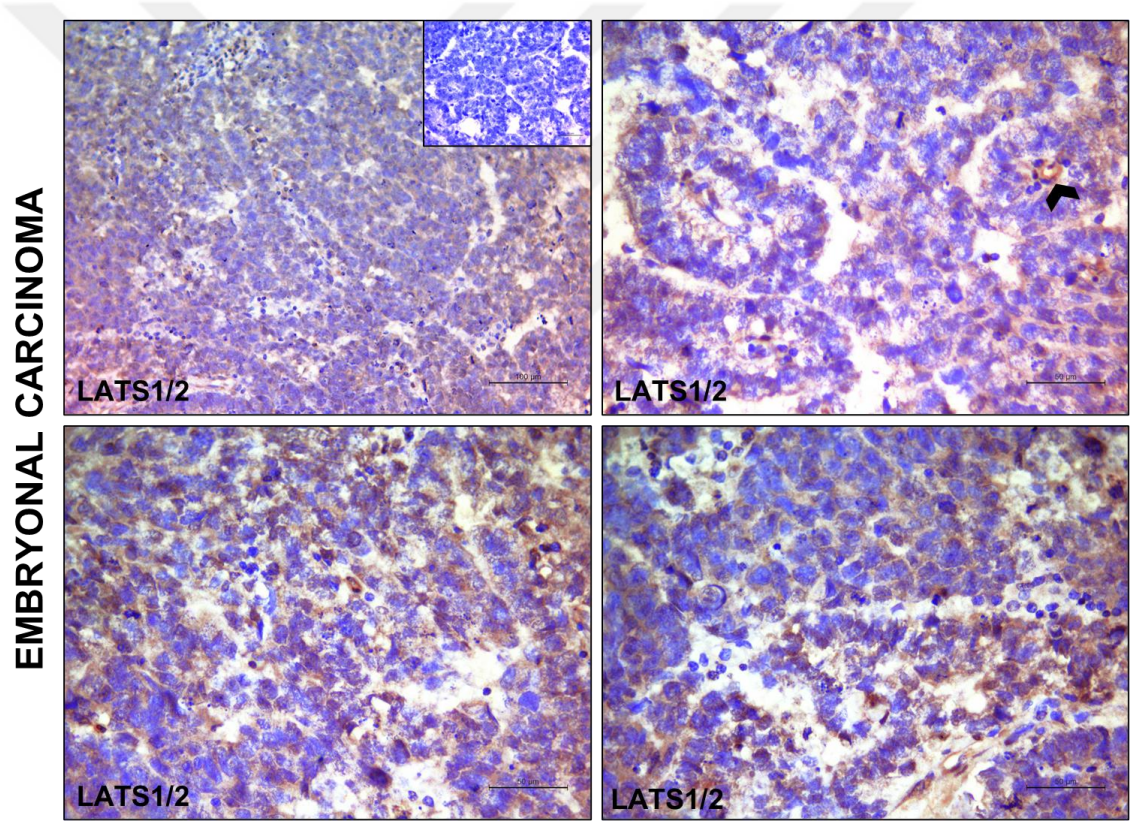

Figure 25. LATS1/2 protein localization in human embryonal carcinoma tissue is demonstrated by immunohistochemistry staining. The chevrons indicate the vascular endothelium. There is no staining pattern in the negative control which is indicated in the insert image.

In seminoma human testis tissue, we see seminoma cells are large uniform round to polygonal cells with distinct cell borders, clear cytoplasm and round nuclei (Figure 26 and 50). Lymphocyte cell infiltration is observed in the fibrous septa between the

seminoma cells (Figure 26, dashed line and Figure 50, Table 8). For the first time, we detected a strong expression of LATS1/2 in the nucleus of seminoma cells. Some of the lymphocyte cells showed cytoplasmic and some nuclear LATS1/2 expression (Figure 26, dashed line and Figure 50, Table 8), which are abundant on the septa separating the seminoma cells.

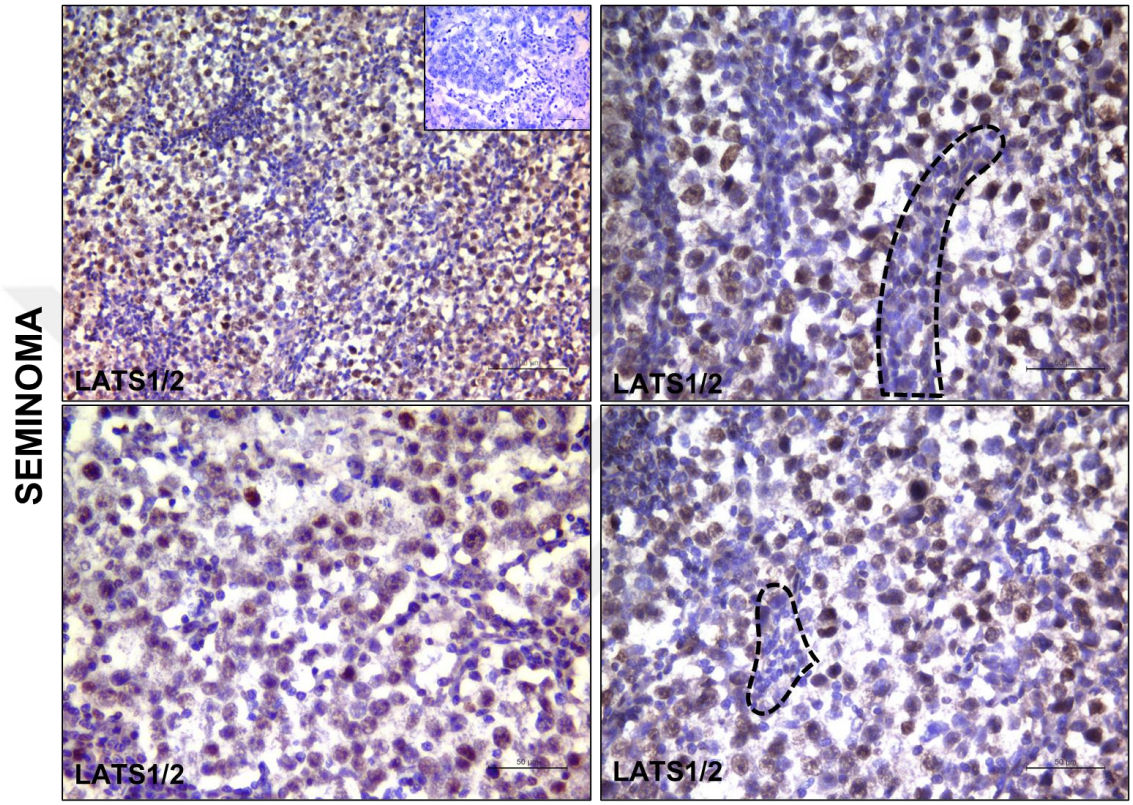

Figure 26. LATS1/2 protein localization in human seminoma tissue is demonstrated by immunohistochemistry staining. Dashed line indicates lymphocytes arrayed on fibrous septa between seminoma cells. There is no staining pattern in the negative control which is indicated in the insert image.

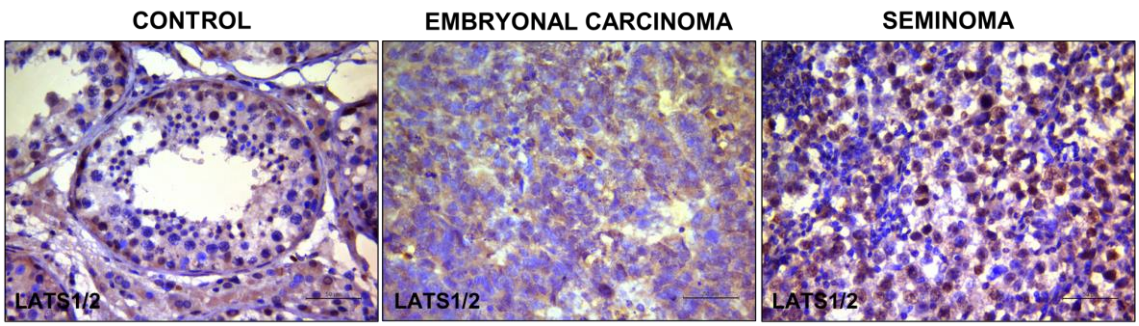

Figure 27. LATS1/2 protein localization in human control, embryonal carcinoma and seminoma tissue is demonstrated by immunohistochemistry staining.

To elucidate in detail the cell type and developmental stage-specific localization of the p-LATS1/2 protein in the human testis, we examined the expression of the p-LATS1/2 protein in germ cells at various stages of seminiferous tubule classification. Leydig cells in the interstitial space between the seminiferous tubules showed cytoplasmic immunoreactivity for p-LATS1/2 (Figure 28, star and Figure 48, Table 6). p-LATS1/2 expression was not observed in myoid cells (Figure 28, thin arrow and 48, Table 6). Spermatogonium cells located at the base of the seminiferous tubule showed a strong cytoplasmic staining pattern for the p-LATS1/2 protein (Figure 28, arrowhead and Figure 48, Table 6). We also determined a strong p-LATS1/2 expression in spermatocytes (Figure 28, thick arrow and Figure 48, Table 6). Cytoplasmic p-LATS1/2 expression was observed in round spermatids in the adluminal compartment of the seminiferous tubule (Figure 28, ellipse and Figure 48, Table 6), while p-LATS1/2 expression was not detected in elongated spermatids (Figure 28, square and Figure 48, Table 6).

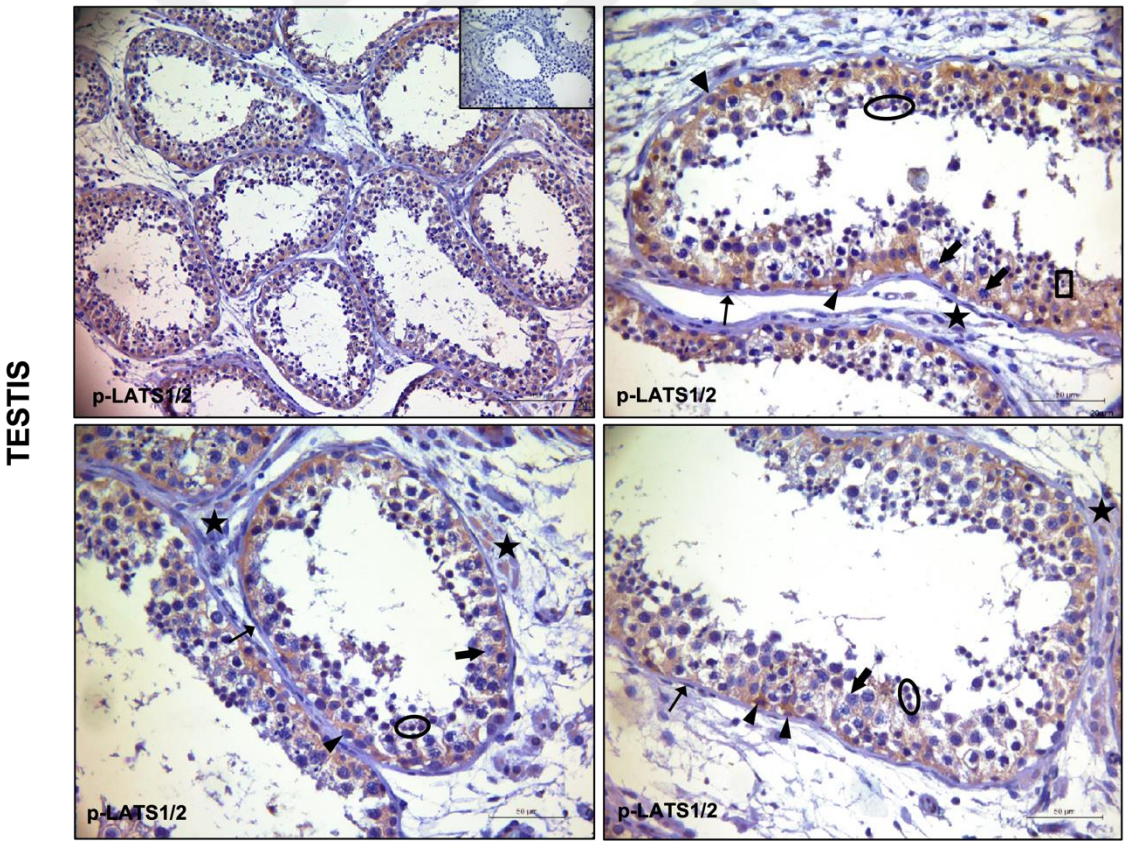

Figure 28. p-LATS1/2 protein localization in human testis tissue is demonstrated by immunohistochemistry staining. The star refers to Leydig cells in the interstitial space between the seminiferous tubules. Thin arrow, myoid cells; arrowhead, spermatogonium; thick arrow, spermatocytes; ellipse represents round spermatids and square represents

elongated spermatids. There is no staining pattern in the negative control which is indicated in the insert image.

Embryonal carcinoma human testicular tissue showed a large number of carcinoma cells with large cytoplasm and vesicular nuclei and prominent nucleoli. It is observed that carcinoma cells are found in groups and form a glandular structure. Mitotic cells (Figure 29, thin arrow and Figure 49, Table 7) are seen (Figure 29 and 49). The p-LATS1/2 showed cytoplasmic staining pattern in carcinoma cells (Figure 29 and 49). A strong positive nuclear p-LATS1/2 immunoreactivity is observed in mitotic (Figure 29, thin arrow and Figure 49, Table 7) cells.

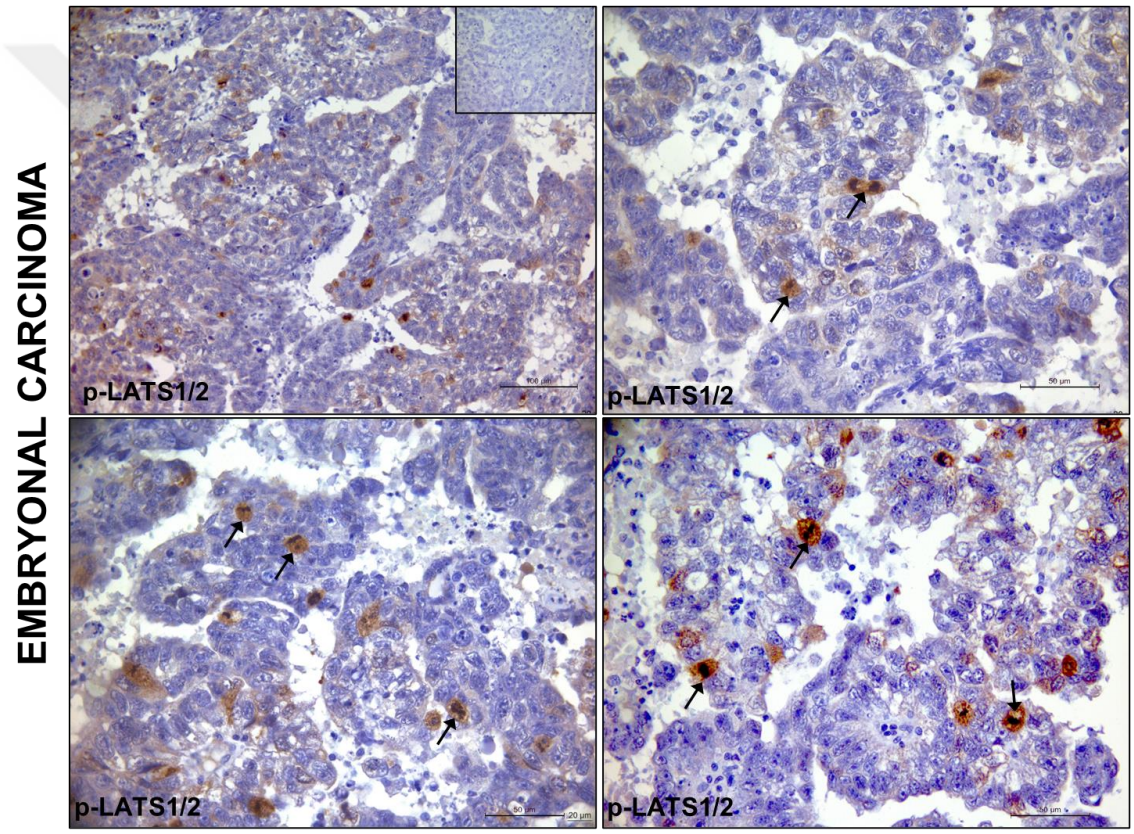

Figure 29. p-LATS1/2 protein localization in human embryonal carcinoma tissue is demonstrated by immunohistochemistry staining. The thin arrow indicates the mitotic cells. There is no staining pattern in the negative control which is indicated in the insert image.

In seminoma human testis tissue, we seen seminoma cells are large uniform round to polygonal cells with distinct cell borders, clear cytoplasm and round nuclei (Figure 30 and 50). Lymphocyte cell infiltration is observed in the fibrous septa between the

seminoma cells (Figure 30, dashed line and Figure 50, Table 8). We detected cytoplasmic expression of p-LATS1/2 in the seminoma cells. Lymphocyte cells showed a very weak cytoplasmic p-LATS1/2 expression (Figure 30, dashed line and Figure 50, Table 8), which are abundant on the septa separating the seminoma cells. We detected expression of p-LATS1/2 in the vascular endothelia.

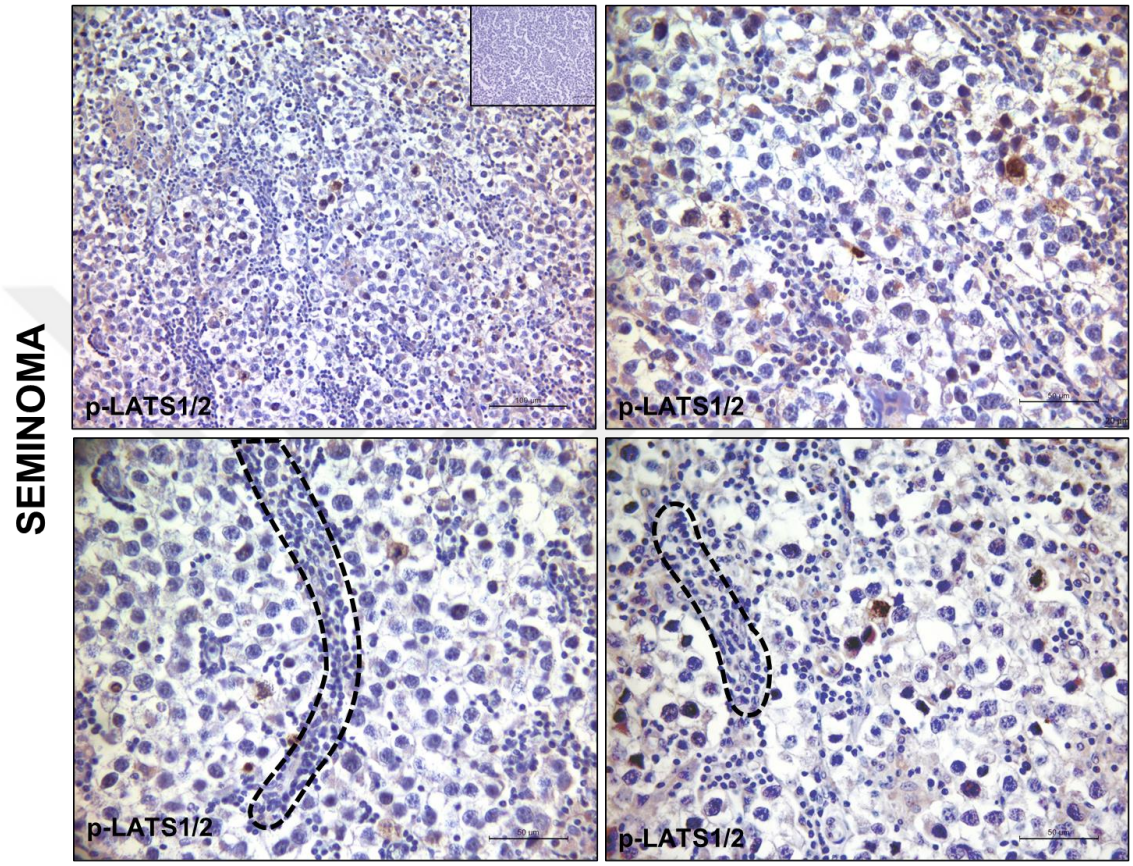

Figure 30. p-LATS1/2 protein localization in human seminoma tissue is demonstrated by immunohistochemistry staining. Dashed line indicates lymphocytes arrayed on fibrous septa between seminoma cells. There is no staining pattern in the negative control which is indicated in the insert image.

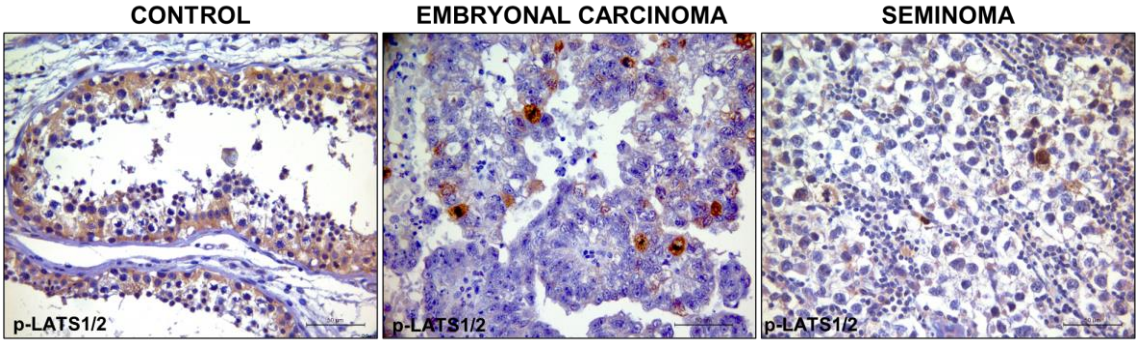

Figure 31. p-LATS1/2 protein localization in human control, embryonal carcinoma and seminoma tissue is demonstrated by immunohistochemistry staining.

YAP1 encodes a downstream nuclear effector of the Hippo signaling pathway involved in development, growth, repair, and homeostasis. This gene is known to be involved in the development and progression of multiple cancers as a transcriptional regulator of this signaling pathway and may serve as a potential target for cancer therapy (13). To elucidate in detail the cell type and developmental stage-specific localization of the YAP1 in the human testis, we examined the expression of the YAP1 in germ cells at various stages of seminiferous tubule classification. Leydig cells in the interstitial space between the seminiferous tubules showed both cytoplasmic and nuclear immunoreactivity for YAP1 (Figure 32, star and Figure 48, Table 6). We detected YAP1 expression in vascular endothelium (Figure 32, chevrons and Figure 48). Similarly, myoid cells showed both a strong cytoplasmic and nuclear immunoreactivity for YAP1 (Figure 32, thin arrow and Figure 48, Table 6). Spermatogonium cells located at the base of the seminiferous tubule showed a strong cytoplasmic staining pattern for the YAP1 (Figure 32, arrowhead and Figure 48, Table 6). We also determined cytoplasmic YAP1 expression in spermatocytes (Figure 32, thick arrow and Figure 48, Table 6). Cytoplasmic YAP1 expression was observed in round spermatids in the adluminal compartment of the seminiferous tubule (Figure 32, ellipse and Figure 48, Table 6), while YAP1 expression was not detected in elongated spermatids (Figure 32, square and Figure 48, Table 6).

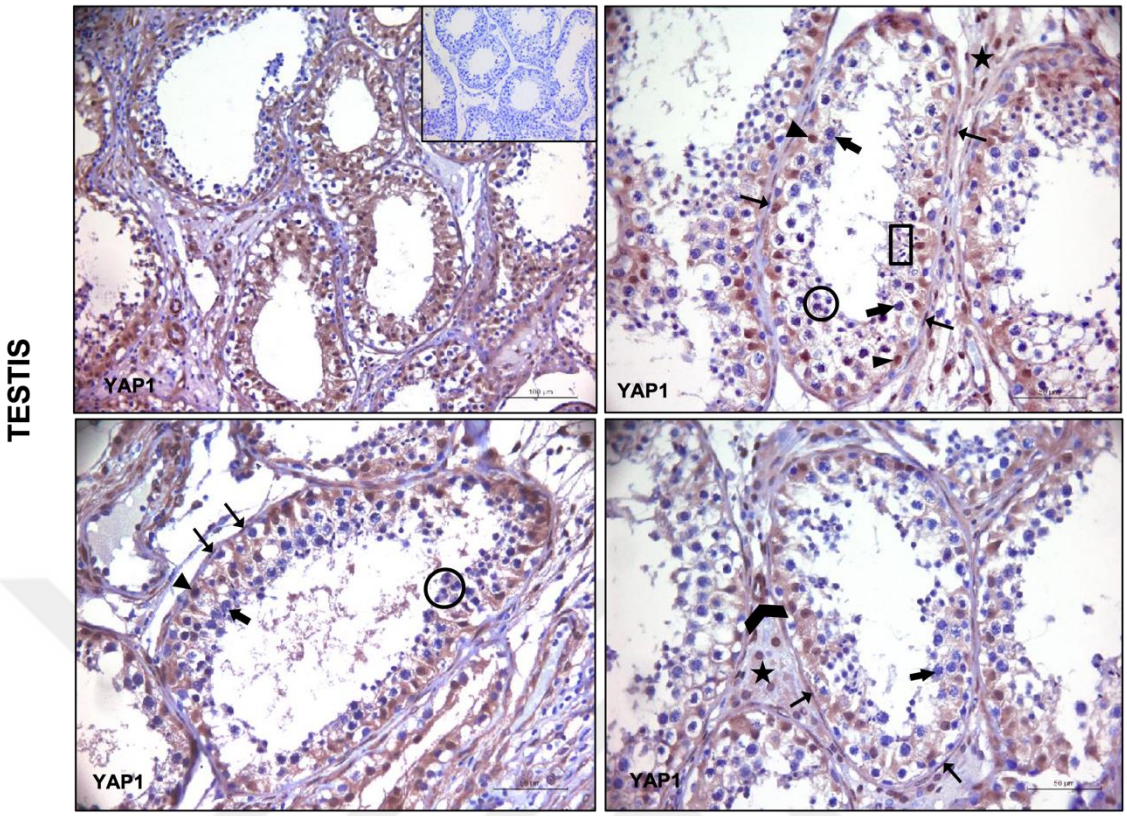

Figure 32. YAP1 localization in human testis tissue is demonstrated by immunohistochemistry staining. The star, Leydig cells and chevrons refers to vascular endothelia in the interstitial space between the seminiferous tubules. Thin arrow, myoid cells; arrowhead, spermatogonium; thick arrow, spermatocytes; ellipse represents round spermatids and square represents elongated spermatids. There is no staining pattern in the negative control which is indicated in the insert image.

Embryonal carcinoma human testicular tissue showed a large number of carcinoma cells with large cytoplasm and vesicular nuclei and prominent nucleoli. It is observed that carcinoma cells are found in groups and form a glandular structure. Mitotic cells (Figure 33, thin arrow and Figure 49, Table 7) are seen (Figure 33 and 49). The YAP1 showed strong cytoplasmic staining pattern in carcinoma cells (Figure 33 and 49). A strong positive nuclear YAP1 immunoreactivity is observed in mitotic (Figure 33, thin arrow and Figure 49, Table 7) cells.

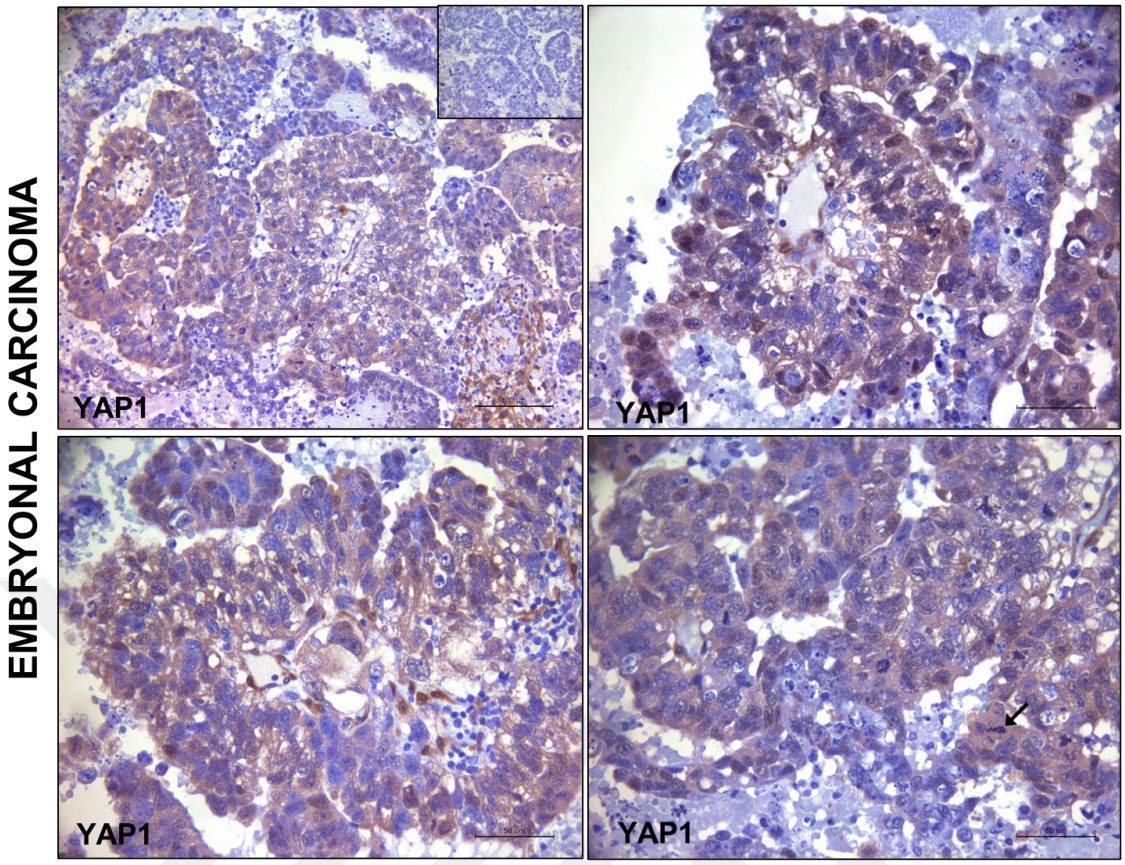

Figure 33. YAP1 localization in human embryonal carcinoma tissue is demonstrated by immunohistochemistry staining. The thin arrow indicates the mitotic cells. There is no staining pattern in the negative control which is indicated in the insert image.

In seminoma human testis tissue, we seen seminoma cells are large uniform round to polygonal cells with distinct cell borders, clear cytoplasm, and round nuclei (Figure 34 and 50). Lymphocyte cell infiltration is observed in the fibrous septa between the seminoma cells (Figure 34, dashed line and Figure 50, Table 8). We detected cytoplasmic expression of YAP1 in the seminoma cells. Lymphocyte cells showed a very weak cytoplasmic YAP1 expression (Figure 34, dashed line and Figure 50, Table 8), which are abundant on the septa separating the seminoma cells. We detected expression of YAP1 in the vascular endothelia.

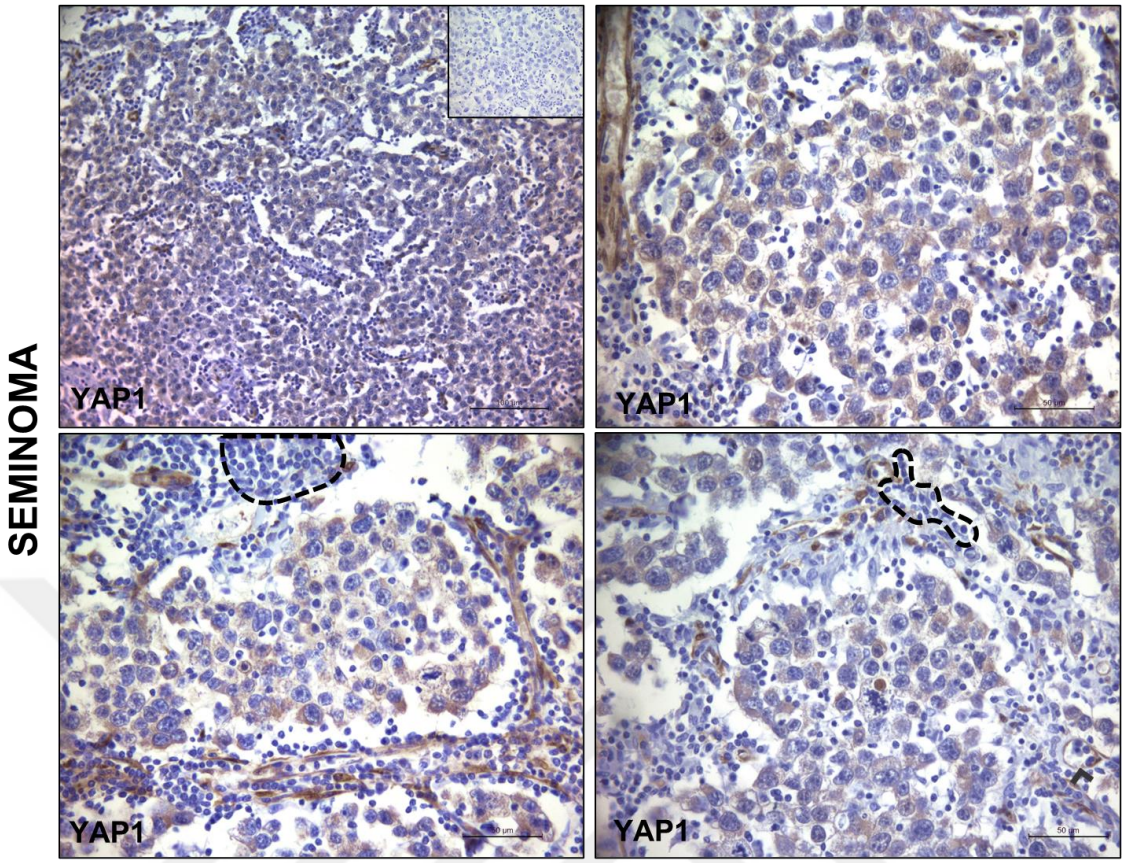

Figure 34. YAP1 localization in human seminoma tissue is demonstrated by immunohistochemistry staining. Dashed line indicates lymphocytes arrayed on fibrous septa between seminoma cells. There is no staining pattern in the negative control which is indicated in the insert image.

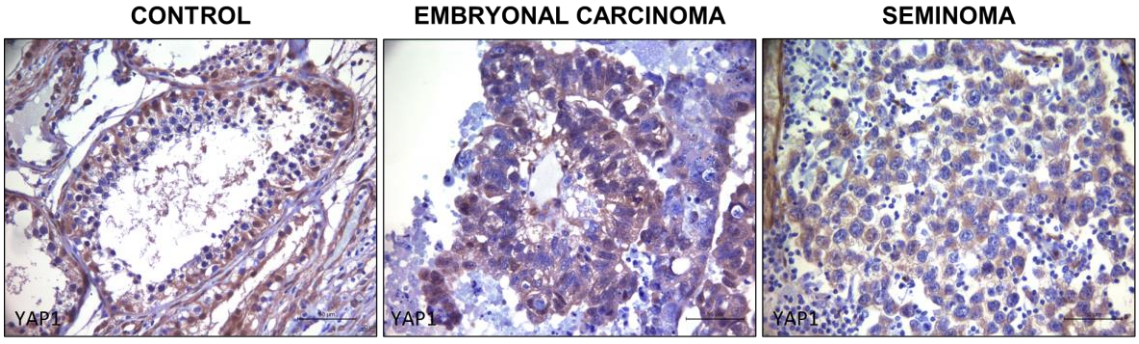

Figure 35. YAP localization in human control, embryonal carcinoma and seminoma tissue is demonstrated by immunohistochemistry staining.

To elucidate in detail the cell type and developmental stage-specific localization of the p-YAP1 in the human testis, we examined the expression of the p-YAP1 in germ cells at various stages of seminiferous tubule classification. Leydig cells in the interstitial

space between the seminiferous tubules showed a strong cytoplasmic immunoreactivity for p-YAP1 (Figure 36, star and Figure 48, Table 6). We detected p-YAP1 expression in vascular endothelium (Figure 36, chevrons and Figure 48, Table 6). Myoid cells showed both a strong cytoplasmic and nuclear immunoreactivity for p-YAP1 (Figure 36, thin arrow and Figure 48, Table 6). Spermatogonium cells located at the base of the seminiferous tubule showed a strong cytoplasmic staining pattern for the p-YAP1 (Figure 36, arrowhead and Figure 48, Table 6). We also determined a strong p-YAP1 expression in spermatocytes (Figure 36, thick arrow and Figure 48, Table 6). Cytoplasmic p-YAP1 expression was observed in round spermatids in the adluminal compartment of the seminiferous tubule (Figure 36, ellipse and Figure 48, Table 6), while p-YAP1 expression was not detected in elongated spermatids (Figure 36, square and Figure 48, Table 6).

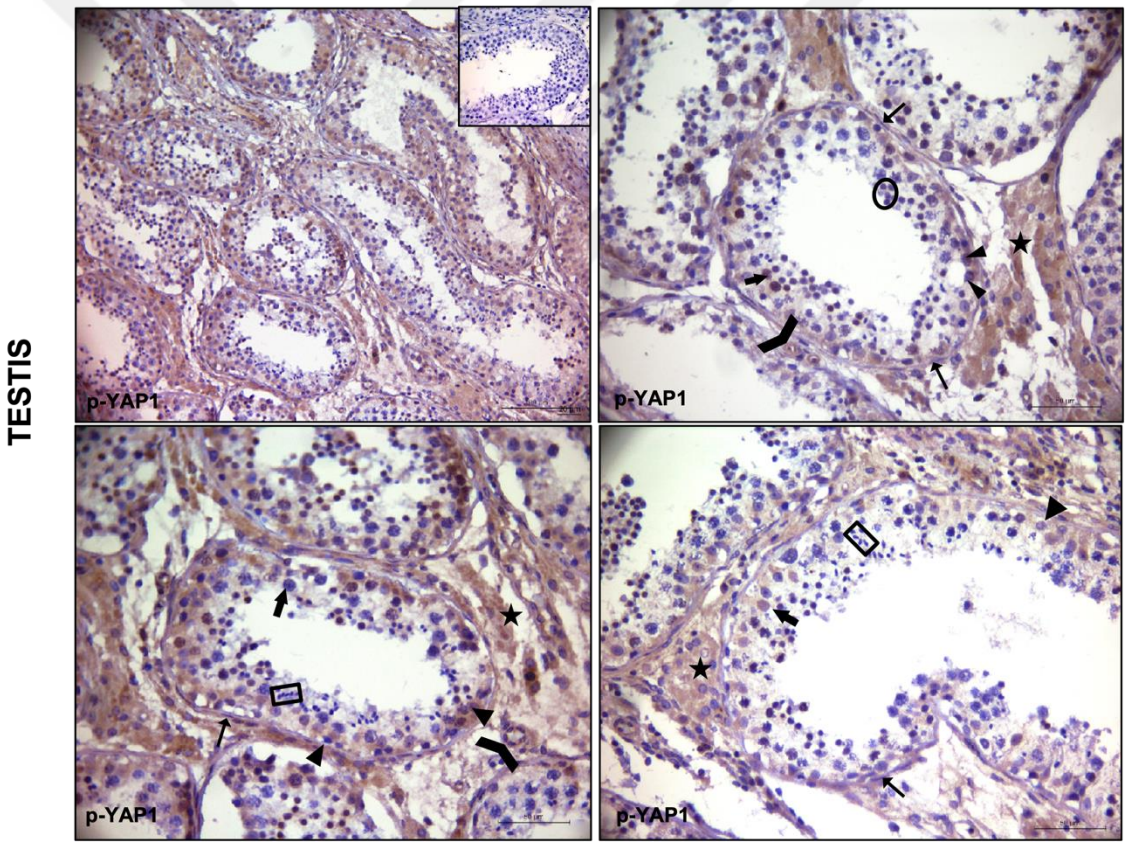

Figure 36. p-YAP1 localization in human testis tissue is demonstrated by immunohistochemistry staining. The star, Leydig cells and chevrons refers to vascular endothelia in the interstitial space between the seminiferous tubules. Thin arrow, myoid cells; arrowhead, spermatogonium; thick arrow, spermatocytes; ellipse represents round spermatids and square represents elongated spermatids. There is no staining pattern in the negative control which is indicated in the insert image.

Embryonal carcinoma human testicular tissue showed many of carcinoma cells with large cytoplasm and vesicular nuclei and prominent nucleoli. It is observed that carcinoma cells are found in groups and form a glandular structure. The p-YAP1 showed strong cytoplasmic staining pattern in carcinoma cells (Figure 37 and 49, Table 7).

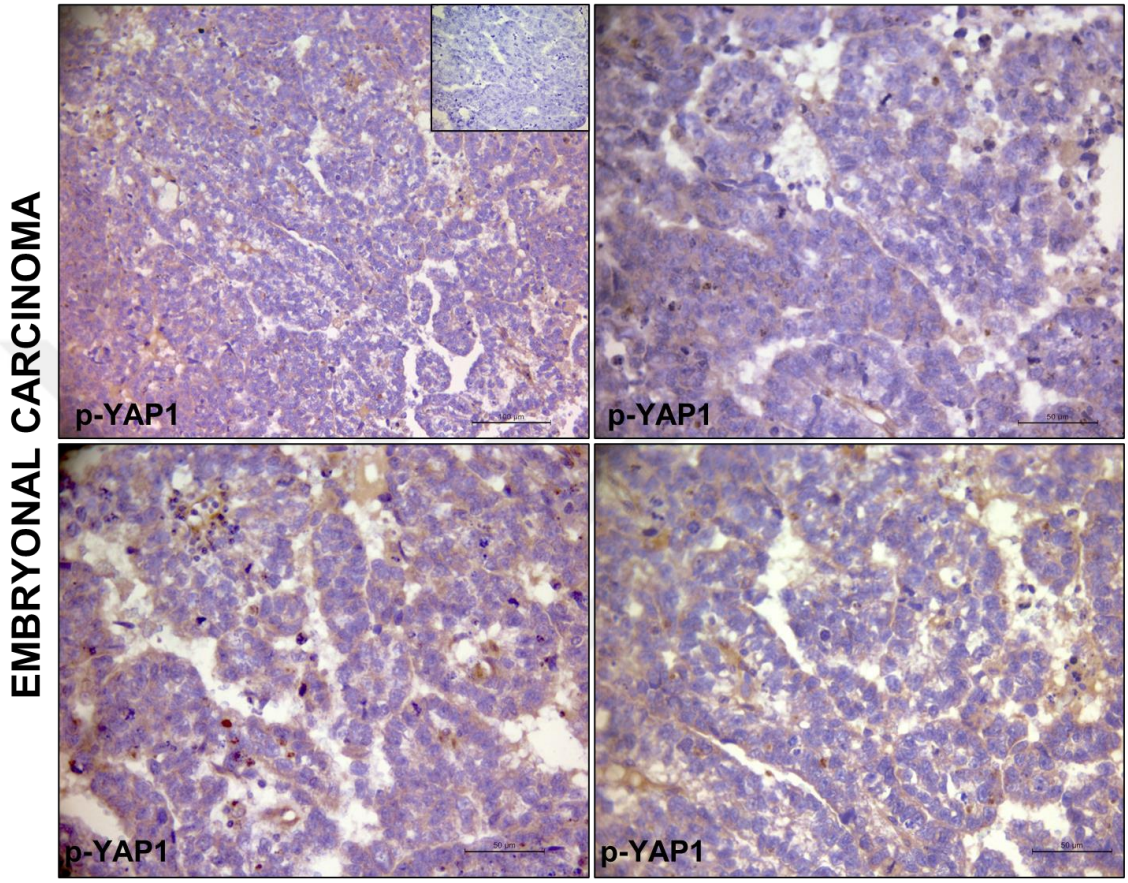

Figure 37. p-YAP1 localization in human embryonal carcinoma tissue is demonstrated by immunohistochemistry staining. There is no staining pattern in the negative control which is indicated in the insert image.

In seminoma human testis tissue, we seen seminoma cells are large uniform round to polygonal cells with distinct cell borders, clear cytoplasm and round nuclei (Figure 38 and 50). Lymphocyte cell infiltration is observed in the fibrous septa between the seminoma cells (Figure 38, dashed line and Figure 50, Table 8). We detected cytoplasmic expression of p-YAP1 in the seminoma cells. Lymphocyte cells showed a very weak cytoplasmic p-YAP1 expression (Figure 38, dashed line and Figure 50, Table 8), which are abundant on the septa separating the seminoma cells. We detected expression of p-YAP1 in the vascular endothelia.

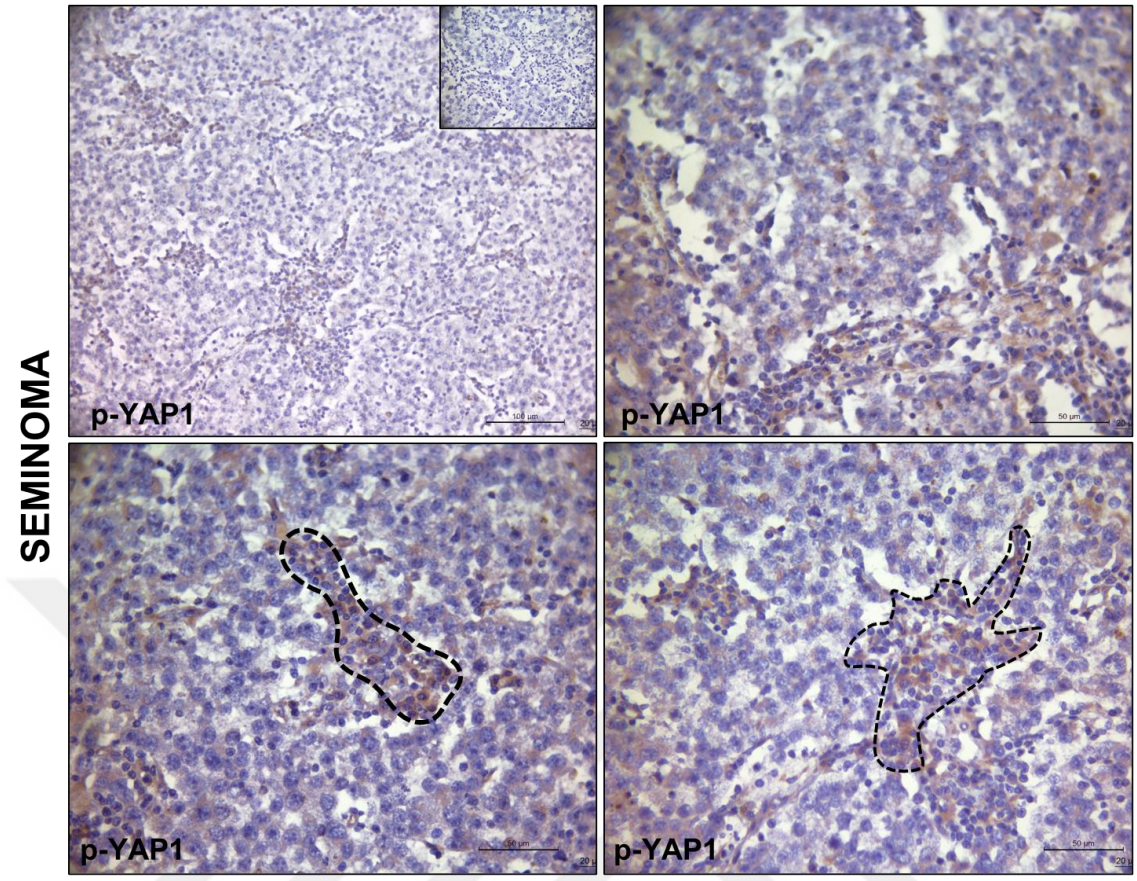

Figure 38. p-YAP1 localization in human seminoma tissue is demonstrated by immunohistochemistry staining. Dashed line indicates lymphocytes arrayed on fibrous septa between seminoma cells. There is no staining pattern in the negative control which is indicated in the insert image.

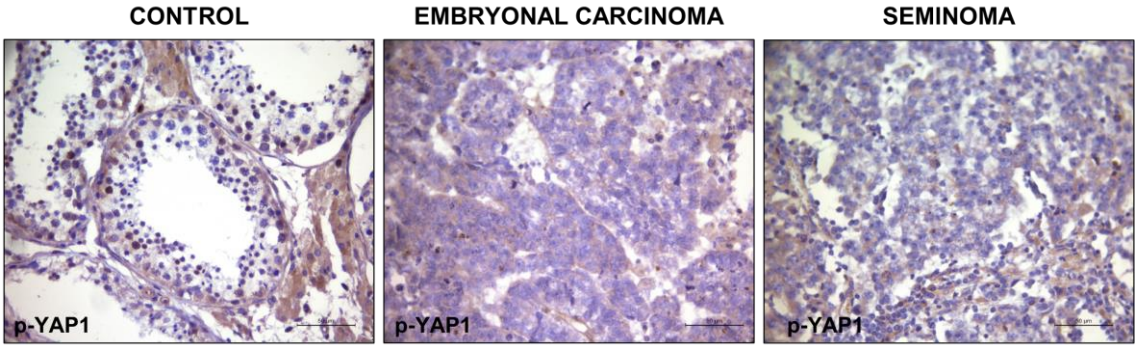

Figure 39. p-YAP1 localization in human control, embryonal carcinoma and seminoma tissue is demonstrated by immunohistochemistry staining.

As a downstream effector of the Hippo pathway, TEAD4 has essential roles in cell proliferation, cell survival, tissue regeneration and stem cell maintenance (194). To

elucidate in detail the cell type and developmental stage-specific localization of the TEAD4 in the human testis, we examined the expression of the TEAD4 in germ cells at various stages of seminiferous tubule classification. Leydig cells in the interstitial space between the seminiferous tubules showed a strong cytoplasmic immunoreactivity for TEAD4 (Figure 40, star and Figure 48, Table 6). Myoid cells showed a strong cytoplasmic immunoreactivity for TEAD4 (Figure 40, thin arrow and Figure 48, Table 6). Spermatogonium cells located at the base of the seminiferous tubule showed a strong cytoplasmic staining pattern for the TEAD4 (Figure 40, arrowhead and Figure 48, Table 6). We also determined a strong both cytoplasmic and nuvclear TEAD4 expression in spermatocytes (Figure 40, thick arrow and Figure 48, Table 6). Similarly, cytoplasmic, and nuclear TEAD4 expression was observed in round spermatids in the adluminal compartment of the seminiferous tubule (Figure 40, ellipse and Figure 48, Table 6), while TEAD4 expression was not detected in elongated spermatids (Figure 40, square and Figure 48, Table 6).

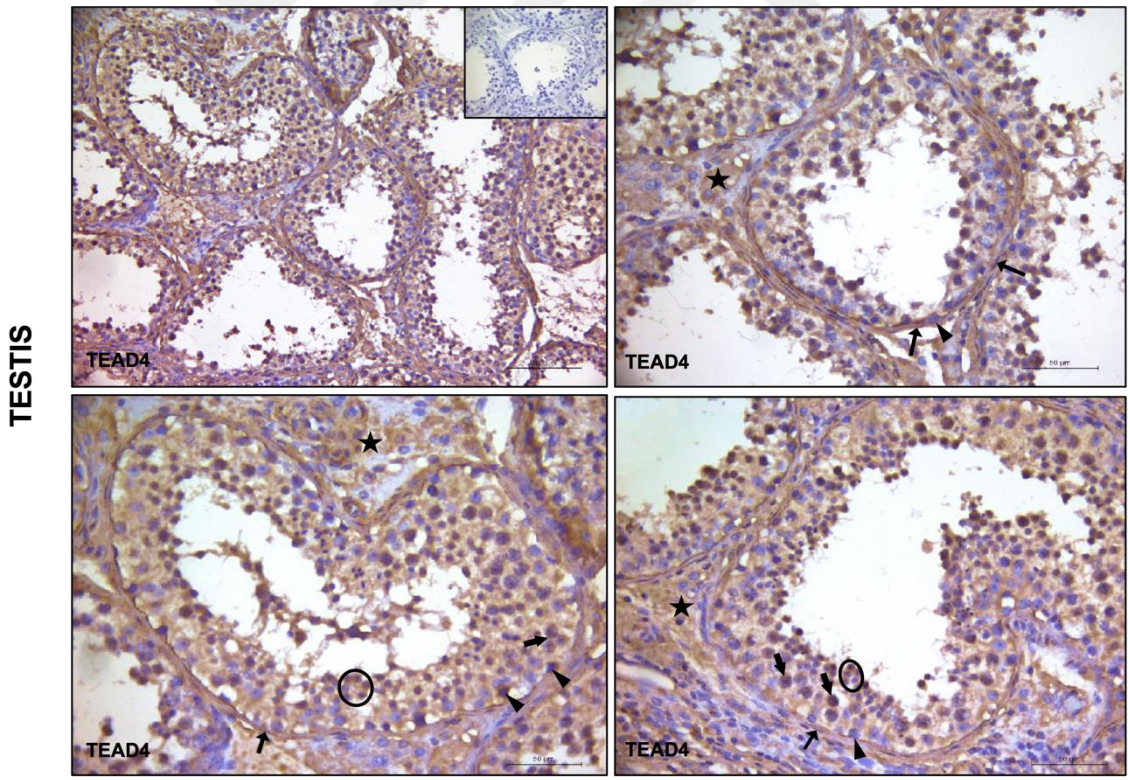

Figure 40. TEAD4 localization in human testis tissue is demonstrated by immunohistochemistry staining. The star refers to Leydig cells in the interstitial space between the seminiferous tubules. Thin arrow, myoid cells; arrowhead, spermatogonium; thick arrow, spermatocytes; ellipse represents round spermatids and square represents

elongated spermatids. There is no staining pattern in the negative control which is indicated in the insert image.

Embryonal carcinoma human testicular tissue showed many of carcinoma cells with large cytoplasm and vesicular nuclei and prominent nucleoli. It is observed that carcinoma cells are found in groups and form a glandular structure. TEAD4 a strong immunoreactivity showed in carcinoma cells cytoplasm (Figure 41 and 49).

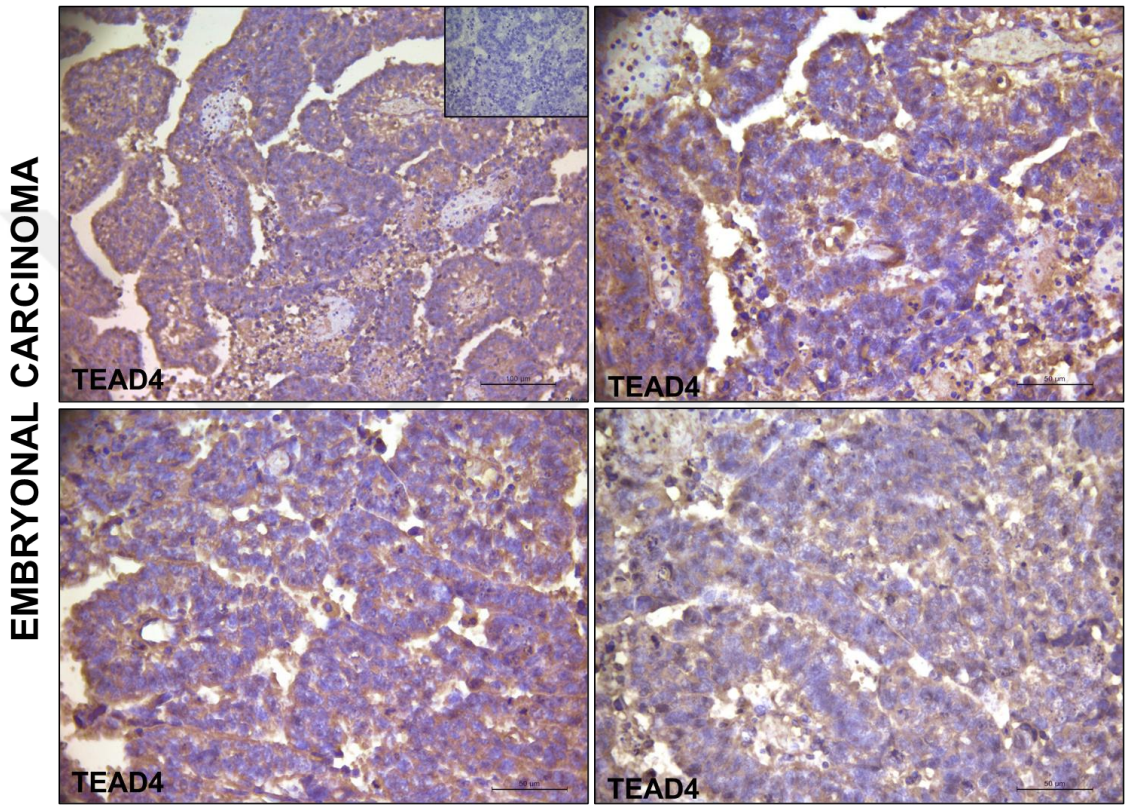

Figure 41. TEAD4 localization in human embryonal carcinoma tissue is demonstrated by immunohistochemistry staining. There is no staining pattern in the negative control which is indicated in the insert image.

In seminoma human testis tissue, we seen seminoma cells are large uniform round to polygonal cells with distinct cell borders, clear cytoplasm, and round nuclei (Figure 42 and 50). Lymphocyte cell infiltration is seen on the fibrous septa between the seminoma cells (Figure 42, dashed line and Figure 50, Table 8). Seminoma cells showed a strong cytoplasmic staining for TEAD4. TEAD4 observed a weak expression in lymphocyte cells, which are found in large numbers on the septa separating the seminoma cells (Figure 42, dashed line and 50, Table 8).

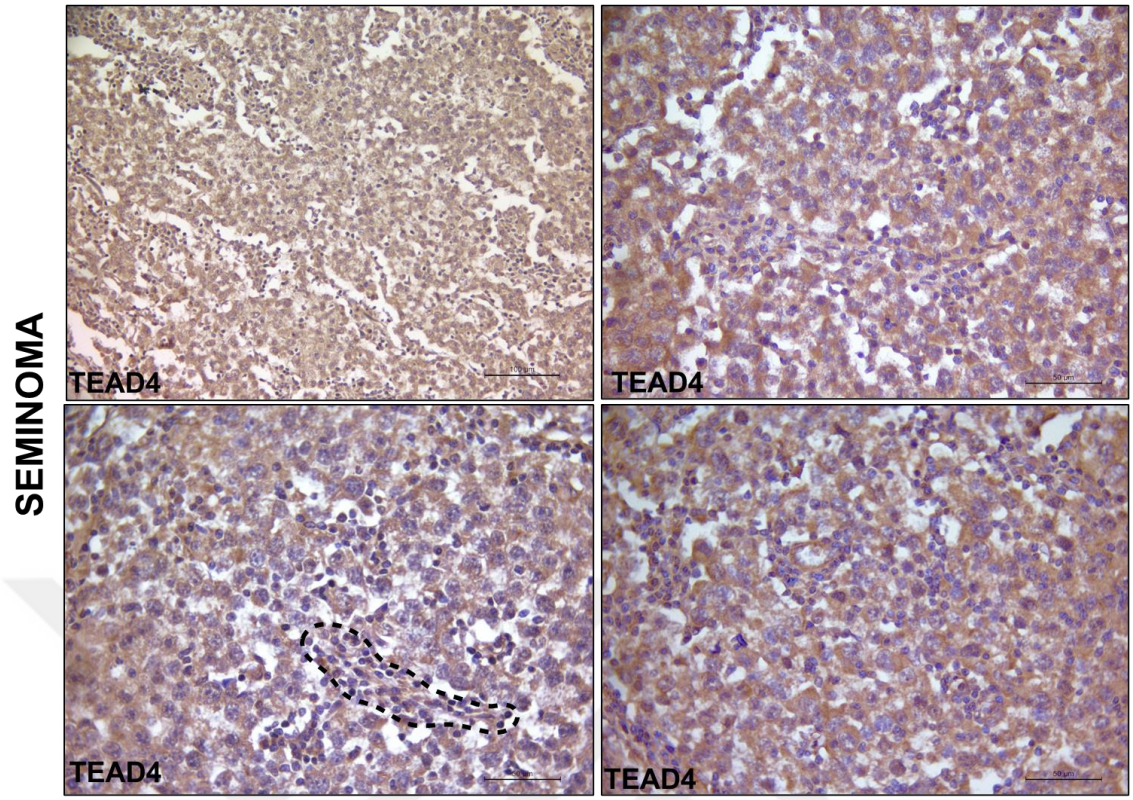

Figure 42. TEAD4 localization in human seminoma tissue is demonstrated by immunohistochemistry staining. Dashed line indicates lymphocytes arrayed on fibrous septa between seminoma cells. There is no staining pattern in the negative control which is indicated in the insert image.

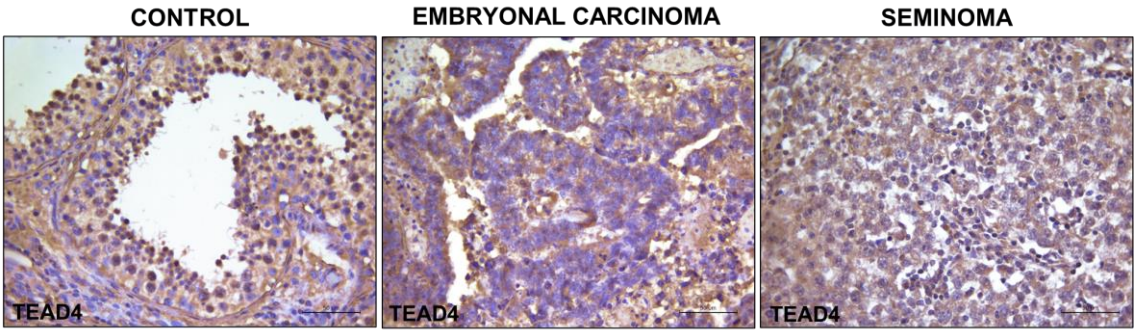

Figure 43. TEAD4 localization in human control, embryonal carcinoma and seminoma tissue is demonstrated by immunohistochemistry staining.

Zonula occludens-1 (ZO-1), one of the tight junction proteins between cells in testicular tissue, and the regular actin network it forms play a role in testicular development and sperm production (195). As a control of our immunostaining, we performed ZO-1 immunostaining in human testis, embryonal carcinoma and seminoma

testicular tissues. As shown in previous studies (195), ZO-1 showed a membranous staining pattern in control testicular tissue (Figure 44, arrow). We detected a linear localization of the blood-testicular barrier in the basolateral region and basal of the seminiferous epithelium (Figure 44, arrow).

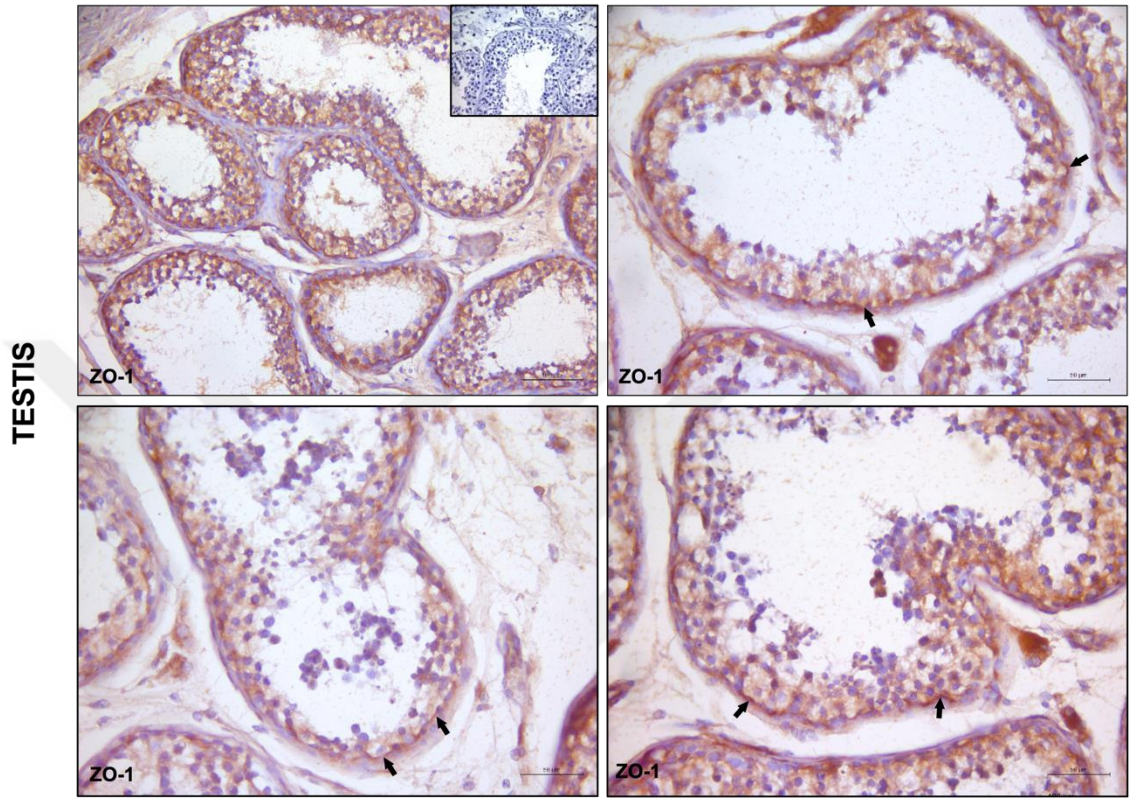

Figure 44. ZO-1 localization in human testis tissue is demonstrated by immunohistochemistry staining.

Embryonal carcinoma human testicular tissue showed a large number of carcinoma cells with large cytoplasm and vesicular nuclei and prominent nucleoli. Weak ZO-1 immunostaining was detected in embryonal carcinoma testis tissue due to disruption of the normal seminiferous tubule structure and loss of intercellular connections. A weak cytoplasmic ZO-1 expression pattern was demonstrated in embryonal carcinoma cells (Figure 45).

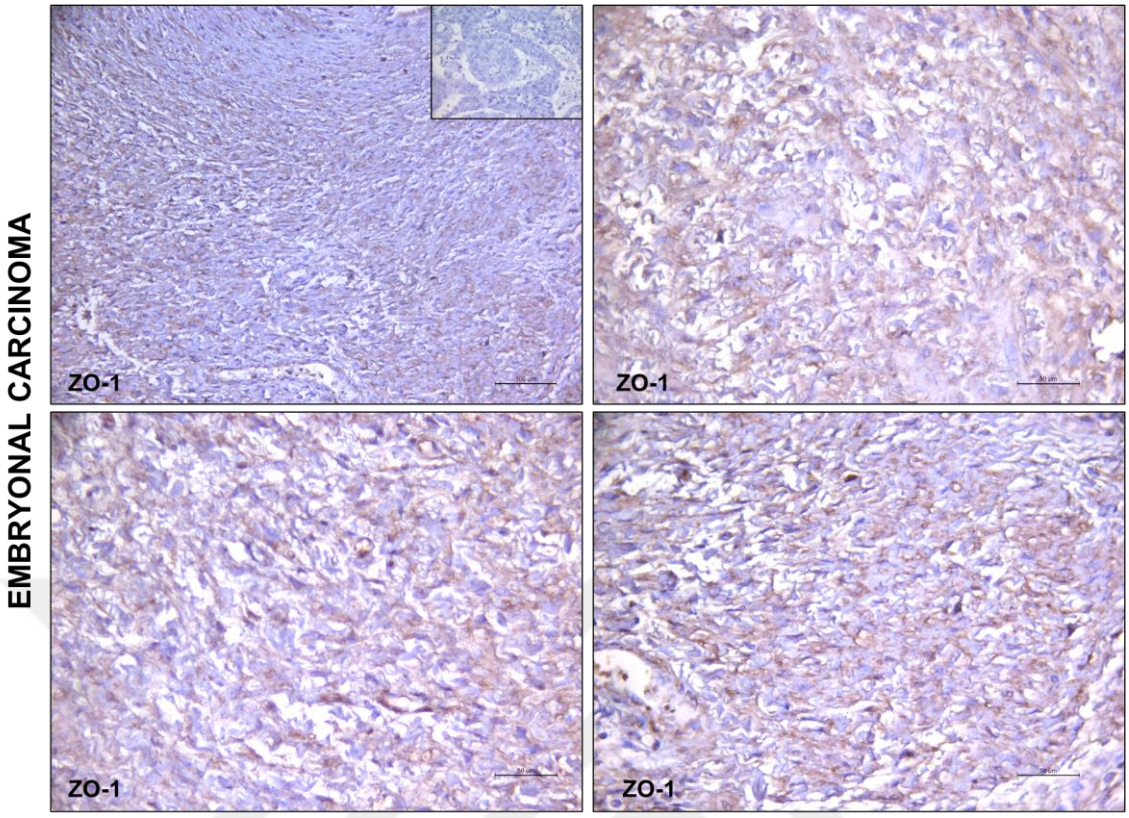

Figure 45. ZO-1 localization in human embryonal carcinoma tissue is demonstrated by immunohistochemistry staining. There is no staining pattern in the negative control which is indicated in the insert image.

In seminoma human testis tissue, we seen seminoma cells are large uniform round to polygonal cells with distinct cell borders, clear cytoplasm and round nuclei. Lymphocyte cell infiltration is seen on the fibrous septa between the seminoma cells. It is observed that the normal seminiferous tubule structures are disrupted in seminoma tissue, and the disrupted seminiferous tubules are devoid of spermatogenic series cells. Therefore, in seminoma cells, the ZO-1 protein showed a diffuse, non-specific, cytoplasmic immunostaining pattern (Figure 46).

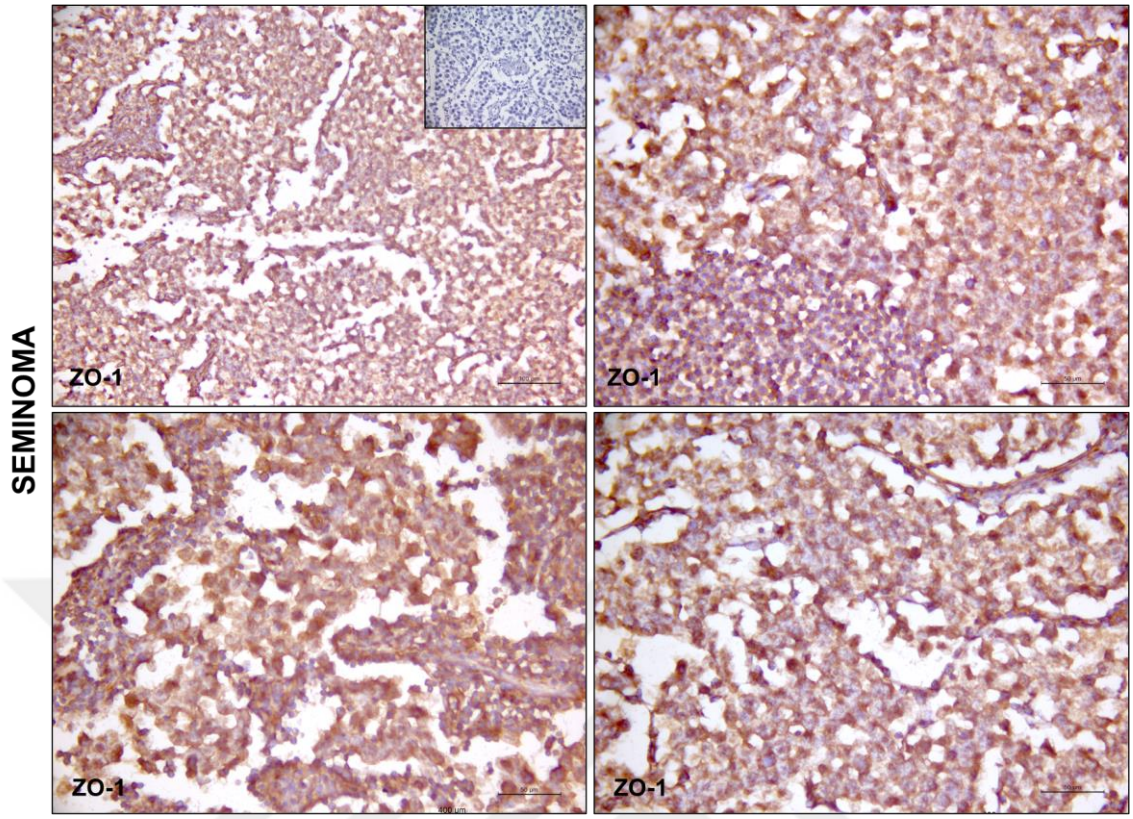

Figure 46. ZO-1 localization in human seminoma tissue is demonstrated by immunohistochemistry staining. There is no staining pattern in the negative control which is indicated in the insert image.

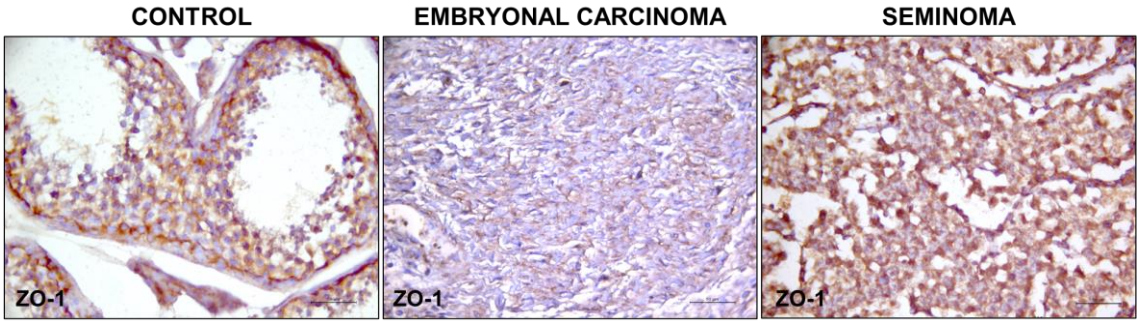

Figure 47. ZO-1 localization in human control, embryonal carcinoma and seminoma tissue is demonstrated by immunohistochemistry staining.

Table 6. Evaluation of the IHC scores of the tissues for testis. The scoring of the cells in the testicular tissue according to their staining intensities is as follows: +: absent, ++: faint, +++: moderate, ++++: strong.

	MST1/2	pMST1/2	LATS1/2	pLATS1/2	YAP1	pYAP1	TEAD4
Leydig Cell	++++	++	++	+	+++	+++	+++
Myoid Cell	+++	+	+	-	+++	+++	+++
Spermatogonium	+++	++	+++	+++	+++	++	+++
Spermatocyte	+++	++	+	+++	+++	++	+++
Round Spermatid	+++	++	++	++	++	+	+++
Elongated Spermatid	+	-	-	-	-	-	-
Endothelia	+++	+++	+	+	+++	++	+++

Table 7. Evaluation of the IHC scores of the tissues for embryonal carcinoma group. The scoring of the cells in the embryonal carcinoma tissue according to their staining intensities is as follows: +: absent, ++: faint, +++: moderate, ++++: strong.

	MST1/2	pMST1/2	LATS1/2	pLATS1/2	YAP1	pYAP1	TEAD4
Carcinoma Cell	+++	++	++	++	++++	+++	+++
Lymphocyte	-	-	-	-	-	-	-
Mitotic Cell	-	-	-	++++	+	-	-
Atypical Cell	+++	-	-	-	-	-	-
Neutrophil	++	-	-	-	-	-	-
Endothelia	++	++	++	-	++	++	++

Table 8. Evaluation of the IHC scores of the tissues for seminoma group. The scoring of the cells in the seminoma tissue according to their staining intensities is as follows: +: absent, ++: faint, +++: moderate, ++++: strong.

		MST1/2	pMST1/2	LATS1/2	pLATS1/2	YAP1	pYAP1	TEAD4
Seminoma	Cell	+++	+	+++	++	+++	++	++++
Lymphocyte		++++	+	++	+	-	+	++
Endothelia		-	+	+	+	+	+	++

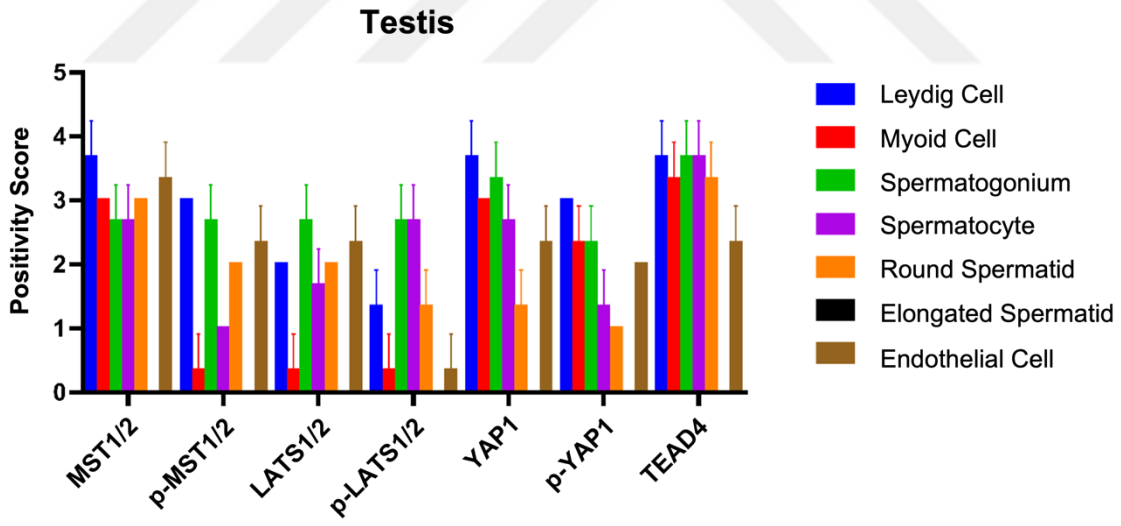

Figure 48. Immunopositivity scores of Hippo signaling pathway proteins in testis tissue.

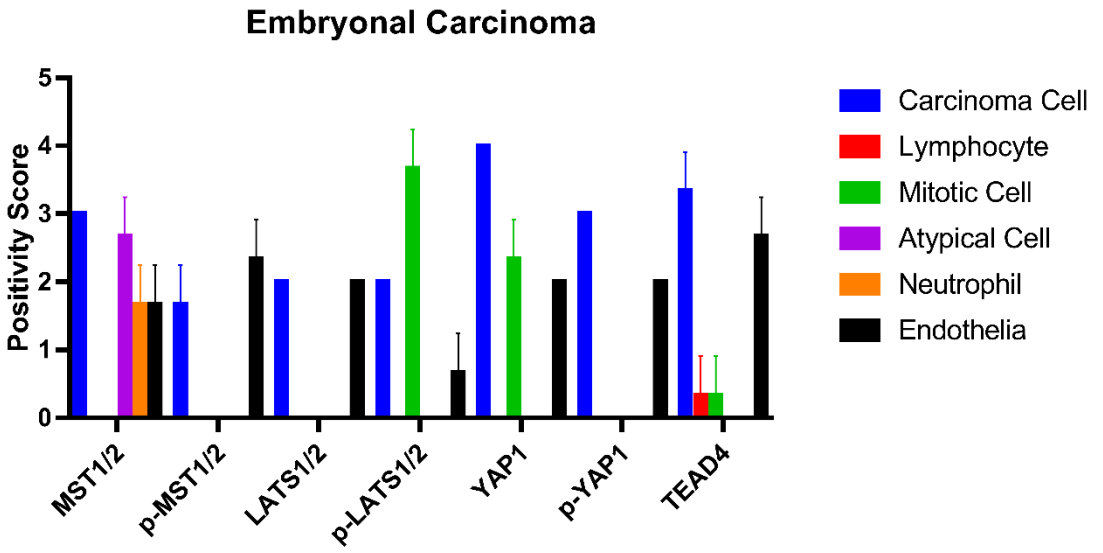

Figure 49. Immunopositivity scores of Hippo signaling pathway proteins in embryonal carcinoma tissue.

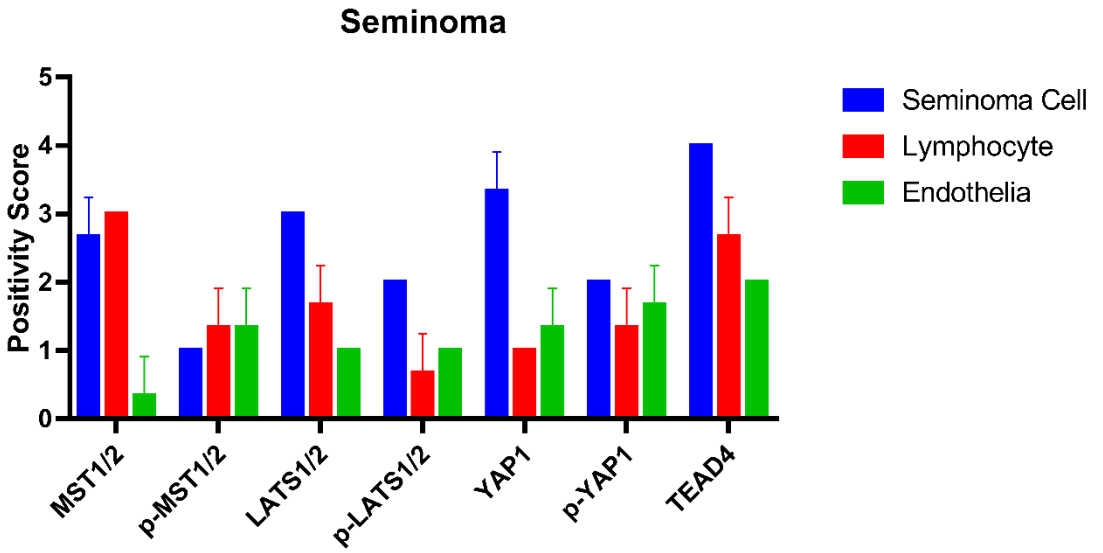

Figure 50. Immunopositivity scores of Hippo signaling pathway proteins in seminoma tissue.

4.3. Evaluation of Hippo Signaling Pathway Proteins by Western Blot

Protein expression levels obtained from TCam-2 cells were analyzed by western blot method. Expression of Hippo signaling pathway protein expression levels were determined in TCam-2 cells treated with different concentrations of verteporfin (control, 1 μM, 5 μM, 10 μM, 20 μM and 40 μM, verteporfin) for 24, 48 and 72 h. Results were confirmed using the β-actin internal control group. Intensities of signal pathway proteins were determined in experimental groups by western blot method. Verteporfin treatment caused significant decrease in protein levels of MST1/2, p-MST1/2, LATS1/2, p-LATS1/2, YAP1, p-YAP1 and TEAD4 dose- and time-dependent. When the duration of verteporfin treatment and the dosage of verteporfin increased, the negative effect of verteporfin on the protein levels increased.

MST 1/2 protein expression level decreased at 40 μM verteporfin dose compared to control, while there was no difference between groups in p-MST 1/2 protein level after 24 h of verteporfin treatment ($p<0.05$; Figure 51). Similarly, there was no difference in LATS1/2 protein level in TCam-2 cells. However, p-LATS1/2 protein level was decreased at 40 μM verteporfin dose compared to control ($p<0.05$; Figure 51). No difference was observed in YAP1 protein expression level. However, p-YAP1 protein expression level was decreased at 40 μM verteporfin dose compared to control (**$p<0.01$; Figure 51). Finally, TEAD4 protein expression levels were reduced at a dose of 40 μM verteporfin compared to control (**$p<0.01$; Figure 51).

After 48 h of verteporfin treatment, a decrease was found in MST1/2 and p-MST1/2 protein levels at 20 μM and 40 μM verteporfin doses compared to the control ($p<0.05$, ****$p<0.0001$; Figure 52). A decrease was demonstrated in TCam-2 cells at LATS1/2 protein levels at 1 μM and 40 μM verteporfin doses, and at p-LATS1/2 protein levels also at 40 μM verteporfin doses compared to the control ($p<0.05$, **$p<0.01$; Figure 52). YAP1 protein expression level was decreased at 5 μM, 20 μM and 40 μM verteporfin doses compared to control ($p<0.05$, **$p<0.01$, ****$p<0.0001$; Figure 52). Similarly, p-YAP1 protein level decreased in all verteporfin doses compared to control (**$p<0.01$, ***$p<0.001$, ****$p<0.0001$; Figure 52). Finally, TEAD4 protein expression level was shown to be decreased at 5 μM, 10 μM, 20 μM, and 40 μM verteporfin doses compared to control (****$p<0.0001$; Figure 52).

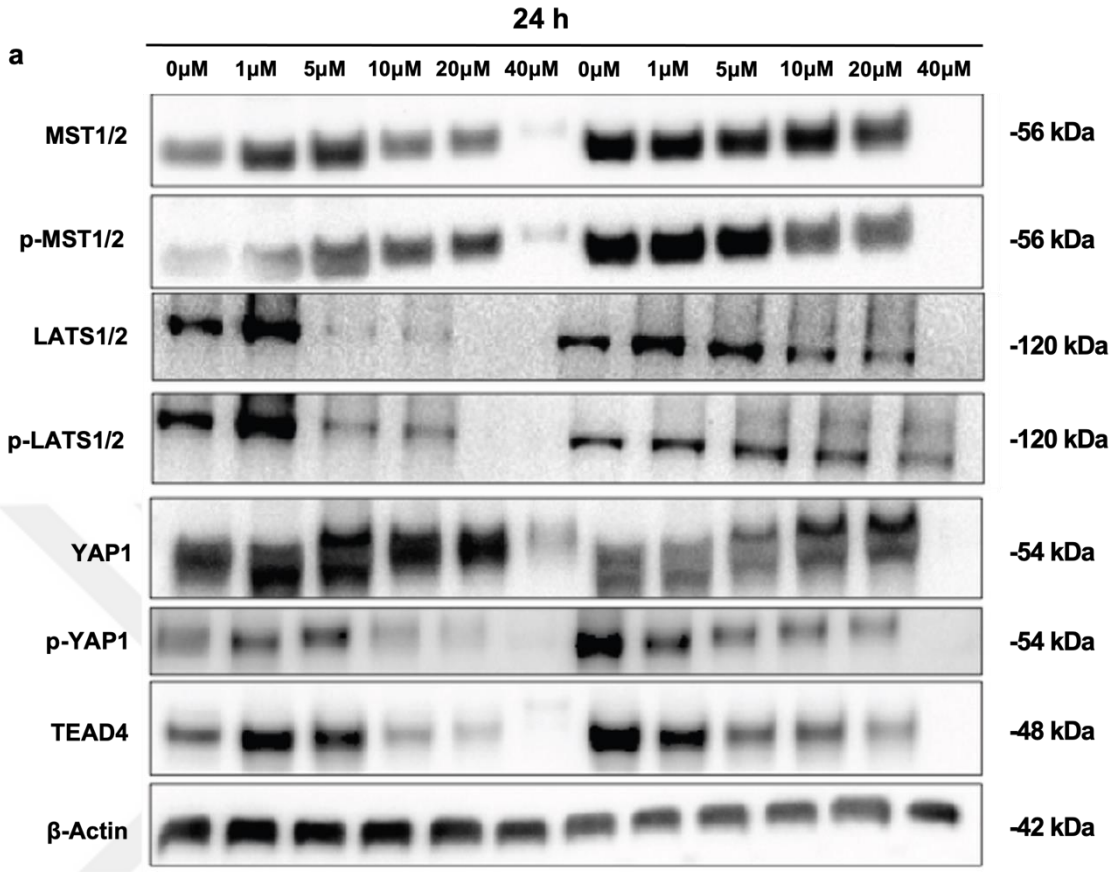
a
24 h
0μM 1μM 5μM 10μM 20μM 40μM 0μM 1μM 5μM 10μM 20μM 40μM
MST1/2
-56 kDa
p-MST1/2
-56 kDa
LATS1/2
-120 kDa
p-LATS1/2
-120 kDa
YAP1
-54 kDa
p-YAP1
-54 kDa
TEAD4
-48 kDa
β-Actin
-42 kDa

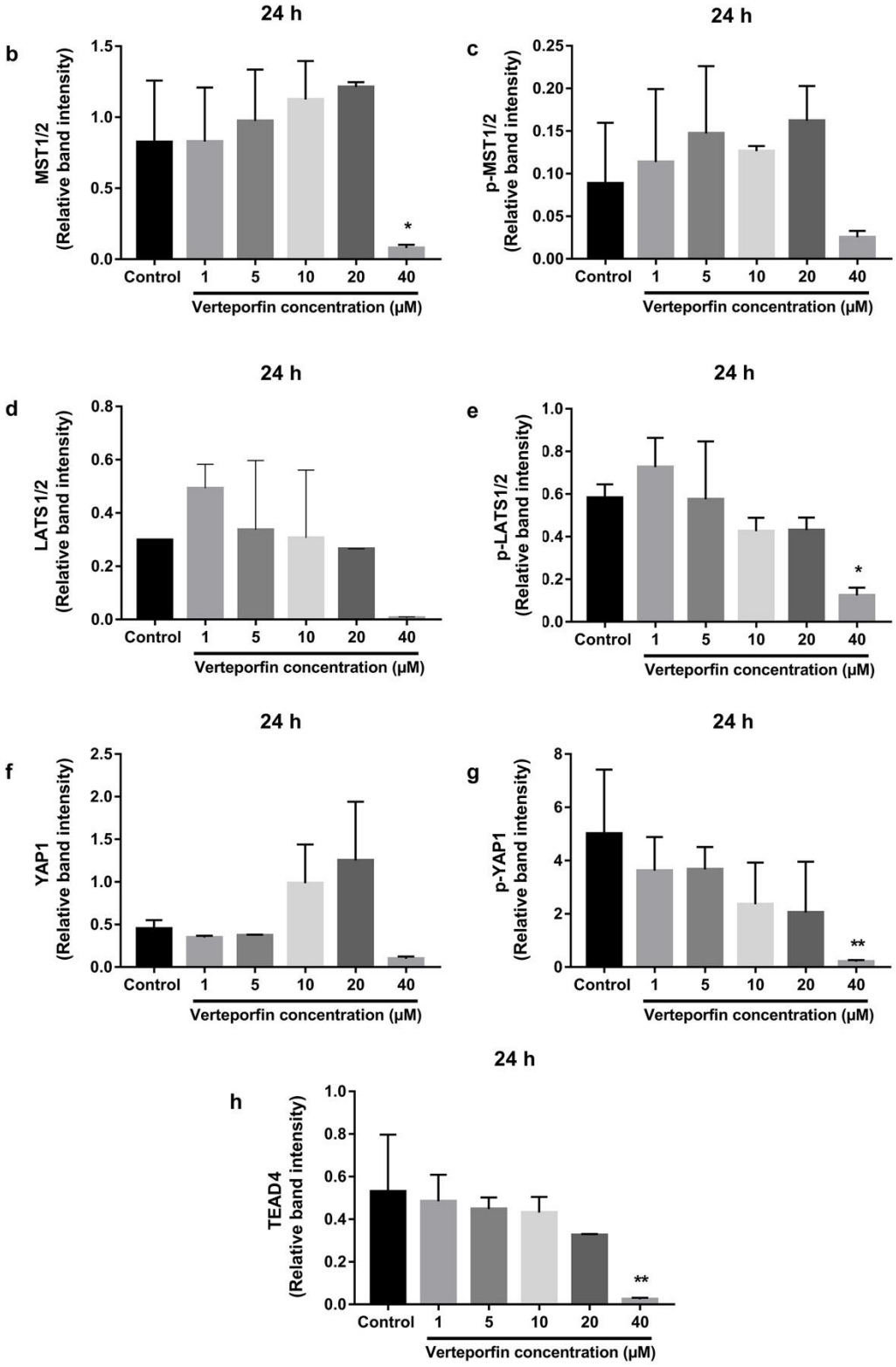

Figure 51. Results of the western blot experiment. a. Representative immunoblot image for MST1/2, p-MST1/2, LATS1/2, p-LATS1/2, YAP1, p-YAP1 and TEAD4 at control - 40 μM verteporfin doses at 24 h. b. MST1/2, c. p-MST/2, d. LATS1/2, e. p-LATS1/2, f. YAP1, g. p-YAP1 and h. TEAD4 protein expression levels (*$p<0.05$, **$p<0.01$).

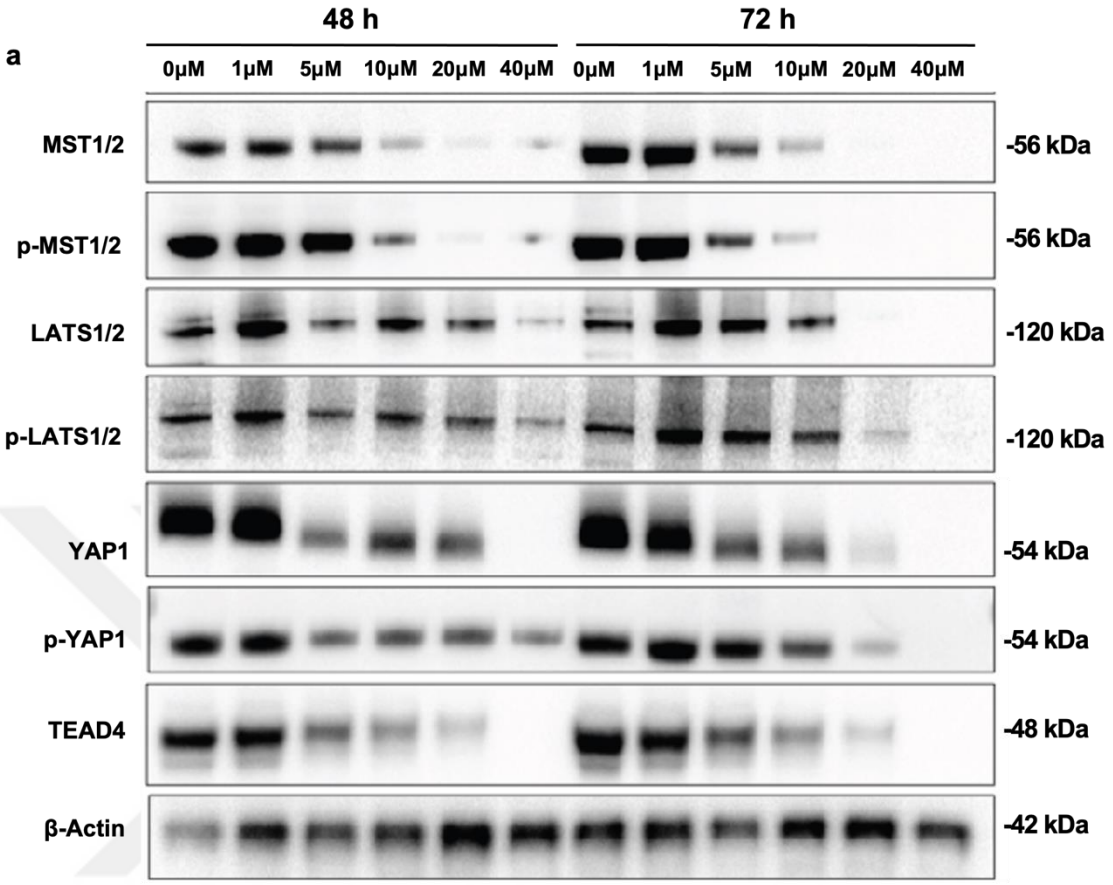
a
48 h
72 h
0μM 1μM 5μM 10μM 20μM 40μM 0μM 1μM 5μM 10μM 20μM 40μM
MST1/2
-56 kDa
p-MST1/2
-56 kDa
LATS1/2
-120 kDa
p-LATS1/2
-120 kDa
YAP1
-54 kDa
p-YAP1
-54 kDa
TEAD4
-48 kDa
β-Actin
-42 kDa

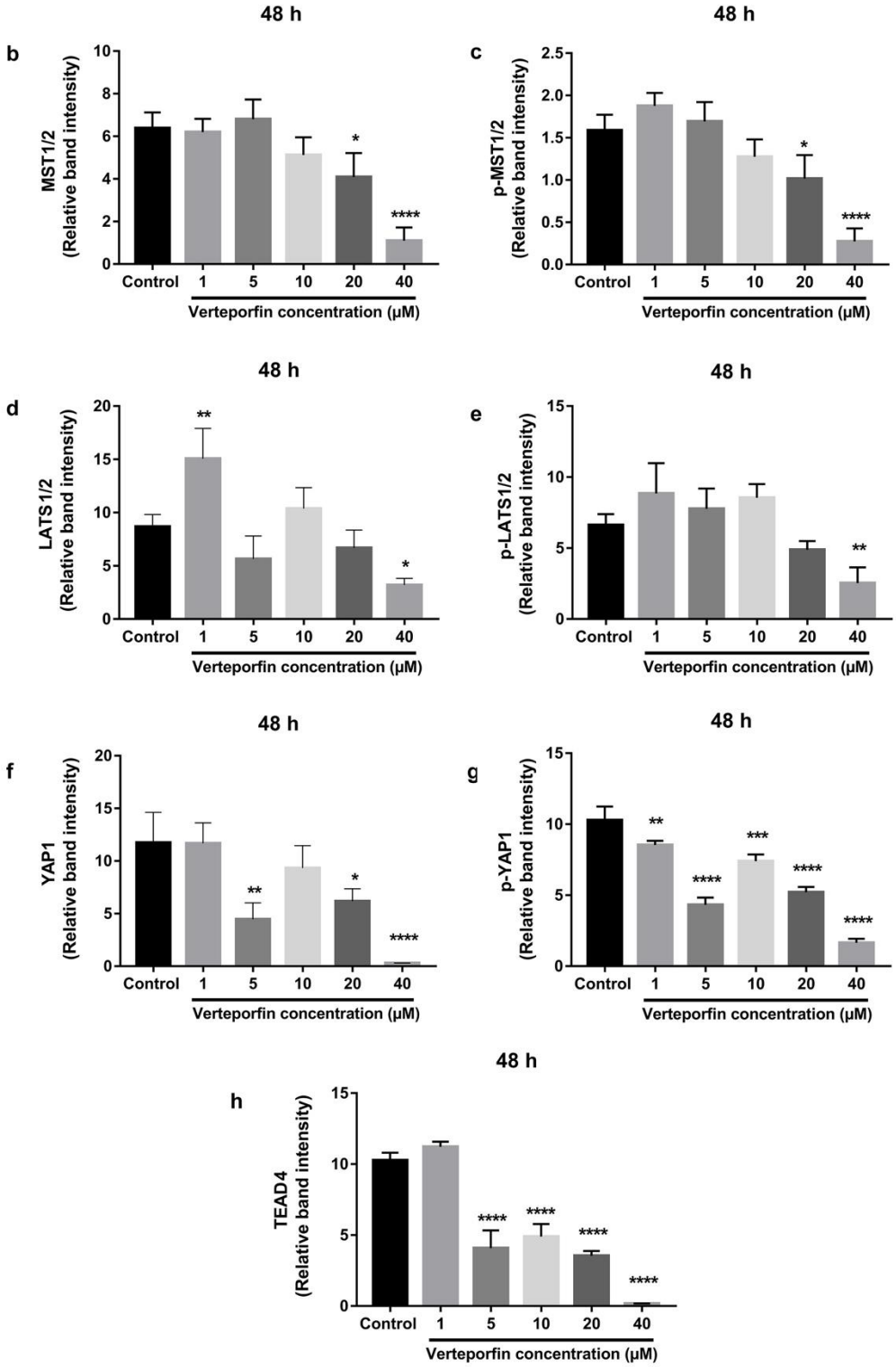

Figure 52. Results of the western blot experiment. a. Representative immunoblot image for MST1/2, p-MST1/2, LATS1/2, p-LATS1/2, YAP1, p-YAP1 and TEAD4 at control - 40 μM verteporfin doses at 24 h. b. MST1/2, c. p-MST/2, d. LATS1/2, e. p-LATS1/2, f. YAP1, g. p-YAP1 and h. TEAD4 protein expression levels (*p<0.05, **p<0.01, ***p<0.001, ****p<0.0001).

After 72 h of verteporfin treatment led to decrease in MST1/2 and p-MST1/2 protein levels only at the dose of 40 μM verteporfin compared to the control ($p<0.05$; Figure 53). A decrease in LATS1/2 protein levels at doses of 20 μM and 40 μM and p-LATS1/2 protein at a dose of 40 μM verteporfin compared to control ($p<0.05$; Figure 53). YAP1 protein expression level was reduced at all verteporfin doses compared to control (**$p<0.01$, ***$p<0.001$, ****$p<0.0001$; Figure 53). On the other hand, p-YAP1 protein level showed decrease in only 40 μM verteporfin dose compared to the control (**$p<0.01$; Figure 53). Finally, TEAD4 protein expression level was shown to be decreased at all verteporfin doses compared to control (***$p<0.001$, ****$p<0.0001$; Figure 53).

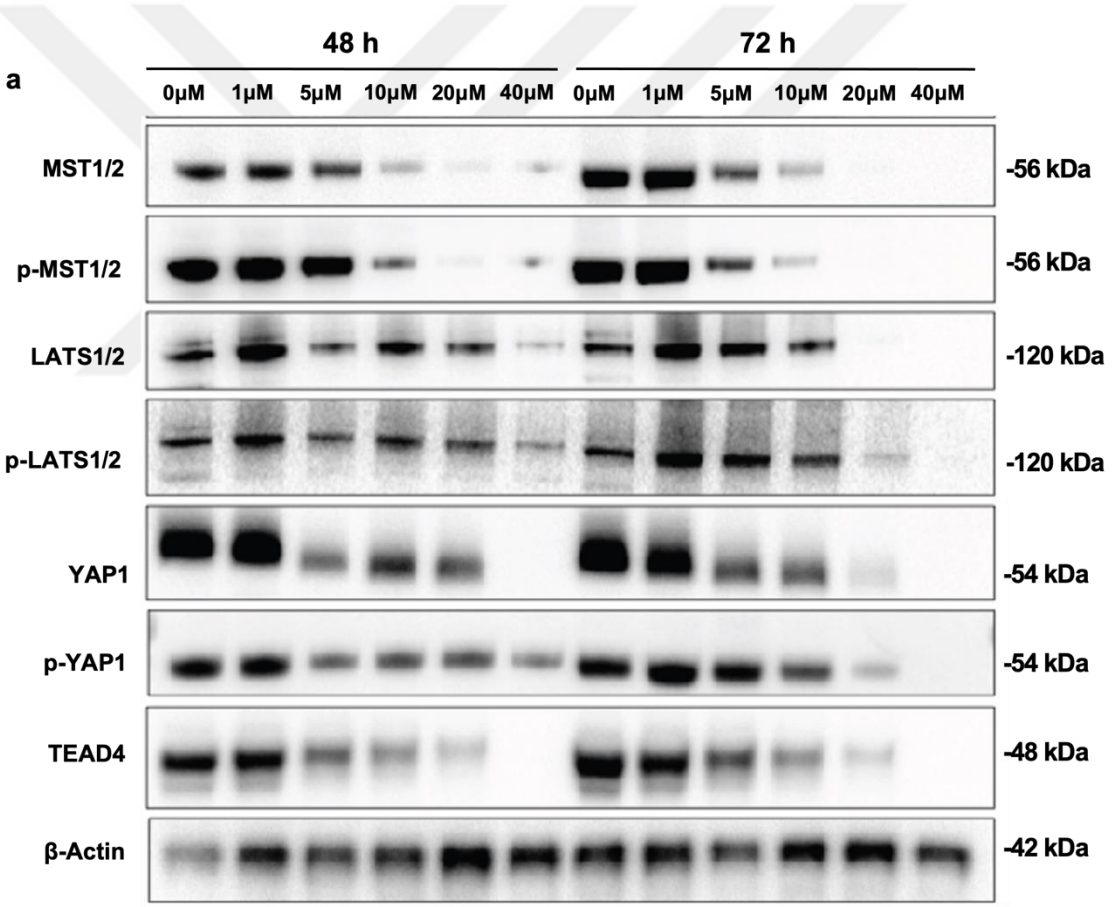

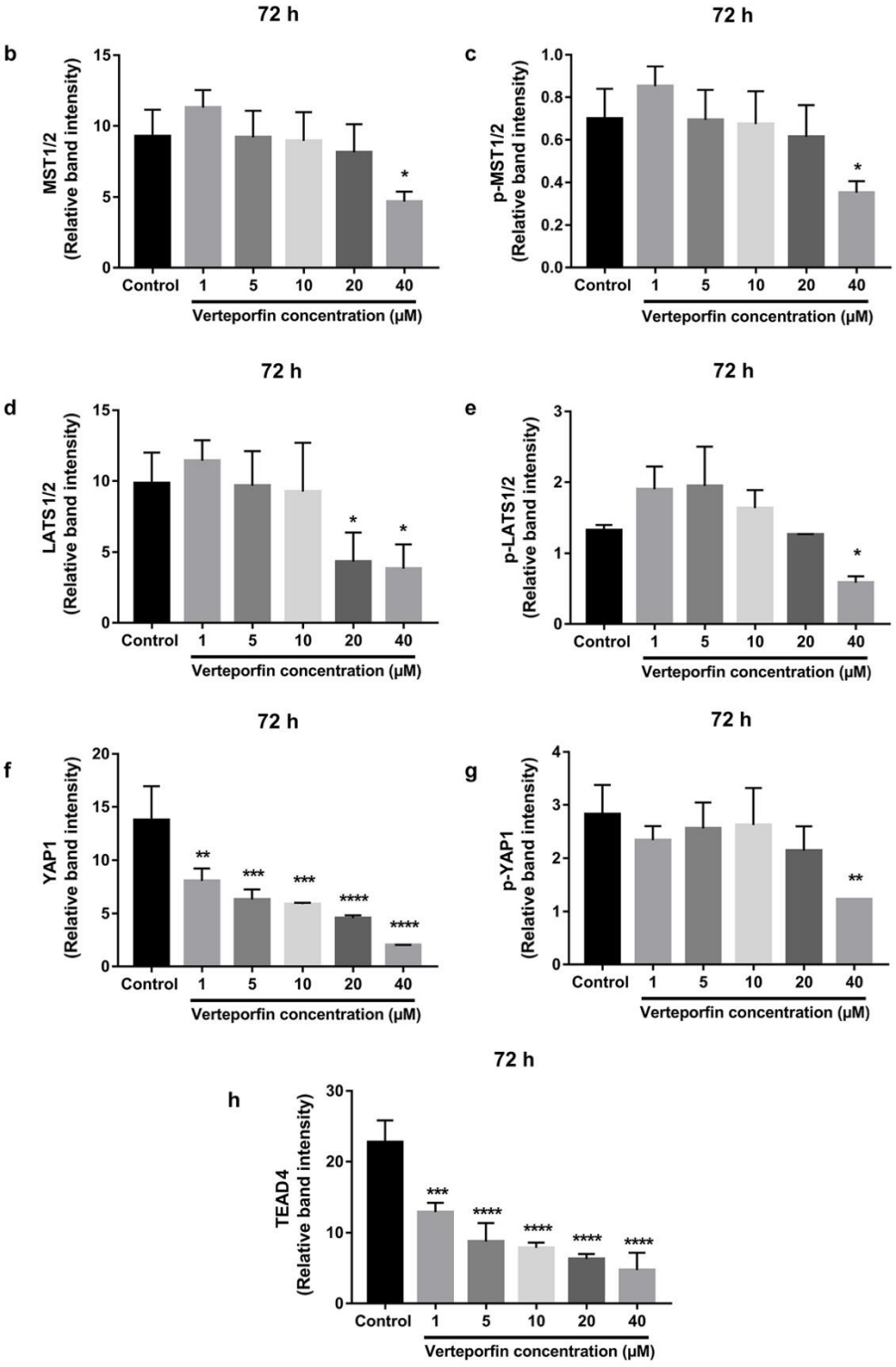

Figure 53. Results of the western blot experiment. a. Representative immunoblot image for MST1/2, p-MST1/2, LATS1/2, p-LATS1/2, YAP1, p-YAP1 and TEAD4 at control - 40 μM verteporfin doses at 24 h. b. MST1/2, c. p-MST/2, d. LATS1/2, e. p-LATS1/2, f. YAP1, g. p-YAP1 and h. TEAD4 protein expression levels (*p<0.05, **p<0.01, ***p<0.001, ****p<0.0001).

4.4. Confocal Microscopy Imaging of TCam-2 Cells

Immunofluorescence staining was performed at specific concentration (control, 1 μM, 5 μM, 10 μM, 20 μM, and 40 μM) at 24 h determine the localization of MST1/2, p-MST1/2, LATS1/2, p-LATS1/2, YAP1, p-YAP1 and TEAD4 in TCam-2 cells.

Protein localization obtained from TCam-2 cells were determined immunofluorescence staining by confocal microscopy. Expression of Hippo signaling pathway protein localization was determined in TCam-2 cells treated with different concentrations of verteporfin (control, 1 μM, 5 μM, 10 μM, 20 μM and 40 μM, verteporfin) for 24 h.

After 24 h of incubation, MST1/2 protein localization showed nuclear pattern in control group. 24 h after treatment of 1 μM verteporfin, MST1/2 protein localization showed a nuclear staining pattern similar to control. After treatment of higher doses of verteporfin, 5 μM and 10 μM, MST1/2 protein localization was observed in the strong nuclear and perinuclear area between the nucleus and the cytoplasm. After treatment dose of 20 μM and 40 μM verteporfin, most TCam-2 cells appear to be deformed in structure and distorted morphology. MST1/2 protein localization could not be detected (Figure 54).

After 24 h of incubation, p-MST 1/2 showed nuclear protein localization in the control group and after treatment of 1 μM verteporfin. After 24 h of 5 μM and 10 μM verteporfin treatment, p-MST1/2 protein localization was strong in the nucleus and weak in the cytoplasm. After a treatment dose of 20 μM and 40 μM verteporfin, most TCam-2 cells appear to be structurally deformed and morphologically impaired. p-MST1/2 protein localization could not be detected (Figure 55).

After 24 h of incubation, LATS1/2 showed nuclear protein localization in the control group. After 24 h of 1 μM and 5 μM and 10 μM verteporfin treatment, LATS1/2 protein localization was detected in the nucleus and cytoplasm. After a treatment dose of 20 μM and 40 μM verteporfin, most TCam-2 cells appear to be structurally deformed and morphologically impaired. LATS1/2 protein localization could not be detected (Figure 56).

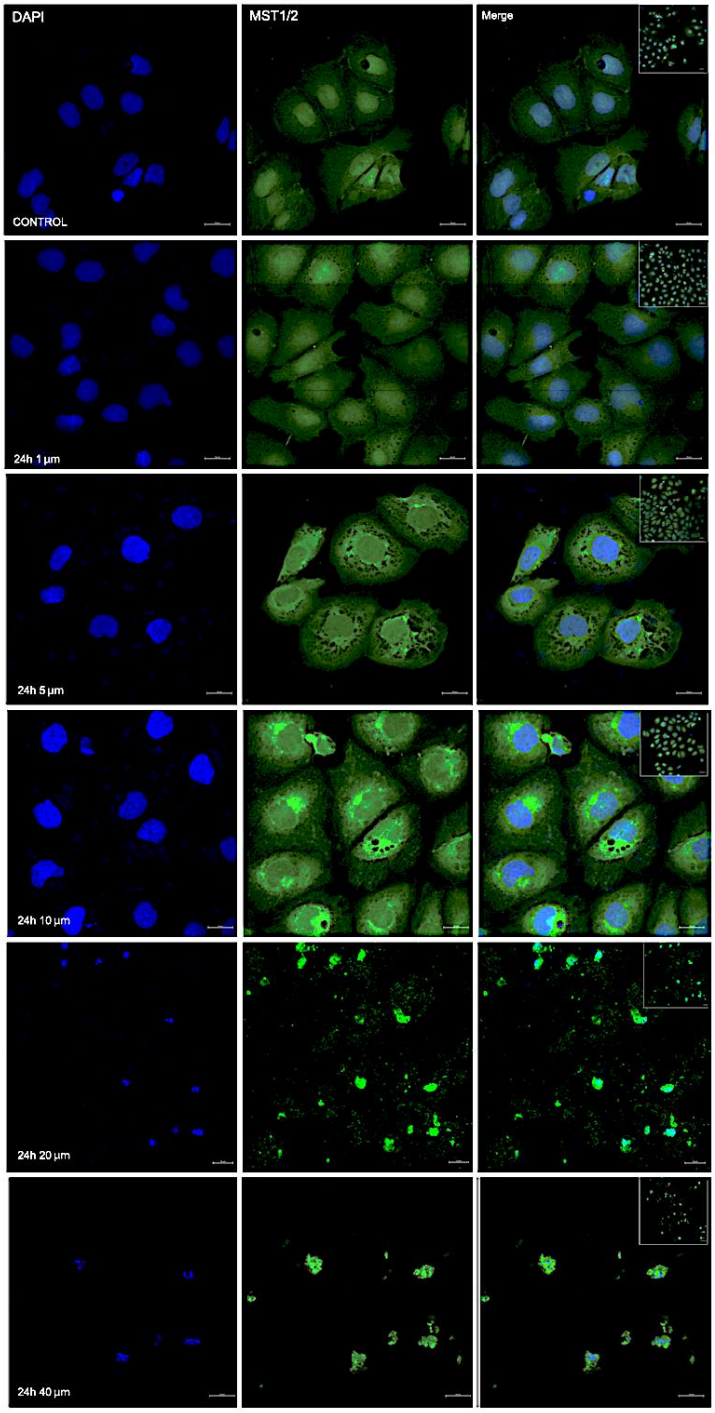

Figure 54. The above confocal microscope images, the control group observed the protein localization of MST1/2 in TCam-2 cells 24 h after 1 µM, 5 µM, 10 µM, 20 µM, and 40 µM verteporfin treatment. Image of TCam-2 cells under a confocal microscope with a 63X objective. Additional images were taken with a 20X objective. DAPI stained cell nuclei. There is no staining pattern in the negative control which is indicated in the insert image.

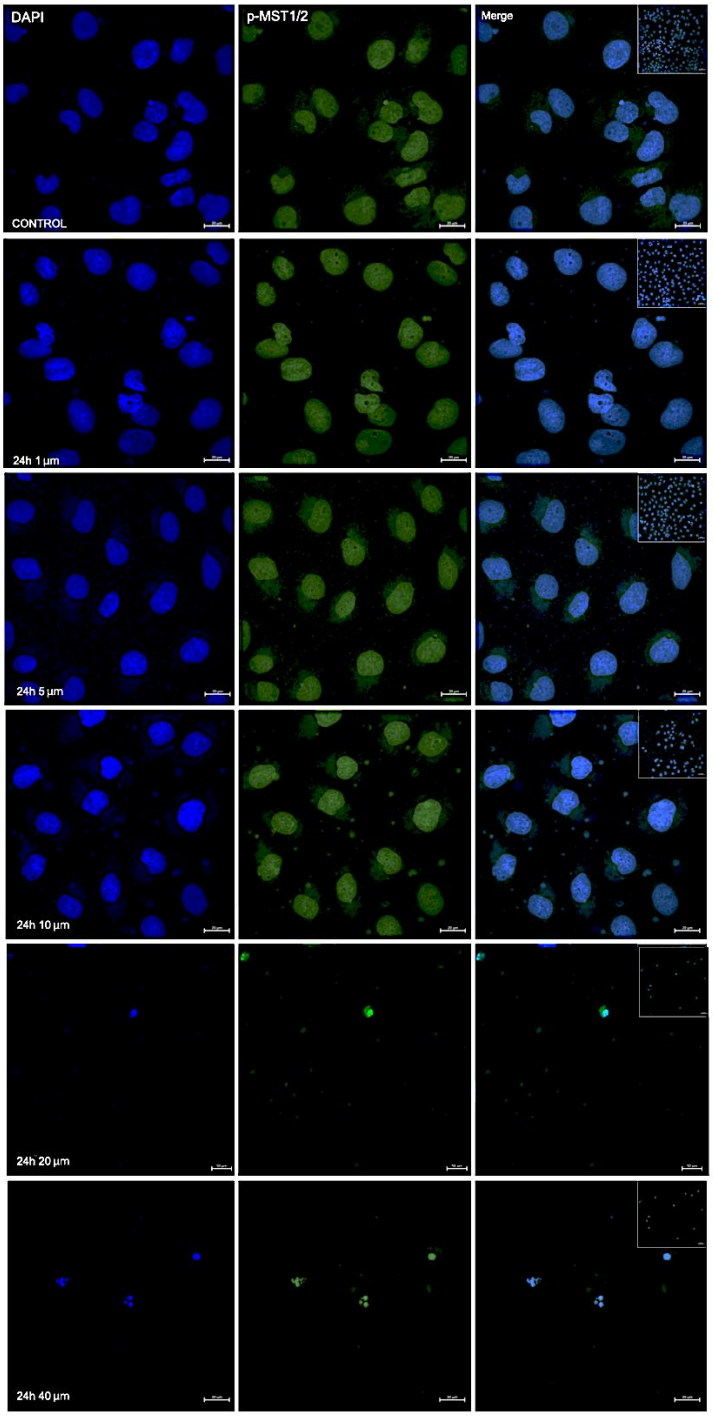

Figure 55. The above confocal microscope images, the control group observed the protein localization of p-MST1/2 in TCam-2 cells 24 h after 1 µM, 5 µM, 10 µM, 20 µM, and 40 µM verteporfin treatment. Image of TCam-2 cells under a confocal microscope with a 63X objective. Additional images were taken with a 20X objective. DAPI stained cell nuclei. There is no staining pattern in the negative control which is indicated in the insert image.

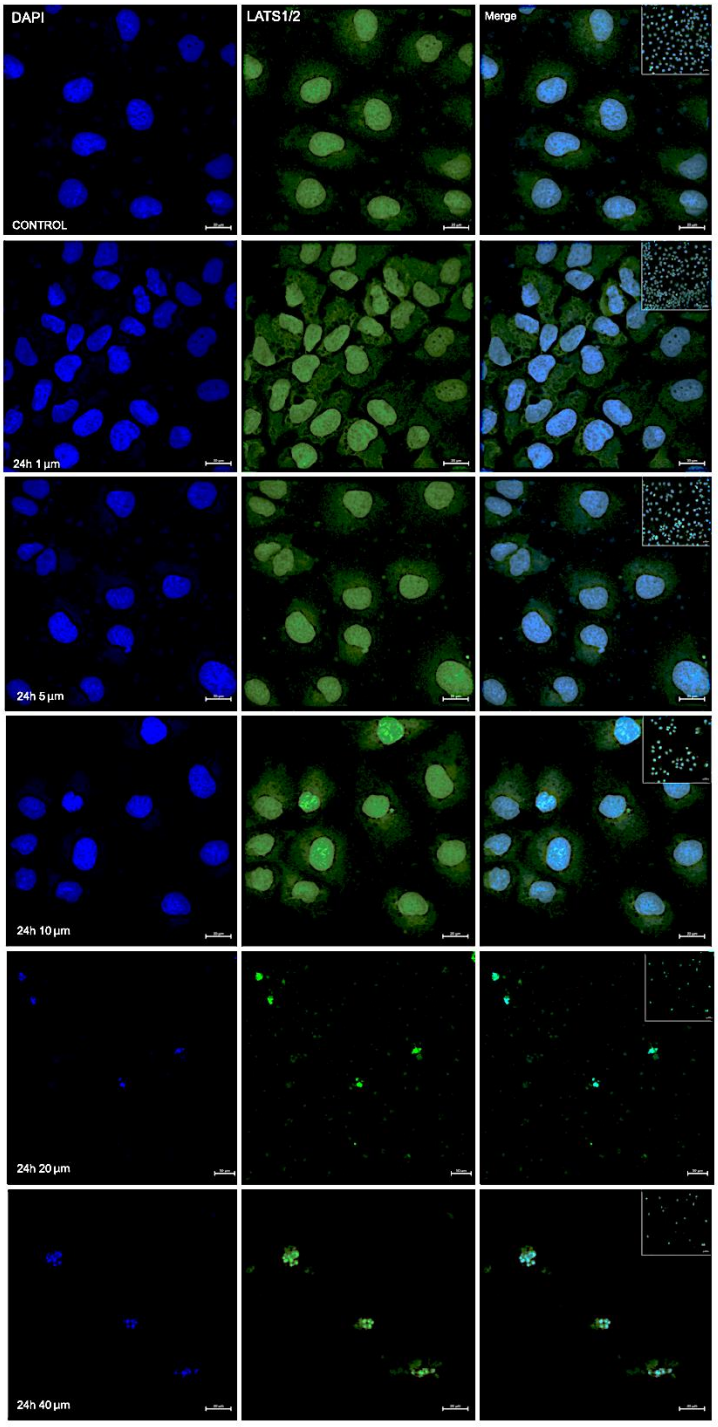

Figure 56. The above confocal microscope images, the control group observe the protein localization of LATS1/2 in TCam-2 cells 24 h after 1 µM, 5 µM, 10 µM, 20 µM, and 40 µM verteporfin treatment. Image of TCam-2 cells under a confocal microscope with a 63X objective. Additional images were taken with a 20X objective. DAPI stained cell nuclei. There is no staining pattern in the negative control which is indicated in the insert image.

After 24 h of incubation, p-LATS1/2 showed intense nuclear weak cytoplasmic protein localization in the control group. After 24 h treatment of 1, 5 and 10 μM verteporfin, p-LATS1/2 protein localization was detected weak in the cytoplasm and strong in the nucleus, similar to the control. After treatment with 20 μM and 40 μM verteporfin, most TCam-2 cells appear to be structurally deformed and morphologically impaired. p-LATS1/2 protein localization could not be detected (Figure 57).

After 24 h of incubation, YAP1 showed intense nuclear weak cytoplasmic protein localization in the control group. After 24 h treatment of 1, 5 and 10 μM verteporfin, YAP1 protein localization was detected weak in the cytoplasm and strong in the nucleus, similar to the control. After treatment with 20 μM and 40 μM verteporfin, most TCam-2 cells appear to be structurally deformed and morphologically impaired. YAP1 protein localization could not be detected (Figure 58).

After 24 h of incubation, p-YAP1 protein localization showed nuclear pattern in control group. 24 h after treatment of 1 μM verteporfin, p-YAP1 protein localization showed a nuclear staining pattern similar to control. After treatment of higher doses of verteporfin, 5 μM and 10 μM, p-YAP1 protein localization was observed in the strong nuclear and weak cytoplasm. After treatment dose of 20 μM and 40 μM verteporfin, most TCam-2 cells appear to be deformed in structure and distorted morphology. p-YAP1 protein localization could not be detected (Figure 59).

After 24 h of incubation, TEAD4 showed both nuclear and cytoplasmic protein localization in control group. Similarly, after 24 h treatment of 1 μM 5 μM and 10 μM verteporfin treatment, TEAD4 protein localization showed nuclear and cytoplasmic pattern in TCam-2 cells. Especially, TEAD4 localization after 5 μM and 10 μM verteporfin administration showed both a strong nuclear and cytoplasmic pattern in cells. Following administration of verteporfin with 20 μM and 40 μM, most TCam-2 cells appear to be structurally deformed and morphologically impaired. TEAD4 protein localization could not be detected (Figure 60).

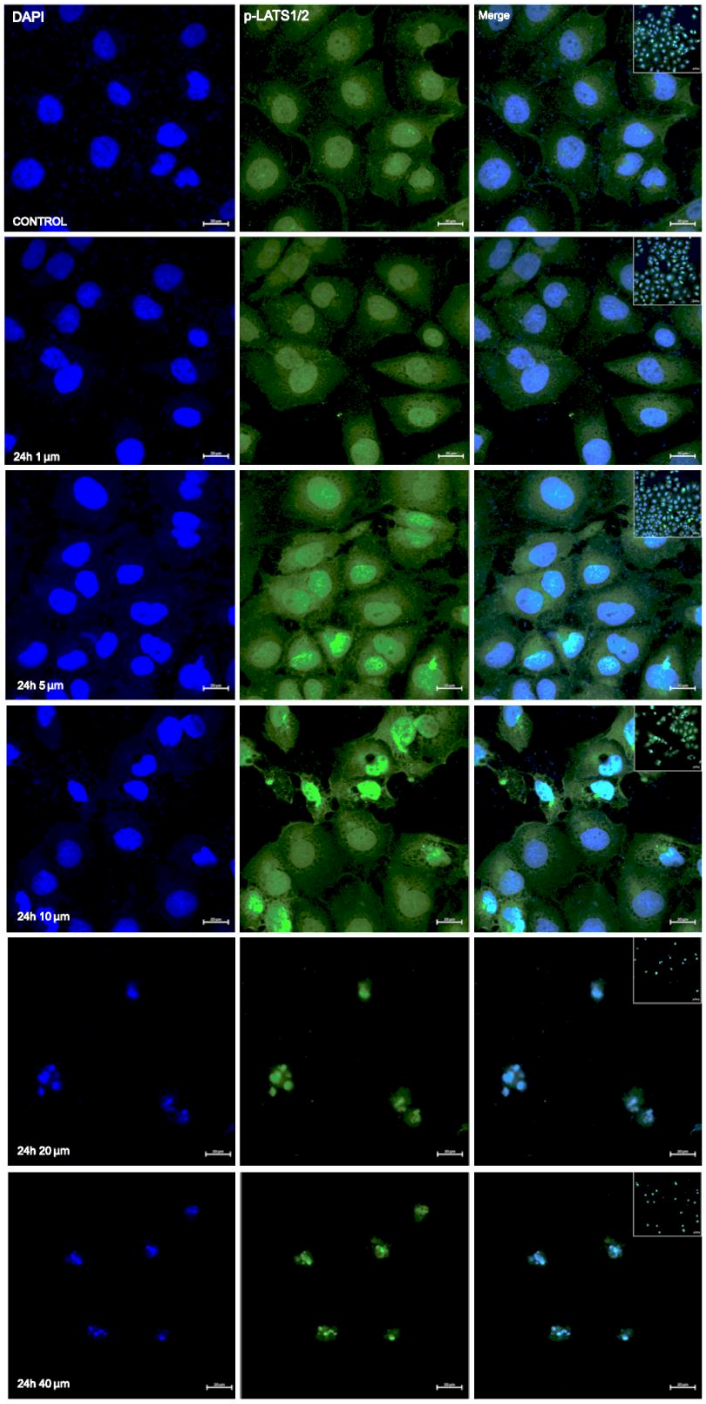

Figure 57. The above confocal microscope images, the control group observe the protein localization of p-LATS1/2 in TCam-2 cells 24 h after 1 µM, 5 µM, 10 µM, 20 µM, and 40 µM verteporfin treatment. Image of TCam-2 cells under a confocal microscope with a 63X objective. Additional images were taken with a 20X objective. DAPI stained cell nuclei. There is no staining pattern in the negative control which is indicated in the insert image.

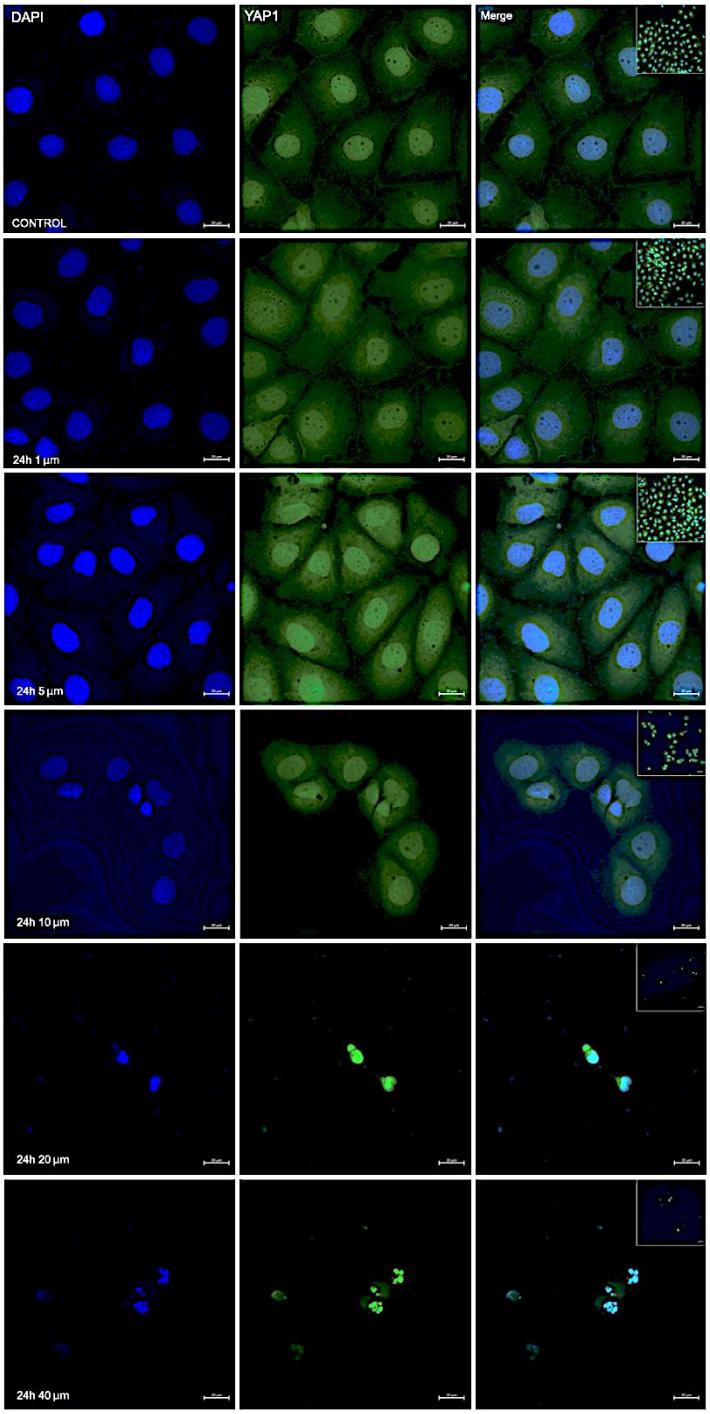

Figure 58. The above confocal microscope images, the control group observe the protein localization of YAP1 in TCam-2 cells 24 h after 1 µM, 5 µM, 10 µM, 20 µM, and 40 µM verteporfin treatment. Image of TCam-2 cells under a confocal microscope with a 63X objective. Additional images were taken with a 20X objective. DAPI stained cell nuclei. There is no staining pattern in the negative control which is indicated in the insert image.

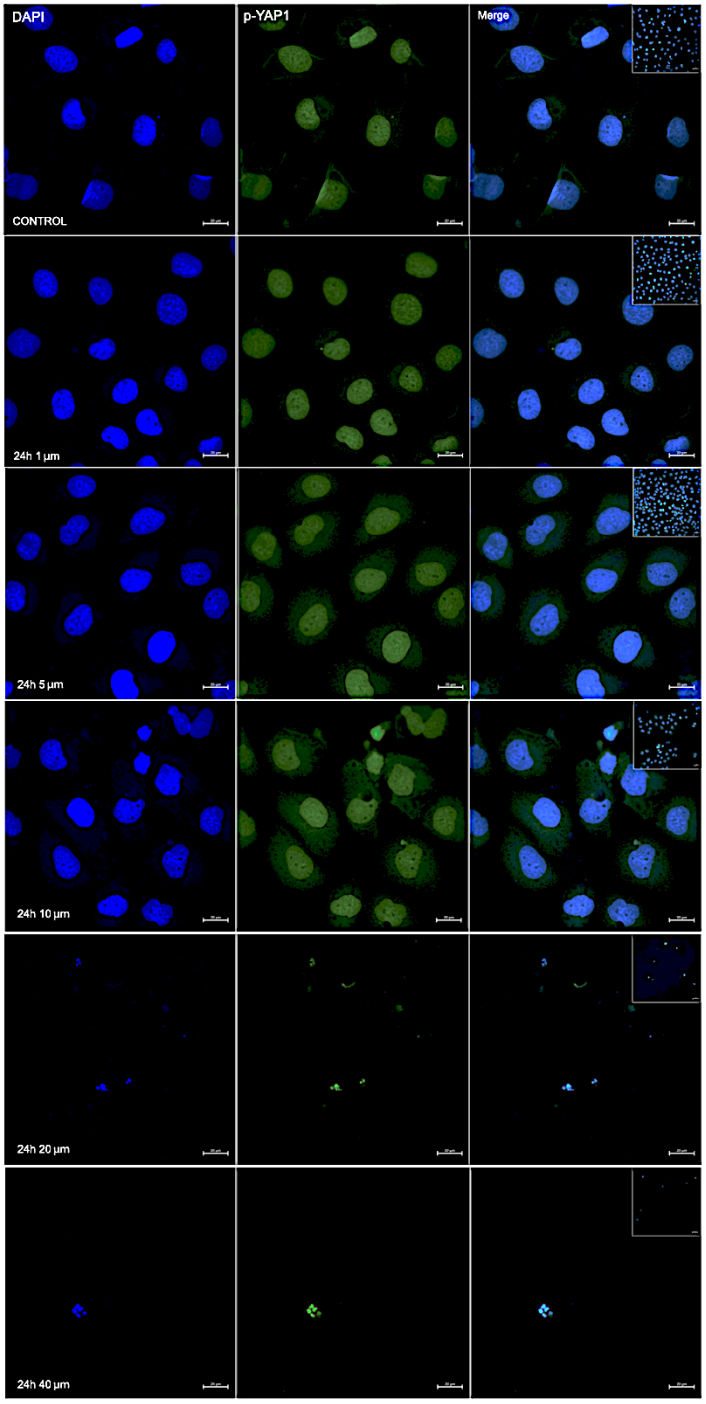

Figure 59. The above confocal microscope images, the control group observe the protein localization of p-YAP1 in TCam-2 cells 24 h after 1 µM, 5 µM, 10 µM, 20 µM, and 40 µM verteporfin treatment. Image of TCam-2 cells under a confocal microscope with a 63X objective. Additional images were taken with a 20X objective. DAPI stained cell nuclei. There is no staining pattern in the negative control which is indicated in the insert image.

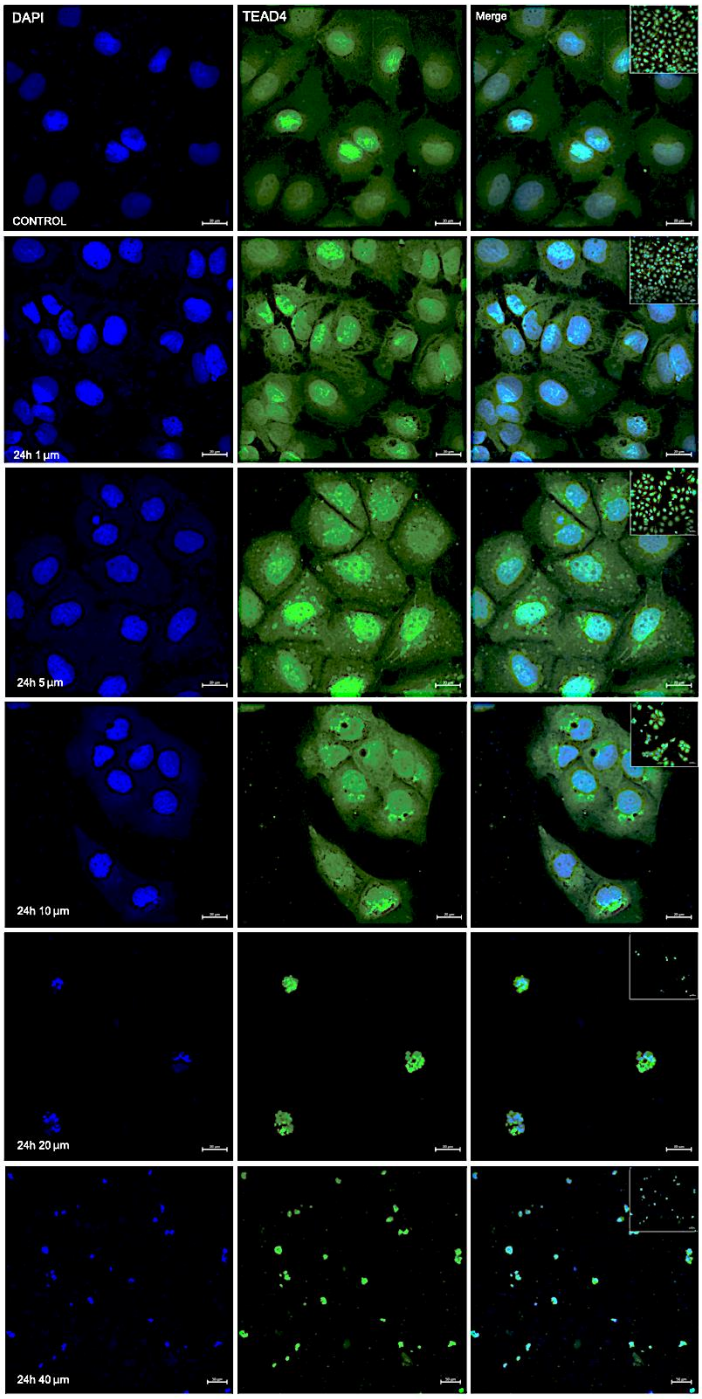

Figure 60. The above confocal microscope images, the control group observe the protein localization of TEAD4 in TCam-2 cells 24 h after 1 µM, 5 µM, 10 µM, 20 µM, and 40 µM verteporfin treatment. Image of TCam-2 cells under a confocal microscope with a 63X objective. Additional images were taken with a 20X objective. DAPI stained cell nuclei. There is no staining pattern in the negative control which is indicated in the insert image.

4.5. Effect of Verteporfin Treatment on the Expression of the Hippo Pathway mRNA Expression Levels

mRNAs obtained from TCam-2 cells were translated into cDNA by RT-PCR method and amplified. Expression of Hippo signaling pathway genes was determined in TCam-2 cells treated with different concentrations of verteporfin (control (no verteporfin treatment), 1 μM, 5 μM, 10 μM, 20 μM and 40 μM, verteporfin) for 24, 48 and 72 h.

After 24 h of verteporfin treatment, no difference was observed in the expression of *MST1*, *MST2*, *LATS1*, *LATS2*, *YAP1* and *TEAD4* mRNA expression levels in TCam-2 cells compared to control at doses of 1, 5, 10, 20 and 40 μM verteporfin (Figure 61).

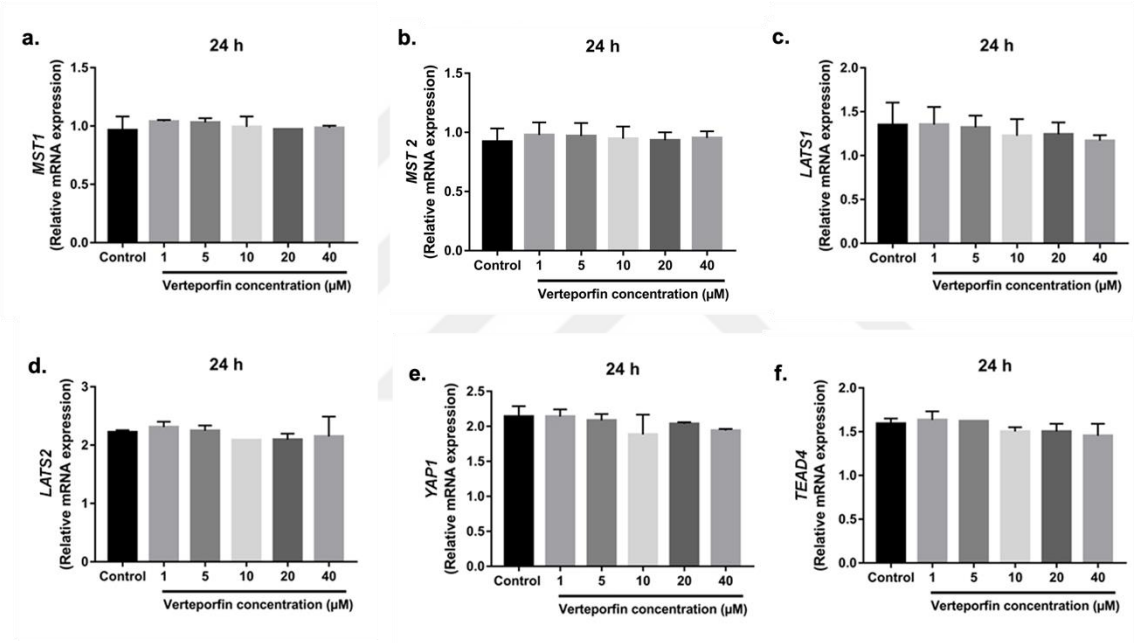

Figure 61. Results of the qRT-PCR experiment. ***a.*** *MST1*, ***b.*** *MST2*, ***c.*** *LATS1*, ***d.*** *LATS2*, ***e.*** *YAP1* and ***f.*** *TEAD4* mRNA expression levels.

After 48 h of verteporfin treatment, no difference was observed in the expression of *MST1*, *MST2*, *LATS1*, *LATS2* and *YAP1* mRNA expression levels in TCam-2 cells compared to control at doses of 1, 5, 10, 20 and 40 μM verteporfin (Figure 62a, b, c, e). After 48 h of verteporfin treatment, only *TEAD4* mRNA expression level was decreased at 20 and 40 μM compared to control ($p<0.05$, $^{**}p<0.01$; Figure 62d).

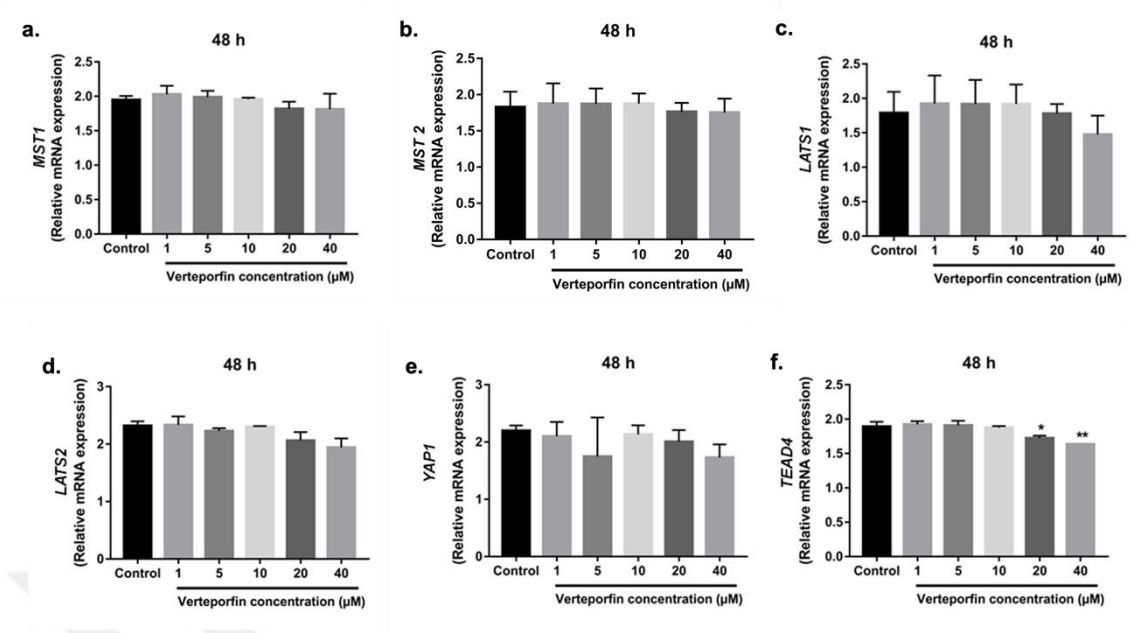

Figure 62. Results of the qRT-PCR experiment. ***a.*** *MST1,* ***b.*** *MST2,* ***c.*** *LATS1,* ***d.*** *LATS2,* ***e.*** *YAP1* and ***f.*** *TEAD4* mRNA expression levels ($p<0.05$, $^{**}p<0.01$).

After 72 h of verteporfin treatment, no difference was observed in the expression of *MST1*, *MST2*, *LATS1*, *LATS2* and *YAP1* mRNA expression levels in TCam-2 cells compared to control at doses of 1, 5, 10, 20 and 40 μM verteporfin (Figure 63a, b, c, e). After 72 h of verteporfin treatment, only *TEAD4* mRNA expression level was decreased at 20 and 40 μM compared to control ($^{**}p<0.01$, $^{***}p<0.001$; Figure 63d).

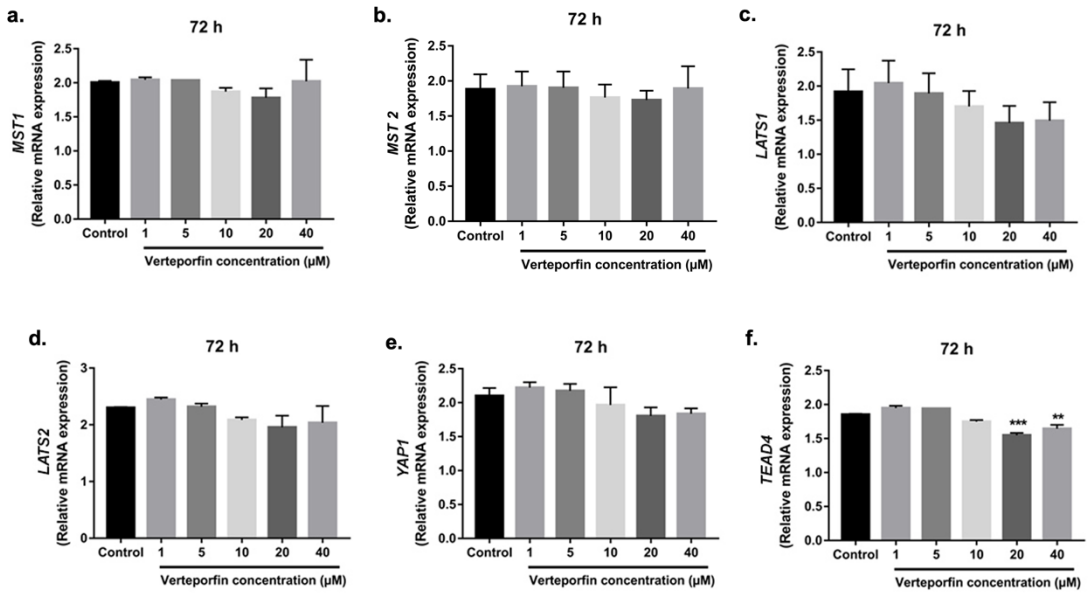

Figure 63. Results of the RT-PCR experiment. ***a.*** *MST1,* ***b.*** *MST2,* ***c.*** *LATS1,* ***d.*** *LATS2,* ***e.*** *YAP1* and ***f.*** *TEAD4* mRNA expression levels (**p<0.01, ***p<0.001).

4.6. Effect of Verteporfin Treatment on the Cell Counts

The Hippo pathway is a highly conserved signaling pathway that controls organ size, tissue homeostasis, and cancer development. In mammals, the Hippo pathway consists of the MST1/2, LATS1/2, YAP1 and its transcriptional cofactor TAZ. Verteporfin has been proven to inhibit the YAP–TEAD complex in studies and has been shown to have a potential role in anticancer therapy. In thesis study, TCam-2 cells were treated with different concentrations of verteporfin (control, 1 μM, 5 μM, 10 μM, 20 μM, and 40 μM, verteporfin) for 24, 48 and 72 h. Afterwards, cell counting were performed for all groups to determine the effect of verteporfin on number of TCam-2 cell.

After 24 h of verteporfin treatment, number of TCam-2 cell was decreased at 1, 5, 10, 20 and 40 μM, compared to control (****p<0.0001; Figure 64b). After 48 h of verteporfin treatment, the number of TCam-2 cell was decreased in 1, 5, 10, 20 and 40 μM, verteporfin treatment compared to control (***p<0.001, ****p<0.0001; Figure 64b). Similarly, after 72 h of verteporfin treatment, the number of TCam-2 cell was decreased in 1, 5, 10, 20 and 40 μM, verteporfin treatment compared to control (**p<0.01, ****p<0.0001; Figure 64c).

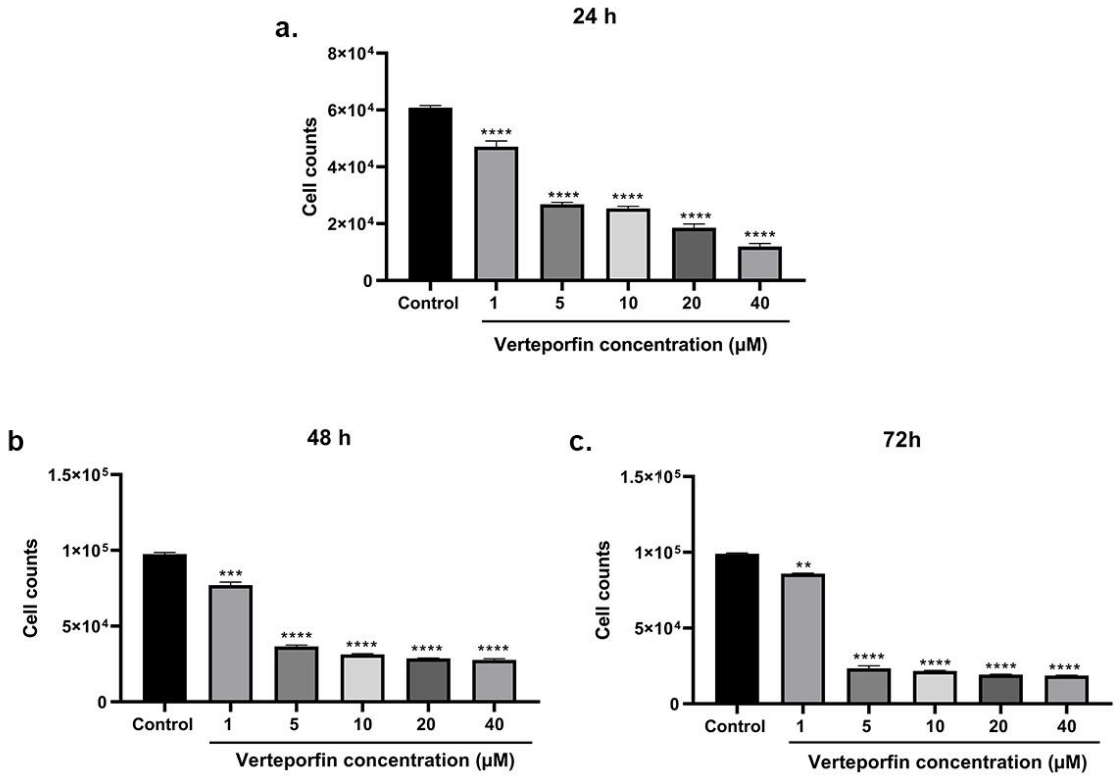

Figure 64. Effect of verteporfin on cell counts at a.24 h, b.48 h and c.72 h. ($p<0.05$, $^{**}p<0.01$, $^{****}p<0.0001$).

4.7. Effect of Verteporfin Treatment on the Cell Migration

To investigate whether 24, 48, and 72 h incubation of verteporfin at concentrations of 1, 5, 10, 20, and 40 μm affects TCam-2 cell migration, insertion-based scratch migration experiments of TCam-2 were performed. When the control group and verteporfin groups were evaluated in terms of migration, we could not perform a quantitative evaluation at these doses, since verteporfin doses of 10 μM and above caused the cells to lose their adhesion and migration properties in 24, 48 and 72 h of verteporfin applications.

We observed that 1, 5, 10 μM verteporfin treatment had no effect on migration in 24 h. Verteporfin incubation of 20 and 40 μm for 24 h has been shown to negatively affect migration in TCam-2 cells. At these doses the cells appear to have lost contact with the surface. High verteporfin concentrations induced TCam-2 cell death and decreased migration (Figure 65).

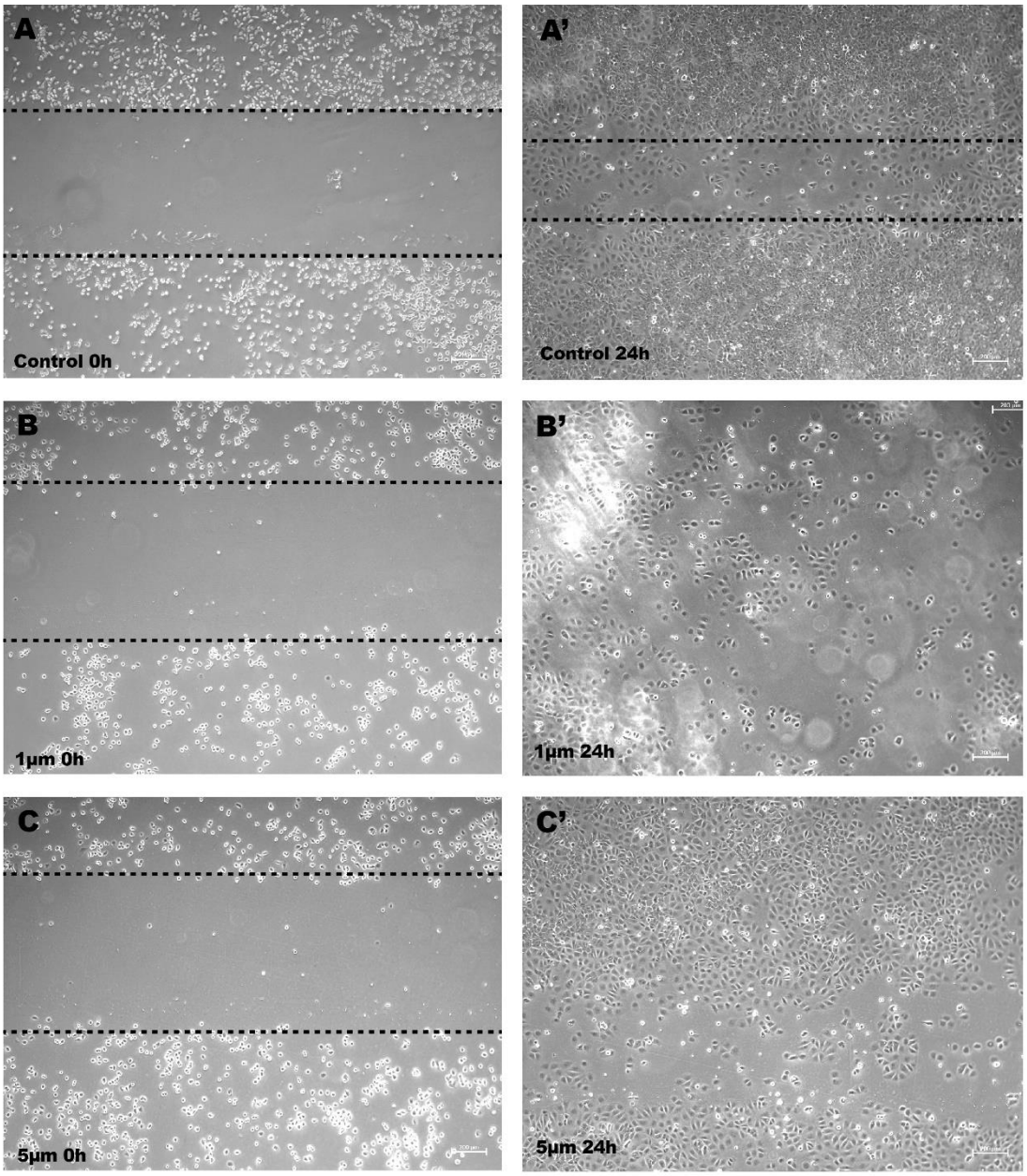
A
Control 0h
A'
Control 24h
B
1µm 0h
B'
1µm 24h
C
5µm 0h
C'
5µm 24h

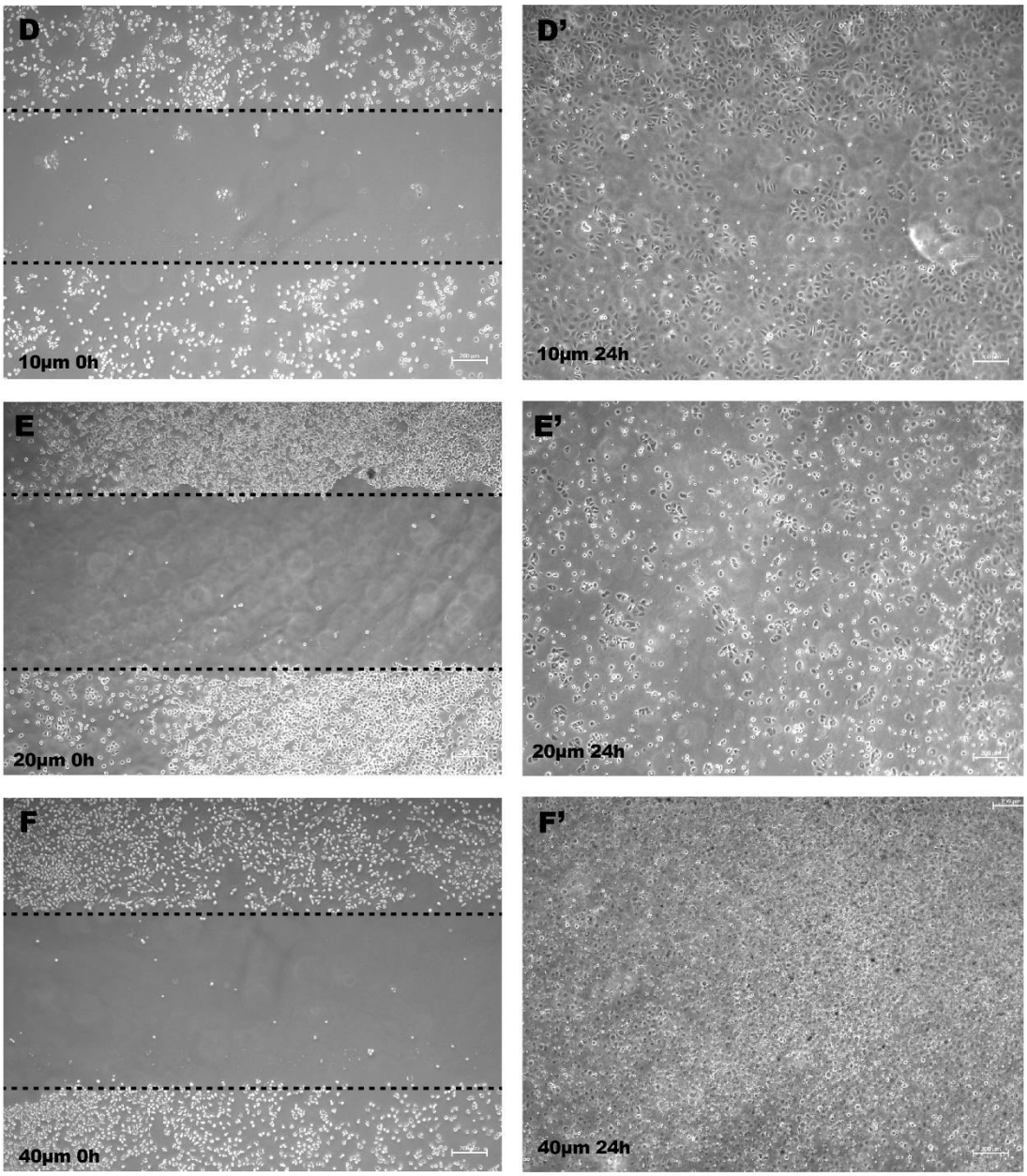

Figure 65. Verteporfin inhibits the migration of TCam-2 cells. The insert-based scratch migration assay. After 24 h of verteporfin treatment, TCam-2 migration was decreased at 10, 20 and 40 µM compared to control.

Verteporfin incubation of 1, 5 µm for 48 h has been shown to negatively affect migration in TCam-2 cells. At these doses the cells appear to have lost contact with the surface. 10, 20 and 40 µm verteporfin concentrations induced TCam-2 cell death and decreased migration (Figure 66).

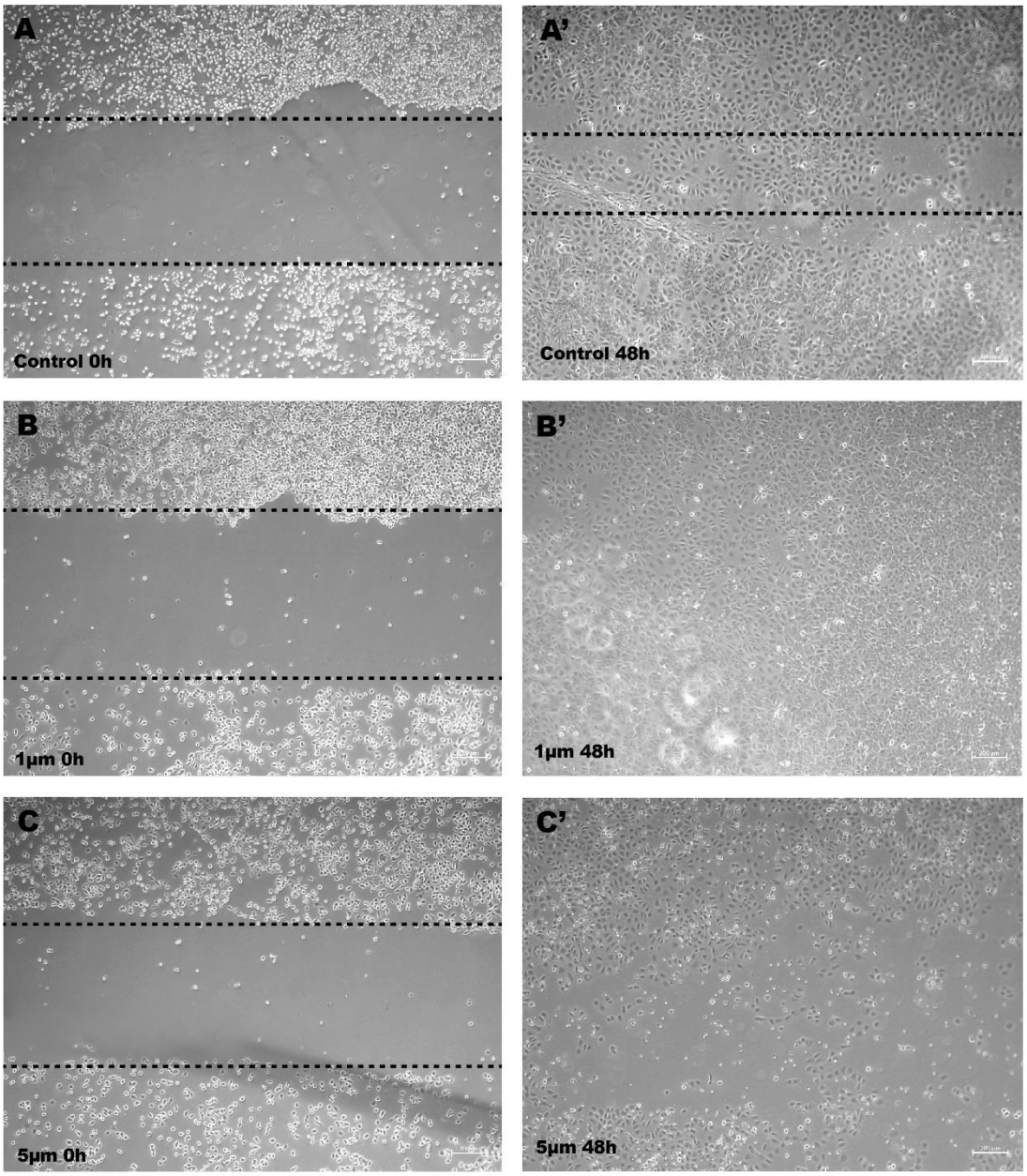
A
Control 0h
A'
Control 48h
B
1µm 0h
B'
1µm 48h
C
5µm 0h
C'
5µm 48h

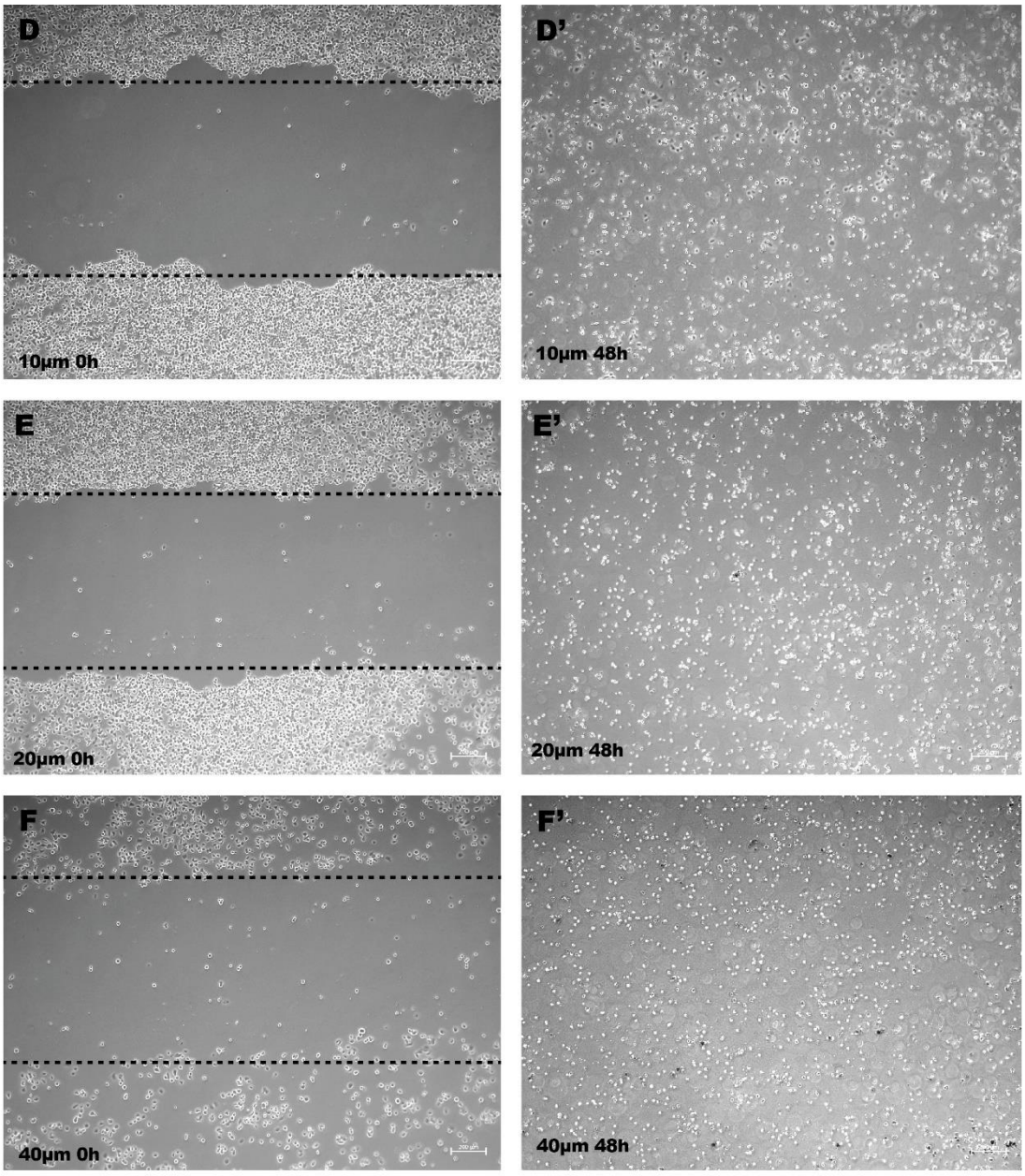

Figure 66. Verteporfin inhibits the migration of TCam-2 cells. The insert-based scratch migration assay. After 48 h of verteporfin treatment, TCam-2 migration was decreased at 5, 10, 20 and 40 µM compared to control.

Similar to the 48 h verteporfin treatment results, it has been shown that verteporfin treatment of 1 µm for 72 h has a negative effect on migration in TCam-2 cells. At these doses the cells appear to have lost contact with the surface. 5, 10, 20 and 40 µm verteporfin concentrations induced TCam-2 cell death and decreased migration (Figure 67).

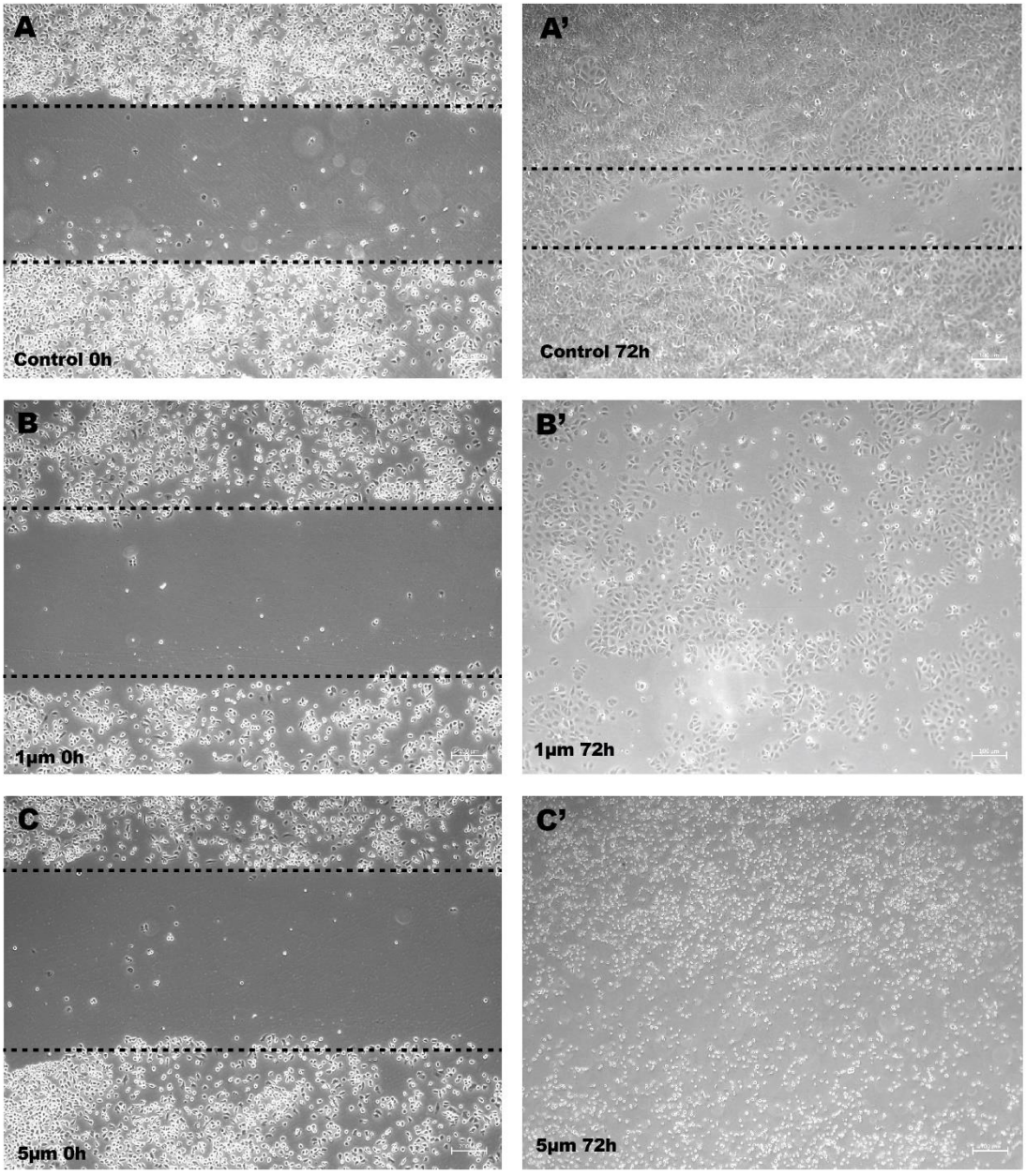
A
Control 0h
A'
Control 72h
B
1µm 0h
B'
1µm 72h
C
5µm 0h
C'
5µm 72h

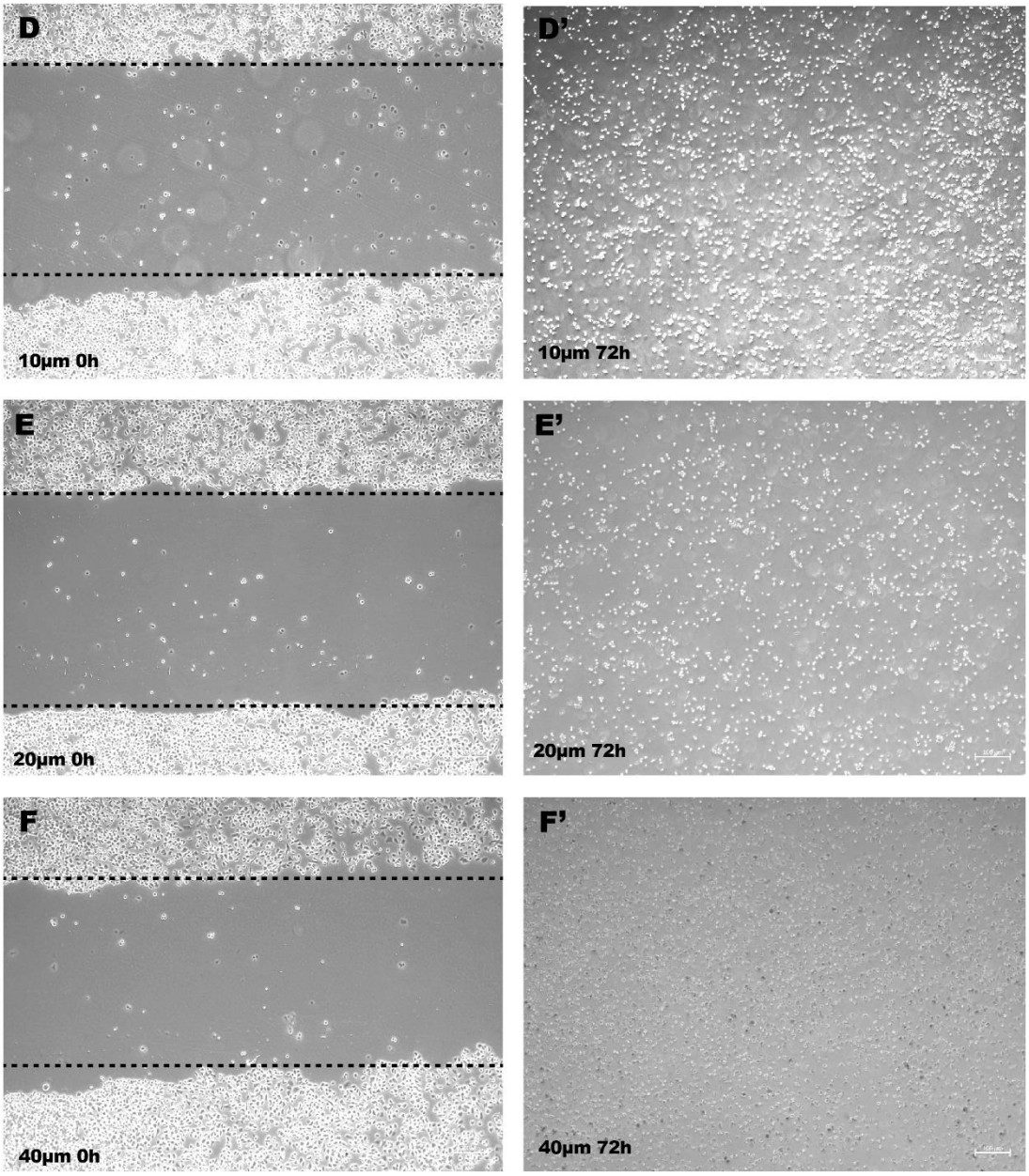

Figure 67. Verteporfin insert-based scratch migration assay. The insert-based scratch migration assay. After 72 h of verteporfin treatment, TCam-2 migration was decreased at 5, 10, 20 and 40 µM compared to control.

4.8. Effect of Verteporfin Treatment on Apoptosis

TCam-2 cells were treated with different concentrations of verteporfin (control 1 µM, 5 µM, 10 µM, 20 µM and 40 µM) for 24, 48 and 72 h. In our thesis study effect of verteporfin treatment at the indicated concentrations and time points on TCam-2 cell

viability, early-late apoptosis, and necrosis rate. The apoptotic effect of verteporfin mediated YAP1 inhibition was evaluated by Annexin V/PI staining after 24, 48 and 72 h.

When the control group and verteporfin groups were evaluated in terms of apoptosis and cell viability, it was shown that cell viability decreased significantly and the apoptosis rate increased depending on the dose increase. There was decrease in cell viability between the verteporfin groups and the control group in 24 h verteporfin treatment (****$p<0.0001$; Figure 68a, b). In addition to cell viability, early and late apoptosis rates were also evaluated between the control and verteporfin groups. When the control and verteporfin groups were evaluated in 24 h verteporfin treatment, there was no difference in early apoptosis in the control and 1 μM and 40 μM verteporfin groups, but an increase was observed between the other groups. When the late period apoptosis rates were evaluated in 24 h verteporfin treatment, increase was observed between the control and verteporfin groups (**$p<0.01$, ***$p<0.001$, ****$p<0.0001$; Figure 68a, d). Finally, necrosis rates were also evaluated between the control and verteporfin groups. When the control and verteporfin groups were evaluated in 24 h verteporfin administration, increase was observed in the 1uM verteporfin group compared to the control ($p<0.05$, Figure 68a, e), but there was difference between the other groups.

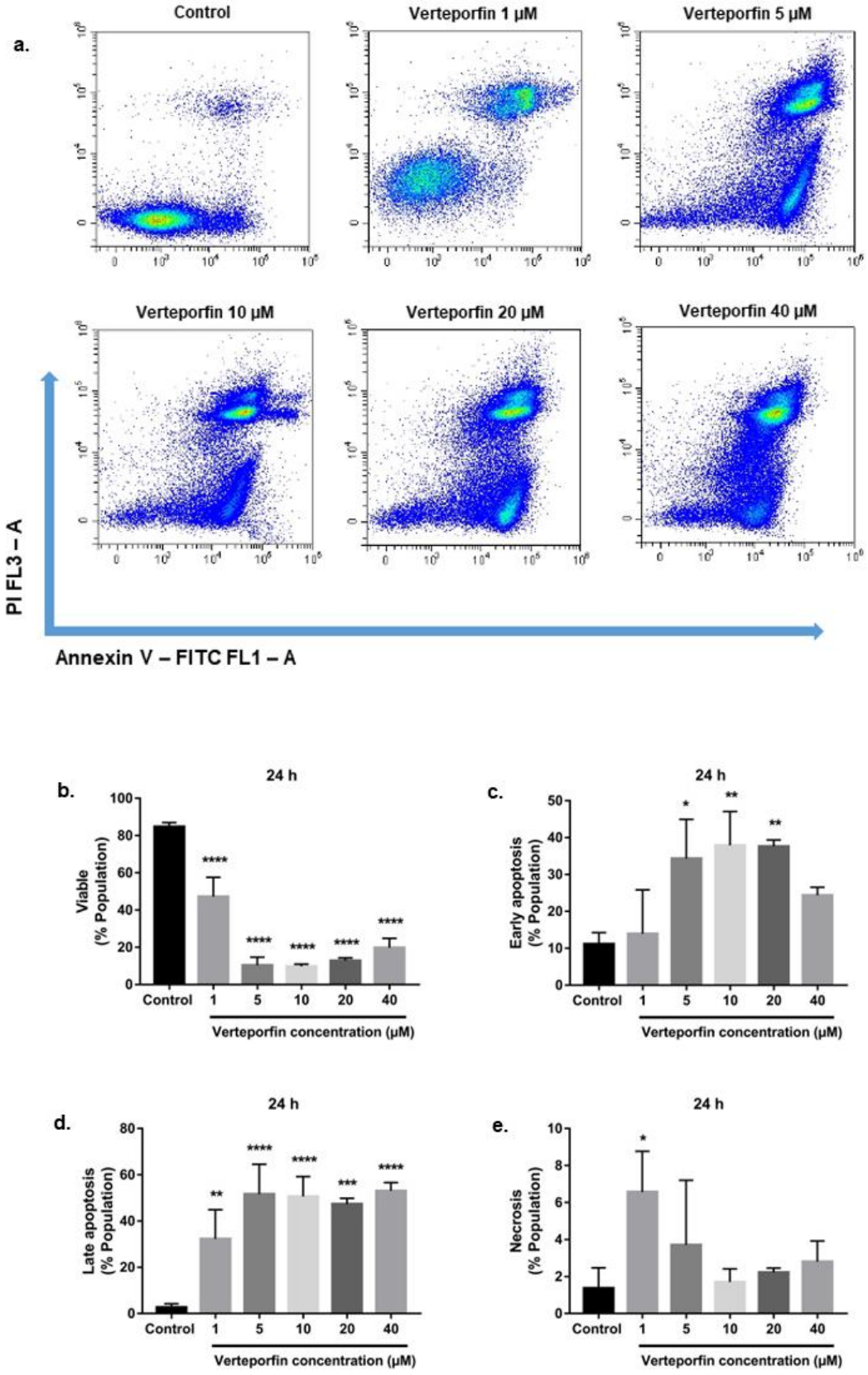

Figure 68. a. Representative flow cytometry histograms, b. viability, c. early apoptosis, d. late apoptosis and e. necrosis rates. (*p<0.05, **p<0.01, ***p<0.001, ****p<0.0001).

Similarly, a decrease was observed between the control and verteporfin groups in 48 h of verteporfin treatment (****p<0.0001; Figure 69a, b). When the control and verteporfin groups were evaluated in 48 h of verteporfin treatment, no difference was observed in early apoptosis in the control and 1 μM verteporfin groups, but an increase was observed between the other groups (p<0.05, **p<0.01, ***p<0.001; Figure 69a, c). When the late period apoptosis rates were evaluated in 48 h verteporfin administration, an increase was observed between the control and verteporfin groups (***p<0.001, ****p<0.0001; Figure 69a, d). When the control and verteporfin groups were evaluated in 48 hours of verteporfin treatment, no difference was observed between the groups in terms of necrosis (Figure 69a, e).

Finally, when the dose-dependent cell viability was evaluated in the 72 h verteporfin administration, a decrease in cell viability was observed between the control and verteporfin groups, depending on the dose increase (****p<0.0001; Figure 68a, b). When the control and verteporfin groups were evaluated in 72 h of verteporfin treatment, no difference was observed in early apoptosis in the control and 1 μM verteporfin groups, but an increase was observed between the other groups (**p<0.01, ***p<0.001, ****p<0.0001; Figure 70a, c). When the late period apoptosis rates were evaluated in 72 h verteporfin treatment, an increase was observed between the control and verteporfin groups (1, 5, 10, 20 and 40 μM) tested (**p<0.01, ****p<0.0001; Figure 70a, d). On the other hand, necrosis rates increased at only 1 μM (****p<0.0001; Figure 68a, d). When the control and verteporfin groups were evaluated in 72 h of verteporfin treatment, an increase was observed in the 1 μM verteporfin group compared to the control, but no difference was found between the other groups (Figure 70a, e).

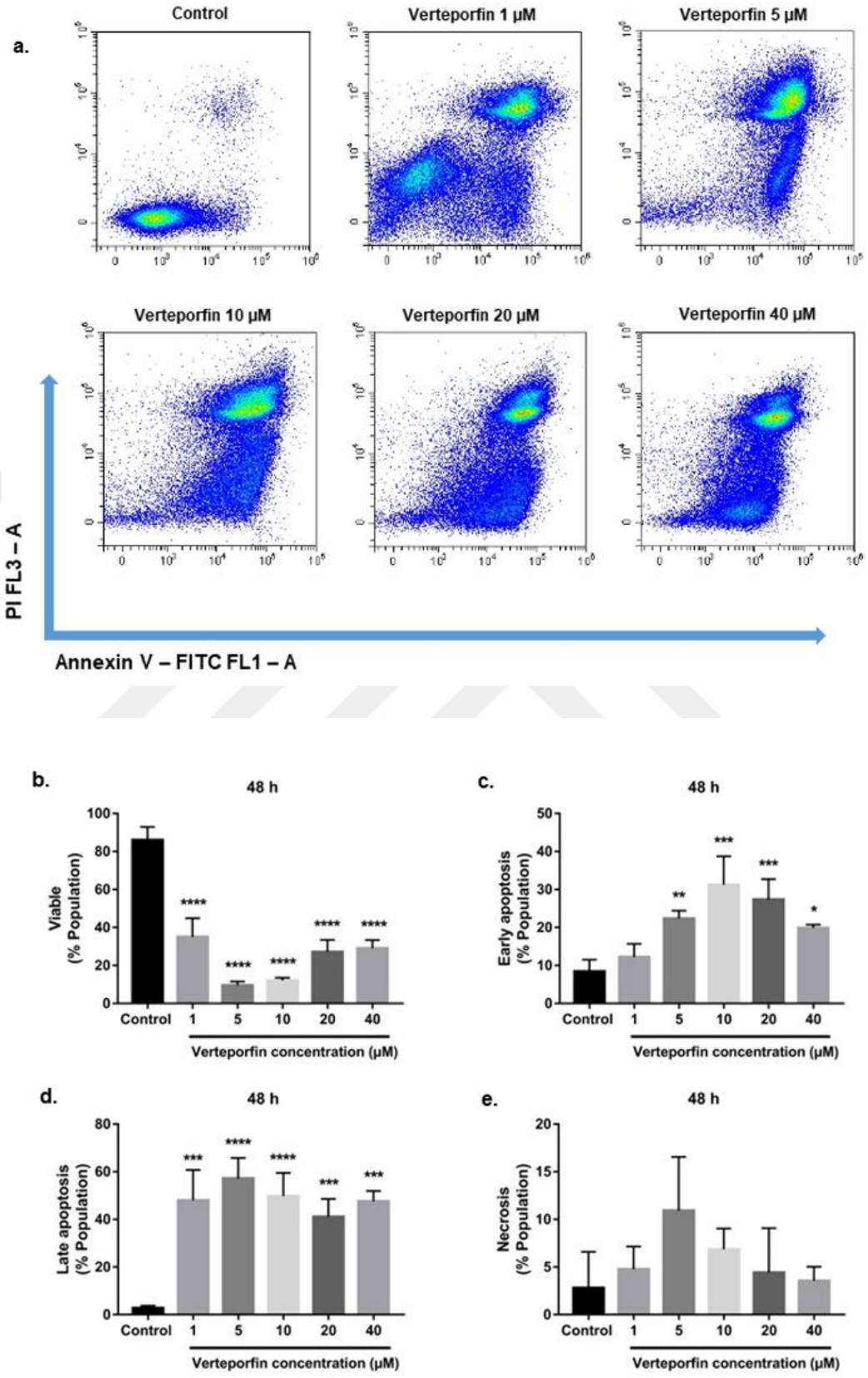
a.
Control
Verteporfin 1 μM
Verteporfin 5 μM
Verteporfin 10 μM
Verteporfin 20 μM
Verteporfin 40 μM
PI FL3 – A
Annexin V – FITC FL1 – A
b.
48 h
Viable (% Population)
Control
1
5
10
20
40
Verteporfin concentration (μM)
c.
48 h
Early apoptosis (% Population)
Verteporfin concentration (μM)
d.
48 h
Late apoptosis (% Population)
Verteporfin concentration (μM)
e.
48 h
Necrosis (% Population)
Verteporfin concentration (μM)

Figure 69. a. Representative flow cytometry histograms, b. viability, c. early apoptosis, d. late apoptosis and e. necrosis rates. (*p<0.05, **p<0.01, ***p<0.001, ****p<0.0001).

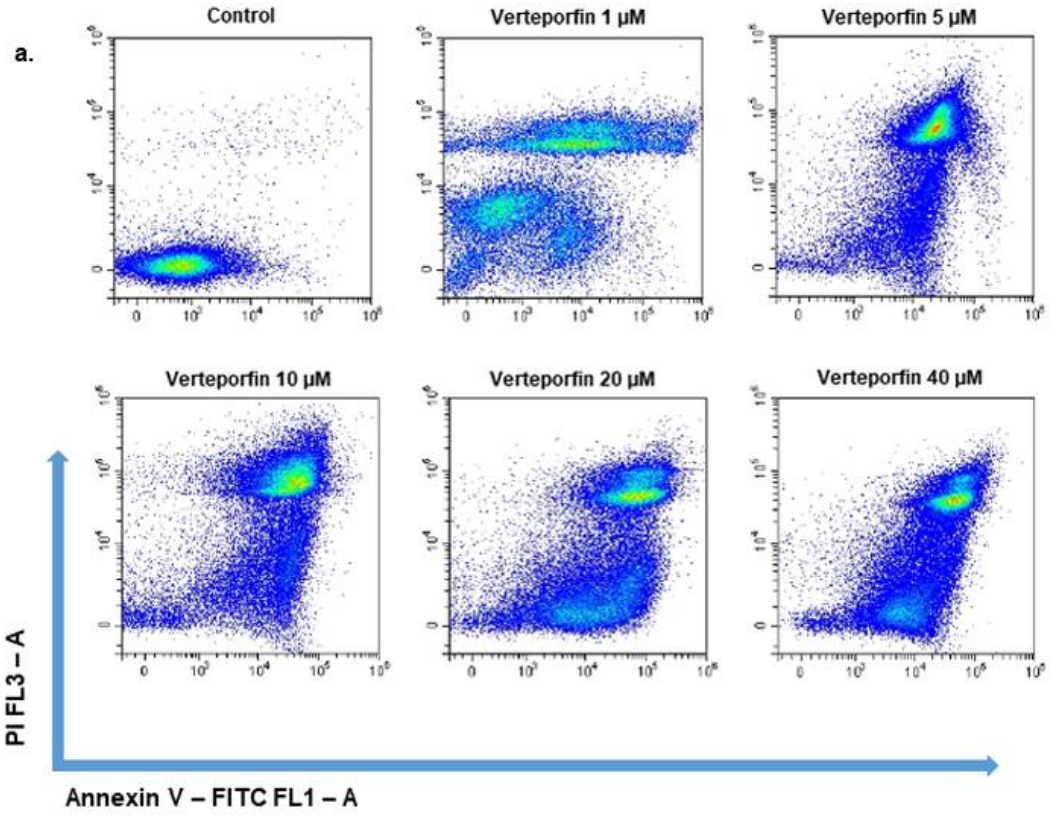

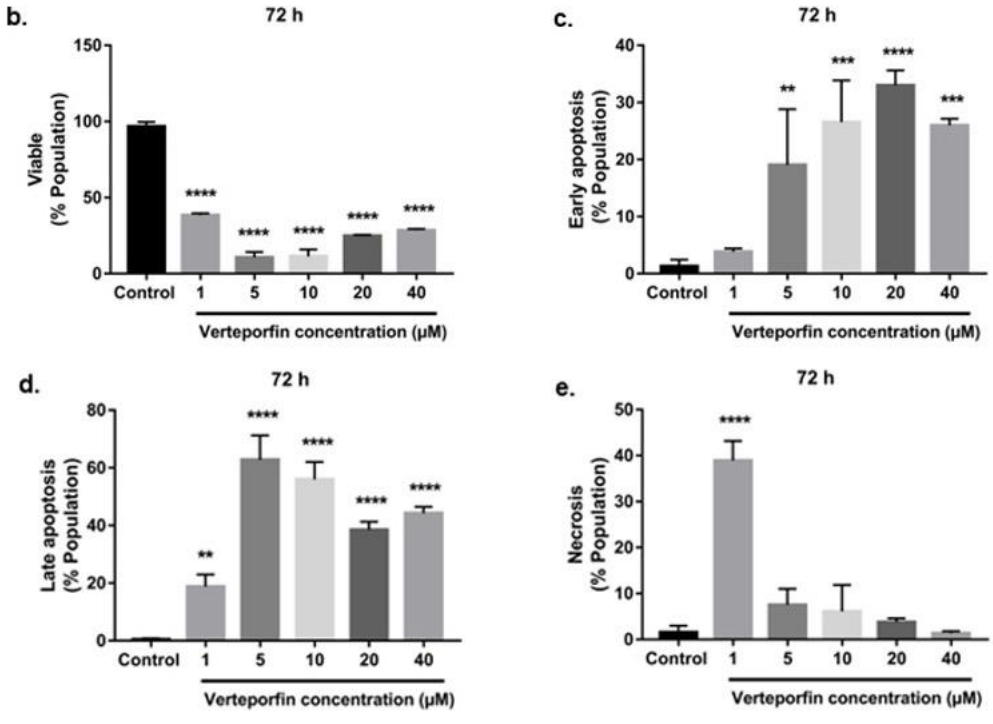

Figure 70. a. Representative flow cytometry histograms, b. viability, c. early apoptosis, d. late apoptosis and e. necrosis rates. (**p<0.01, ***p<0.001, ****p<0.0001).

5. DISCUSSION AND CONCLUSION

The Hippo signaling pathway is known to control organ size, tissue homeostasis, and cancer development (124). It plays important roles in cell differentiation and proliferation. Dysregulated Hippo signaling pathway is contribute to the invasion, mesenchymal differentation and tumorigenesis process (158, 196). Therefore, Hippo signaling pathway is frequently studied in cancer. In addition, YAP1, which is the main component of the Hippo signaling pathway, is ubiquitiously active in various human cancers and functions as an oncogene (160, 197). YAP1 is not only involved in the cancer cell proliferation, but also plays a central role in the resistance to cancer treatment such as targeted therapies, immunotherapy, radiotherapy and chemotherapy (161). Verteporfin (VP), anFDA-approved drug for macular degeneration, was recently discovered to act as an inhibitor of YAP-TEAD (198) and TAZ-TEAD (199) activity, and was subsequently shown to have anti-cancer activity in various solid tumor types (200). Although Hippo signaling pathway is mostly studied in cancer related studies, studies on Hippo signaling pathway and seminoma are limited. In this study, we have shown the expression of Hippo signaling pathway components in human testis tissue and human testicular cancer for the first time. Also, we have shown how Hippo signaling pathway components are affected in human testicular cancer. Besides, by this study, the effect of verteporfin on Hippo signaling pathway components in human testicular cancer was investigated for the first time.

We first evaluated the localization of Hippo signaling pathway components in human control testis tissue, non-seminoma and seminoma tissues after histomorphological evaluation. MST1/2, component of Hippo signaling pathway, is a type of pro-apoptotic kinase and activates LATS1/2 which is known as tumour suppressor homologs through multiple mechanisms in the protein kinase cascade of the Hippo signaling pathway (201). In our study, the interstitial area and spermatogonia cells in the control testicular tissue, carcinoma cells in embryonal carcinoma tissue and seminoma cells in seminoma tissue (Figure 71) showed positive immunostaining in cytoplasm for MST1/2. p-MST1/2 localization showed negative immunostaining pattern in spermatocyte cells, carcinoma and seminoma cells in (Figure 71) all related tissues. George et al. showed that MST1/2, p-MST1/2 localization in pancreatic islets, with very weak staining pattern in the acinar and ductal compartments (202). Selective localization

of MST1/2 was shown in the renal tubules of kidney (203). Similarly, deletion of MST1/2 in both studies causes nuclear accumulation of YAP, which affects inflammation and proliferation processes. Besides, MST1 localization was also demonstarted by immunostaining in breast tissue (204). MST1/2 localization in cervical cancer cell line and p-MST1/2 localization in colorectal cancer cells were also demonstrated (205, 206). In another study, MST1 localization was also reported in breast carcinoma tissues (207). Su et al. showed increased MST1 localization in cardiomyocytes of diet-exposed embryos compared to the control (204).

Like MST1/2, the localization of LATS1/2 has not been demonstrated in human testicular and human testicular cancer tissues. In our study, we reported that the interstitial area and the spermatogonic serie cells showed LATS1/2 and p-LATS1/2 positive immunostaining pattern in the control testicular tissue. Similarly; mitotic carcinoma cells in carcinoma tissue and mitotic seminoma cells in seminoma tissue (Figure 71) showed positive nuclear immunostaining pattern. We detected strong immunoreactivity for LATS1/2 and p-LATS1/2 in mitotic cells. Previously, Yabuta et al. showed that LATS2 is localized to the centrosome and is involved in the regulation of cell cycle and apoptosis (208, 209). There is also the centrosome involved in LATS1/2 cell division and mitotic progression. When we evaluated our data, we also observed strong immunostaining pattern in mitotic seminoma cells. Consistent with these studies, we demonstrated that there is high expression of LATS1/2 in mitotic cells due to the high mitotic activity of seminoma cells (Figure 71). Shen et al. showed that LATS1 expression is less in colorectal cancer tissues compared to control colorectal tissues (210). Also; Wang et al. showed a very weak signal of LATS1 in the cytoplasm of human hepatocellular carcinoma cells compared to para-cancerous cells (211). Consistent with the studies, we also detected cytoplasmic LATS1/2 expression in seminoma cells. Weak and cytoplasmic expression of LATS1/2 in seminoma cells can negatively regulate its transcriptional and transformational functions by inhibiting nuclear translocation of YAP. Therefore, LATS1 may be a potential therapeutic target molecule for cancer therapy.

Activated LATS1/2 phosphorylates YAP which is the main effector of the Hippo signaling pathway (212, 213). The localization of YAP was also demonstrated for the first time in human testicular tissue and different types of testicular cancer in our study. YAP1 and p-YAP1 localizations were observed in the interstitial area and spermatogenic cells

in the control testis. Total YAP1 localization in carcinoma and seminoma cells (Figure 71). Li et al. demonstrated increased nuclear localization of YAP in human gastric carcinoma tissues compared to normal tissues (214). Morvaridi et al. showed that YAP is localized in the nucleus in pancreatic ductal adenocarcinoma cells (215). Besides, Cha et al. reported that metastasis in breast cancer patients was strongly correlated with nuclear YAP1 localization (216). In another study, it was reported that strong YAP localization was found in the nucleus in breast, ovarian and liver carcinomas (217), additionally, both cytoplasmic and nuclear YAP localizations were also demonstrated in prostate cancer (218). In a different study, while high nuclear YAP expression in ovarian cancer cells was associated with prognosis, it was also reported that low cytoplasmic YAP expression was not an indicator of survival (219). Similarly, Lee et al. showed that nuclear YAP expression was not found significant in lymph node metastasis (220). One may suggest that the localization of YAP in seminoma may vary depending on the degree of prognosis. In addition, YAP may play a role as an independent prognostic factor. When the Hippo signaling pathway is active, MST1/2 phosphorylates LATS1/2, then phosphorylated LATS1/2 activates YAP and induces its cytoplasmic localization. In contrast, unphosphorylated YAP translocates into the nucleus as a transcription cofactor, particularly in cancer cells, to induce expression of many genes. In our study, we determined the localization of YAP in seminoma cells as cytoplasmic (Figure 71) may be because the Hippo signal pathway was not active in seminoma and YAP was not translocated to the nucleus. Zakaria et al. demonstrated the localization of cytoplasmic p-YAP in lung cancer tissue (221). Similarly, high cytoplasmic p-YAP localization was detected in breast cancer (222), esophageal squamous cell carcinoma (223). Also, another study reported high cyoplasmic p-YAP expression in head and neck squamous cell carcinoma (224). Consistent with these studies, we detected cytoplasmic p-YAP expression in seminoma cells (Figure 71). Strong cytoplasmic YAP and pYAP protein expression in seminoma tissues suggest activation of the Hippo signaling pathway.

YAP and TAZ are critical effectors in the Hippo pathway. When YAP is phosphorylated by the upstream kinases LATS1 and LATS2, YAP and TAZ accumulate in the cytoplasm and are unable to bind TEAD, inducing their ubiquitin-mediated proteolysis and autophagy-induced degradation. Upon dephosphorylation, YAP and TAZ are translocated into the nucleus, where they interact with TEADs to drive transcription of various target genes involved in cell proliferation, metastasis, and apoptosis (225).

Until our study, there is no study which demonstrate the TEAD4 localization in human testicular tissue and different types of human testicular cancer. We observed that TEAD4 showed positive immunostaining pattern in interstitial area and spermatogenic cells in the human testis. TEAD4 localization was also demonstrated in carcinoma and seminoma cells (Figure 71) in related cancer tissues. Previosuly; Zhang et al. showed nuclear localization of TEAD4 in head and neck squamous cell carcinoma and similarly, in another study localization of TEAD4 in hepatocellular carcinoma was also noted in nucleus of cell (226, 227). Wang et al. also showed increased nuclear localization of TEAD4 in colorectal cancer tissue (228). YAP and TEAD4 immunolabeling in both cancer cells and stromal cells were also reported in a subset of gallbladder cancer and YAP and TEAD4 localizations were demonstrated to be associated significantly with aggressive cancer behavior (229). It has also been shown that environmental stress and various signals, such as osmotic stress, cell separation and cell crowding, can direct the cytoplasmic translocation of TEAD4 as a predominantly nuclear protein. Environmental stress can induce cytoplasmic translocation of TEADs in a Hippo-independent manner (230). In our study, we detected a strong cytoplasmic TEAD4 expression pattern in carcinoma and seminoma cells (Figure 71). This indicates that TEAD4 expression is translocated to the cytoplasm by other variables independent of the Hippo signaling pathway. The mechanism of TEAD4 translocation still remains unclear.

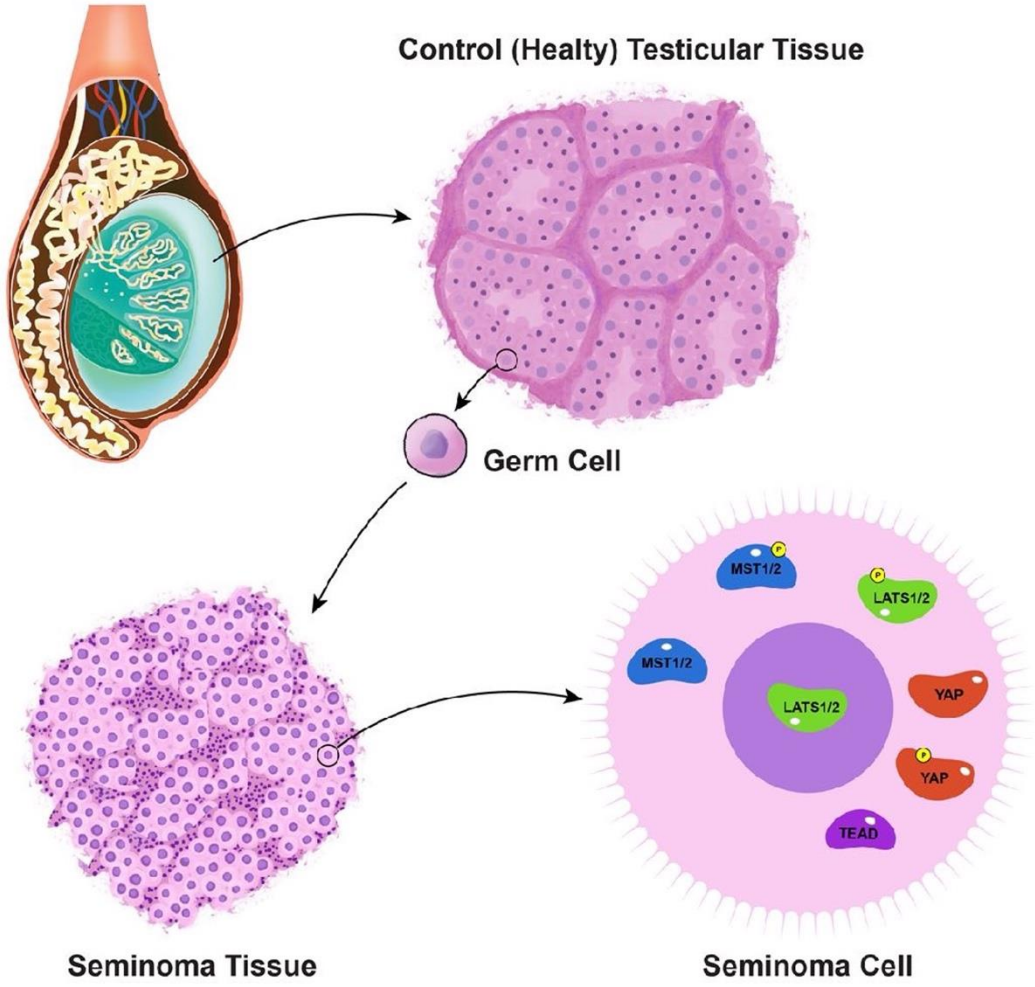

Figure 71. Germ cells are specialized cells found in control (healthy) testes. They are known as 'primitive' cells because of their ability to differentiate into all types of cells. After puberty, germ cells undergo mitosis to develop into spermatogonia. Most mixed germ cell tumors may contain seminoma tissue. Seminoma is the most common type among germ cell tumors. When viewed under the microscope, seminoma tumor cells are large cells arranged in groups. The cytoplasm of tumor cells is usually clear. The cells are separated from each other by a thin connective tissue structure called fibrous septa. Tumor cells are surrounded by lymphocytes on fibrous septa. Localization of Hippo signaling pathway proteins in seminoma cells has been shown.

Afterwards; we performed TCam-2 human seminoma cell culture to perform verteporfin treatment with different doses. TCam-2 cell line is the first cell line derived from seminoma and it shares many characteristic features with human seminoma such as aneuploidy, hypomethylation and germ cell gene expressions as pluripotency markers

(107, 231). We analyzed the components of Hippo signaling pathway in TCam-2 human seminoma cell line.

There are limited studies on the effects of VP on TCam-2 cells (232). In this study, we demonstrated thethe protein and mRNA expression levels of Hippo signaling pathway components in human seminoma cell line. This study is the first one investigating the protein and mRNA level analysis of these components (MST1/2, p-MST1/2, LATS1/2, p-LATS1/2, YAP1, p-YAP1, TEAD4) and TCam-2 seminoma cell line as the positive control as the seminoma cell line to be able to analyze the effect of verteporfin on these components in seminoma cells.

Verteporfin treatment caused significant decrease in protein levels of MST1/2, p-MST1/2, LATS1/2, p-LATS1/2, YAP1, p-YAP1 and TEAD-4 in dose- and time-dependent manner. When the duration and the dosage of verteporfin treatment increased, the negative effect of verteporfin on the protein levels increased as well. Wang et al. showed that 1 μm verteporfin treatment at 24, 48 and 72 h time intervals reduced the protein levels of the Hippo pathway (p-LATS1, LATS1, p-YAP, YAP, p-MST1, MST1) on a cervical cancer cell line (233). Wei et al. showed that different doses (0, 1, 2, 4, 8 μM) of 24 h verteporfin administration disrupted the YAP-TEAD interaction, reducing the YAP, p-YAP, TEAD protein expression levels in pancreatic ductal adenocarcinoma (167). Similarly, Fu et al. also demonstrated that verteporfin administration (1 μmol/L and 2 μmol/L) decreased the protein expressions of YAP and the downstream effector TAZ in cholangiocarcinoma cells (234). Consistent with our results, Hasegawa et al. also reported that dose- (15 μM) and time- (12 and 24 h) dependent application of verteporfin decreased the expression of YAP and TAZ protein levels in two different gastric cancer cells (235). Besides, it has been showed that different doses (0, 4, 8, 12 μMm) of 24 h verteporfin administration inhibited YAP, p-YAP and TEAD protein expression in three different breast cancer cell lines (236), and again different doses (0, 2.5, 5 μM) of 24 h verteporfin treatment reduced YAP1 and TEAD1 protein expression levels in osteosarcoma cell line (237). Takeda et al. reported that the application of 10, 100, 200 and 500 nM verteporfin in lung cancer cell lines decreased the expression of YAP protein levels (238). Similar results were also obtained from different studies using the similar verteporfin treatment durations as in our study. For instance, Zucchini et al. showed that different doses (0.5, 1, 2 μM) and durations (12, 24, 48 h) of verteporfin treatment caused

decreased YAP protein expression (178) and Cheng et al. reported that different durations of (24, 48, 72 h) of 3 μm verteporfin treatment in lung cancer cells caused to decrease total and phosphorylated YAP protein expression (239). Shi et al. showed that dose- and time- dependent administration of verteporfin in LOVO/TAX human lung cancer cell line lead to decreased YAP expression (240). Verteporfin treatment in HER-2 positive breast cancer cell line is also showed decrease the protein levels of YAP1 and p-YAP1 (241). 10 or 20 μmol/L verteporfin administration has been shown to decrease the expression of total YAP protein in two different intrahepatic cholangiocarcinoma cell lines (242). Chen et al. showed that the treatment of 0.5, 1 and 2 μM verteporfin for 24 h decreased the expression of YAP protein but had no effect on p-YAP. Furthermore; in a different study, Choe et al. showed down-regulated YAP and p-YAP protein expression in human embryonic stem cells after 300 nM verteporfin treatment for 24 h (243). Besides *in vitro* studies, Quan et al. demonstrated that verteporfin administration in transplanted hepatocarcinoma tissues also reduced significantly the protein expression levels of MST1, MST2, LATS1, TAZ, YAP, TEAD1, and TEAD2 (244).

According to our results, we noted that only 40 μM of verteporfin treatment for 48 h and 72 h caused decrease in only TEAD4 mRNA levels. Altough there are limited studies on mRNA levels of Hippo signaling pathway components in seminoma line and human seminoma line treated with verteporfin. In a previous study, TEAD1 mRNA expression levels were shown to be decreased in osteosarcoma cell lines after verteporfin treatment (237). To determine whether verteporfin affects YAP upstream factors, Feng et al. measured the mRNA levels of MST1/2 and LATS1/2 in ovarian cancer cells at different verteporfin concentrations (0, 1.25, 2.5, 5 and 10 μM) and no significant differences in mRNA levels were detected (200). Verteporfin treatment in a hepatocellular carcinoma xenograft model was also shown to reduce mRNA levels of TEAD4 (241). On the other hand, Ouan et al. showed that administration of verteporfin in transplanted hepatocellular carcinoma cells significantly reduced the mRNA expressions of effectors (MST1, MST2, LAST1, LAST2, TAZ, YAP, TEAD1, TEAD2, TEAD3, and TEAD4) in the Hippo/YAP signaling pathway (245). Our results showed that Hippo signaling pathway is regulated via translational or posttranslational modifications level rather than the transcriptional level following verteporfin treatment.

After protein and mRNA levels were evaluated, immunofluorescence staining performed and especially p-MST1/2, p-LATS1/2 and p-YAP1 localizations were observed in the nucleus of TCam-2 seminoma cells. While MST1/2, LATS1/2, YAP1 and TEAD4 showed nuclear localization in the control group (no treatment), they were also seen in the cytoplasm in addition to the nucleus, depending on the increasing dose. Li et al. and George et al. showed MST1 localization in the cytoplasm in pancreatic cells (246, 247). MST1/2 localization was also reported in cervical cancer cells (248). Britschgi et al. showed that LATS1/2 localization in control breast tissue and breast tumors is mostly nuclear in basal cells and cytoplasmic in luminal cells (249).

MST1/2 and LATS1/2 show nuclear localization in TCam-2 seminoma cells before verteporfin treatment. However, it is also known that the localization of MST1/2 and LATS1/2 is in the cytoplasm of healthy cell. When our results are evaluated, it is seen that the localization from the nucleus to the cytoplasm increases as the dose and time of verteporfin treatment increases (perinuclear). This situation can be explained as follows, verteporfin can also change the localization of the components of Hippo signaling pathway by generating a therapeutic effect in human seminoma cells.

In our study; we observed nuclear localization of YAP1 in seminoma cells. It is not surprising to observe YAP1 in the nucleus because of Hippo signaling is off in cancer cells (250). When YAP1 is tranclocated in the nucleus, it can stimulate continous expression of the genes related to cell proliferation and cell growth, thence, nuclear localization of YAP1 in seminoma cells are consistent with literature. Similarly, Wu et al. showed that YAP1 was located more in nucleus in bladder cancer cells in the cytoplasm. Kim et al. reported that YAP and TAZ localizations are found in the nucleus in tumorigenesis (251) and Morvaidi et al. reported that the localization of YAP in pancreatic cancer cells was strong in both the nucleus and cytoplasm (252, 253). Similarly, in another study, YAP1 localization in human ovarian epithelial cells was shown to be found both in the nucleus and in the cytoplasm (254). On the other hand; YAP/TAZ is observed in the cytoplasm in colon cancer cells (255) and Moroishi et al. showed that YAP/TAZ was localized in the cytoplasm in different murine syngeneic tumor cells. We observed that verteprofin treatment caused perinuclear and cytoplasmic localization of YAP1.

It has been reported in previous studies that verteporfin inhibits the proliferation of cells originating from esophageal cancer, lung cancer and different cancer types (167). In our study, we analyzed the effect of verteporfin on cell proliferation in TCam-2 human seminoma cells (Figure 73). Consistent with the studies on verteporfin and other cancer types, we observed that verteporfin treatment decreased cell proliferation as the dose (0, 1, 5, 10, 20 and 40 μM) and incubation time (24, 48 and 72 h) increased (Figure 73). In another study which supports our results, Wei et al. showed that dose- (2, 4, 6, 8, 10 μM) and time-dependent (24, 48 and 72 h) verteporfin treatment in pancreatic ductus adenocarcinoma cells arrested the cell cycle in the G1 phase and decreased cell proliferation in direct proportion to the treatment dose and incubation period (167). In our study, a significant decrease was observed between the control and verteporfin groups after 24 h verteporfin administration (Figure 73). Similarly, Zucchini et al. showed that 2 μM verteporfin of 24 h treatment significantly inhibited cell proliferation in the osteosarcoma cell line (178). In addition, in our study, it was shown that there was a significant decrease between the control and verteporfin groups after 48 h verteporfin treatment (Figure 73). However, there was no significant difference between the control and 1uM verteporfin group in 48h of verteporfin treatment. Consistently, Lin et al. showed that cell proliferation was inhibited after a 2 μg/ml dose and 48h of verteporfin treatment (256). Finally, when the dose-related proliferation was evaluated in the 72 h verteporfin treatment, there was no significant difference between the 72 h 1 μM verteporfin treated group and the control group, while a similarly significant decrease was observed between the control and the other verteporfin-treated groups (Figure 73). Similarly, Gurda et al. showed that cell proliferation was inhibited in cholangiocyte and cholangiocarcinoma cells with dose- (1.25, 2.5 and 5 μM) and time-dependent (72 h) verteporfin treatment, even at the lowest verteporfin dose in carcinoma cells compared to cholangiocytes. In the highest dose (5 μM) verteporfin treatment, cell proliferation decreased by 80-90% (257). We also showed that 48 h and 72 h of verteporfin treatment caused a decrease in cell proliferation more effectively than 24 h of verteporfin treatment. Hasegawa et al. showed that verteporfin treatment at different doses (10, 15, 20 μM) and incubation times (24, 48 and 72 h) caused cell proliferation in two different poorly and moderately differentiated adenocarcinoma cell lines. Interestingly, it has been shown that there is less cell proliferation in mildly differentiated adenocarcinoma cells compared to moderately differentiated adenocarcinoma cells with 24 h verteporfin treatment due to

dose escalation. Effectively, decreased cell proliferation due to increasing dose at 48 h and 72 h (235). At the same time, in our study, we also showed that proliferation decreased as the dose of verteporfin increased. In the proliferation evaluation, it was shown that the treatment of 40 μM verteporfin for 72 h caused the most significant decrease in proliferation of TCam-2 seminoma cells. Similarly, Brodowska et al. treated human retinoblastoma cells with verteporfin at different doses (2 and 10 μg/ml) for 5 days, and showed that cell proliferation decreased due to increasing dose until the 3 rd day of treatment, and the highest verteporfin dose (10 μg/ml) was the most effective on proliferation inhibition (258). Jiang et al. reported that cell proliferation decreased in proportion to the increase in dose (0, 4, 8, 12, 16 μmol/ml) in human breast cancer cells. Even the lowest dose of verteporfin (4μmmol/ml) significantly reduced cell proliferation (259). Besides, Yin et al. showed that dose (0.5, 1, 2, 5 μM) and time-dependent (24, 48 and 72 h) verteporfin treatment inhibited cell proliferation in Hela cells in direct proportion to the increase in dose and time of the treatment. Verteporfin treatment at 5 μM and 72 h was most effective treatment for reduction in cell proliferation (260). Also, Kang et al. reported that dose- and time-dependent treatment of verteporfin in granulosa cell lines increased cell proliferation but did not affect proliferation in normal gastric cell lines (261). This suggests that verteporfin application has a selective effect on cell lines. Therefore, we showed that verteporfin treatment had a negative effect on proliferation, which was correlated with dose increase and longer incubation times (48 and 72 h). In addition, verteporfin administration may also inhibit the migratory and invasive capacity of seminoma cells. In our study, we reported that verteporfin treatment played a role as an anti-cancer agent by inhibiting TCam-2 cell proliferation, which is a seminoma cell line. On the other hand, as a result of verteporfin administration, Hippo signaling pathway can be reactivated in seminoma cells and thus regulate critical processes such as decreased cell proliferation.

When the control group and verteporfin treated groups were evaluated in terms of migration, we could not perform a quantitative evaluation at these doses, since verteporfin doses of 5 μM and above caused the cells to lose their adhesion and migration properties in 24, 48 and 72 h of verteporfin administration. We observed that 1uM verteporfin treatment had no effect on migration in 24 hours. On the other hand, Wang et al. showed that verteporfin significantly reduced cell migration in cervical cancer cells after a dose of 1 μM and a time of 24h incubation. The researchers found that a 1 μM dose of

verteporfin significantly reduced cell viability and used this concentration for other experiments (262). In 24 h verteporfin treatment when the control and 5μM verteporfin groups were evaluated, we showed that 5 μM verteporfin caused reduction in migration. Brodowska et al. showed that dose- (2 and 10 μg/mol) and time- (6, 24, 48 h) dependent treatment of verteporfin reduced migration-related protein expression levels in human retinoblastoma cells (258). Zucchini et al. showed that a 2 μM dose and 24 h treatment of verteporfin significantly inhibited cell proliferation in the osteosarcoma cell line (178). In another study; Yin et al. performed 5 μM verteporfin treatment for 24 h and showed that the migration rate in Hela cells reduced significantly compared to the control (260). Besides, Wei et al. treated 3 different breast cancer cell subtypes with 8 μM verteporfin treatment for 24 h and showed that migration was inhibited compared to control (213). Garcia et al. showed that the treatment of 500 nM verteporfin administration for 24 h in gallbladder cancer cells reduced cell migration significantly compared to the control (263).

Similarly, we did not observe the difference in migration between the control and 1μM verteporfin group in 48 h of verteporfin treatment. However, when the control group and 5μM verteporfin group were evaluated, we observed that 5 μM verteporfin treatment reduced migration of TCam-2 cells in 48 h (Figure 73). Jiang et al. Reported that cell proliferation decreased in proportion to the increase in dose (0, 4, 8, 12, 16 μmol/ml) in human breast cancer cells (259). It has been shown that dose (2 and 10 μg/mol) and time (6, 24, 48 h) dependent treatment of verteporfin reduces migration-related protein expression levels in human retinoblastoma cells (258). In another study, it was reported that verteporfin reduced cell migration in NCI-H1975 lung cancer cells (260).

Finally, we could not make a quantitative evaluation at higher doses, since verteporfin doses of 5μM and above caused the cells to lose their adhesion properties in 72 h of verteporfin administration. Almost all cells after 72 h treatment group were floating and lost their attachment to the culture plate, thence migration evaluations could not be done. There are different studies which shows that verteporfin effect adherence properties of cells negatively (264). In a related study, it was shown that the inhibition of YAP by verteporfin treatment caused a significant decrease in desmosomal genes and proteins, resulting in weakening of cell cohesion (265). Similarly, Kang et al. showed that 3 μM verteporfin treatment for 24 h caused to decrease in cell migration by inhibiting an

adhesion molecule in gastric cancer cells (261). Therefore, we might suggest that verteporfin treatment in different doses for 72 h might affect the cell adhesion molecules so the cells lost their adherence properties. By this way, migration of cells might be decreased by verteporfin treatment (Figure 73).

When the control group and verteporfin groups were evaluated in terms of apoptosis and cell viability, we showed that cell viability decreased significantly and apoptosis rate increased depending on the increasing dose (Figure 73). We reported significant decrease in cell viability between the verteporfin groups and the control group in 24 h (Figure 73). Chen et al. showed that verteporfin treatment for 24 h at different doses in the trabecular meshwork of the eye lead to decrease cell viability (266). Saini et al. performed dose- (1, 5, 10 µM) and time- (1, 6, 24, 48 h) dependent verteporfin treatment in osteosarcoma cells and showed that 1 and 6 h incubation and 1µM verteporfin treatment did not affect cell viability. However, after 24 h incubation, it was determined that as the dose increased, cell viability in all groups decreased (267).

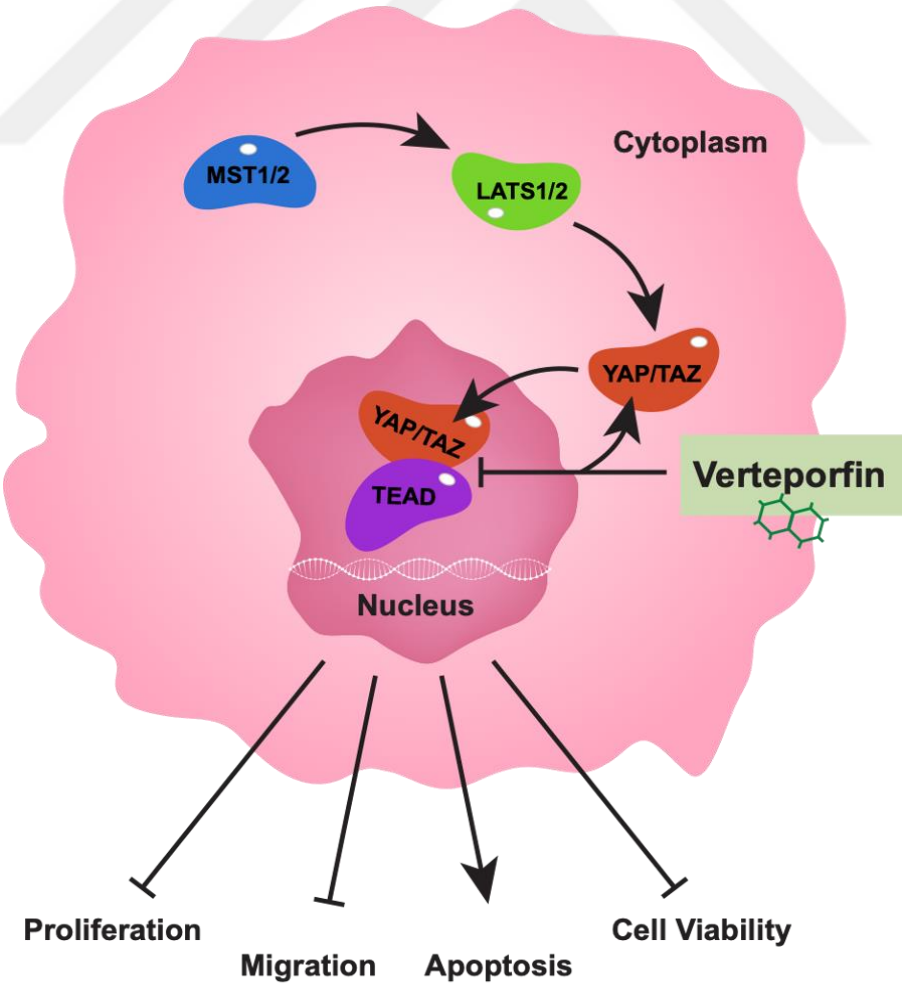

Figure 72. Verteporfin is a YAP-TEAD inhibitor. Verteporfin-mediated inhibition in cancer cells decreases cell proliferation, viability and migration, while increasing apoptosis.

Similarly, we reported a significant decrease in 48 h of verteporfin treatment. Wang et al. showed that the cell viability of two different cervical cancer cells decreased depending on the time with 1 μM and 0, 12, 24, 36 and 48 h incubation of verteporfin (268). Brodowska et al. showed that dose- (2 and 10 μg/mol) and time- (6, 24, 48 h) dependent treatment of verteporfin significantly reduced cell viability in human retinoblastoma cells (258). Finally, when the dose-dependent cell viability was evaluated after 72 h verteporfin treatment, we showed a significant decrease in cell viability in verteporfin-treated groups in a dose-dependent manner (Figure 73). Wang et al. showed that verteporfin decreased cell viability in cervical cancer cells in a dose- (0.5, 1, 5, 10 μM) and time- (24, 48 and 72 h) dependent manner. The researchers found that 1 μM of verteporfin treatment significantly reduced cell viability (268). Wei et al. administered verteporfin at different doses (0, 2, 4, 6, 8 μM) and time (24, 48, 72 h) intervals in 3 different breast cancer cell subtypes and showed that cell viability decreased with increasing doses and time (213). Similarly, Fu et al. demonstrated that verteporfin in cholangiocarcinoma cells caused the cell viability rate to decrease (234). Yang et al. also showed that verteporfin promotes apoptosis by downregulating the expression of the Hippo signaling pathway proteins YAP1 and TEAD1 (260). Besides, Jeong et al. reported that verteporfin treatment inhibited cell viability in lung cancer cells (269). We demonstrated nuclear expression of YAP-TEAD complex as a transcription factor in seminoma cells. However, we found that verteporfin administered dose- and time-dependently in TCam-2 seminoma cells decreased cell proliferation, migration and viability by inducing cytoplasmic translocation of YAP-TEAD complex.

In addition to cell viability, early and late apoptosis rates were also evaluated between the control and verteporfin groups. In our study, early apoptosis rates were higher than late apoptosis rates. The underlying reason of this situation might be the dose- and time-dependent verteporfin saturation limit treated in TCam-2 cells may be reached. So cells switch to the recovery mechanism in the early apoptosis period, and late apoptosis rates may be found to be lower compared to early apoptosis rates (270). Although studies related to apoptosis and vertoporfin are quite numerous, the studies of the effect of

verteporfin on early and late periods seperately are very limited. Although apoptotic effects of verteporfin have been extensively studied, the studies on the effect of verteporfin on early and late apoptosis in seminoma are scarce. There are quite a few studies that have found similar results to our results. When the control and verteporfin groups were evaluated in 24 h verteporfin treatment, there was no significant difference in early apoptosis in the control and 1 μM and 40 μM verteporfin groups, but a significant increase was observed between the other groups. When the late period apoptosis rates were evaluated in 24h verteporfin treatment, a significant increase was observed between the control and verteporfin doses (Figure 73). Wei et al. showed that 8 μM dose and 24 h teatment of verteporfin increased apoptosis rate in pancreatic ductus adenocarcinoma cells compared to control (167). Besides, Chen et al. showed that the treatment of 10 and 20 μM verteporfin for 24 h in NB4 cells, a human leukemia cell line, induced apoptosis depending on the dose increase (271). 10 μM verteporfin treatment for 24 h has been reported to induce apoptosis in osteosarcoma cells (267). When the control and verteporfin groups were evaluated in 48 h of verteporfin treatment, we observed no significant difference in early apoptosis in the control and 1 μM verteporfin groups, but a significant increase was observed between the other groups. When the late apoptosis rates were evaluated in 48 h verteporfin treatment, we reported a significant increase between the control and verteporfin groups. When the control and verteporfin groups were evaluated at 72 h, we observed no significant difference in early apoptosis between the control and 1 μM verteporfin groups, but a significant increase in the early apoptosis was observed as the verteporfin dose increased (Figure 73). Similarly, Wang et al. showed that verteporfin in cervical cancer cells increased cell apoptosis in 1μm verteporfin treatment at different time 0, 12, 24, 36 and 48 h intervals (268). Ma et al. showed that apoptosis increased significantly dose- (0, 1.5, 2.5, 5 μM) and time- (0, 12, 24, 48 h) dependent manner of verteporfin treatment in uveal melonam cells (272). When the late apoptosis rates were evaluated in 72 h verteporfin treatment, a significant increase was observed between the control and verteporfin groups in our study. Studies reported that verteporfin treatment induced apoptosis in lung cancer cells (269), cholangiocarcinoma cells (234), rhabdomyosarcoma cells (273), human leukemia HL-60 cells (274), chronic myeloid leukemia cells (275) and human leukemia NB4 cells (271).

The necrosis was also evaluated between the control and verteporfin groups. We observed significant increase in necrosis rates only in 1 μM verteporfin treatment for 24

h and 72 h but no significant difference between groups independently the dose and time interval of the verteporfin treatment. There are few studies on the effect of verteporfin treatment on necrosis of cells found in different cancer types. However, similar to our study, Sanna et al. demonstrated that verteporfin treatment induced necrosis in rhabdomyosarcoma cells (273). On the other hand, Wei et al. showed that dose- (0, 4, 8, 12 μM) and time- (24 h) dependent verteporfin administration inhibited the expression of necrosis-related protein in pancreatic ductal adenocarcinoma cells by disrupting the YAP-TEAD interaction (167). According to these controversial results obtained from our study and previous studies, further studies on the relationship between verteporfin treatment and necrosis of cancer cells is needed. However, when the current situation is considered, we suggest that verteporfin treatment may exert its affects on cell death by apoptosis which is known as a programmed cell death mechanism, rather than necrosis. Therefore, verteporfin may be a clinically adaptable cancer therapy as it may offer a controlled treatment mechanism.

Although Hippo signaling pathway has been studied in testicular tissue of other species (131, 132, 135, 276), in our study, Hippo signaling pathway components were first identified in human testis tissue. Additionally, the Hippo signaling pathway has been demonstrated in many different cancer types with previous studies, but our thesis study is the first to demonstrate the components of Hippo signaling pathway in human testicular cancer tissue. We suggested that it may be important to define the Hippo signaling pathway in human seminoma, to reveal its potential role in pathogenesis of testicular cancer and to predict/plan possible treatment methods in the future.

In addition, verteporfin used in the TCam-2 human seminoma cell line, has been reported to affect critical processes such as cell proliferation, migration and apoptosis. It has been reported in previous studies that verteporfin administration is a promising treatment for endometrial cancer (277), ovarian cancer (200), glioblastoma (278) and retinoblastoma (258) by reducing cell proliferation. However, it has not been shown yet in testicular cancer. In this study, we showed inhibitory effect of verteporfin in cell proliferation, migration and apoptosis in seminoma cells via Hippo signaling pathway. According to our results, we suggested that verteporfin may improve outcome of seminoma cancer treatment in dose and treatment period dependent manner. The development of long term and more effective, at the same time minimal toxic treatment

methologies are needed to provide effective treatment in cancer. Therefore, development of new strategies will be very fundamental to manegment of testicular seminoma. In our study, we aimed to contribute literature that the Hippo signaling pathway may be a therapeutic target for seminoma. Further *in vivo* and *in vitro* seminoma cancer studies are needed to better understand the underlying mechanism of seminoma and the treatmental role of Hippo signal pathway to earn new insights on the seminoma therapies.

REFERENCES

1. O'Donnell K, Nirenberg HI, Aoki T, Cigelnik E. A Multigene phylogeny of the Gibberella fujikuroi species complex: Detection of additional phylogenetically distinct species. Mycoscience. 2000;41(1):61-78.
2. O'Donnell L, Smith LB, Rebourcet D. Sertoli cells as key drivers of testis function. Seminars in Cell & Developmental Biology. 2022;121:2-9.
3. de Lima e Martins Lara N, Costa G, Figueiredo A, França L. The Sertoli cell: what can we learn from different vertebrate models? Animal reproduction. 2019;16.
4. Setchell B. Blood-Testis Barrier, Junctional and Transport Proteins and Spermatogenesis. Advances in experimental medicine and biology. 2008;636:212-33.
5. Cheng L, Albers P, Berney DM, Feldman DR, Daugaard G, Gilligan T, et al. Testicular cancer. Nature reviews Disease primers. 2018;4(1):29.
6. Young RH. Sex cord-stromal tumors of the ovary and testis: their similarities and differences with consideration of selected problems. Modern Pathology. 2005;18(2):S81-S98.
7. Parekh NV, Lundy SD, Vij SC. Fertility considerations in men with testicular cancer. Translational andrology and urology. 2020;9(Suppl 1):S14-s23.
8. Zeng Q, Hong W. The emerging role of the hippo pathway in cell contact inhibition, organ size control, and cancer development in mammals. Cancer cell. 2008;13(3):188-92.
9. Zeng Q, Hong W. The Emerging Role of the Hippo Pathway in Cell Contact Inhibition, Organ Size Control, and Cancer Development in Mammals. Cancer cell. 2008;13(3):188-92.
10. Schroeder M, Halder G. Regulation of the Hippo pathway by cell architecture and mechanical signals. Seminars in cell & developmental biology. 2012;23:803-11.
11. Fu M, Hu Y, Lan T, Guan K-L, Luo T, Luo M. The Hippo signalling pathway and its implications in human health and diseases. Signal Transduction and Targeted Therapy. 2022;7(1):376.
12. Kodaka M, Hata Y. The mammalian Hippo pathway: regulation and function of YAP1 and TAZ. Cell Mol Life Sci. 2015;72(2):285-306.
13. Szulzewsky F, Holland EC, Vasioukhin V. YAP1 and its fusion proteins in cancer initiation, progression and therapeutic resistance. Developmental Biology. 2021;475:205-21.
14. Franklin JM, Ghosh RP, Shi Q, Reddick MP, Liphardt JT. Concerted localization-resets precede YAP-dependent transcription. Nature communications. 2020;11(1):4581.
15. Moody SC, Wakitani S, Young JC, Western PS, Loveland KL. Evidence that activin A directly modulates early human male germline differentiation status. Reproduction (Cambridge, England). 2020;160(1):141-54.
16. Smialek MJ, Ilaslan E, Sajek MP, Swiercz A, Janecki DM. Characterization of RNP Networks of PUM1 and PUM2 Post-Transcriptional Regulators in TCam-2 Cells, a Human Male Germ Cell Model. 2020;9(4).
17. James ER, Carrell DT, Aston KI, Jenkins TG, Yeste M. The Role of the Epididymis and the Contribution of Epididymosomes to Mammalian Reproduction. 2020;21(15).
18. Muniyan S, Chaturvedi NK, Dwyer JG, Lagrange CA, Chaney WG, Lin MF. Human prostatic acid phosphatase: structure, function and regulation. Int J Mol Sci. 2013;14(5):10438-64.
19. Johnson LR. Essential medical physiology: Elsevier; 2003.

20. White BA, Porterfield SP. Endocrine and Reproductive Physiology: Mosby Physiology Monograph Series. Endocrine and Reproductive Physiology: Mosby Physiology Monograph Series. 2012:1-302.
21. De Groot LJ, Jameson JL. Endocrinology adult and pediatric: the thyroid gland: Elsevier Health Sciences; 2013.
22. Jones RC. To store or mature spermatozoa? The primary role of the epididymis. International journal of andrology. 1999;22(2):57-67.
23. Sandlow J. An introduction to male reproductive medicine. Fertility and sterility. 2012;98:769.
24. Ramírez-González JA, Sansone A. Chapter 2 - Male reproductive system. In: Vaamonde D, Hackney AC, Garcia-Manso JM, editors. Fertility, Pregnancy, and Wellness: Elsevier; 2022. p. 23-36.
25. Foster RA. Male Genital System.
26. Fernando L. Sperm intrauterine fluid interaction test - A new sperm function test 2007.
27. Middendorff R, Müller D, Mewe M, Mukhopadhyay AK, Holstein AF, Davidoff MS. The tunica albuginea of the human testis is characterized by complex contraction and relaxation activities regulated by cyclic GMP. The Journal of clinical endocrinology and metabolism. 2002;87(7):3486-99.
28. Ivell R. Lifestyle impact and the biology of the human scrotum. Reproductive biology and endocrinology : RB&E. 2007;5:15.
29. Setchell BP. The Parkes Lecture. Heat and the testis. Journal of reproduction and fertility. 1998;114(2):179-94.
30. Molecular biology of the male reproductive system / edited by David de Kretser. De Kretser DM, editor. San Diego: Academic Press; 1993.
31. França LR, Hess RA, Dufour JM, Hofmann MC, Griswold MD. The Sertoli cell: one hundred fifty years of beauty and plasticity. Andrology. 2016;4(2):189-212.
32. Ni F-D, Hao S-L, Yang W-X. Multiple signaling pathways in Sertoli cells: recent findings in spermatogenesis. Cell death & disease. 2019;10(8):541.
33. Kaur G, Thompson LA, Dufour JM. Sertoli cells--immunological sentinels of spermatogenesis. Semin Cell Dev Biol. 2014;30:36-44.
34. Thakur RK, Yadav VK, Kumar A, Singh A, Pal K, Hoeppner L, et al. Non-metastatic 2 (NME2)-mediated suppression of lung cancer metastasis involves transcriptional regulation of key cell adhesion factor vinculin. Nucleic Acids Res. 2014;42(18):11589-600.
35. Peschon JJ, Behringer RR, Brinster RL, Palmiter RD. Spermatid-specific expression of protamine 1 in transgenic mice. Proc Natl Acad Sci U S A. 1987;84(15):5316-9.
36. Ferguson S, Panos J. Blood-Brain-Barrier Development and Function2016. 66-7 p.
37. Setchell BP. Blood-testis barrier, junctional and transport proteins and spermatogenesis. Advances in experimental medicine and biology. 2008;636:212-33.
38. Setchell BP, Waites GM. Changes in the permeability of the testicular capillaries and of the 'blood-testis barrier' after injection of cadmium chloride in the rat. The Journal of endocrinology. 1970;47(1):81-6.
39. Siu MK, Cheng CY. Dynamic cross-talk between cells and the extracellular matrix in the testis. BioEssays : news and reviews in molecular, cellular and developmental biology. 2004;26(9):978-92.

40. Siu MK, Cheng CY. Extracellular matrix and its role in spermatogenesis. Advances in experimental medicine and biology. 2008;636:74-91.
41. Mruk DD, Cheng CY. Sertoli-Sertoli and Sertoli-germ cell interactions and their significance in germ cell movement in the seminiferous epithelium during spermatogenesis. Endocrine reviews. 2004;25(5):747-806.
42. Francavilla F, Santucci R, Barbonetti A, Francavilla S. Naturally-occurring antisperm antibodies in men: interference with fertility and clinical implications. An update. Frontiers in bioscience : a journal and virtual library. 2007;12:2890-911.
43. Mazumdar S, Levine AS. Antisperm antibodies: etiology, pathogenesis, diagnosis, and treatment. Fertility and sterility. 1998;70(5):799-810.
44. Alexander NJ, Anderson DJ. Vasectomy: consequences of autoimmunity to sperm antigens. Fertility and sterility. 1979;32(3):253-60.
45. Mandelbaum SL, Diamond MP, DeCherney AH. The impact of antisperm antibodies on human infertility. The Journal of urology. 1987;138(1):1-8.
46. Arora P, Sudhan MD, Sharma RK. INCIDENCE OF ANTI-SPERM ANTIBODIES IN INFERTILE MALE POPULATION. Medical journal, Armed Forces India. 1999;55(3):206-8.
47. Adeghe JH. Male subfertility due to sperm antibodies: a clinical overview. Obstetrical & gynecological survey. 1993;48(1):1-8.
48. Jager S, Kremer J, van Slochteren-Draaisma T. A simple method of screening for antisperm antibodies in the human male. Detection of spermatozoal surface IgG with the direct mixed antiglobulin reaction carried out on untreated fresh human semen. International journal of fertility. 1978;23(1):12-21.
49. Aitken RJ, Rudak EA, Richardson DW, Dor J, Djahanbahkch O, Templeton AA. The influence of anti-zona and anti-sperm antibodies on sperm--egg interactions. Journal of reproduction and fertility. 1981;62(2):597-606.
50. Junk SM, Matson PL, Yovich JM, Bootsma B, Yovich JL. The fertilization of human oocytes by spermatozoa from men with antispermatozoal antibodies in semen. Journal of in vitro fertilization and embryo transfer : IVF. 1986;3(6):350-2.
51. Chereshnev V, Pichugova S, Beikin Y, Chereshneva M, Iukhta A, Stroev Y, et al. Pathogenesis of Autoimmune Male Infertility: Juxtacrine, Paracrine, and Endocrine Dysregulation. Pathophysiology. 2021;28:471-89.
52. Zimmer SE, Kowalczyk AP. The desmosome as a model for lipid raft driven membrane domain organization. Biochimica et Biophysica Acta (BBA) - Biomembranes. 2020;1862(9):183329.
53. Segretain D, Fiorini C, Decrouy X, Defamie N, Prat JR, Pointis G. A proposed role for ZO-1 in targeting connexin 43 gap junctions to the endocytic pathway. Biochimie. 2004;86(4-5):241-4.
54. Gilligan T. Testis cancer: rare, but curable with prompt referral. Cleveland Clinic journal of medicine. 2007;74(11):817-25.
55. Khan O, Protheroe A. Testis cancer. Postgraduate medical journal. 2007;83(984):624-32.
56. Huyghe E, Plante P, Thonneau PF. Testicular cancer variations in time and space in Europe. European urology. 2007;51(3):621-8.
57. Regalado Porras GO, Chávez Nogueda J, Poitevin Chacón A. Chemotherapy and molecular therapy in cervical cancer. Reports of practical oncology and radiotherapy : journal of Greatpoland Cancer Center in Poznan and Polish Society of Radiation Oncology. 2018;23(6):533-9.

58. Jones RH, Vasey PA. Part I: testicular cancer--management of early disease. The Lancet Oncology. 2003;4(12):730-7.
59. Faja F, Finocchi F, Carlini T, Rizzo F, Pallotti F, Spaziani M, et al. PDE11A gene polymorphism in testicular cancer: sperm parameters and hormonal profile. Journal of Endocrinological Investigation. 2021;44(10):2273-84.
60. Litchfield K, Levy M, Dudakia D, Proszek P, Shipley C, Basten S, et al. Rare disruptive mutations in ciliary function genes contribute to testicular cancer susceptibility. Nature communications. 2016;7(1):13840.
61. di Pietro A, Vries EG, Gietema JA, Spierings DC, de Jong S. Testicular germ cell tumours: the paradigm of chemo-sensitive solid tumours. The international journal of biochemistry & cell biology. 2005;37(12):2437-56.
62. Lutke Holzik MF, Rapley EA, Hoekstra HJ, Sleijfer DT, Nolte IM, Sijmons RH. Genetic predisposition to testicular germ-cell tumours. The Lancet Oncology. 2004;5(6):363-71.
63. Chung CC, Kanetsky PA, Wang Z, Hildebrandt MA, Koster R, Skotheim RI, et al. Meta-analysis identifies four new loci associated with testicular germ cell tumor. Nat Genet. 2013;45(6):680-5.
64. LeBron C, Pal P, Brait M, Dasgupta S, Guerrero-Preston R, Looijenga LH, et al. Genome-wide analysis of genetic alterations in testicular primary seminoma using high resolution single nucleotide polymorphism arrays. Genomics. 2011;97(6):341-9.
65. Béranger R, Le Cornet C, Schüz J, Fervers B. Occupational and environmental exposures associated with testicular germ cell tumours: systematic review of prenatal and life-long exposures. PloS one. 2013;8(10):e77130.
66. Cook MB, Akre O, Forman D, Madigan MP, Richiardi L, McGlynn KA. A systematic review and meta-analysis of perinatal variables in relation to the risk of testicular cancer--experiences of the mother. International journal of epidemiology. 2009;38(6):1532-42.
67. Looijenga LH, Van Agthoven T, Biermann K. Development of malignant germ cells - the genvironmental hypothesis. The International journal of developmental biology. 2013;57(2-4):241-53.
68. Ponti G, Ponzoni M, Ferreri AJM, Foppoli M, Mazzucchelli L, Zucca E. The impact of histopathologic diagnosis on the proper management of testis neoplasms. Nature Clinical Practice Oncology. 2008;5(10):619-22.
69. Skakkebaek NE, Rajpert-De Meyts E, Main KM. Testicular dysgenesis syndrome: an increasingly common developmental disorder with environmental aspects. Hum Reprod. 2001;16(5):972-8.
70. Rajpert-De Meyts E. Developmental model for the pathogenesis of testicular carcinoma in situ: genetic and environmental aspects. Human reproduction update. 2006;12(3):303-23.
71. Zhang XS, Zhang ZH, Jin X, Wei P, Hu XQ, Chen M, et al. Dedifferentiation of adult monkey Sertoli cells through activation of extracellularly regulated kinase 1/2 induced by heat treatment. Endocrinology. 2006;147(3):1237-45.
72. Fink C, Baal N, Wilhelm J, Sarode P, Weigel R, Schumacher V, et al. On the origin of germ cell neoplasia in situ: Dedifferentiation of human adult Sertoli cells in cross talk with seminoma cells in vitro. Neoplasia. 2021;23(7):731-42.
73. Sesterhenn IA, Davis CJ, Jr. Pathology of germ cell tumors of the testis. Cancer control : journal of the Moffitt Cancer Center. 2004;11(6):374-87.

74. McIver SC, Roman SD, Nixon B, Loveland KL, McLaughlin EA. The rise of testicular germ cell tumours: the search for causes, risk factors and novel therapeutic targets. F1000Research. 2013;2:55.
75. Frazier AL, Weldon C, Amatruda J. Fetal and neonatal germ cell tumors. Seminars in fetal & neonatal medicine. 2012;17(4):222-30.
76. Looijenga LH, Gillis AJ, Stoop H, Biermann K, Oosterhuis JW. Dissecting the molecular pathways of (testicular) germ cell tumour pathogenesis; from initiation to treatment-resistance. International journal of andrology. 2011;34(4 Pt 2):e234-51.
77. Bahrami A, Ro JY, Ayala AG. An overview of testicular germ cell tumors. Archives of pathology & laboratory medicine. 2007;131(8):1267-80.
78. Carver BS, Sheinfeld J. Germ cell tumors of the testis. Annals of surgical oncology. 2005;12(11):871-80.
79. Richiardi L, Pettersson A, Akre O. Genetic and environmental risk factors for testicular cancer. International journal of andrology. 2007;30(4):230-40; discussion 40-1.
80. Gaddam SJ, Chesnut GT. Testicle Cancer. StatPearls. Treasure Island (FL): StatPearls Publishing

81. Granfors T, Modig H, Damber JE, Tomic R. Combined orchiectomy and external radiotherapy versus radiotherapy alone for nonmetastatic prostate cancer with or without pelvic lymph node involvement: a prospective randomized study. The Journal of urology. 1998;159(6):2030-4.
82. Pinar G, Oksuz E, Beder A, Elbaş N. Reliability and validity of the Turkish adaptation of the Champion's health belief model scale at testicular cancer screening. 2011.
83. Nichols CR. Testicular cancer. Current problems in cancer. 1998;22(4):187-274.
84. Park DS, Prow DM, Amato RJ, Ro JY, Logothetis CJ. Clinical characteristics of metachronous bilateral testicular tumors in the chemotherapeutic era. Yonsei medical journal. 1999;40(2):137-43.
85. Kattuoa ML, Kumar A. Yolk Sac Tumors. StatPearls. Treasure Island (FL): StatPearls Publishing

86. Szymendera JJ, Zborzil J, Sikorowa L, Kamińska JA, Gadek A. Value of five tumor markers (AFP, CEA, hCG, hPL and SP1) in diagnosis and staging of testicular germ cell tumors. Oncology. 1981;38(4):222-9.
87. Lawton AJ, Mead GM. Staging and prognostic factors in testicular cancer. Seminars in surgical oncology. 1999;17(4):223-9.
88. von Eyben FE. A systematic review of lactate dehydrogenase isoenzyme 1 and germ cell tumors. Clinical biochemistry. 2001;34(6):441-54.
89. Simpson AJG, Caballero OL, Jungbluth A, Chen Y-T, Old LJ. Cancer/testis antigens, gametogenesis and cancer. Nature Reviews Cancer. 2005;5(8):615-25.
90. Shabbir M, Morgan RJ. Testicular cancer. The journal of the Royal Society for the Promotion of Health. 2004;124(5):217-8.
91. McGlynn KA, Devesa SS, Graubard BI, Castle PE. Increasing incidence of testicular germ cell tumors among black men in the United States. Journal of clinical oncology : official journal of the American Society of Clinical Oncology. 2005;23(24):5757-61.

92. Oosterhuis JW, Looijenga LH. Testicular germ-cell tumours in a broader perspective. Nature reviews Cancer. 2005;5(3):210-22.
93. Berney DM, Looijenga LH, Idrees M, Oosterhuis JW, Rajpert-De Meyts E, Ulbright TM, et al. Germ cell neoplasia in situ (GCNIS): evolution of the current nomenclature for testicular pre-invasive germ cell malignancy. Histopathology. 2016;69(1):7-10.
94. de Jong J, Stoop H, Gillis AJ, Hersmus R, van Gurp RJ, van de Geijn GJ, et al. Further characterization of the first seminoma cell line TCam-2. Genes, chromosomes & cancer. 2008;47(3):185-96.
95. Stoop H, Honecker F, van de Geijn GJ, Gillis AJ, Cools MC, de Boer M, et al. Stem cell factor as a novel diagnostic marker for early malignant germ cells. The Journal of pathology. 2008;216(1):43-54.
96. Irie N, Weinberger L, Tang WW, Kobayashi T, Viukov S, Manor YS, et al. SOX17 is a critical specifier of human primordial germ cell fate. Cell. 2015;160(1-2):253-68.
97. Nettersheim D, Westernströer B, Haas N, Leinhaas A, Brüstle O, Schlatt S, et al. Establishment of a versatile seminoma model indicates cellular plasticity of germ cell tumor cells. Genes, chromosomes & cancer. 2012;51(7):717-26.
98. Nettersheim D, Jostes S, Sharma R, Schneider S, Hofmann A, Ferreira HJ, et al. BMP Inhibition in Seminomas Initiates Acquisition of Pluripotency via NODAL Signaling Resulting in Reprogramming to an Embryonal Carcinoma. PLoS genetics. 2015;11(7):e1005415.
99. Pierce GB, Pantazis CG, Caldwell JE, Wells RS. Specificity of the control of tumor formation by the blastocyst. Cancer research. 1982;42(3):1082-7.
100. Goddard NC, McIntyre A, Summersgill B, Gilbert D, Kitazawa S, Shipley J. KIT and RAS signalling pathways in testicular germ cell tumours: new data and a review of the literature. International journal of andrology. 2007;30(4):337-48; discussion 49.
101. Hochedlinger K, Blelloch R, Brennan C, Yamada Y, Kim M, Chin L, et al. Reprogramming of a melanoma genome by nuclear transplantation. Genes Dev. 2004;18(15):1875-85.
102. Lee LM, Seftor EA, Bonde G, Cornell RA, Hendrix MJ. The fate of human malignant melanoma cells transplanted into zebrafish embryos: assessment of migration and cell division in the absence of tumor formation. Developmental dynamics : an official publication of the American Association of Anatomists. 2005;233(4):1560-70.
103. Ferranti F, D'Anselmi F, Caruso M, Lei V, Dinicola S, Pasqualato A, et al. TCam-2 seminoma cells exposed to egg-derived microenvironment modify their shape, adhesive pattern and migratory behaviour: a molecular and morphometric analysis. PloS one. 2013;8(10):e76192.
104. Young J, Wakitani S, Loveland K. TGF-β superfamily signaling in testis formation and early male germline development. Seminars in Cell and Developmental Biology. 2015;45:94-103.
105. Nettersheim D, Schorle H. The plasticity of germ cell cancers and its dependence on the cellular microenvironment. Journal of cellular and molecular medicine. 2017;21:1463-7.
106. Nettersheim D, Vadder S, Jostes S, Heimsoeth A, Schorle H. TCam-2 cells deficient for SOX2 and FOXA2 are blocked in differentiation and maintain a seminoma-like cell fate in vivo. Cancers. 2019;11:E728.
107. Young JC, Jaiprakash A, Mithraprabhu S, Itman C, Kitazawa R, Looijenga LH, et al. TCam-2 seminoma cell line exhibits characteristic foetal germ cell responses to

TGF-beta ligands and retinoic acid. International journal of andrology. 2011;34(4 Pt 2):e204-17.
108. Ferranti F, Caruso M, Cammarota M, Masiello MG. Cytoskeleton modifications and autophagy induction in TCam-2 seminoma cells exposed to simulated microgravity. 2014;2014:904396.
109. Peng D, Wei J, Gan Y, Yang J, Jiang X, Kitazawa R, et al. Testis developmental related gene 1 regulates the chemosensitivity of seminoma TCam-2 cells to cisplatin via autophagy. Journal of cellular and molecular medicine. 2019;23(11):7773-84.
110. Liu C, Wei J, Xu K, Sun X, Zhang H, Xiong C. CSE1L participates in regulating cell mitosis in human seminoma. Cell proliferation. 2019;52(2):e12549.
111. Panza S, Gelsomino L, Malivindi R, Rago V, Barone I, Giordano C, et al. Leptin Receptor as a Potential Target to Inhibit Human Testicular Seminoma Growth. The American journal of pathology. 2019;189(3):687-98.
112. Harvey KF, Zhang X, Thomas DM. The Hippo pathway and human cancer. Nature reviews Cancer. 2013;13(4):246-57.
113. Varelas X. The Hippo pathway effectors TAZ and YAP in development, homeostasis and disease. Development. 2014;141(8):1614-26.
114. Mo JS, Park HW, Guan KL. The Hippo signaling pathway in stem cell biology and cancer. EMBO reports. 2014;15(6):642-56.
115. Meng Z, Moroishi T, Guan KL. Mechanisms of Hippo pathway regulation. Genes Dev. 2016;30(1):1-17.
116. Yu FX, Guan KL. The Hippo pathway: regulators and regulations. Genes Dev. 2013;27(4):355-71.
117. Boggiano JC, Vanderzalm PJ, Fehon RG. Tao-1 phosphorylates Hippo/MST kinases to regulate the Hippo-Salvador-Warts tumor suppressor pathway. Dev Cell. 2011;21(5):888-95.
118. Poon CL, Lin JI, Zhang X, Harvey KF. The sterile 20-like kinase Tao-1 controls tissue growth by regulating the Salvador-Warts-Hippo pathway. Dev Cell. 2011;21(5):896-906.
119. Praskova M, Khoklatchev A, Ortiz-Vega S, Avruch J. Regulation of the MST1 kinase by autophosphorylation, by the growth inhibitory proteins, RASSF1 and NORE1, and by Ras. Biochem J. 2004;381(Pt 2):453-62.
120. Glantschnig H, Rodan GA, Reszka AA. Mapping of MST1 kinase sites of phosphorylation. Activation and autophosphorylation. J Biol Chem. 2002;277(45):42987-96.
121. Hergovich A, Schmitz D, Hemmings BA. The human tumour suppressor LATS1 is activated by human MOB1 at the membrane. Biochem Biophys Res Commun. 2006;345(1):50-8.
122. Yin F, Yu J, Zheng Y, Chen Q, Zhang N, Pan D. Spatial organization of Hippo signaling at the plasma membrane mediated by the tumor suppressor Merlin/NF2. Cell. 2013;154(6):1342-55.
123. Chan EH, Nousiainen M, Chalamalasetty RB, Schäfer A, Nigg EA, Silljé HH. The Ste20-like kinase Mst2 activates the human large tumor suppressor kinase Lats1. Oncogene. 2005;24(12):2076-86.
124. Yu F-X, Zhao B, Guan K-L. Hippo Pathway in Organ Size Control, Tissue Homeostasis, and Cancer. Cell. 2015;163:811-28.
125. Liu AM, Wong KF, Jiang X, Qiao Y, Luk JM. Regulators of mammalian Hippo pathway in cancer. Biochimica et biophysica acta. 2012;1826(2):357-64.

126. Harvey KF, Zhang X, Thomas DM. The Hippo pathway and human cancer. Nature Reviews Cancer. 2013;13(4):246-57.
127. McPherson JP, Tamblyn L, Elia A, Migon E, Shehabeldin A, Matysiak-Zablocki E, et al. Lats2/Kpm is required for embryonic development, proliferation control and genomic integrity. The EMBO journal. 2004;23(18):3677-88.
128. Morin-Kensicki EM, Boone BN, Howell M, Stonebraker JR, Teed J, Alb JG, et al. Defects in yolk sac vasculogenesis, chorioallantoic fusion, and embryonic axis elongation in mice with targeted disruption of Yap65. Molecular and cellular biology. 2006;26(1):77-87.
129. Hossain Z, Ali SM, Ko HL, Xu J, Ng CP, Guo K, et al. Glomerulocystic kidney disease in mice with a targeted inactivation of Wwtr1. Proc Natl Acad Sci U S A. 2007;104(5):1631-6.
130. St John MA, Tao W, Fei X, Fukumoto R, Carcangiu ML, Brownstein DG, et al. Mice deficient of Lats1 develop soft-tissue sarcomas, ovarian tumours and pituitary dysfunction. Nat Genet. 1999;21(2):182-6.
131. Levasseur A, Paquet M, Boerboom D, Boyer A. Yes-associated protein and WW-containing transcription regulator 1 regulate the expression of sex-determining genes in Sertoli cells, but their inactivation does not cause sex reversal. Biol Reprod. 2017;97(1):162-75.
132. Kjærner-Semb E, Ayllon F, Kleppe L, Sørhus E, Skaftnesmo K, Furmanek T, et al. Vgll3 and the Hippo pathway are regulated in Sertoli cells upon entry and during puberty in Atlantic salmon testis. 2018;8(1):1912.
133. Sen Sharma S, Majumdar SS. Transcriptional co-activator YAP regulates cAMP signaling in Sertoli cells. Molecular and cellular endocrinology. 2017;450:64-73.
134. Chi X, Luo W, Song J, Li B, Su T, Yu M, et al. Kindlin-2 in Sertoli cells is essential for testis development and male fertility in mice. Cell death & disease. 2021;12(6):604.
135. Abou Nader N, Levasseur A, Zhang X, Boerboom D, Nagano MC, Boyer A. Yes-associated protein expression in germ cells is dispensable for spermatogenesis in mice. 2019;57(10):e23330.
136. Sen Sharma S, Vats A, Majumdar S. Regulation of Hippo pathway components by FSH in testis. Reproductive biology. 2019;19(1):61-6.
137. Pfleger CM. The Hippo Pathway: A Master Regulatory Network Important in Development and Dysregulated in Disease. Curr Top Dev Biol. 2017;123:181-228.
138. Ma S, Meng Z, Chen R, Guan KL. The Hippo Pathway: Biology and Pathophysiology. Annual review of biochemistry. 2019;88:577-604.
139. Tapon N, Harvey KF, Bell DW, Wahrer DC, Schiripo TA, Haber D, et al. salvador Promotes both cell cycle exit and apoptosis in Drosophila and is mutated in human cancer cell lines. Cell. 2002;110(4):467-78.
140. Camargo FD, Gokhale S, Johnnidis JB, Fu D, Bell GW, Jaenisch R, et al. YAP1 increases organ size and expands undifferentiated progenitor cells. Curr Biol. 2007;17(23):2054-60.
141. Schlegelmilch K, Mohseni M, Kirak O, Pruszak J, Rodriguez JR, Zhou D, et al. Yap1 acts downstream of α-catenin to control epidermal proliferation. Cell. 2011;144(5):782-95.
142. Heallen T, Zhang M, Wang J, Bonilla-Claudio M, Klysik E, Johnson RL, et al. Hippo pathway inhibits Wnt signaling to restrain cardiomyocyte proliferation and heart size. Science. 2011;332(6028):458-61.

143. Serrano M, Lin AW, McCurrach ME, Beach D, Lowe SW. Oncogenic ras provokes premature cell senescence associated with accumulation of p53 and p16INK4a. Cell. 1997;88(5):593-602.
144. Dong J, Feldmann G, Huang J, Wu S, Zhang N, Comerford SA, et al. Elucidation of a universal size-control mechanism in Drosophila and mammals. Cell. 2007;130(6):1120-33.
145. Ramalho-Santos M, Yoon S, Matsuzaki Y, Mulligan RC, Melton DA. "Stemness": transcriptional profiling of embryonic and adult stem cells. Science. 2002;298(5593):597-600.
146. Steinhardt AA, Gayyed MF, Klein AP, Dong J, Maitra A, Pan D, et al. Expression of Yes-associated protein in common solid tumors. Human pathology. 2008;39(11):1582-9.
147. Lian I, Kim J, Okazawa H, Zhao J, Zhao B, Yu J, et al. The role of YAP transcription coactivator in regulating stem cell self-renewal and differentiation. Genes Dev. 2010;24(11):1106-18.
148. Varelas X, Sakuma R, Samavarchi-Tehrani P, Peerani R, Rao BM, Dembowy J, et al. TAZ controls Smad nucleocytoplasmic shuttling and regulates human embryonic stem-cell self-renewal. Nat Cell Biol. 2008;10(7):837-48.
149. Hong JH, Hwang ES, McManus MT, Amsterdam A, Tian Y, Kalmukova R, et al. TAZ, a transcriptional modulator of mesenchymal stem cell differentiation. Science. 2005;309(5737):1074-8.
150. Cordenonsi M, Zanconato F, Azzolin L, Forcato M, Rosato A, Frasson C, et al. The Hippo transducer TAZ confers cancer stem cell-related traits on breast cancer cells. Cell. 2011;147(4):759-72.
151. Zanconato F, Cordenonsi M, Piccolo S. YAP/TAZ at the Roots of Cancer. Cancer cell. 2016;29(6):783-803.
152. Pan D. The Hippo Signaling Pathway in Development and Cancer. Developmental Cell. 2010;19(4):491-505.
153. Pavel M, Renna M, Park SJ, Menzies FM, Ricketts T, Füllgrabe J, et al. Contact inhibition controls cell survival and proliferation via YAP/TAZ-autophagy axis. Nature communications. 2018;9(1):2961.
154. Cunningham R, Hansen CG. The Hippo pathway in cancer: YAP/TAZ and TEAD as therapeutic targets in cancer. 2022;136(3):197-222.
155. Moya IM, Halder G. Hippo-YAP/TAZ signalling in organ regeneration and regenerative medicine. 2019;20(4):211-26.
156. Zhao B, Wei X, Li W, Udan RS, Yang Q, Kim J, et al. Inactivation of YAP oncoprotein by the Hippo pathway is involved in cell contact inhibition and tissue growth control. Genes & development. 2007;21(21):2747-61.
157. Barron DA, Kagey JD. The role of the Hippo pathway in human disease and tumorigenesis. Clinical and translational medicine. 2014;3:25.
158. Dai M, Yan G, Wang N, Daliah G. In vivo genome-wide CRISPR screen reveals breast cancer vulnerabilities and synergistic mTOR/Hippo targeted combination therapy. 2021;12(1):3055.
159. Luo M, Meng Z, Moroishi T. Heat stress activates YAP/TAZ to induce the heat shock transcriptome. 2020;22(12):1447-59.
160. Kim MH, Kim J. Role of YAP/TAZ transcriptional regulators in resistance to anti-cancer therapies. Cell Mol Life Sci. 2017;74(8):1457-74.

161. Yu M, Peng Z, Qin M, Liu Y, Wang J, Zhang C, et al. Interferon-γ induces tumor resistance to anti-PD-1 immunotherapy by promoting YAP phase separation. Molecular cell. 2021;81(6):1216-30.e9.
162. He K, Li Z, Ye K, Zhou Y, Yan M, Qi H, et al. Novel sequential therapy with metformin enhances the effects of cisplatin in testicular germ cell tumours via YAP1 signalling. 2022;22(1):113.
163. Bressler N. Age related macular degeneration. New hope for a common problem comes from photodynamic therapy. BMJ (Clinical research ed). 2001;321:1425-7.
164. Wei C, Li X. The Role of Photoactivated and Non-Photoactivated Verteporfin on Tumor. Frontiers in pharmacology. 2020;11:557429.
165. Rytlewski JD, Scalora N. Photodynamic Therapy Using Hippo Pathway Inhibitor Verteporfin: A Potential Dual Mechanistic Approach in Treatment of Soft Tissue Sarcomas. 2021;13(4).
166. Panciera T, Azzolin L, Cordenonsi M, Piccolo S. Mechanobiology of YAP and TAZ in physiology and disease. Nat Rev Mol Cell Biol. 2017;18(12):758-70.
167. Wei H, Wang F, Wang Y, Li T, Xiu P, Zhong J, et al. Verteporfin suppresses cell survival, angiogenesis and vasculogenic mimicry of pancreatic ductal adenocarcinoma via disrupting the YAP-TEAD complex. Cancer science. 2017;108(3):478-87.
168. Zhao W, Zhang LN, Wang XL, Zhang J, Yu HX. Long noncoding RNA NSCLCAT1 increases non-small cell lung cancer cell invasion and migration through the Hippo signaling pathway by interacting with CDH1. FASEB journal : official publication of the Federation of American Societies for Experimental Biology. 2019;33(1):1151-66.
169. Trautmann M, Cheng YY, Jensen P, Azoitei N, Brunner I, Hüllein J, et al. Requirement for YAP1 signaling in myxoid liposarcoma. EMBO molecular medicine. 2019;11(5):e9889.
170. Yu FX, Luo J, Mo JS, Liu G, Kim YC, Meng Z, et al. Mutant Gq/11 promote uveal melanoma tumorigenesis by activating YAP. Cancer cell. 2014;25(6):822-30.
171. Kang W, Huang T, Zhou Y, Zhang J, Lung RWM, Tong JHM. miR-375 is involved in Hippo pathway by targeting YAP1/TEAD4-CTGF axis in gastric carcinogenesis. 2018;9(2):92.
172. Li N, Feng Y, Hu Y, He C, Xie C, Ouyang Y, et al. Helicobacter pylori CagA promotes epithelial mesenchymal transition in gastric carcinogenesis via triggering oncogenic YAP pathway. Journal of Experimental & Clinical Cancer Research. 2018;37(1):1-15.
173. Shen Y, Wang X. STAT3-YAP/TAZ signaling in endothelial cells promotes tumor angiogenesis. 2021;14(712):eabj8393.
174. Dong L, Lin F, Wu W, Liu Y, Huang W. Verteporfin inhibits YAP-induced bladder cancer cell growth and invasion via Hippo signaling pathway. International journal of medical sciences. 2018;15(6):645-52.
175. Jin D, Guo J, Wang D, Wu Y, Wang X, Gao Y, et al. RETRACTED: The antineoplastic drug metformin downregulates YAP by interfering with IRF-1 binding to the YAP promoter in NSCLC. EBioMedicine. 2018;37:188-204.
176. Garcia-Rendueles ME, Ricarte-Filho JC, Untch BR, Landa I, Knauf JA, Voza F, et al. NF2 Loss Promotes Oncogenic RAS-Induced Thyroid Cancers via YAP-Dependent Transactivation of RAS Proteins and Sensitizes Them to MEK Inhibition. Cancer discovery. 2015;5(11):1178-93.
177. Zhang WQ, Dai YY. Targeting YAP in malignant pleural mesothelioma. 2017;21(11):2663-76.

178. Zucchini C, Manara MC, Cristalli C, Carrabotta M, Greco S, Pinca RS, et al. ROCK2 deprivation leads to the inhibition of tumor growth and metastatic potential in osteosarcoma cells through the modulation of YAP activity. Journal of experimental & clinical cancer research : CR. 2019;38(1):503.
179. Hua G, Lv X, He C, Remmenga SW, Rodabough KJ, Dong J, et al. YAP induces high-grade serous carcinoma in fallopian tube secretory epithelial cells. Oncogene. 2016;35(17):2247-65.
180. Aparicio J, Terrasa J, Durán I, Germà-Lluch JR, Gironés R, González-Billalabeitia E, et al. SEOM clinical guidelines for the management of germ cell testicular cancer (2016). Clinical & translational oncology : official publication of the Federation of Spanish Oncology Societies and of the National Cancer Institute of Mexico. 2016;18(12):1187-96.
181. Williamson SR, Delahunt B, Magi-Galluzzi C, Algaba F, Egevad L, Ulbright TM, et al. The World Health Organization 2016 classification of testicular germ cell tumours: a review and update from the International Society of Urological Pathology Testis Consultation Panel. Histopathology. 2017;70(3):335-46.
182. Saeed-Zidane M, Linden L, Salilew-Wondim D, Held E, Neuhoff C, Tholen E, et al. Cellular and exosome mediated molecular defense mechanism in bovine granulosa cells exposed to oxidative stress. 2017;12(11):e0187569.
183. Xu C, Liu C, Huang W, Tu S, Wan F. Effect of Mst1 overexpression on the growth of human hepatocellular carcinoma HepG2 cells and the sensitivity to cisplatin in vitro. Acta biochimica et biophysica Sinica. 2013;45(4):268-79.
184. Najafi M, Kordi-Tamandani DM, Arish M. Evaluation of LATS1 and LATS2 Promoter Methylation with the Risk of Pterygium Formation. Journal of ophthalmology. 2016;2016:5431021.
185. Liu JY, Li YH, Lin HX, Liao YJ, Mai SJ, Liu ZW, et al. Overexpression of YAP 1 contributes to progressive features and poor prognosis of human urothelial carcinoma of the bladder. BMC cancer. 2013;13:349.
186. Zhang J, Liu P, Tao J, Wang P, Zhang Y, Song X, et al. TEA domain transcription factor 4 (TEAD4) is the major mediator of Yap oncogenic activity in mouse and human hepatoblastoma. The American Journal of Pathology. 2019;189.
187. Suarez-Arnedo A, Torres Figueroa F, Clavijo C, Arbeláez P, Cruz JC, Muñoz-Camargo C. An image J plugin for the high throughput image analysis of in vitro scratch wound healing assays. PLoS One. 2020;15(7):e0232565.
188. Gelles JD, Chipuk JE. Robust high-throughput kinetic analysis of apoptosis with real-time high-content live-cell imaging. Cell Death Dis. 2017;8(5):e2758.
189. Eray M, Mättö M, Kaartinen M, Andersson L, Pelkonen J. Flow cytometric analysis of apoptotic subpopulations with a combination of annexin V-FITC, propidium iodide, and SYTO 17. Cytometry. 2001;43(2):134-42.
190. Ekici K, Temelli O, Parlakpınar H, Samdanci E, Polat A, Beytur A, et al. Beneficial effects of aminoguanidine on radiotherapy- induced kidney and testis injury. Andrologia. 2015;48.
191. Wang L, Matloob A, Asiry S, Khader S. Educational Case: Testicular Germ Cell Tumor: Clinical Presentation, Pathogenesis, and Diagnostic and Therapeutic Modalities. Academic Pathology. 2020;7:237428952097517.
192. Ciaputa R, Nowak M, Kiełbowicz M, Antończyk A, Błasiak K, Madej J. Seminoma, Sertolioma, and Leydigoma in Dogs: Clinical and Morphological Correlations. Bulletin of the Veterinary Institute in Pulawy. 2012;56.

193. Pan W-W, Moroishi T, Koo J, Guan K-L. Cell type-dependent function of LATS1/2 in cancer cell growth. Oncogene. 2019;38.
194. Chen M, Huang B, Zhu L. Structural and Functional Overview of TEAD4 in Cancer Biology. 2020;13:9865-74.
195. Fink C, Weigel R, Hembes T, Lauke-Wettwer H, Kliesch S, Bergmann M, et al. Altered expression of ZO-1 and ZO-2 in Sertoli cells and loss of blood-testis barrier integrity in testicular carcinoma in situ. Neoplasia. 2006;8(12):1019-27.
196. Lin KC, Shen G.
197. Ciamporcero E, Daga M, Pizzimenti S, Roetto A, Dianzani C, Compagnone A, et al. Crosstalk between Nrf2 and YAP contributes to maintaining the antioxidant potential and chemoresistance in bladder cancer. Free radical biology & medicine. 2018;115:447-57.
198. Liu-Chittenden Y, Huang B, Shim JS, Chen Q, Lee SJ, Anders RA, et al. Genetic and pharmacological disruption of the TEAD-YAP complex suppresses the oncogenic activity of YAP. Genes Dev. 2012;26(12):1300-5.
199. Szeto SG, Narimatsu M, Lu M, He X, Sidiqi AM, Tolosa MF, et al. YAP/TAZ Are Mechanoregulators of TGF-β-Smad Signaling and Renal Fibrogenesis. Journal of the American Society of Nephrology : JASN. 2016;27(10):3117-28.
200. Feng J, Gou J, Jia J, Yi T, Cui T, Li Z. Verteporfin, a suppressor of YAP-TEAD complex, presents promising antitumor properties on ovarian cancer. OncoTargets and therapy. 2016;9:5371-81.
201. Bae SJ, Luo X. Activation mechanisms of the Hippo kinase signaling cascade. Biosci Rep. 2018;38(4).
202. George NM, Day CE, Boerner BP, Johnson RL, Sarvetnick NE. Hippo signaling regulates pancreas development through inactivation of Yap. Molecular and cellular biology. 2012;32(24):5116-28.
203. Xu C, Wang L, Zhang Y, Li W, Li J, Wang Y, et al. Tubule-Specific Mst1/2 Deficiency Induces CKD via YAP and Non-YAP Mechanisms. 2020;31(5):946-61.
204. Su D, Li Y, Guan L, Li Q, Shi C, Ma X, et al. Elevated MST1 leads to apoptosis via depletion of YAP1 in cardiomyocytes exposed to high glucose. Molecular Medicine. 2021;27(1):13.
205. Zhang Y-R, Zheng P-S. NEK2 inactivates the Hippo pathway to advance the proliferation of cervical cancer cells by cooperating with STRIPAK complexes. Cancer letters. 2022;549:215917.
206. Liu X, Quan J, Shen Z, Zhang Z, Chen Z, Li L, et al. Metallothionein 2A (MT2A) controls cell proliferation and liver metastasis by controlling the MST1/LATS2/YAP1 signaling pathway in colorectal cancer. Cancer cell international. 2022;22(1):205.
207. Li L, Fang R, Liu B, Shi H, Wang Y, Zhang W, et al. Deacetylation of tumor-suppressor MST1 in Hippo pathway induces its degradation through HBXIP-elevated HDAC6 in promotion of breast cancer growth. Oncogene. 2016;35(31):4048-57.
208. Yabuta N, Okada N, Ito A, Hosomi T, Nishihara S, Sasayama Y, et al. Lats2 Is an Essential Mitotic Regulator Required for the Coordination of Cell Division*. Journal of Biological Chemistry. 2007;282(26):19259-71.
209. Furth N, Aylon Y. The LATS1 and LATS2 tumor suppressors: beyond the Hippo pathway. Cell death and differentiation. 2017;24(9):1488-501.
210. Shen Z, Pan Y, Chen P, Jiang B, Fang X, Jiang Y. LATS1 exerts tumor suppressor functions via targeting Gli1 in colorectal cancer. J Cancer. 2021;12(24):7311-9.
211. Wang C, Zhu ZM, Liu CL, He XJ, Zhang HY, Dong JH. Knockdown of yes-associated protein inhibits proliferation and downregulates large tumor suppressor 1

expression in MHCC97H human hepatocellular carcinoma cells. Molecular medicine reports. 2015;11(6):4101-8.
212. Chang Y, Fu XR, Cui M, Li WM, Zhang L, Li X, et al. Activated hippo signal pathway inhibits cell proliferation and promotes apoptosis in NK/T cell lymphoma cells. 2019;8(8):3892-904.
213. Wei C, Li X. Determination of the migration effect and molecular docking of verteporfin in different subtypes of breast cancer cells. Molecular medicine reports. 2020;22(5):3955-61.
214. Li N, Feng Y, Hu Y, He C, Xie C, Ouyang Y, et al. Helicobacter pylori CagA promotes epithelial mesenchymal transition in gastric carcinogenesis via triggering oncogenic YAP pathway. Journal of experimental & clinical cancer research : CR. 2018;37(1):280.
215. Morvaridi S, Dhall D, Greene MI, Pandol SJ, Wang Q. Role of YAP and TAZ in pancreatic ductal adenocarcinoma and in stellate cells associated with cancer and chronic pancreatitis. Scientific reports. 2015;5(1):16759.
216. Cha YJ, Bae SJ, Kim D, Ahn SG, Jeong J, Koo JS, et al. High Nuclear Expression of Yes-Associated Protein 1 Correlates With Metastasis in Patients With Breast Cancer. Frontiers in oncology. 2021;11:609743.
217. Han H, Yang B, Nakaoka HJ, Yang J, Zhao Y-f, Le Nguyen K, et al. Hippo signaling dysfunction induces cancer cell addiction to YAP. Oncogene. 2018;37:6414 - 24.
218. Sheng X, Li WB, Wang DL, Chen KH, Cao JJ, Luo Z, et al. YAP is closely correlated with castration-resistant prostate cancer, and downregulation of YAP reduces proliferation and induces apoptosis of PC-3 cells. Molecular medicine reports. 2015;12(4):4867-76.
219. Xia Y, Chang T, Wang Y, Liu Y, Li W, Li M, et al. YAP promotes ovarian cancer cell tumorigenesis and is indicative of a poor prognosis for ovarian cancer patients. PloS one. 2014;9(3):e91770.
220. Lee CK, Jeong SH, Jang C. Tumor metastasis to lymph nodes requires YAP-dependent metabolic adaptation. 2019;363(6427):644-9.
221. Zakaria MA, Kiew MC, Rajab NF. Rigid Tissue Increases Cytoplasmic pYAP Expression in Pre-Malignant Stage of Lung Squamous Cell Carcinoma (SCC) In Vivo. 2022;44(10):4528-39.
222. Cao L, Sun P-L, Yao M, Jia M, Gao H. Expression of YES-associated protein (YAP) and its clinical significance in breast cancer tissues. Human pathology. 2017;68:166-74.
223. Yeo M-K, Kim S-H, Kim JM, Huang S-M, Kim M-R, Song KS, et al. Correlation of expression of phosphorylated and non-phosphorylated Yes-associated protein with clinicopathological parameters in esophageal squamous cell carcinoma in a Korean population. Anticancer research. 2012;32(9):3835-40.
224. Wang Y, Gersten A, Moleirinho S, Gunn-Moore FJ, Reynolds PA, Prystowsky MB. Fibroblasts in head and neck squamous cell carcinoma associated with perineural invasion have high-level nuclear Yes-Associated Protein (YAP) Expression. Academic pathology. 2015;2(4):2374289515616972.
225. Huh HD, Kim DH, Jeong HS. Regulation of TEAD Transcription Factors in Cancer Biology. 2019;8(6).
226. Zhang W, Li J, Wu Y, Ge H, Song Y, Wang D, et al. TEAD4 overexpression promotes epithelial-mesenchymal transition and associates with aggressiveness and adverse prognosis in head neck squamous cell carcinoma. 2018;18:178.

227. Coto-Llerena M, Tosti N, Taha-Mehlitz S, Kancherla V, Paradiso V, Gallon J. Transcriptional Enhancer Factor Domain Family member 4 Exerts an Oncogenic Role in Hepatocellular Carcinoma by Hippo-Independent Regulation of Heat Shock Protein 70 Family Members. 2021;5(4):661-74.
228. Liu Y, Wang G, Yang Y, Mei Z, Liang Z, Cui A, et al. Increased TEAD4 expression and nuclear localization in colorectal cancer promote epithelial–mesenchymal transition and metastasis in a YAP-independent manner. Oncogene. 2016;35(21):2789-800.
229. Kim JY, Sung YN, Hong SM. High YAP and TEAD4 immunolabelings are associated with poor prognosis in patients with gallbladder cancer. APMIS : acta pathologica, microbiologica, et immunologica Scandinavica. 2021;129(12):729-42.
230. Bunney PE, Zink AN, Holm AA, Billington CJ, Kotz CM. Orexin activation counteracts decreases in nonexercise activity thermogenesis (NEAT) caused by high-fat diet. Physiology & behavior. 2017;176:139-48.
231. De Jong J, Stoop H, Gillis A, Hersmus R, Van Gurp R, Van De Geijn G, et al. Further characterization of the first seminoma cell line TCam-2. Genes, Chromosomes and Cancer. 2008;47:185-96.
232. He K, Li Z, Ye K, Zhou Y, Yan M, Qi H, et al. Novel sequential therapy with metformin enhances the effects of cisplatin in testicular germ cell tumours via YAP1 signalling. Cancer Cell Int. 2022;22(1):113.
233. Wang L, Li J, Wang R, Chen H, Wang R, Wang W, et al. NGF Signaling Interacts With the Hippo/YAP Pathway to Regulate Cervical Cancer Progression. Frontiers in oncology. 2021;11:688794.
234. Fu J, McGrath NA, Lee J, Wang X, Brar G, Xie C. Verteporfin synergizes the efficacy of anti-PD-1 in cholangiocarcinoma. Hepatobiliary & pancreatic diseases international : HBPD INT. 2022;21(5):485-92.
235. Hasegawa T, Sugihara T, Hoshino Y, Tarumoto R, Matsuki Y, Kanda T, et al. Photosensitizer verteporfin inhibits the growth of YAP- and TAZ-dominant gastric cancer cells by suppressing the anti-apoptotic protein Survivin in a light-independent manner. Oncology letters. 2021;22(4):703.
236. Wei C, Li X. Verteporfin inhibits cell proliferation and induces apoptosis in different subtypes of breast cancer cell lines without light activation. BMC cancer. 2020;20(1):1042.
237. Yang X, Xu Y, Jiang C, Ma Z, Jin L. Verteporfin suppresses osteosarcoma progression by targeting the Hippo signaling pathway. Oncology letters. 2021;22(4):724.
238. Takeda T, Tsubaki M, Genno S, Matsuda T, Yamamoto Y, Kimura A, et al. Inhibition of yes-associated protein suppresses migration, invasion, and metastasis in non-small cell lung cancer in vitro and in vivo. 2022;22(2):221-8.
239. Cheng H, Zhang Z, Rodriguez-Barrueco R, Borczuk A, Liu H, Yu J, et al. Functional genomics screen identifies YAP1 as a key determinant to enhance treatment sensitivity in lung cancer cells. Oncotarget. 2016;7(20):28976-88.
240. Shi G, Wang H, Han H, Gan J, Wang H. Verteporfin enhances the sensitivity of LOVO/TAX cells to taxol via YAP inhibition. Experimental and therapeutic medicine. 2018;16(3):2751-5.
241. González-Alonso P, Zazo S, Martín-Aparicio E, Luque M, Chamizo C, Sanz-Álvarez M, et al. The Hippo Pathway Transducers YAP1/TEAD Induce Acquired Resistance to Trastuzumab in HER2-Positive Breast Cancer. 2020;12(5).
242. Sugiura K, Mishima T, Takano S, Yoshitomi H, Furukawa K, Takayashiki T, et al. The Expression of Yes-Associated Protein (YAP) Maintains Putative Cancer Stemness

and Is Associated with Poor Prognosis in Intrahepatic Cholangiocarcinoma. The American journal of pathology. 2019;189(9):1863-77.
243. Choe MS, Bae CM, Kim SJ, Oh ST, Kown YJ, Choi WY, et al. Human embryonic stem cell-specific role of YAP in maintenance of self-renewal and survival. 2022;79(11):544.
244. Quan Y, Li Z, Zhu K, Liang J. Transcatheter arterial chemoembolization combined with Hippo/YAP inhibition significantly improve the survival of rats with transplanted hepatocellular carcinoma. Lipids in health and disease. 2021;20(1):74.
245. Quan Y, Li Z, Zhu K, Liang J. Transcatheter arterial chemoembolization combined with Hippo/YAP inhibition significantly improve the survival of rats with transplanted hepatocellular carcinoma. Lipids in health and disease. 2021;20(1):74.
246. Li JA, Kuang T, Pu N, Fang Y, Han X, Zhang L, et al. TRAF6 regulates YAP signaling by promoting the ubiquitination and degradation of MST1 in pancreatic cancer. 2019;19(2):211-8.
247. George NM, Day CE, Boerner BP, Johnson RL, Sarvetnick NE. Hippo Signaling Regulates Pancreas Development through Inactivation of Yap. Molecular and cellular biology. 2012;32(24):5116-28.
248. Reiser J, Hurst J, Voges M, Krauss P, Münch P, Iftner T, et al. High-risk human papillomaviruses repress constitutive kappa interferon transcription via E6 to prevent pathogen recognition receptor and antiviral-gene expression. Journal of virology. 2011;85(21):11372-80.
249. Britschgi A, Duss S, Kim S, Couto JP, Brinkhaus H, Koren S, et al. The Hippo kinases LATS1 and 2 control human breast cell fate via crosstalk with ERα. Nature. 2017;541(7638):541-5.
250. Han Y. Analysis of the role of the Hippo pathway in cancer. J Transl Med. 2019;17(1):116.
251. Kim J, Kwon H, Shin YK, Song G, Lee T. MAML1/2 promote YAP/TAZ nuclear localization and tumorigenesis. 2020;117(24):13529-40.
252. Morvaridi S, Dhall D, Greene MI, Pandol SJ, Wang Q. Role of YAP and TAZ in pancreatic ductal adenocarcinoma and in stellate cells associated with cancer and chronic pancreatitis. Scientific reports. 2015;5:16759.
253. Moroishi T, Hayashi T, Pan WW, Fujita Y, Holt MV, Qin J, et al. The Hippo Pathway Kinases LATS1/2 Suppress Cancer Immunity. Cell. 2016;167(6):1525-39.e17.
254. He C, Lv X, Huang C, Hua G, Ma B, Chen X, et al. YAP1-LATS2 feedback loop dictates senescent or malignant cell fate to maintain tissue homeostasis. 2019;20(3).
255. Pan WW, Moroishi T. Cell type-dependent function of LATS1/2 in cancer cell growth. 2019;38(14):2595-610.
256. Lin M, Yuan W, Su Z, Lin C, Huang T, Chen Y, et al. Yes-associated protein mediates angiotensin II-induced vascular smooth muscle cell phenotypic modulation and hypertensive vascular remodelling. 2018;51(6):e12517.
257. Gurda GT, Zhu Q, Bai H, Pan D, Schwarz KB, Anders RA. The use of Yes-associated protein expression in the diagnosis of persistent neonatal cholestatic liver disease. Human pathology. 2014;45(5):1057-64.
258. Brodowska K, Al-Moujahed A, Marmalidou A, Meyer Zu Horste M, Cichy J, Miller JW, et al. The clinically used photosensitizer Verteporfin (VP) inhibits YAP-TEAD and human retinoblastoma cell growth in vitro without light activation. Experimental eye research. 2014;124:67-73.
259. Jiang Y, Liu Y, Zhang Z, Yang J, Ye X, Jin Q, et al. [Verteporfin inhibits proliferation, invasion and migration of MDA-MB-231 human breast cancer cells by

down-regulating the expression of Yes-associated protein]. Xi bao yu fen zi mian yi xue za zhi = Chinese journal of cellular and molecular immunology. 2017;33(9):1223-7.
260. Yin L, Chen G. Verteporfin Promotes the Apoptosis and Inhibits the Proliferation, Migration, and Invasion of Cervical Cancer Cells by Downregulating SULT2B1 Expression. Medical science monitor : international medical journal of experimental and clinical research. 2020;26:e926780.
261. Kang MH, Jeong GS, Smoot DT, Ashktorab H, Hwang CM, Kim BS, et al. Correction: Verteporfin inhibits gastric cancer cell growth by suppressing adhesion molecule FAT1. Oncotarget. 2018;9(98):37268.
262. Wang M, Liu C, Li Y, Zhang Q, Zhu L, Fang Z, et al. Verteporfin Is a Promising Anti-Tumor Agent for Cervical Carcinoma by Targeting Endoplasmic Reticulum Stress Pathway. Frontiers in oncology. 2020;10:1781.
263. García P, Rosa L, Vargas S, Weber H, Espinoza JA, Suárez F, et al. Hippo-YAP1 Is a Prognosis Marker and Potentially Targetable Pathway in Advanced Gallbladder Cancer. Cancers. 2020;12(4).
264. Lui JW, Xiao S, Ogomori K, Hammarstedt JE, Little EC, Lang D. The Efficiency of Verteporfin as a Therapeutic Option in Pre-Clinical Models of Melanoma. J Cancer. 2019;10(1):1-10.
265. Huang Y, Ahmad US. YAP Inhibition by Verteporfin Causes Downregulation of Desmosomal Genes and Proteins Leading to the Disintegration of Intercellular Junctions. 2022;12(6).
266. Chen WS, Cao Z, Krishnan C, Panjwani N. Verteporfin without light stimulation inhibits YAP activation in trabecular meshwork cells: Implications for glaucoma treatment. Biochem Biophys Res Commun. 2015;466(2):221-5.
267. Saini H, Sharma H, Mukherjee S, Chowdhury S, Chowdhury R. Verteporfin disrupts multiple steps of autophagy and regulates p53 to sensitize osteosarcoma cells. 2021;21(1):52.
268. Wang M, Liu C, Li Y, Zhang Q, Zhu L, Fang Z, et al. Verteporfin Is a Promising Anti-Tumor Agent for Cervical Carcinoma by Targeting Endoplasmic Reticulum Stress Pathway. Frontiers in oncology. 2020;10:1781.
269. Jeong SB, Das R, Kim DH, Lee S, Oh HI, Jo S, et al. Anticancer effect of verteporfin on non-small cell lung cancer via downregulation of ANO1. Biomedicine & pharmacotherapy = Biomedecine & pharmacotherapie. 2022;153:113373.
270. Calori IR, Caetano W, Tedesco AC, Hioka N. Self-aggregation of verteporfin in glioblastoma multiforme cells: a static and time-resolved fluorescence study. Dyes and Pigments. 2020;182:108598.
271. Chen M, Zhong L, Yao SF, Zhao Y, Liu L, Li LW, et al. Verteporfin Inhibits Cell Proliferation and Induces Apoptosis in Human Leukemia NB4 Cells without Light Activation. International journal of medical sciences. 2017;14(10):1031-9.
272. Ma YW, Liu YZ, Pan JX. Verteporfin induces apoptosis and eliminates cancer stem-like cells in uveal melanoma in the absence of light activation. American journal of cancer research. 2016;6(12):2816-30.
273. Sanna L, Piredda R, Marchesi I, Bordoni V, Forcales SV, Calvisi DF, et al. "Verteporfin exhibits anti-proliferative activity in embryonal and alveolar rhabdomyosarcoma cell lines". Chemico-biological interactions. 2019;312:108813.
274. Chen M, Zhong L, Yao S-F, Zhao Y, Liu L, Li L-W, et al. Verteporfin Inhibits Cell Proliferation and Induces Apoptosis in Human Leukemia NB4 Cells without Light Activation. International journal of medical sciences. 2017;14:1031-9.

275. Li H, Huang Z, Gao M, Huang N, Luo Z, Shen H, et al. Inhibition of YAP suppresses CML cell proliferation and enhances efficacy of imatinib in vitro and in vivo. Journal of experimental & clinical cancer research : CR. 2016;35(1):134.
276. Abou Nader N, Ménard A, Levasseur A, St-Jean G. Targeted Disruption of Lats1 and Lats2 in Mice Impairs Testis Development and Alters Somatic Cell Fate. 2022;23(21).
277. Bang LG, Dasari VR, Kim D, Gogoi RP. Differential gene expression induced by Verteporfin in endometrial cancer cells. 2019;9(1):3839.
278. Al-Moujahed A, Brodowska K, Stryjewski TP, Efstathiou NE, Vasilikos I. Verteporfin inhibits growth of human glioma in vitro without light activation. 2017;7(1):7602.

6. APPENDICES

6.1. EHICAL APPROVAL

T.C. YEDİTEPE ÜNİVERSİTESİ

Sayı : 37068608-6100-15- 1966 **24/09/2020**
Konu: Klinik Araştırmalar
Etik Kurul Başvurusu hk.

İlgili Makama (Tuğçe Önel)

Yeditepe Üniversitesi Tıp Fakültesi Histoloji ve Embriyoloji A.B. Doç. Dr. Aylin Yaba Uçar'ın sorumlu araştırmacı olduğu **"İnsan Normal ve Seminoma Testis Dokularında Hippo Sinyal Yolağı Proteinlerinin Retrospektif Olarak Belirlenmesi"** isimli araştırma projesine ait Klinik Araştırmalar Etik Kurulu (KAEK) Başvuru Dosyası **(1957)** kayıtlı Numaralı KAEK Başvuru Dosyası, Yeditepe Üniversitesi Klinik Araştırmalar Etik Kurulu tarafından **23.09.2020** tarihli toplantıda incelenmiştir.

Kurul tarafından yapılan inceleme sonucu, yukarıdaki isim belirtilen çalışmanın yapılmasının etik ve bilimsel açıdan uygun olduğuna karar verilmiştir. **(KAEK Karar No:1292)**

Prof. Dr. Turgay Çelik

Yeditepe Üniversitesi
Klinik Araştırmalar Etik Kurul Başkanı

6.2. CURRICULUM VITAE

Personal Information

Adı		**Surname**	
Name		**Date of Birth**	
Nationality		**TR ID Number**	
E-mail		**Phone number**	

Education

Degree	Department	The name of the Institution Graduated From	Graduation year
Master	Institute of Health Sciences/Department of Histology and Embryology	İstanbul Medipol Univesity	2016
University	Faculty of Science and Letters/Biology	Marmara Univesity	2014
High school	Science Branch	Şenesenevler High School	2010

[#] All the grades must be listed if there is more than one (KPDS, ÜDS, TOEFL; EELTS vs),

Languages	**Grades ([#]) **
English (YÖKDİL)	75

Work Experience (Sort from present to past)

Position	**Institute**	**Duration (Year - Year)**
Technical Personnel	Yeditepe University	2022-
Department of Histology and Embryology - Assistant	İstanbul Medipol University, Center for Restorative and Regenerative Medicine (REMER)	2014-2016

Computer Skills

Program	**Level**
Microsoft Office (Excel, Word, Powerpoint)	Good
GraphPad	Good
EndNote	Good
Image Lab	Good
Photoshop	Good

****Excellent, good, average or basic**

Scientific works

The articles published in the journals indexed by SCI, SSCI, AHCI

T. Onel, C. S. Erdogan, B. Aru, E. Yildirim, G.Y. Demirel, A. Yaba. Effect of Rapamycin Treatment in Human Seminoma TCam-2 Cells through Inhibition of G1-S Transition. Nauy-nyn-Schmiedeberg's Archives of Pharmacology. 2022.
T. Onel, E. Yildirim, S. Dogan, A. Yaba. Determination of mTOR Signal Pathway in MMTV-TGF-α Mice Ovary at Different Ages. Research Article. The Journal of Histotechnology. 2022.
E. Yildirim, G. Bora, **T. Onel,** N. Talas, A. Yaba. Cell fate determination and Hippo signalingpathway in preimplantation mouse embryo. Review Article. Cell Tissue Research. 2021.
E. Yildirim, S. Aksoy, **T. Onel,** A. Yaba. Gonadal development and sex determination in mouse. Review Article. Reproductive Biology. 2020.
Onel T, Ayla Ş, Keskin İ, Parlayan C, Yiğitbaşı T, Kolbaşı B, Varlı Yelke T, Şenel Ustabaş T. Leptin in sperm analysis can be a new indicator. Research Article. Acta Histochemica. 2018

Articles published in other journals

Ayla Ş, Keskin İ, Varlı Yelke T, **Onel T**, Karahüseyinoğlu S. The Relationship of Seminal Leptin Levels with Semen Parameters and DNA Fragmentation. Orijinal Araştırma. Zeynep Kamil Tıp Bülteni (ZKTB). 2017.

Proceedings presented in international scientific meetings and published in proceedings book.

T. Önel, E. Yıldırım, S. Doğan & A. Yaba Ucar.The Acceleration of Reproductive Aging in MMTV- TGF-α Mice, Poster Presentation, 34th Annual Meeting Of The European Society Of Human Reproduction And Embryology, 01 July 2018, 04 August 2018.
H. K. Parlaktaş, E. Yıldırım, **T. Önel**, H. Zortul, F. Arıcıoğlu & A. Yaba Uçar. Effect Of Maternal Separation Stress and Use of Antidepressants on Rat Ovarian Reserve, Poster Presentation, 34th Annual Meeting of The European Society of Human Reproduction and Embryology, 01 July 2018, 04 August 2018.
T. Önel, E. Yıldırım, H.K. Parlaktaş, S. Doğan, A. Yaba Ucar. Effect of TGF-α Activation on Follicle Development in Mice. Poster Presentation. Awakening of the genome: The maternal-to-zygotic transition. EMBO Workshop. Prague/Czech Republic. 15-18 May 2019. Embryos. Poster Presentation. Awakening of the genome: The maternal-to-zygotic transition. EMBO Workshop. Prague/Czech Republic. 15-18 May 2019.
E. Yıldırım, Ö. Başer, **T. Önel**, H.K. Parlaktaş, Y. Yavuz, N. Talaş, B. Yılmaz, A. Yaba. Kisspeptin is mediated mTOR Signal Pathway in Ovarian Follicular Development in Mouse. Poster Presentation. Awakening of the genome: The maternal-to-zygotic transition. EMBO Workshop. Prague/Czech Republic. 15-18 May 2019.
G. Bora, **T. Önel**, E. Yıldırım, A. Yaba. The effect of circadian rhythm disruption due to constant light on ovarian and oocyte aging through possible relationship between PER2 and mTOR signaling pathway. Oral Presentation. European Society of Human Reproduction and Embryology (ESHRE) 2021.
E. Yıldırım, **T. Onel**, A. Yaba. Determination of the Role of c-Abl Tyrosine Kinase During Mouse Compaction Stage Preimplantation Embryos. Oral Presentation. 4th East Mediterranean Congressof Laboratory Animal Science. 9-11 Dec 2021.
T. Onel, N. Talas, E. Yıldırım, A. Yaba. Determination of the c-Abl Tyrosine Kinase in Response to DNA Damage in Mouse Granulosa Cells. Oral Presentation. 4th East Mediterranean Congress of Laboratory Animal Science. 9-11 Dec 2021.
T. Onel, C.S. Erdogan, E. Yildirim, A. Yaba. Inhibition of Mammalian Target of Rapamycin (mTOR) in Tcam-2 Seminoma Cell Line. 15th National and 1st International Congress of Histology and Embryology. 26-28 May 2022.
E. Yildirim**, T. Onel**, A. Yaba. The Role of C-Abl Tyrosine Kinase in Cell Fate Specification and Morphogenesis in Preimplantation Mouse Embryo. 15th National and 1st International Congress of Histology and Embryology. 26-28 May 2022.
E. Yildirim, Y. Yavuz, **T. Onel**, Z.Y. Erol, A. Yaba, B. Yilmaz. Effects Of Chemogenetıc Modulatıon of Hypothalamıc Arcuate Nucleus Kısspeptın Neurons on Folliculogenesıs in Kıss-Cre Polycystıc Ovarıan Syndrome Mouse Model. FENS Forum. Paris/France. 9-14 July 2022.

Journals in the proceedings book of the refereed conference / symposium

H. K. Parlaktaş, E. Yıldırım, **T. Önel**, H. Zortul. F. Arıcıoğlu & A. Yaba Uçar, Anneden Ayrılma Stresinin ve Antidepresan Kullanımının Sıçan Ovaryumları Üzerindeki Etkisinin Gösterilmesi, Poster Sunumu, 14. Ulusal Histoloji ve Embriyoloji Kongresi, 10 Mayıs 2018, 13 Mayıs 2018.
A. Yaba Uçar, E. Yıldırım, **T. Önel**, H. K. Parlaktaş. Farede DMBA İle Indüklenmiş Ovotoksisitede c-Abl Ve mTERT Ekspresyonlarının Belirlenmesi, Poster Sunumu, 14. Ulusal Histoloji ve Embriyoloji Kongresi, 10 Mayıs 2018, 13 Mayıs 2018.
T. Önel, E. Yıldırım, S. Doğan & A. Yaba Uçar. Mmtv-TGF-a Farelerde Ovariyal YaşlanmaSürecinde mTOR Ekspresyonunun Belirlenmesi, Poster Presentation, 14. Ulusal Histoloji ve Embriyoloji Kongresi, 10 Mayıs 2018, 13 Mayıs 2018.
E. Yıldırım, Ö. Başer, **T. Önel**, H.K. Parlaktaş, Y. Yavuz, N. Talaş, B. Yılmaz, A. Yaba. Farede Kisspeptin Aktivasyonu ile Ovaryumlarda Foliküler Gelişimin, mTOR ve p-mTOR Seviyelerinin Değerlendirilmesi, Sözlü sunum, 24. Ulusal Elektron Mikroskobi Kongresi, 24-26 Nisan 2019
G. Bora, E. Yıldırım, **T. Önel**, E. Günalan, H.K. Parlaktaş, N. Talaş, B. Gemici Başol, A. YabaUçar. Yüksek yağlı diyetin sıçan ovaryumlarında foliküler gelişim ve mTOR sinyal yolağı üzerindeki etkisi. Poster sunumu. 24. Ulusal Elektron Mikroskobi Kongresi, 24-26 Nisan 2019.
H.K. Parlaktaş, E. Yıldırım, **T. Önel**, H. Zortul, F. Arıcıoğlu, A. Yaba Uçar. Anneden ayrılmastresinin sıçan

ovaryumları üzerindeki etkisinin mTOR yolağı üzerinden değerlendirilmesi. Poster sunumu. 24. Ulusal Elektron Mikroskobi Kongresi, 24-26 Nisan 2019.
A. Yaba Uçar, E. Yıldırım, **T. Önel**, H.K. Parlaktaş, N. Demir. Farede DMBA maruziyeti ile oluşturulan prematüre over yetmezliğinde foliküllerin ultrastrüktürel olarak incelenmesi. Poster sunumu. 24. Ulusal Elektron Mikroskobi Kongresi, 24-26 Nisan 2019.
T. Önel, E. Yıldırım, H.K. Parlaktaş, S. Doğan, A. Yaba Uçar. TGF-α aktivasyonunun farelerde folikül gelişimi üzerindeki etkisinin gösterilmesi. Sözlü sunum. 24. Ulusal Elektron Mikroskobi Kongresi, 24-26 Nisan 2019.

Others (Projects / Certificates / Rewards)

Polikistik Over Sendromu (PKOS)'nun Tedavisinde mTOR (Mammalian Target of Rapamycin) Sinyal Mekanizmasının Rolü, **TUBİTAK** #214S328, Bursiyer
Farede Prematüre Over Yetmezliğinde mTERT Telomeraz Katalitik Alt Ünitesinin Rolünün Belirlenmesi, **TUBİTAK** #215S867, Bursiyer
Polikistik Over Sendromu Oluşturulan Transgenik Kisspeptin-Cre Farelerde Optogenetik ve Farmakogenetik Yöntemlerle Ovaryum Fonksiyonlarının Santral Düzenlenmesinin ve Mekanizmalarının Araştırılması, **TUBİTAK** #219S554, Bursiyer
Scholarship for workshop participation. Awakening of the genome: The maternal-to-zygotic transition. EMBO Workshop. Prague/Czech Republic. 15-18 May 2019.
4th East Mediterranean Congress of Laboratory Animal Science Oral Presentation 1st Award**.** E. Yıldırım, **T. Onel**, A. Yaba. Determination of the Role of c-Abl Tyrosine Kinase During Mouse Compaction Stage Preimplantation Embryos. 9-11 Dec 2021.